How cellulose and microtubules contribute to plant cell and organ growth : a temporal and spatial multi-scale analysis

Corentin Mollier

Numéro National de Thèse : **2022ENSL0041**

THESE

en vue de l'obtention du grade de Docteur, délivré par

l'ECOLE NORMALE SUPERIEURE DE LYON

Ecole Doctorale N° 340
Biologie Moléculaire, Intégrative et Cellulaire (BMIC)

Discipline : Sciences de la vie et de la santé

Soutenue publiquement le 25/11/2022, par :

Corentin MOLLIER

How cellulose and microtubules contribute to plant cell and organ growth: a temporal and spatial multi-scale analysis

Comment la cellulose et les microtubules contribuent à la croissance des cellules et des organes végétaux : une analyse temporelle et spatiale multi-échelles

---

Devant le jury composé de :

HERMAN Höfte	Directeur de recherche INRAE	Rapporteur
SUZANNE Magali	Directrice de recherche CNRS	Rapporteure
DELATTRE Marie	Directrice de recherche ENS de Lyon	Examinatrice
GRIENEISEN Veronica	Professeure Université de Cardiff	Examinatrice
PERSSON Staffan	Professeur Université de Copenhague	Examinateur
BOUDAOUD Arezki	Professeur des universités ENS de Lyon	Directeur de thèse

PhD manuscript

How cellulose and microtubules contribute to plant cell and organ growth: a temporal and spatial multi-scale analysis

Corentin Mollier

2019-2022

Under the supervision of Arezki Boudaoud and Françoise Monéger

Template

Template for this PhD is based on the work of Ken Arroyo Ohori. Source code is available at https://github.com/fmarotta/kaobook.

"Truth is singular. Its 'versions' are mistruths"

– *Sonmi 451*, Cloud Atlas, David Mitchell

Acknowledgements/Remerciements

First, I would like to thank Herman Höfte, Magali Suzanne, Marie Delattre, Staffan Persson and Veronica Grieneisen for accepting to review my work. I will switch to French, but just for this page.

Arezki est un encadrant de thèse assez particulier, et , au moment où j'écris ces mots, j'ai encore du mal à réaliser tout ce qu'il a fait pour moi. Globalement il cherche à faire de vous une meilleure personne, que ce soit humainement et scientifiquement (prenez garde à vous). Pour ça je lui en serai toujours reconnaissant.

Merci à toute l'équipe biophysique pour les échanges stimulants (virtuels ou pas) et pour les croissants (virtuels ou pas) du jeudi matin. Merci à Fanfan d'avoir accepté de participer à l'encadrement de ma thèse, à Mathilde d'avoir initié le projet, à Simone pour les nombreuses tentatives d'AFM, à Annamaria pour les discussions autour de l'analyse d'image et à Virginie de m'avoir supporté moi qui arrive avec ma petite goutte sur le front avec des questions de bio-mol, et mes trois forêts à ranger. Merci aux voisins de l'équipe mécano dévo pour les projets partagés, en particulier à Matthieu, Olivier, Christophe et Claire, et merci à Vincent pour le TIRF salvateur. Many thanks to all the contributors of the project who hosted me across Europe. Cześć my friends. Hallo, Köln.

Merci au département de biologie de l'ENS de Lyon, pour la supervision pendant ma scolarité mais également pour m'avoir donné l'opportunité d'enseigner à mon tour sur ses bancs pendant ma thèse.

Je voudrais aussi remercier mes élèves, que j'ai encadré de plus ou moins près pendant plus ou moins longtemps. Parce que la connaissance n'a de valeur que si elle est partagée, et probablement aussi parce que j'ai au moins autant appris qu'eux au cours de ces échanges. Merci en particulier à mes deux supers stagiaires Emilie et Mylan de m'avoir accompagné pendant ces périodes, vous trouverez votre travail joint à cette thèse.

Une thèse c'est du travail, mais c'est aussi un environnement de travail, et cet environnement c'est vous, le GN1 1.0, le GN1 2.0, les jeux du midi, la danse, la Zumba, le club murder, le café tricot, le BeeRDP et le RDP en général. Je ne sais pas expliquer pourquoi la sauce prend, mais si quelqu'un a la recette n'oubliez pas de la transmettre.

Enfin, à tous les gens qui me sont proches, prenez soin de vous comme vous avez pris soin de moi pendant ma thèse (sans nécessairement en avoir conscience).

Bonne lecture :)

Corentin Mollier

Ce n'est pas parce que la tartine est courte que la confiture est moins reconnaissante.

Contents

General introduction

Preface to the introduction: biology, time and space

Time and space are the two main aspects of our world. Biologists basically try to understand the behavior of wobbly spheres (known as molecules, well they're not really spheres but you get the point) which, sometimes, aggregate to form an organism. Even though biologists usually focus on a particular scale to understand a particular phenomenon, in the end, the goal is to provide an explanation that goes from the molecule to the organism. The sequence of scales one must go through ranges from atoms in some cases, to molecule, groups of molecules, compartment of the cell, cell, groups of cells, tissue, interaction between tissue and finally organism. Fortunately, these interactions only span from about a nanometer to a meter, about 9 orders of magnitude, which is much less compared to some systems studied by physicists. Another good news is that tools that allow for visualization of processes have been developed at all scales. As biologists, our task is to use them wisely to better understand the world around us.

Temporal analysis must also be considered cautiously. If one was to take pictures of a clock every hour, it would be tempting to say that the small hand moves while the big hand stays put. Here again, access to the truth is often dependent on our ability to quantify and track changes over time. In a developmental context, faster events usually occur at small spatial scales, while slower events occur at large spatial scales. For instance, a small glucose molecule diffuse in a water volume of its size in about a tenth of a nanosecond (Koirala et al. 2022), while a cell migrates up to its size in about a minute (Cai et al. 2016).

Relevant spatial scales in developmental biology: 10^{-9}m-1m
Relevant temporal scales in developmental biology: 10^{-9}s-10^{7}s (one year)
Small margin notes like this one are spread out throughout the introduction to give the reader an anthology of orders of magnitude in biology.

Energy produced by a reaction & Boltzzman constant k_bT

A few boxes like this one are spread out across the introduction. These give some insights on biological or physical models that should help the reader understand my manuscript. Every molecular interaction or reaction is associated with an energy. Quantifying this energy allows us to do qualitative evaluation of the plausibility of a phenomenon. Numerous units are used to describe the same phenomenon. In the main text of this manuscript we will try, when possible to use the Boltzmann constant (Boltzmann 1995):

$$k_bT = \frac{RT}{N_A}$$

where R corresponds to the molar gas constant, T corresponds to the temperature, N_A is the Avogadro number. At room temperature, k_bT is equal to 0.59kcal/mol or 4114 pN nm. To give a few ideas of order of magnitude, a hydrogen bond usually present an associated energy of $5k_bT$, a covalent bond an energy of $200k_bT$ and nuclear fusion an energy of $10^{11}k_bT$

Developmental biologists in particular aim at explaining the origin of complex morphogenetic events from molecular behaviors. In the introduction of this manuscript, I will try to give a non-exclusive overview of the phenomena that are linked with my biological questions. First, I will describe the rapid dynamics of the cytoskeleton with the example of microtubules. Then I will present the different components of the cell wall that influence the growth of plant cells. Finally, I will illustrate how morphogenesis involves the coordinated behavior of various cells in a tissue context. This will be followed by a brief introduction of the biological questions of my PhD prior to the presentation of the results.

The cytoskeleton, nanometers and seconds

1

The beginning of this chapter gives basic knowledge about cytoskeleton elements. This may seem trivial to some, but I thought it was important to go back to the fundamentals to better understand the biological questions asked in my PhD.

1.1 Molecular structure of microtubules

1.1.1 Microtubule elongation : α and β-tubulin

Microtubules are 25nm wide polymers of tubulins that fulfill various cellular functions. Tubulins are highly conserved evolutionary and their primitive role was likely involved in cell division (Pilhofer et al. 2011). The two most common tubulins in eukaryotes, α and β-tubulin, share around 90% sequence similarity (Fygenson et al. 2004). Cotton β-tubulin have been shown to complement β-tubulin deficient yeast cells, suggesting conserved functions (He et al. 2008). Both α and β-tubulin present a molecular weight of 50kDa (Desai and T. J. Mitchison 1997), bind to nucleotides, and form $\alpha\beta$ heterodimers. α-tubulin binds to guanosine-tri-phosphate (GTP) only, whereas β-tubulin binds to both GTP and guanosine-di-phosphate (GDP) (Geahlen and Haley 1977).

Tubulins represent 3-4% of the total protein content in a cell (Oakley 2000), leading to a high concentration of α and β tubulins in the cytoplasm which favors the formation of the $\alpha\beta$-tubulin complex, with an association speed of about 10^5-10^6 s^{-1} (Montecinos-Franjola et al. 2016). Intra-dimer strength of bonds has not been measured experimentally but are believed to be higher than the inter-dimer association energy (Kononova et al. 2014; Fedorov et al. 2019). Dissociation of the $\alpha\beta$ dimer was found to be relatively slow, with a dissociation rate of about 10^{-3}-10^{-2} s^{-1}, and does not require hydrolysis of the bound nucleotides (Montecinos-Franjola et al. 2016).

1.1.2 Microtubule nucleation : γ-tubulin and associated proteins

Microtubules' first step of polymerization is called nucleation and involves the assembly of another type of tubulin called γ-tubulin. γ-tubulin is found only at the base of microtubules, represents about 1% of total tubulins (Stearns et al. 1991) and presents about 40% sequence similarity with α and β tubulins (Burns 1991). These γ-tubulins form classically a 13 unit ring, on top of other scaffolding proteins, with a slight shift between units that gives it a helicoidal structure (Kollman et al. 2011). The

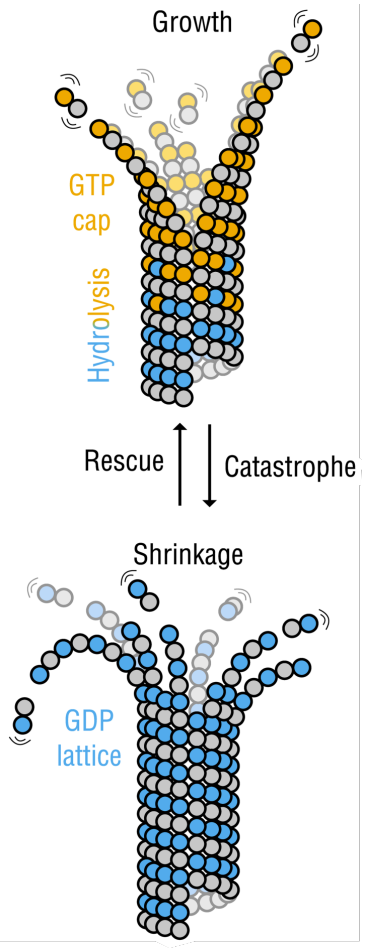

Figure 1.1: Microtubule dynamics. α-tubulin bound to GTP is represented in grey. β-tubulin is shown in orange bound to GTP and blue bound to GDP. Microtubules oscillate between phases of growth and shrinkage (extracted from Igaev and Grubmüller 2020). *γ-tubulin is not represented here but would form a ring at the base of the microtubue.*

$\alpha\beta$-tubulin dimer length : 8nm
Polymerisation speed : 10-20nm s^{-1} = 1-2 units s^{-1}, dependant on tubulin concentration (Gudimchuk and McIntosh 2021)
Depolymerisation speed : 500nm s^{-1} = 50 units s^{-1}, dependant on tubulin concentration (Gudimchuk and McIntosh 2021; Walker et al. 1988)
k_{on} : 3.4 $\mu M^{-1}s^{-1}$ per tip or 0.26 $\mu M^{-1}s^{-1}$ per protofilament (Mickolajczyk et al. 2019)

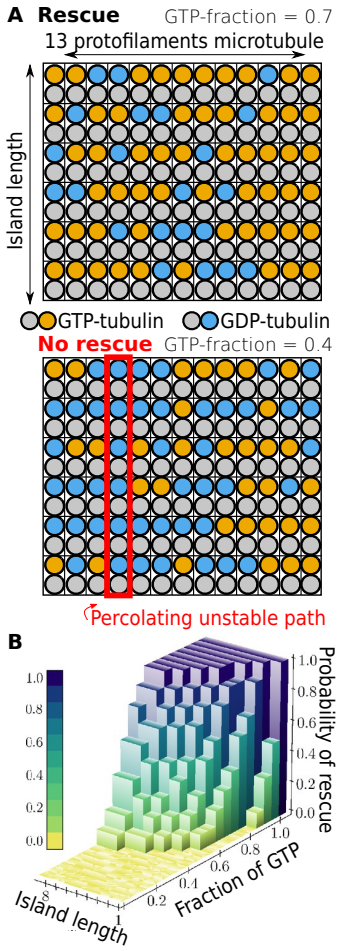

Figure 1.2: Model of microtubule instability and GTP/GDP ratio. A) GTP status of the 13 filaments composing a microtubule, in the top panel the microtubule is stable because no path of GDP bound tubulin goes from the top to the bottom. This creates a GTP island that may rescue a catastrophe. In the bottom panel, the catastrophe can not be prevented (redrawn from Michaels et al. 2020). B) Evolution of the probability of rescue in the model depending on the island length and the fraction of GTP. Areas where the fraction of GTP is close to 1, such as the tip, never undergo catastrophe (extracted from Michaels et al. 2020).

α-tubulin of a free $\alpha\beta$-tubulin dimer can bind to the top of a γ-tubulin or β tubulin of another dimer. This form filaments composed of a γ-tubulin followed by many $\alpha\beta$-tubulin dimers, which are called protofilaments. 13 of these filaments associate laterally to form a microtubule (Figure 1.1). The base formed by the protein complex associated with γ-tubulin, called nucleus, actually does not form a perfect circle but rather a helicoidal structure. The shift induced by the nucleus makes the ring of one type of tubulin be shifted by 3 monomers along the microtubule, creating an asymmetrical seam (Kollman et al. 2011). Protofilaments are linked longitudinally and laterally with a dissociation energy associated to the tubulin-tubulin interactions of 11 and $25k_bT$, respectively (Kononova et al. 2014). Polymerization on all protofilaments is relatively independent, and protofilaments are observed bending apart from the microtubule. This bending is related to the relaxed state of the $\alpha\beta$-tubulin dimer that presents an angle between 9-12°out (Campanacci et al. 2019). Once all 13 protofilaments are formed at one point of the microtubule, the energy provided by the lateral bonds brings them together and the angle between dimers becomes null making the protofilaments straight in the microtubule rod (Alushin et al. 2014).

1.1.3 Tubulin configuration and microtubule instability

α-tubulins do not present hydrolytic activity and are only found associated with GTP (David-Pfeuty et al. 1977). β tubulins can hydrolyse the nucleotide they are bound to and are added to the protofilaments only if they are bound to GTP (Carlier 1989). With a delay after insertion, this GTP is hydrolysed to GDP (Brouhard and Rice 2018). Most literature agrees that the status of the nucleotide bound affects the shape of the tubulin dimer, whether by a shortening of the dimer (Alushin et al. 2014; LaFrance et al. 2022), or by other rearrangements (Nawrotek et al. 2011). This leads to a relatively stable GTP bound cap at the end of the microtubule followed by a GDP bound body that is unstable (Alushin et al. 2014). Microtubules can be in one of two states: a slow polymerisation where dimers are added to the microtubule, or events of rapid depolymerisation, called catastrophe. During a catastrophe, the GTP bound tubulin cap present at the end of the microtubule shrinks, and the stabilizing forces, coming from lateral bonds of GTP associated tubulins, become smaller than the tension induced by GDP bound tubulin in the microtubule body, which are in a non relaxed state (Igaev and Grubmüller 2020). This mechanicals stress is therefore released by curving the protofilaments outwards eventually leading to their depolymerisation (Brouhard and Rice 2018). Occasionally, this catastrophe reaches an area where the GTP has not been hydrolyzed and where less stress has therefore been accumulated (Brouhard and Rice 2018). This may prevent the microtubule from depolymerizing further and start growing back again, leading to an event called a rescue.

Microtubule dynamic instability therefore depends on various parameters such as tubulin concentration, GTP hydrolysis activity of the tubulins, etc. Recent studies show that it is possible to predict microtubule's evolution depending on these parameters. The modeling approach described by Michaels et al. 2020 revealed, as expected, that the ratio between the rate of GTP hydrolysis and the rate of addition of GTP subunits at the end of the microtubule was determinant for the stability of the microtubule. Another key factor for the stability highlighted in this study was the presence of "GTP island" along the microtubule axis (Figure 1.2). While most of the microtubule body is composed of GDP tubulin, small groups of GTP bound tubulin can still be present. Because the stability of the structure is so dependent on the hydrolysis status of the nucleotide, if a microtubule undergoing catastrophe reaches a GTP island it may undergo a rescue. This study suggests that the microtubule will be rescued if there is no GDP percolating path (a connected path of GDP tubulin, see Figure 1.2), and that the probability of existence of such a path presents a sharp transition depending on the GDP/GTP proportions.

1.2 Regulation of microtubule dynamics by microtubule associated proteins

Microtubule dynamics, characterized by a time scale of seconds to minutes (Zwetsloot et al. 2018), can only be described by a probability distribution as it depends on random molecular events. Such processes are called stochastic. Microtubules, despite their stochastic behavior, fulfill various functions vital for the cell, which suggest that their activity is regulated by additional factors. Here, we will describe a few proteins known to regulate microtubule dynamics, which play a role in morphogenesis apart from cell division. We will focus on three key actors : End Binding (EB) proteins that act as a hub for the growing tip of microtubules, CLASPs (cytoplasmic-linker-associating proteins) that locally stabilizes microtubules and KATANIN, a microtubule severing protein that likely belongs to the stress sensing pathway.

1.2.1 End-binding proteins, a central hub for the growing tip

End binding proteins (EB) bind specifically to the GTP cap present at the end of microtubules (Figure 1.3, Roostalu et al. 2020). In vitro, EB1 and EB3, two of the three members of the EB family, induce the hydrolysis of the GTP (R. Zhang et al. 2015) and increase the catastrophe rate (Zanic et al. 2013; Maurer et al. 2014). Counterintuitively, EB1 also increases the rescue rate, possibly by stabilizing the lateral junctions between tubulin dimers (Vitre et al. 2008).

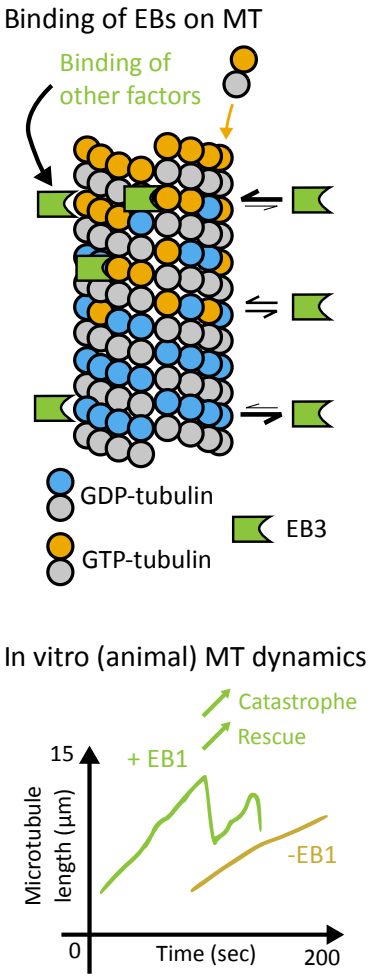

Figure 1.3: End-Binding proteins (EB) and influence on microtubules A) Binding of EB proteins is dependant on the hydrolysis status of tubulin (redrawn from Roostalu et al. 2020 with style copied from Igaev and Grubmüller 2020) B) In vitro influence of animal EB on microtubules (redrawn from Vitre et al. 2008).

As microtubule formation is prone to error, with for instance changes in the number of protofilaments (Chrétien et al. 1992; Rai et al. 2021), higher microtubule dynamics in presence of EB proteins is thought to reduce lattice defects and stabilize microtubules (Vitre et al. 2008). EB proteins are conserved in eukaryotes Mathur et al. 2003, with Arabidopsis presenting three variants all related to EB1 : EB1a, EB1b, EB1c (Bisgrove et al. 2008). However their influence on microtubules in vitro already presents some opposite effects, with plant EB that reduces polymerization speed and diminishes catastrophe rates (Molines, Stoppin-Mellet, et al. 2020).

EB proteins also recruit numerous proteins at the plus growing end of microtubules which are involved in depolymerisation, dynamics, nucleation, etc (Kumar and Wittmann 2012). These partners all share a short hydrophobic sequence, Ser-x-Ile-Pro (SxIP), recognized by all EB proteins which pinpoints their role as a hub for + end regulation of microtubule dynamics (Honnappa et al. 2009). The high number of partners associated with EB proteins makes it difficult to differentiate in vivo if the role of EB proteins in microtubule dynamics is direct or if it is achieved via the recruitment of other factors. In mammalian cells, EB proteins have been reported to decrease catastrophe rate, which is the opposite of the results obtained in vitro (Komarova et al. 2009). Contrary to discrepancies found in vitro between plants and animals, mutant plants lacking EB proteins also display reduced catastrophe rates (Komarova et al. 2009; Molines, Marion, et al. 2018). In plant cells, EB proteins additionally contribute to the association of microtubules into bundles (Molines, Marion, et al. 2018).

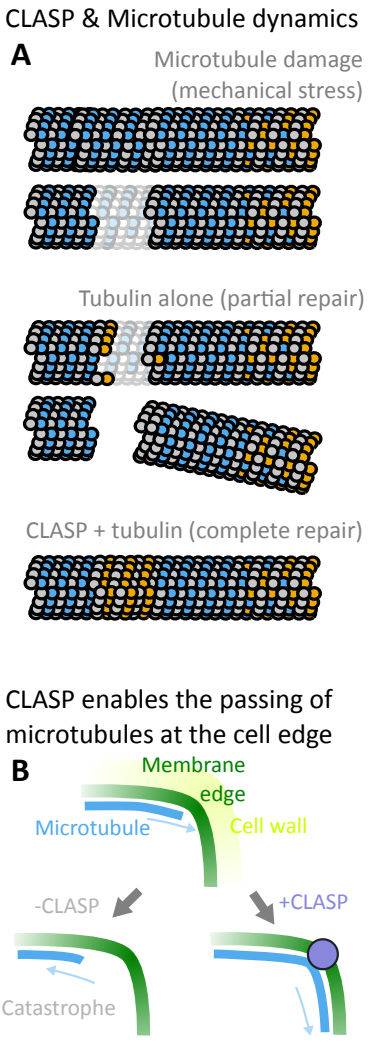

Figure 1.4: CLASP binding and influence on microtubules A) Microtubules often get damaged. In the presence of tubulin alone, the repair that occurs is only partial and the microtubule eventually ruptures. CLASP binds to damaged zones of microtubules and enable for a complete repair (redrawn from Aher et al. 2020 with style copied from Igaev and Grubmüller 2020) B) In plant cells CLASP is required at cell edges for MT to go from one face to another. In the absence of CLASP, microtubules that encounter the cell edge undergo catastrophe.

1.2.2 Cytoplasmic-linker-associating proteins, a stabilizer of microtubules

CLASPs, for cytoplasmic-linker-associating proteins, are another evolutionary conserved family of microtubule associated proteins, with two paralogues in humans, and one gene in Arabidopsis. In vitro, CLASPs bind to microtubules + ends via EB proteins but also independently and directly to the microtubule body (E. J. Lawrence et al. 2020). CLASPs binding to EB at the + end promotes assembly of protofilaments into a complete microtubule (Aher et al. 2020). CLASPs bind directly to the microtubule body and preferentially to defects in the lattice. After binding, CLASPs favor the insertion of GTP tubulin, which stabilizes microtubules, by reducing catastrophe duration (Aher et al. 2020) and preventing microtubule rupture (Figure 1.4, Aher et al. 2020).

Despite evolutionary conservation of CLASPs, they fulfill different functions in plants and animals. In animal cells, CLASPs are associated with stabilization of microtubules at the leading edge of motile cells (Akhmanova et al. 2001; Wittmann and Waterman-Storer 2005). CLASPs

also play a role in nucleation of microtubules as they are required for non-centrosomal MTOC (Efimov et al. 2007). Surprisingly, overexpression of CLASPs leads to defects in microtubule elongation, with microtubules not being able to expand to the axon growth cone (Hur et al. 2011).

A specificity of plant cells is that geometry of the cell wall impose sharp angles at the cell edges. As a consequence, because microtubules are stiff and bound to the membrane, polymerizing microtubules end up facing the cell edge with an angle that does not allow for bending, which leads to depolymerization (Dixit and Cyr 2004). CLASPs are enriched at the cell edges and *clasp* mutants in plants do not present microtubules with sharp turns (Ambrose, Allard, et al. 2011). CLASPs also contribute to stabilizing microtubules that have been severed, spontaneously (Aher et al. 2020), or by other proteins (Lindeboom, Nakamura, Saltini, et al. 2018). Overall, CLASPs are precisely localized in the cells and stabilize microtubules in contexts that are not mechanically favorable, revealing that microtubule dynamics is not homogeneously distributed within cells.

1.2.3 Katanin, a destabilizer of microtubules

KATANIN is a microtubule severing protein that was initially named after the japanese expression for sword, katana (McNally and Vale 1993). In vitro, KATANIN has been shown to severe microtubules (Stoppin-Mellet et al. 2002; Hartman et al. 1998). Recent studies suggest that, in vitro, KATANIN may actually present an additional activity of exchanging GDP-tubulin against GTP-tubulin, which stabilizes microtubules after severing (Vemu et al. 2020).

In animals, in vivo studies have revealed the role of KATANIN in different processes. KATANIN plays a role in mitosis and meiosis that we will not describe here (Buster et al. 2002; Lombino et al. 2019; Dunleavy et al. 2017; Pleuger et al. 2016), and also contributes to cilia dynamics (Lynn et al. 2021). Cilia are membrane protrusions created by a skeleton of microtubules that are required for various processes, including signaling processes such as chemosensation and osmosensing (Waters and Beales 2011). The different variants of KATANIN in vertebrates contribute to rapid deciliation (Mirvis et al. 2019) and stabilization of the cilia by preventing bifurcation and bending (Banks et al. 2018). During corticogenesis, KATANIN severes microtubules, which generates smaller fragments that can be transported to the outgrowths of the axon (Ahmad et al. 1999). This transport then allows for a correct stabilization of the outgrowths and correct migration and growth of the neuron (Toyo-Oka et al. 2005).

In plants, KATANIN severs microtubules specifically at the crossovers (Figure 1.5, Lindeboom, Nakamura, Hibbel, et al. 2013). Crossovers correspond to an intersection between two microtubules present. In plants, because cortical microtubules are close to the membrane, crossovers are relatively frequent when there is variability in the orientations of

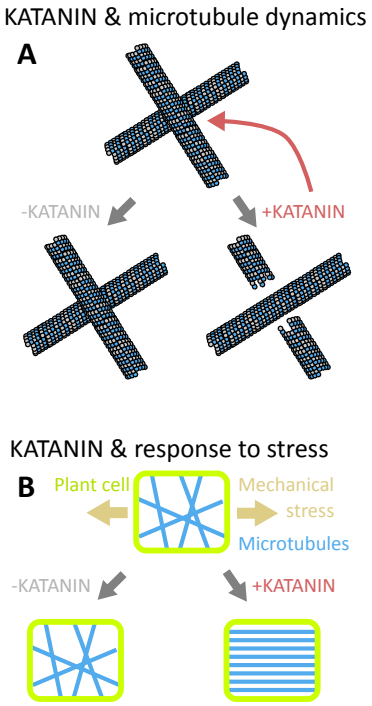

Figure 1.5: Katanin binding and influence on microtubules A) KATANIN severs microtubules at crossover sites (redrawn from C. Wang et al. 2017 with style copied from Igaev and Grubmüller 2020) B) In plant cells, a mechanical stimulus such as an ablation leads to a reorganisation of the microtubules, so that they become aligned with the stress direction. In the absence of KATANIN, there is no response of microtubules to ablations (inspired from Uyttewaal et al. 2012).

microtubules. This specific severing rapidly increases the number of microtubules that are orthogonal to the existing microtubules and induces a change in the microtubules orientation (Lindeboom, Nakamura, Hibbel, et al. 2013). KATANIN is also recruited by the Mitotic spindle disanchored 1 - WD40-repeat protein 8 (MSD1-WDR8) complex at the branching nucleation sites and separates the newly polymerized microtubule from the main one (Yagi et al. 2021), increasing the total number of microtubules. Regulation of KATANIN activity appears to depend on environmental cues such as light (Lindeboom, Nakamura, Hibbel, et al. 2013) and surrounding mechanical stress (Uyttewaal et al. 2012; Eng et al. 2021). In a developmental context, this leads to KATANIN participating to patterning of the cell wall in the pollen grain (Riglet et al. 2020), and supporting robustness of morphogenesis in the sepal and the shoot apical meristem of Arabidopsis (Uyttewaal et al. 2012; Hervieux, Tsugawa, et al. 2017).

Microtubules can also be modified post-translationnally, with for instance acetylation of the lysin 40 of α-tubulin by the acetyltransferase 1, that has been shown to soften microtubule thus preventing crack formations (Janke and Montagnac 2017). However, the role of post translationnal modification in plant is not evident, as modification of the lysin 40 by a non acetylable amino acid had no consequence on the plant phenotype (Xiong et al. 2013).

1.3 Impact of the physical environment on microtubule dynamics

1.3.1 In vitro mechanics of the microtubules

Characterization of polymers : the persistence length

Persistence length is used to characterize the mechanical properties of a polymer that does not remain straight due to thermal fluctuations. This persistence length corresponds to the maximal length for which the first and the last monomer orientation are significantly correlated. Practically, the larger the persistence length, the higher the scale at which a polymer will be straight. For a rigid and uniform rod (as an approximation for biological polymers), this length can be expressed as (Gittes et al. 1993; Baumann et al. 1997) :

$$L = \frac{E\pi a^3 h}{4k_B T}$$

where L is the persistence length, E corresponds to the Young's modulus of the material, a corresponds to the radius of the rod and h it's thickness, k_b is Boltzmann's constant and T corresponds to the temperature. The exponent of the radius is partly the reason why DNA (2nm wide, full) has a shorter persistence length than microtubules

(25nm wide, 5nm thick). Based on the radius and thickness alone and assuming other parameters similar, we would expect the persistence length microtubule/DNA ratio to be of about 5 000 fold, similar to the actual value observed here.

The first method used to quantify microtubule stiffness was based on thermal fluctuation (Gittes et al. 1993). This method consisted in visualizing labeled microtubules oscillate under brownian motion, movement coming from molecular agitation present in fluids, and to fit this oscillation with mechanical models. Other methods used optical tweezers (Kurachi et al. 1995), gliding on molecular motors (D. S. Martin 2013), curvature under perpendicular electric forces (Van den Heuvel et al. 2008), etc. All these methods lead to a coherent measurement for the persistence length of microtubules in the range of the millimeters. Some studies suggest that microtubule persistence length increases with the size of the microtubule, with short microtubules having a persistence length in the range of tens or hundreds of micrometers (Van den Heuvel et al. 2008; Pampaloni et al. 2006; Sharma and Vershinin 2020).

These stiff microtubules can then generate forces by three main means : polymerization, depolymerization and gliding on molecular motors. Polymerization forces were estimated either by measuring the buckling of a microtubule growing against a wall (Dogterom and Yurke 1997) or by using an optically trapped microtubule pushing against a barrier (Laan et al. 2008). Both methods lead to a coherent pushing force of about 2.7pN. Conceptually, it is important to note that the force, generated by the synthesis of a polymer against a surface, relates to the insertion of a monomer during thermal fluctuation that creates gaps between the polymer and the surface. If a monomer was inserted during this short period of time, then the relative position of the polymer and the surface would effectively be increased by one monomer. Thermal fluctuations can then again create a new gap, which may further extend the distance (Laan et al. 2008).

Work generated by a polymerizing microtubule for a displacement of 10nm : $6.10^{-3} k_b T$
Work generated by a depolymerizing microtubule for a displacement of 10nm : $2.10^{-1} k_b T$ (Molodtsov et al. 2005)

Depolymerization of microtubules has been mostly studied by linking the plus end of a microtubule with an optically trapped bead, which lead to forces ranging from 1 to 30pN (Grishchuk et al. 2008; Volkov et al. 2013). This force originates from the release of the stress accumulated in the microtubule body from non relaxed tubulins, and is, to my knowledge, only present in the separation of chromosomes during mitosis (Coue et al. 1991).

Microtubule, can generate pulling and pushing forces on their own, however, they can also be acted upon by other cellular elements. Kinesins are molecular motors that generate a displacement between their head and the microtubules. If the microtubule is more tightly fixed than the head, the head will move, otherwise the microtubule will move. Each step moves one tubulin dimer towards the plus end and generates a force of 3-5pN (Valentine et al. 2006; Bodrug et al. 2020). This force generation

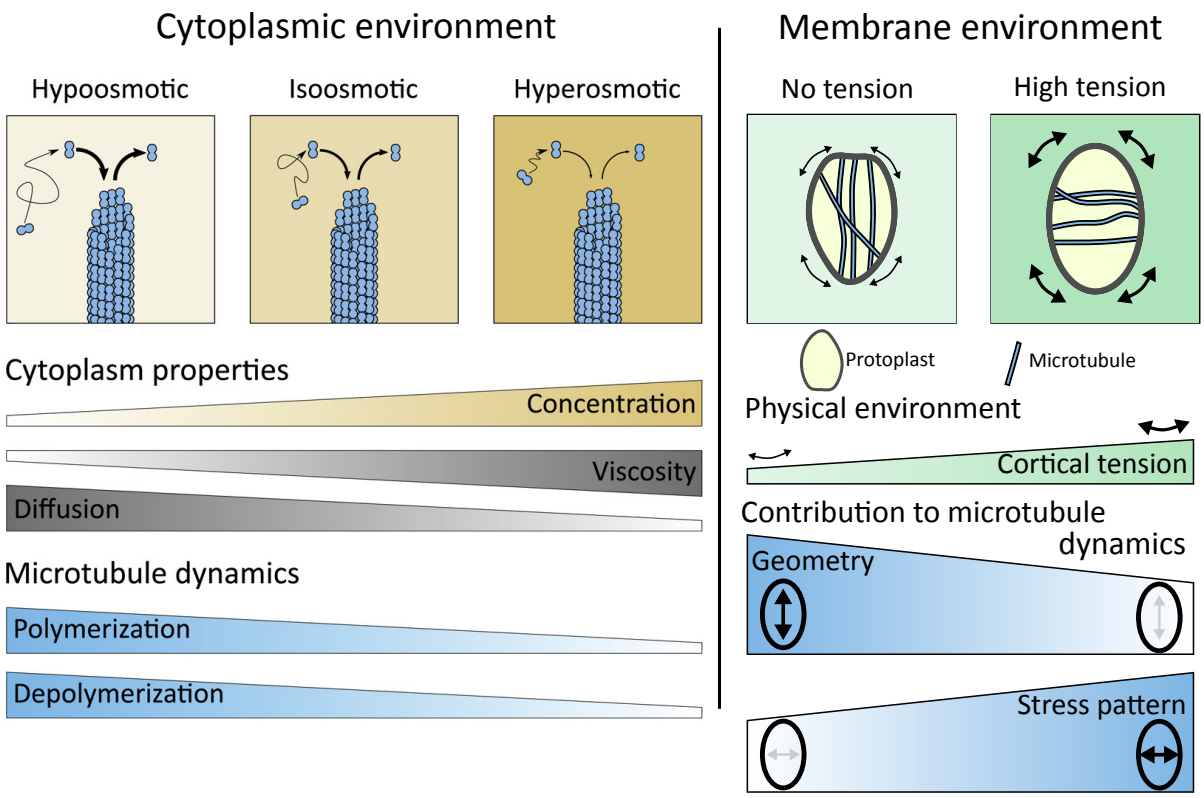

Figure 1.6: Microtubule dynamics is dependent on their physico-chemical environment. A) Cytoplasmic crowding affects microtubule polymerization and depolymerization rates. In a hypoosmotic medium, diffusion favors the association and dissociation of tubulin. In a hyperomsotic medium, viscosity slows tubulin, which reduces its association and dissociation dynamics (extracted from Molines, Lemière, et al. 2022). B) Geometry determines microtubule orientation at low surface tension, and stress patterns are determinant for microtubule orientation at high cortical tension. In a protoplast, if there is no membrane tension, then the preferiential orientation of microtubules correspond to the long axis of the protoplast. In a turgid and confined cell, a stress circumferential stress pattern arise orthogonal to the long axis of the cell, which orients microtubules (inspired from Leia Colin et al. 2020).

however mostly plays a role in vesicle trafficking and does not directly affect morphogenesis.

1.3.2 Direct regulation of microtubule dynamics by the environment

Microtubule dynamics greatly depend on the local concentration of tubulin. Recent studies have shown, both in vitro and in vivo that indeed, viscosity of the cytoplasm greatly impacts the diffusion rates of tubulin, and therefore the polymerization rates of microtubules (Molines, Lemière, et al. 2022). Additionally, there is now evidence for intracellular heterogeneity in viscosity (Odermatt et al. 2021; Garner et al. 2022), but whether this physiologically plays a role in varying microtubules dynamics within a cell has not been studied yet.

Surrounding geometry could also influence microtubule orientation, with in vitro microtubule responding to the geometry of microwells (Lagomarsino et al. 2007). Purified tubulins were polymerized inside wells with an elipsoid shape. Spontaneously, microtubules were found in

this study to align with the long axis of the elips. Modeling approaches confirmed that geometry could influence the main orientation in the absence of other guiding cues (Mirabet et al. 2018), which was studied in more realistic conditions using protoplasts, i.e. plant cells with digested cell walls (Durand-Smet et al. 2020). These cells were confined in micro-wells and indeed, microtubules followed the cell long axis in these non pressurized protoplasts.

Finally, recent studies have shown that microtubules may spontaneously align with mechanical stress in the cell wall (Hamant, Inoue, et al. 2019). The first evidence come from in vitro studies, where microtubules were bound to stretchable polydimethylsiloxane (PDMS) substrate via motor proteins and antibodies (Inoue et al. 2016). This PDMS was then stretched or compressed and microtubules' response was observed. Upon stretching, microtubules appeared to fragment (Kabir et al. 2015), which counterintuitively lead to microtubules aligning with tension over longer time scales (Inoue et al. 2016). A possible explanation is that fragmentation induced by the tension generated numerous seeds that then polymerized into full microtubules. Whether it is the mechanical stress or the geometry that influences microtubule orientation in cells was recently unraveled using confined and pressurized protoplasts (Leia Colin et al. 2020). In this study, plasmolysed protoplasts presented microtubules aligned with the long axis of the cell while pressurized protoplasts, with a tensile stress pattern orthogonal to the long axis, presented microtubules aligned perpendicularly to the cell axis. Surprisingly, microtubules' response actually appeared to depend on variations in stress levels as protoplasts that were kept in a pressurized state recovered the alignment with the long axis over long periods of time. Several questions still need to be elucidated : at what time scale is this stress perceived in vitro? How is the stress present at the membrane and/or cell wall perceived by the microtubules? Is this perception direct or are there other elements sensitive to the stress in the membrane and/or cell wall?

1.4 Contribution of microtubules to morphogenesis

Microtubules contribute to two different aspects of morphogenesis: a direct modification of the cell shape by mechanical forces, and an indirect contribution via the guidance of delivery of materials to the periphery or to the outside of the cell. Plant cells are much stiffer than animal cells, and likely too stiff for their shapes to be affected by microtubules, which explains why the first aspect is only present in animal cells. Here we will give a few exemples of the direct effect of direct control of morphogenesis by microtubules, and we will elaborate the role of indirect control, with a focus on plants, in the next section.

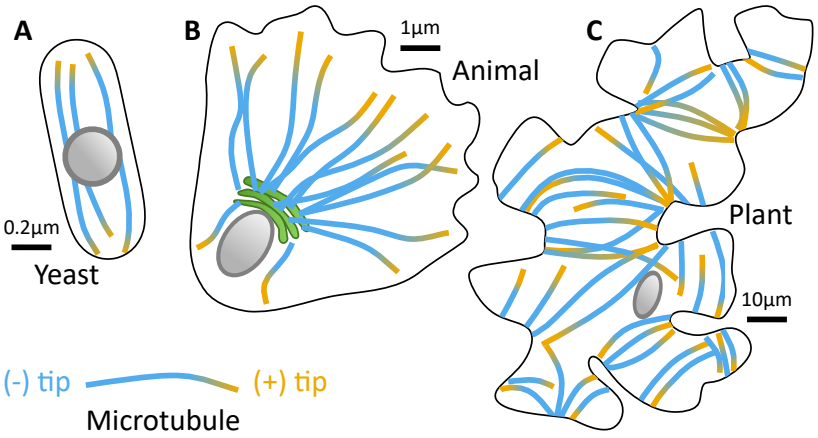

Figure 1.7: Organization of the microtubule network across kingdoms. A) Yeast microtubules are polarized around the spindle pole body. The nucleus is represented as a grey circle. B) Animal microtubules are organized around the nucleus or the Golgi apparatus with (+) tips growing towards the membrane. C) Plant microtubules are cortical (close to the membrane). In pavement cells, microtubules tend to go from neck to neck.

1.4.1 Cellular organization of microtubules across kingdoms

Organization of the microtubule network during interphase varies across kingdoms. During mitosis, particular microtubule structures arise that present similarities between kingdoms, but will not be discussed here. Instead we will focus on the function of microtubules in morphogenesis.

In animals, microtubule-organizing centers (MTOCs) are key to the network, and are divided into two categories : centrosomal MTOC and non-centrosomal MTOC. The centrosome is a non-membranous organelle present next to the nucleus, from which nucleate numerous microtubules (Becker et al. 2020). Centrosome MTOC are mostly related to cell division (Tillery et al. 2018). Microtubules may also nucleate from the side of existing microtubules via the recruitment of γ tubulin (Uehara et al. 2009; Petry et al. 2013). Non-centrosomal MTOCs are present in various types of cells around the Golgi apparatus and involve the recruitment of centrosomal proteins (Figure 1.7 B, Efimov et al. 2007; Chabin-Brion et al. 2001). Their main functions are related to vesicular trafficking, guidance for apical-basal transport in epithelial cells and replacement of MTOC in mature neurons (Nishita et al. 2017).

Number of microtubule in a yeast cell: about 10 (Carminati and Stearns 1997)
Number of microtubule in a dendritic cell: hundreds (Katrukha et al. 2021)
Number of microtubule in a pavement cell: hundreds (Sampathkumar et al. 2014)

In yeast, a few tens of microtubules form antiparallel bundles with the + ends directed towards the cell tips (Figure 1.7 A). Because microtubules are stiff and because they are not bound to the membrane, they reorient during growth when they encounter membranes which lead them to spontaneously align with the cell axis (Carazo-Salas and Nurse 2006; Daga et al. 2006). This network is organized from a structure called the Spindle Pole Body, the functional equivalent of the animal centrosome and helps define the cell axis (S. G. Martin 2009).

In plants, a particular population of microtubules form an array under the membrane, called cortical microtubules (Figure 1.7 C). The cellulose synthase-microtubule uncouplings 1 (CMU1) and CMU2 proteins form a link that binds both the microtubules and the membrane (Z. Liu et al. 2016). Because microtubules are bound to the membrane, they explore mostly a 2D space, which greatly increases the probability that

they encounter another microtubule. Additionally, cortical microtubules are subject to high forces generated by the polymerisation of cellulose synthases, and this anchoring prevents the cellulose synthases from dragging the microtubules along them (Z. Liu et al. 2016).

1.4.2 Microtubule direct role in morphogenesis

As described previously, in animals microtubules play a role in cilia formation and neuron elongation. Blood cells adopt an ellipsoidal shape based on a balance between cortical tension and a ring of microtubules going around the cell, called the marginal band (Dmitrieff et al. 2017). Microtubules in the marginal bands present a curvature which is of the order of the inverse of the cell radius ($C = 1/R$), much smaller than the persistence length of microtubules. This leads to microtubules exerting a force resisting bending because of their rigidity, force that is counterbalanced by cortical tension. Analysis of blood cells from 25 species confirmed this tension compression model with a correlation between the number of microtubules in the marginal band and the size of the blood cell. During Drosophila wing epithelial development, cells also present dual mechanics, with the acto-myosin cortex putting the cell under tension, and microtubule resisting this force (Singh et al. 2018). Indeed, microtubules in these cells were curved under lengths far inferior to their persistence length, which suggest that forces were acting on them. Additionally, local ablation of microtubules lead to a rapid shrinkage of the cell, further supporting their role as a pillar. Interestingly, microtubules were linked from one cell to its neighbors via adherens junctions which lead to the whole tissue being supported by microtubules. Perturbation of the microtubule network indeed leads to defects in cell shape as well as overall tissue elongation. As a summary, microtubules in animal cells mainly play a role of mechanical support opposing tension created elsewhere, which relates to the concept of tensegrity N. Wang et al. 1993; Ingber 2006.

1.4.3 Microtubule indirect role in morphogenesis

Microtubules position is controlled by multiple factors as seen previously, this particular placement makes microtubules good tracks for all the trafficking required for morphogenesis. In the axon, additional marks on the microtubules indicate whether the microtubule goes toward the body or opposite (Tas et al. 2017). Combined with kinesins moving only towards one side of the microtubule, this creates a polar transport along the axon axis.

Structures ranging from migrating cells from animals to the tip growth of the pollen grain rely on polarized transport of material (Sieberer et al. 2005; Stehbens and Wittmann 2012). This material ranges from

membrane, membrane proteins, extracellular components, which will be further described in the next section.

Cell wall and cell shape, micrometers and minutes

2

2.1 Composition of the cell wall

The plant cell wall is an extracellular matrix present outside plant cells. Cell walls observed in nature can be divided into two categories: primary cell walls are extensible and present during cell growth and morphogenesis, and secondary cell walls that are non extensible are formed after the cell reaches its final size. Here we will focus on primary cell walls. Cell walls are composed of four main components (with their respective proportion in the cell wall (O'Neill and York 2018)): cellulose (20-30%), hemi-cellulose (20-35%), pectins (30-45%) and proteins (1-10%). We will describe the nature and synthesis of each of these components. Then, we will describe a model for plant cell growth based on the composition of the cell wall, and relate the contribution of each component to the dynamics of the cell wall.

2.1.1 Cellulose, mechanical anisotropy of the wall

Cellulose is a linear polymer of β-D glucose linked by 1,4-glycosidic bonds (Figure 2.1 A). Cellulose microfibrils are synthesized by a transmembrane protein complex called cellulose synthase complex (CSC). In land plants, the core of CSCs is composed of three cellulose synthases (CeSa) proteins forming a globular catalytic subunit. These units then assemble to form a hexameric rosette-like structure of about 20-30nm in diameter (Kimura et al. 1999), leading to the simultaneous synthesis of 18 cellulose strands per complex (Figure 2.1 B, T. Zhang, Zheng, et al. 2016; Song et al. 2020). The number of strands varies between species (Huang et al. 2020), but the 18 strands model prevails in Arabidopsis thaliana. In Arabidopsis, there are 10 homologous genes encoding CeSa (Doblin et al. 2002). A subunit of the rosette complex is usually composed of 3 different isoforms, with CESA1, 3 and 6 involved in primary cell wall synthesis (Taylor et al. 2003; Desprez et al. 2007).

Cellulose strands are linked with one another only via van der Waal's interaction and hydrogen bonds. Hydrogen bonds are weak bonds with dissociation energy values depending on the atoms involved, ranging from 1 k_bT in C-H···C bonds to 15 k_bT in O-H···O bonds. Hydrogen bonds of cellulose-cellulose in the cell wall are highly exposed to competition from water molecules that form bonds of similar strength. These bonds are weak and non-specific so they break and form rapidly (on a nanosecond timescale). What gives stability to cellulose - cellulose interactions then ? If we take a chain of cellulose tied with N hydrogen bonds, thermal fluctuation exposes this chain to $N^{1/2}k_bT$ energy. If N is large enough, the

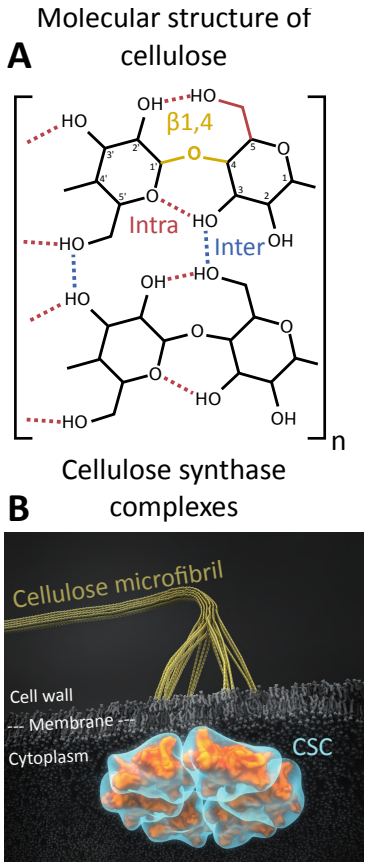

Figure 2.1: Molecular structure & synthesis of cellulose. A) Two strands of cellulose are represented with the β-1,4 glycosidic link in yellow, intramolecular hydrogen bonds in red and intermolecular hydrogen bonds in blue (redrawn from Wohlert et al. 2022) . B) Artistic rendition of cellulose synthase complexes in the membrane (extracted from Vandavasi et al. 2016).

energy required to break most of the bonds at the same time scales with NCk_bT, where Ck_bT is the average energy required to break a bond in the structure. When we compare the random force acting on the chemical bonds scaling on $N^{1/2}$ to the stability of the structure scaling on N, we see that for large N, stability is favored. In other words, this means that in the case of long polymers, there are too many bonds that have to break simultaneously for the chains to be separated by thermal fluctuations alone (Wohlert et al. 2022). Similar reasoning applies for van der Waal's interactions but with an energy of about 6 k_bT.

Cellulose monomer length: 1nm
Cellulose strand diameter: 1nm
Cellulose microfibril diameter (36 strands): 4nm (Ding et al. 2014)
Polymerisation speed: 300nm min^{-1} = 300 units min^{-1} (Paredez et al. 2006)

These lateral bonds favor interaction between cellulose strands to form a crystal arranged cellulose microfibril outside the rosette. Little is known about whether there are mediators for the correct assembly of the strands into a microfibril, but KORRIGAN is assumed to play a role (Vain et al. 2014). Some specific mutants *cesa1*^{aegeus} and *cesa3*$^{ixr1\text{-}2}$ present reduced cellulose crystallinity (D. M. Harris et al. 2012). Two hypotheses could explain this: mutations could affect amino acids involved in the interaction with other proteins that help for the correct assembly of strands, or the mutation could affect part of the CESA that guides the cellulose strand into correct assembly. Strangely, in these mutants cellulose synthesis speed was increased, which suggests that crystallization may be achieved at the expense of polymerization rates. Another more recently discovered crystallinity mutant also affected CESA1 and is known as *any1* (Fujita et al. 2013). While crystallinity was also reduced in the mutant, polymerization was slower compared to WT. The *any1* mutant presented was not affected in cellulose content, Cellulose crystallinity was quantified to be reduced by about 10% in *any1* and *cesa1*^{aegeus}, however both mutants displayed a drastic phenotype. Little is known about the contribution of cellulose crystallinity levels to morphogenesis, and it has been suggested that crystallinity could play a role in the interaction with other components of the cell wall or prevent sliding between fibrils during wall expansion (Martínez-Sanz et al. 2015). These cellulose microfibrils can then bind to one another via hydrogen bonds. The deposition of microfibrils with respect to one another is far less controlled than the deposition of cellulose strands inside a microfibril. Bundles of microfibrils are thought to present only partial crystallinity.

Cellulose lateral bonds: 1-15k_bT
Cellulose longitudinal bonds: 140k_bT
Cellulose strand persistence length: 60nm (Usov et al. 2015)
Cellulose microfibril persistence length: 2.5 µm (Usov et al. 2015)
Cellulose tensile strength: 1-75 GPa (Jakob et al. 2022)

The strength of lateral bonds in cellulose allows for a cohesion between strands but is however much weaker than the covalent bonds established in the body of a cellulose strand, with a strength of about 140 k_bT for C-C and C-O (Huheey et al. 1993). This difference of mechanical properties longitudinally or laterally gives specific properties to the cellulose microfibrils that relate to mechanical anisotropy. The control of mechanical anisotropy in the cell wall is therefore achieved in part via the control of the deposition of cellulose. Control of cellulose deposition presents two modalities: the delivery of CSCs vesicles to the plasma membrane, and the guidance of CSCs in the plasma membrane. Guidance of the CSCs in the plasma membrane will be discussed in another section.

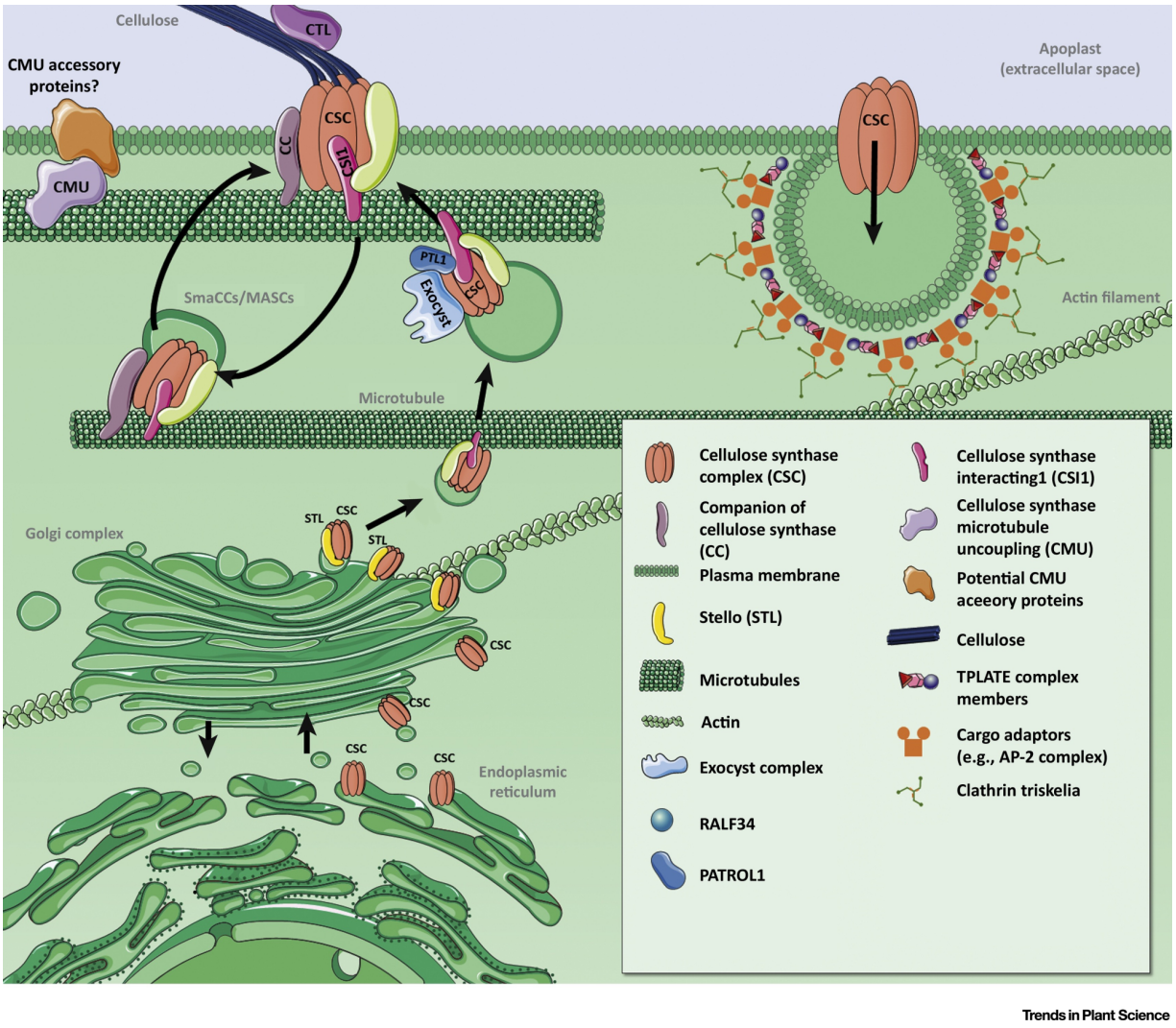

Figure 2.2: Overview of proteins involved in cellulose deposition and their dynamics. Cellulose synthase complexes are synthesized at the endoplasmic reticulum, transit through the Golgi and are delivered to the membrane under the form of vesicles guided by microtubules via CSI1, PTL and the Exocyst complex. After insertion in the membrane, CSC begin cellulose synthesis, and are guided along microtubules via CSI1 and potentially other actors. Finally, CSC are recycled via clathrin mediated endocytosis (extracted from Lampugnani et al. 2019).

CSCs have been observed as rosettes in the Golgi apparatus, suggesting that they may be assembled here (Haigler and Brown 1986). CSCs then enter the trans-Golgi network, and are selectively delivered to the plasma membrane (Figure 2.2, Gutierrez et al. 2009; Crowell et al. 2009). The actin cytoskeleton and microtubules both contribute to transport and selective exocytosis of CSCs (Gutierrez et al. 2009; W. Zhang and Staiger 2022). CELLULOSE SYNTHASE INTERACTIVE 1 (CSI1) marks the docking site on microtubules for delivery (X. Zhu et al. 2018). PROTON ATPASE TRANSLOCATION CONTROL 1 (PATROL1), exocyst and myosin XI then associate transiently with the CSC and CSI1 to mediate exocytosis (W. Zhang and Staiger 2022; X. Zhu et al. 2018). Together, this makes CSC delivery a very regulated process.

CSC complexes can also be endocytosed which then stops cellulose deposition. Endocytosis occurs via clathrin mediated endocytosis (CME) and

involves the proteins CLATHRIN-MEDIATED ENDOCYTOSIS ADAPTATOR PROTEIN 2 (AP2) and TWD40 (Bashline, S. Li, Anderson, et al. 2013; Bashline, S. Li, X. Zhu, et al. 2015), with both mutants displaying drastic reduction in plant size. Endocytosis allows for the recycling of non functional CSC, and is also induced by environmental stresses such as salt stress. During salt stress, CSCs are endocytosed together with Companion of Cellulose synthase (CC), which contributes to the reinsertion of the CSCs after recovery (Endler et al. 2015).

2.1.2 Pectins, modular gel

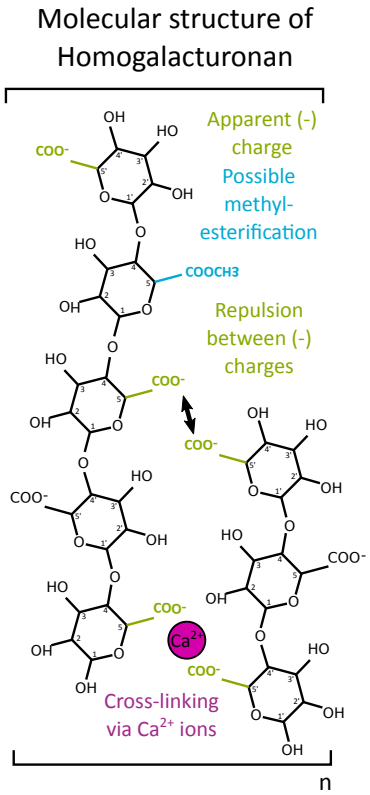

Figure 2.3: Molecular structure of a homogalacturonan chain. Note that the in plane and out of plane bonds are flattened in the figure. Negative charges of the carboxyl groups are represented in green. This group can be methylesterified making it neutral, represented in blue. Ca^{2+} can bind to the positive charges and cross-link the pectin chains, represented in purple.

Pectins are ramified polymers divided into three categories: homogalacturonan (HG), which represent about 65% of pectins in dicots and is composed of α-1,4 linked galacturonic acid backbone (Figure 2.3); rhamnogalacturonan I (RG-I), which represent between 20 and 35% of pectins and is composed of galacturonic acid and rhamnose linked in α-1,2 and α-1,4; and rhamnogalacturonan II (RG-II) with the same backbone as HG. Contrary to cellulose, these polymers can be ramified. Galacturonan possesses a free carboxyl group that presents a pKa of 4, meaning that they usually have a negative charge if the pH is above 4 (cell walls are slightly acidic with a pH between 4 and 6 (Martinière, Gibrat, et al. 2018; Moreau et al. 2022)). This charge creates repulsion between the pectins and favors cell wall hydration (X. Wang et al. 2020). This carboxyl group can however be methyl esterified, which then makes the molecule neutral.

Pectins are synthesized in the Golgi and are delivered to the cell wall inside vesicles. The precise guidance of such vesicles remains elusive, but available data hints toward a dual guidance by the actin (Toyooka et al. 2009; S.-J. Kim and Brandizzi 2014) and microtubule networks (C. Zhu et al. 2015; Domozych et al. 2014). Exocytosis is also controlled and has been shown in the root and the pollen tube to occur at precise sites (McKenna et al. 2009; Anderson et al. 2012). During synthesis in the Golgi and insertion in the cell wall, the carboxyl group is methyl esterified, but can be modified post insertion.

The modifications pectins can undergo in the cell wall are regulated by multiple families of proteins, among which: Pectin Methyl Esterases (PME) and PME Inhibitors (PMEI), which has their name suggest, inhibits PME. In the genome of Arabidopsis, there are 66 PME and 71 PMEI, which suggests that pectin dynamics is precisely regulated (M. Wang et al. 2013). PME are proteins that remove methyl-ester groups, leaving negative charges in the carboxyl groups. The current view for pectin interactions is the following: methyl-esterified pectins interact with each other via weak interactions, and de-esterified pectins, presenting negative charges that should repel themselves, interact with Ca^{2+} ions present in the cell wall to form egg-box motifs (see Figure) (Cao et al. 2020). Formation of these structures have been reported to require long chains

of de-esterified HG, which suggest that the processivity of the PME matters for the emerging mechanics of the cell wall (Zdunek et al. 2021). Interactions between PME and PMEI may be specific between a pair of proteins (Wormit and Usadel 2018), and may also depend on the pH (Sénéchal et al. 2015). Although the selective secretion of PME and PMEI in the cell wall appears important, literature on the subject is quite sparse. One study that analyzed the subcellular localization of a few PME could not highlight hotpots in tomato leaf (Tang et al. 2020).

Pectin fibril persistence length: 5-12nm depending on ramification (Zdunek et al. 2021)
Pectin tensile strength: 30 MPa (Bátori et al. 2017)

Quantifying the mechanical properties associated with the different types of pectins has proven difficult, in part because the properties of pectins are vastly different between in vitro and in vivo. In vitro, pectins have been extensively studied for their role in food chemistry (Gawkowska et al. 2018) and can present sol-gel transitions, from solute (liquide) to gel (solid) (Figure 2.4, Pieczywek et al. 2021). Such transitions differentiate particles in solution from a network of molecules, which present vastly different mechanical properties, notably in terms of viscosity (X. Zhu et al. 2018). The importance of pectin sol-gel transition during plant growth is controversial as cell wall concentrations may only allow the existence of gels.

In vivo analyses are quite difficult because of the complex nature of the cell wall, and the large number of existing PME and PMEI. A few studies exhibited correlation between esterification status and mechanical properties. De-esterified pectins have been reported to be associated with softer growing regions in the pollen tube (Chebli et al. 2012). In the shoot apical meristem and hypocotyl, de-esterified pectins have also been linked with softer regions (Peaucelle, Braybrook, et al. 2011; Peaucelle, Wightman, et al. 2015). However, studies in the hypocotyl also found the opposite phenotype with methyl-esterified pectins that presented an increased indentation stiffness (Bou Daher et al. 2018). These two last studies used PME and PMEI overexpressors. A key benefit is the relatively less perturbed cell wall compared to exogenous chemical treatment of pectins, but the cell wall response pathways may have been triggered nonetheless. Indeed, information from the cell wall status are relayed to the cell which may trigger responses (Rui and Dinneny 2020), with in particular small oligogalacturonides generated by the lysis of pectins that can act as signaling molecules (Wolf et al. 2012). The studies also quantified mechanical properties by indentation, which is not a direct indication of cell wall extensibility. It is assumed that the deformability of the wall perpendicular to the plane act as a proxy for longitudinal deflection but this is not necessarily true, as will be described further in the mechanical imaging section. Another recent study suggested that PMEs increase or decrease cell wall plasticity in the absence or presence of Ca^{2+}, respectively (X. Wang et al. 2020). Together, this suggests that looking exclusively at the methyl-esterification status of the pectins, may not be sufficient to predict plant cell growth.

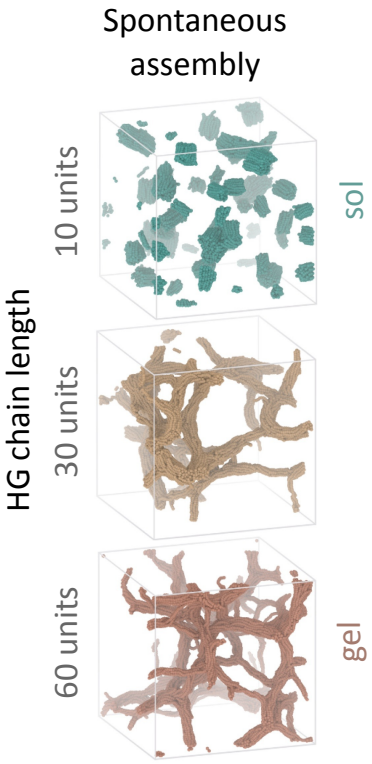

Figure 2.4: Computational modeling of homogalacturonan assembly depending on the chain length. Gel corresponds to a solid state, sol corresponds to a solute state. Fraction of charged galacturonic acids: 50%. Concentration of galacturonic acids: 0.5M (extracted from Pieczywek et al. 2021).

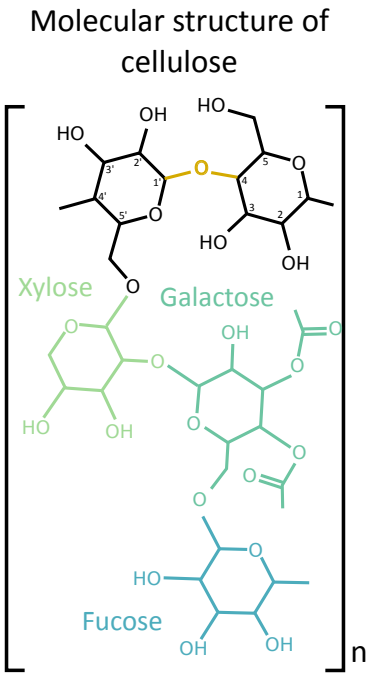

Figure 2.5: Molecular structure of xyloglucan. Main chain of a xyloglucan (black), ramified with three sugars. Xyloglucan can be ramified with one to three sugars, always found in the order xylose, galactose, fucose, or can also be naked. Note that the in plane and out of plane bonds are flattened in the figure.

Xyloglucan fibril persistence length: 6-8nm depending on ramification (Picout et al. 2003)
Xyloglucan tensile strength: 20 MPa (da Silva Braga and Poletto 2020)

2.1.3 Hemicelluloses, universal linker

Hemicelluloses are the third major component of the cell wall. The most common hemicellulose in eudicots, xyloglucan, consists of a backbone of D-glucose linked in β-1,4 (Figure 2.5, Park and Daniel J. Cosgrove 2015), the same as cellulose. This backbone can be ramified with xylose, galactose and fucose. This architecture based on sugar gives similar hydrogen bonds than those found in cellulose-cellulose interactions, and makes hemicellulose a good cellulose binder. Contrarily to cellulose, xyloglucan synthesis occurs in the Golgi, and is then secreted via vesicles (Pauly and Keegstra 2016). Although different levels of xyloglucan have been detected between cells (Xue et al. 2013; J. S. Kim and Daniel 2018), there is no evidence of subcellular heterogeneity, which suggests that hemicelluloses are uniformly synthesized.

In vitro, the study of the dynamics of hemicellulose binding to cellulose revealed the existence of two regimes: a diluted regime where initially coiled xyloglucan rearrange to form flat fibers, and a concentrated regime where the xyloglucan can not uncoil (Villares et al. 2015). In the cell wall, there are reports of foiled and uncoiled xyloglucan, which suggests that these transitions may also occur in native conditions (Zheng et al. 2018).

Hemicellulose can be modified after incorporation in the cell wall by a family of proteins called XYLOGLUCAN TRANS-β-GLUCANASES / HYDROLASES (XTH), with about 30 members in land plants (Yokoyama et al. 2010). These proteins are responsible for covalently linking hemicellulose with pectin (Stratilová et al. 2020), hemicellulose with hemicellulose and hemicellulose with cellulose (Herburger et al. 2020). While such linking could impact cell wall mechanics, little effect of XTH was found in vitro (Saladié et al. 2006) and in vivo (Kaewthai et al. 2013).

Despite their relative abundance in the cell wall, the role of xyloglucans in growth is still elusive as the double mutant *xxt1xxt2* completely lacking xyloglucan displayed only mild phenotype (Cavalier et al. 2008). However, it is important to note that the same mutant displayed increased cellulose microfibril alignment (Xiao, T. Zhang, et al. 2016), which is also backed by in vitro interaction between cellulose and hemicellulose (Stimpson et al. 2020). This greater alignment could originate from xyloglucan preventing cellulose microfibrils from binding to one another (acting as a spacer), but may also be related to the affected microtubule networks observed in *xxt1xxt2* (Xiao, T. Zhang, et al. 2016).

2.1.4 Guidance of cellulose synthases

CESAs were first found to move in linear trajectories and were later found to move along microtubules (Paredez et al. 2006). A few more years were required to find the protein that links them to microtubules. CELLULOSE-SYNTHASE INTERACTIVE 1 (CSI1) is a protein that was

discovered as coexpressed with CESAs (Persson et al. 2005) and that physically interacts with CESA in yeast two-hybrid (Gu et al. 2010). *csi1* mutants were first found to display affected CESA trajectories but no link was made with microtubules at this point. Two years later, several studies demonstrated that the displacement of CESA along microtubules was lost in the absence of CSI1 (Figure 2.6, S. Li et al. 2012; Bringmann et al. 2012; Lei, S. Li, and Gu 2012).

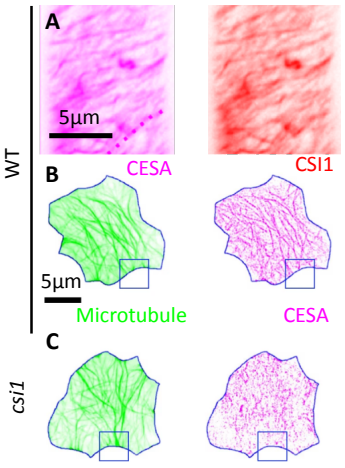

Figure 2.6: CSI1 links CESA and microtubules. A) Colocalization of the temporal integration of CESA and CSI1 tagged proteins in hypocotyl cells (adapted from S. Li et al. 2012) B, C) Signal of microtubules and CESA integrated over time in WT (B) and csi1 (C) pavement cell (adapted from Schneider et al. 2022).

With this, a model of CSI1 guiding CESA along microtubules emerged. A recent study analyzing the displacement of CESA particles upon induced microtubule depolymerisation, found that CESA particles can follow the tracks of previous cellulose microfibrils (Chan and Coen 2020). Modeling suggests that CESA particles are propelled by the energy liberated by synthesis (Diotallevi and Mulder 2007): insertion of a glucose monomer slightly moves the fibril up, but as there is cell wall material above, the fiber bends, this bending transforms the vertical force into a horizontal force between the CESA and the fiber. Because the fiber is anchored in the cell wall, and the CESA is only bound to a fluid membrane, the consequence of the monomer insertion is CESA horizontal displacement. The direction of the force is aligned with the orientation of the depositing cellulose fiber and the surrounding wall material, which explains why previously deposited fibers can guide cellulose deposition.

Recent advance in imaging techniques offered by super-resolution, revealed never seen before behaviors of CESA that displayed U turns (Duncombe et al. 2022). This suggests that we still do not fully understand the guidance of CESA. U-turns could be explained by the presence of previously deposited fibers, but other hypotheses could be possible, notably involving pectins. Pectin methyltransferase mutant quasimodo2 exhibited altered cellulose deposition (Du et al. 2020). Another line of evidence for pectin involvement in guidance comes from the work with the drug cobtorin that removes guidance by microtubules (Yoneda, Higaki, et al. 2007; Yoneda, Ito, et al. 2010). Although the molecular mechanism of action of the drug is not known, cellulose deposited after application was no longer linked with microtubules. Additionally, some pectin related mutants were insensitive to this drug, similarly to polygalacturonase-treated wild type plants. Hemicellulose mutants also display affected cellulose patterns (Xiao, T. Zhang, et al. 2016). Despite a relatively well established guidance by microtubules in normal conditions, there is still lacking knowledge on the guidance of CESA in plants.

2.2 Imaging components of the cell wall

Imaging the different components of the cell wall implies localizing a particular sugar embedded in other sugars and sometimes determining its orientation. Here we try to give an overview of the methods available for such visualization, with potential limitations associated.

Direct molecular visualization by atomic force microscopy consists in scanning the sample with a nanometer sized probe and reporting the height of contact (Figure 2.7 D). The first step of AFM probing consists in exposing the cell wall from the protoplast side, as plant organs are usually covered in a wax layer called cuticle that prevents the use of AFM from outside. This is done by either peeling the cell walls (usually done in onion scales), grinding and isolating the sample or gently removing cell layers mechanically (T. Zhang, Zheng, et al. 2016). Pectins have been observed by AFM in purified samples in vitro (Gawkowska et al. 2018; Posé et al. 2015). However, because of the multi components nature of the cell wall, and the difference in stiffness between cellulose and pectins, imaging of pectins in the cell wall by AFM is not achievable. Cellulose fibrils on the other hand, present the highest stiffness in the cell wall and are one of its most structured components. This allows AFM topography to directly visualize the fibrils (Davies and P. J. Harris 2003). While this imaging method is destructive, potential modifications of the sample are possible, with for example stretching of the sample to observe fibril rearrangement (T. Zhang, Vavylonis, et al. 2017).

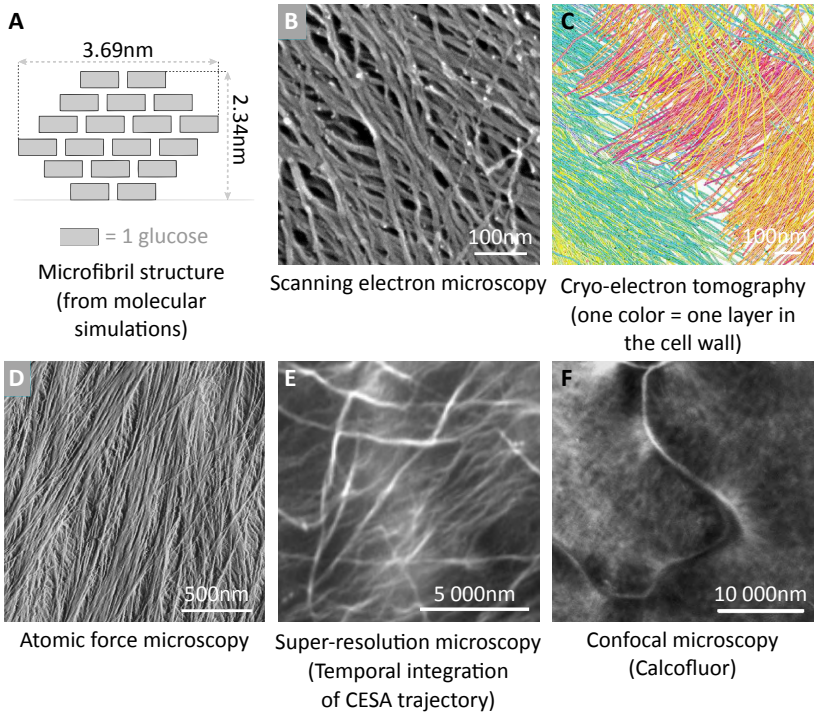

Figure 2.7: Methods for imaging cellulose microfibrils in the cell wall. A) Current model for the structure of a cellulose microfibril with 18 chains (adapted from Song et al. 2020). B) Scanning electron microscopy on the protoplast side (extracted from T. Zhang, Zheng, et al. 2016). C) Cryo-electron tomography from multiple milling sections. Each color corresponds to a different section (extracted from Nicolas et al. 2022). D) Atomic force microscopy from the protoplast side (extracted from T. Zhang, Zheng, et al. 2016). E) Temporal integration of CESA trajector imaged using super resolution microscopy (extracted from Duncombe et al. 2022). F) Confocal microscopy of pavement cells stained with calcofluor (extracted from A. Bidhendi et al. 2020).

Direct imaging is also possible by scanning electron microscopy (SEM, Figure 2.7 B). SEM relies on accelerating a beam of electrons onto the sample. Upon contact, the electrons will bounce and the way they were redirected will be measured by surrounding detectors. Diffraction limits predict that SEM resolution depends on the speed of the electrons, and with current technologies, a resolution of around 1nm has been observed. Sample preparation, similarly to AFM, requires the exposition of the cell wall, and usually also involves clearing from pectins using chemical treatments (Xiao, T. Zhang, et al. 2016). SEM and AFM, despite having the highest resolution of all methods as they allow for the direct visualization

of molecules, only allow for the imaging of the cell wall layer closest to the protoplast surface.

Transmission electron microscopy (TEM) also allows for direct imaging, but requires sectioning of the material. Such sectioning allows for the visualization of transverse section of the cell wall (Kutschera 1992; Xin et al. 2020). However, TEM does not allow for a clear understanding of the alignment or orientation in the wall, but rather allows for an assessment of homogeneity through the thickness of the wall.

Recently, a novel method combining electron tomography with beam milling allowed access to the 3D structure of the cell wall (Figure 2.7 C, Nicolas et al. 2022). This method consists in imaging a small patch of the cell wall using transmission electron microscopy, and progressively removing layers using a separate beam. While technically challenging, this method already gave new insights into the cell wall structure by revealing alternating layers of cellulose deposited at +45° and -45° along the cell axis in onion epidermal cells.

Hypocotyl cell dimensions: 200×50×50 µm (Janková Drdová et al. 2019)
Thickness of the cell wall: 0.2 µm (Derbyshire et al. 2007)
Volume of the cell: 500 000 μm^3
Volume of the cell wall: 5000 μm^3

Confocal imaging of cell wall components require dyes as they do not present fluorescent activities by themselves. Calcofluor and pontamine fast scarlet 4B, also known as direct red 23, are two reported dyes for cellulose and have been associated with various confocal microscopy techniques (Figure 2.7 F,A. Bidhendi et al. 2020; Thomas et al. 2017). Antibodies against all wall components are also available with specificity for sub groups of components (Pedersen et al. 2012; Verhertbruggen et al. 2009). For instance, antibodies targeting pectins with different degrees of methyl esterification have also been developed, which allows to qualitatively map the relative abundance of pectins at different places in the cell wall. Optical techniques are however much more limited than electron microscopy, with a diffraction limit of 250nm, around 10 times the size of a cellulose microfibril. Super resolution techniques could potentially push this technique past this limit (Paës et al. 2018). Dye confocal microscopy approaches are interesting as they allow for live imaging and integrate the information on the thickness of the wall. However, it is still sometimes difficult to interpret how binding of the dye allows for a visualization of the orientation of various materials.

Another technique that is used consists in visualizing the actors that control the deposition of the cell wall elements (Figure 2.7 E). For instance, the displacement of CESA at the membrane can be integrated over time to visualize a fibril being deposited (Duncombe et al. 2022). Here, because these elements are relatively big and spaced, single molecule imaging is achievable. Pectin deposition can also be monitored using click labeling of pectins, where small substitutes for sugars such as fucose can be incorporated into pectins and then click labeled with fluorescent tags (Anderson et al. 2012).

Cellulose stands out from other cell wall components because of its crystallinity. This crystallinity originates from the synthesis of cellulose

microfibrils that produces a highly ordered material. This ordering is of interest for imaging because it deviates polarized light enough for it to be detected. Different cell walls were analyzed with this technique and yielded microfibrils orientation similar to other methods described here (Abraham and Elbaum 2013). The deviation induced is proportional to the thickness of the material the light went through, which limits the application of this method to analysis of orthogonal sections of cell walls.

Finally, spectroscopy methods that rely on the analysis of chemical bonds specific to each component have also been deployed in plants. The two most common methods, FTIR and Raman spectroscopy, both exploit the interaction of chemical bonds with light (Gierlinger 2018). Light going through or reflected by the sample is detected and characterised by its spectrum, with absorption/emission bands that can be associated with the various components of the cell wall. Scanning samples on the plane thus allows for quantification of heterogeneity of the cell wall.

2.3 Determination of physico-chemical properties of the cell wall

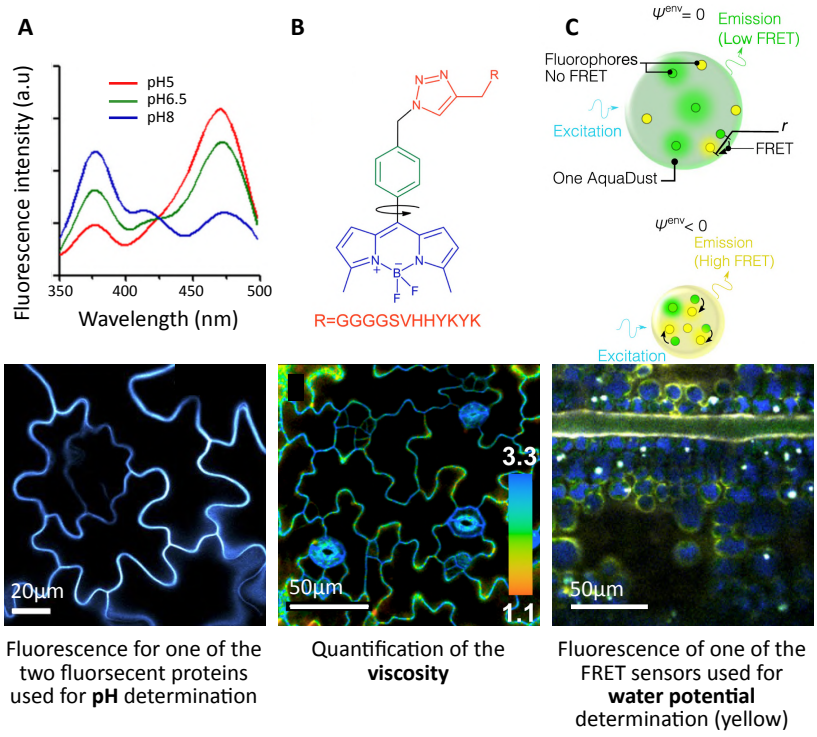

Figure 2.8: Fluorescent probes used for the determination of physicochemical properties of the cell wall. A) Fluorescence of the construct depending on the wavelength for three different values of pH (top). Fluorescence intensity for one of the two fluorescent proteins used for pH determination in the (bottom). Intensity ratio are used to compute the pH (extracted from Martinière, Gibrat, et al. 2018). B) Molecular structure of the viscosity probe, the lifetime of fluorescence is affected by the rotation of the arm, which itself depends on the mechanical environment (top). Fluorescent lifetime of a viscosity probe in the pavement cell (bottom, extracted from Michels et al. 2020). C) Functioning of the AquaDust probe, with two different water potential environments. Fluorescence of one of the FRET sensors used for water potential determination (extracted from Jain et al. 2021).

Knowledge about the physicochemical properties of the cell wall are required in order to build integrative models for cell wall deformation. These properties usually integrate different elements and are difficult to associate with one particular component (cellulose, pectins, etc). pH status is important for all molecular interactions, and determines the

charge of pectins (which is required for Ca^{2+} binding). Fluorescent pH probes are composed of two different fluorescent proteins, with different excitation and emission spectra (Miesenböck et al. 1998). These proteins fluorescent activity is also dependent on the pH and the ratio of fluorescence intensity decreases with the pH (Figure 2.8). These probes are also relatively insensitive to the variation of other cellular parameters such as the presence of ions (Martinière, Bassil, et al. 2013). Genetic constructs expressing the probes are introduced in plant cells and are secreted in the cell wall which allows a quantitative imaging of pH in live tissues (Martinière, Gibrat, et al. 2018).

Viscosity sensors have also been created from molecules with an arm that can freely rotate (Figure 2.8). Viscosity affects the ability of the arm to rotate and the rotation of this arm affects the fluorescence lifetime of the molecule (Michels et al. 2020). These probes are added exogenously and bind to the cell wall which allows for a quantitative imaging of viscosity in the cell wall (Michels et al. 2020).

Water status heterogeneity in the cell wall is still an open question. Probes to quantify its values have been developed by exogenously depositing a hydrogel reporter on top of the cell walls (Figure 2.8, Jain et al. 2021). This gel contains Förster Resonance Energy Transfer (FRET) sensors, which respond to light differently based on their physical distance. The gel expands based on the water potential of the cell wall, which affects the distance between the FRET sensors and thus their optical properties. Water status was also analyzed expressing a genetic construct of a FRET sensor based on molecular crowding, which yielded similar results, although not targeted to the cell wall (Cuevas-Velazquez et al. 2021).

Determination of the tension in the cell wall could also really prove useful. Tension FRET sensors have been created recently in animal cells (LaCroix et al. 2018). Such sensors are composed of two FRET interactants linked by a chain that acts as a spring. Each of these fluorophores is also linked with an element that is sensitive to the tension. In animal cells, actin has been chosen as a target because of its load bearing role. When stress-subjected filaments glide on another, the distance between the two fluorophores will increase, affecting the FRET intensity. Similar approach could be used in plants using cellulose as a target in the cell wall. This method requires a strong binding between the sensor and the element subject to tension. While cellulose binding protein exists, whether the link is strong enough compared to actin is not clear yet. Additionally, it requires insertion before deformation of the element, which may explain why no suitable sensor has been developed yet in plants.

Direct mechanical probing is also possible. AFM, apart from performing topography mapping as described above, also allows for mechanical probing (Figure 2.9 A, Jalili and Laxminarayana 2004). The probe used by the AFM allows quantification of the force and the displacement it triggered in the material; information that can then be used to compute the sample's mechanical properties. This method can be applied on the

walls of sections of plant cells, which revealed asymmetry in wall stiffness (Majda, Grones, et al. 2017). This method was also used on living tissues, and revealed gradients in wall properties at the surface of epidermal cells (Sampathkumar et al. 2014). AFM probes mechanical properties usually orthogonally to the direction of deformation and under compression forces. A potential limit for this approach lies in the non trivial link between this measurement and the deformability of the wall in vivo, which occurs in the plane and under extension forces.

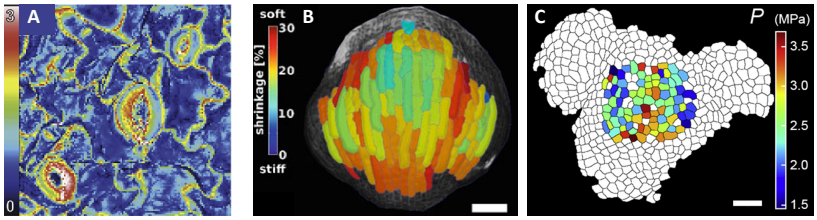

Subcellular cell wall mechanical properties | Cell wall mechanical properties | Cellular turgor pressure measurements

Figure 2.9: Determination of plant cell mechanics. A) AFM measurement of subcellular cell stiffness, on Arabidopsis cotyledon pavement cells. Colorbar is in N/m (extracted from Braybrook 2015). B) Confocal measurement of cell wall relaxation upon osmotic treatment, on Arabidopsis sepal (extracted from Sapala and Smith 2020). C) AFM measurement of cellular turgor pressure, on Arabidopsis shoot apical meristem (extracted from Long et al. 2020).

Probing wall properties with AFM, usually implies using indentation depths that are small compared to the wall thickness. If the indentation depth increases, then the measurements become sensitive to the turgor pressure of the sample. Indeed plant cells behave as a pressurized shell (Beauzamy et al. 2015). Large indentation coupled with modeling of the tissue geometry have allowed quantification of cell pressure at the surface of the tissue (Figure 2.9 C, Long et al. 2020; W. Li et al. 2022).

Finally, material relaxation can also be quantified upon plasmolysis (Sapala and Smith 2020). Plant cells are under pressure which stretch their cell walls. Osmotic treatments induce a decrease in turgor pressure, and a relaxation in the wall. Measurements of wall length before and after treatment allows for a quantification of its properties (Figure 2.9 B).

2.4 Model for cell wall deformation & growth

Modeling of a cylindrical plant cell growth: Lockhart equation

One of the first attempts to model plant cell growth mathematically was done by Lockhart 1965. The model links G, the growth rate or rate of extension of the cell wall, to ϕ, the extensibility of the cell wall, P, the pressure inside the cell and Y a threshold pressure above which deformation occurs.

$$G = \phi(P - Y)$$

When P is below the threshold Y, the cell is not growing, and above this threshold, the growth rate is proportional to the difference in pressure. Here, the cell wall is modeled as an elastic material that is inflated and deformed plastically when the cell is turgid. The balance between

wall properties (that influence ϕ and Y) and turgor pressure is the key regulator in this model. ϕ and Y vary over time, are dependant on cell geometry and are thought to be influenced by molecules interacting with the cell wall such as auxin and expansins (Okamoto et al. 1990).

As described above, the key elements that determine cell wall elongation are the following: 1) insertion of cellulose fibrils and pectins, and subsequent deformations 2) sliding and rearrangement of material based on the tension applied by turgor pressure, and potentially affected by the action of other components such as expansins and calcium, 3) methyl esterification of pectins, which affects their ability to bind to each other and to Ca^{2+} ions. As we saw above, visualization of the respective rearrangement in the cell wall is not achievable yet. However, recent molecular simulations, called coarse grained models, gave insights into the dynamics of the system (Figure 2.10, Y. Zhang et al. 2021). In this study, the three main polymers of the cell wall (cellulose, pectins and hemicellulose) were represented as beads linked by springs. Physical values measured experimentally were implemented so that the spring and bead model behaves similarly to the polymer, in terms of stiffness and persistence length. Interaction between beads of different polymers were also matched with experimental values, with cellulose-cellulose interaction being the strongest followed by cellulose-hemicellulose and then the rest of the interactions.

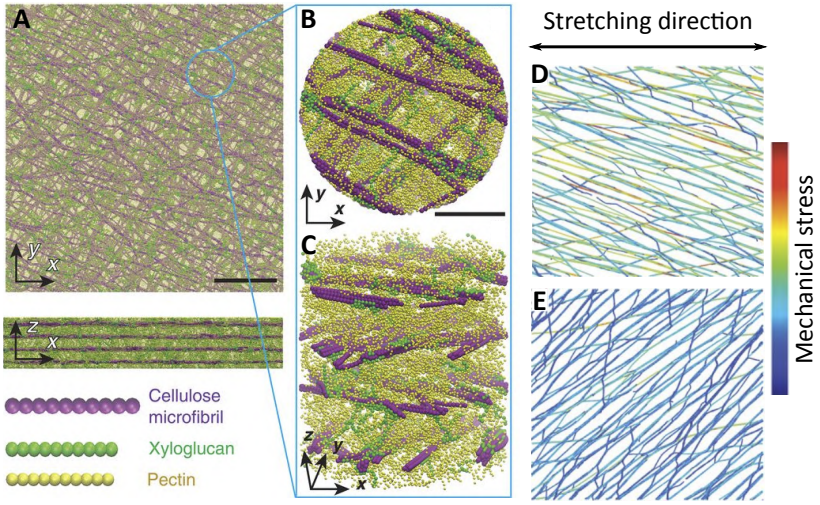

Figure 2.10: Model for cell wall deformation. A) Top view of the components of a small patch of the cell wall. Here four layers of cellulose microfibrils are represented but there is likely more in vivo. B) Zoom on a small section, and C) associated side view. We see better here that D, E) Representation of the stress intensity supported by cellulose fibrils upon stretching. Panels D and E differ by the angle between fibrils and stretch direction. Colors correspond to the stress intensity supported by each fragment of the cellulose microfibril. Note that depending on the relation between cellulose microfibril angle and the stretching direction, large differences in mechanical stress are experienced. (extracted from Y. Zhang et al. 2021).

This model predicts that, upon loading: (1) almost all of the stress accumulates in the cellulose compared to other cell wall elements. This suggests that pectins and hemicellulose play little role in the passive response to stretching. (2) Fibrils that are parallel to the stretching direction are subject to much more stress than those perpendicular. In other words, upon inflation and in absence of material insertion, the cell will stretch most in the direction perpendicular to cellulose fibrils. Experimentally, it has been observed that this direction also corresponds to the direction in which irreversible deformation (growth) occurs.Indeed, it has been observed that cylindrical cells of *Nitella* were growing orthogonally to

the fibril direction (Green 1962). Mechanical testing of the cell wall of onion cells also revealed that cell wall extensibility was significantly higher in the direction perpendicular to the fibrils (Suslov and Verbelen 2006). Some studies use the orientation of microtubules as a proxy for the orientation of cellulose fibrils. In some cases it was observed that microtubules align with the growth direction (Burian et al. 2013), while in other cases changes in growth anisotropy preceded changes in microfibril orientation (Sugimoto et al. 2003; Wiedemeier et al. 2002). This mechanism of control of growth anisotropy by orientation of cellulose microfibrils describes some situations but elements are missing.

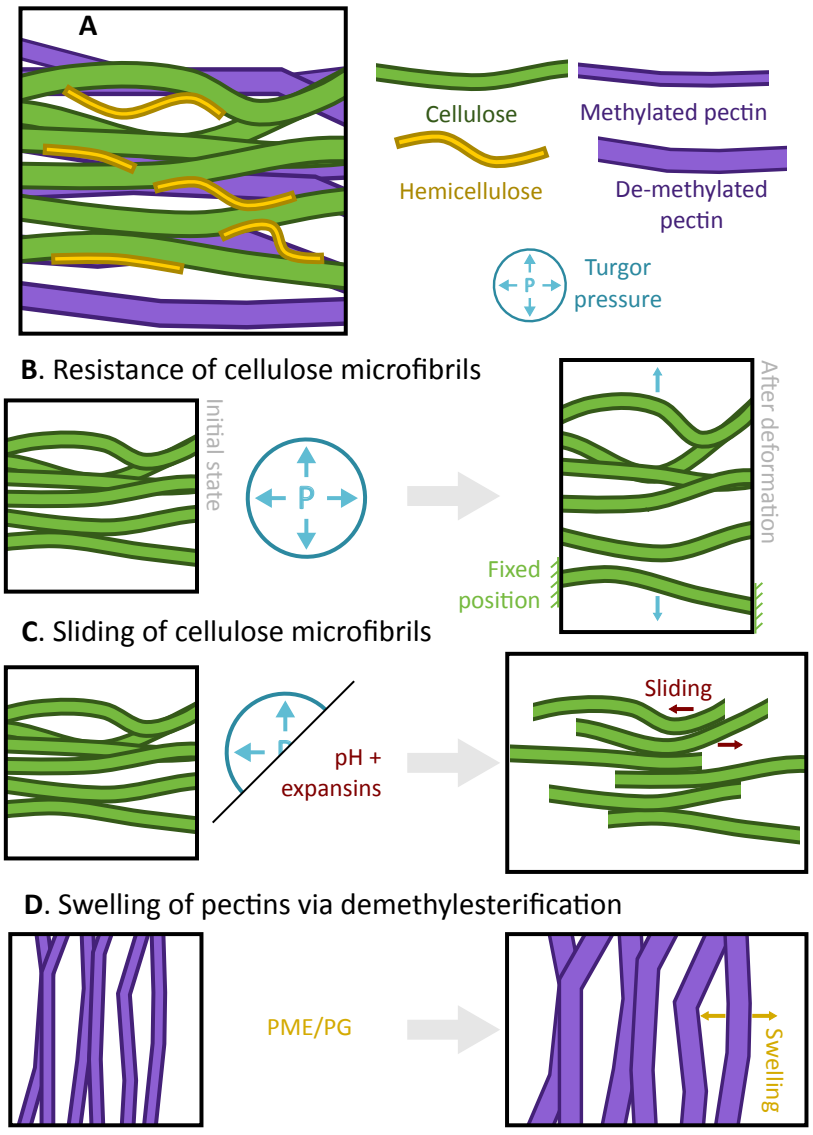

Figure 2.11: Mechanisms of cell wall deformation. A) Representation of the composition of the cell wall. A small patch of the cell wall is represented here, and the subsequent deformation will be denoted as modification of the outline of the black box for each mechanism. B) Mechanism of wall deformation linked with stiffness anisotropy of an ordered cellulose network. Deforming the network orthogonally to the cellulose microfibrils requires less energy. Because turgor pressure is isotropic, this lead to the network deforming orthogonally to the cellulose microfibrils orientation. C) Mechanism of wall deformation linked with the sliding of cellulose microfibrils. Cellulose microfibrils are bound by non covalent links. In the presence of an acidic pH and expansins, these links can be reorganized. In the presence of turgor pressure, this leads to a deformation of the cell wall preferentially in the microfibril orientation. D) Mechanisms of wall deformation linked with the swelling of pectin. Pectins can be deposited as organized filaments in the cell wall. The addition of pectin methylesterases (PME) exposes charges, which lead to filament repulsing each other, and triggers expansion perpendicular to the direction of the filaments.

An alternative mechanism of growth relies on relaxation of the link between cellulose fibrils and hemicelluloses. Expansins are a family of proteins that are thought to rearrange and relax these non covalent bonds (Daniel J. Cosgrove 2015). Expansins lack enzymatic activity, but allow for cell wall creep when added exogenously to the cell wall under acidic conditions (McQueen-Mason et al. 1992; D. J. Cosgrove 2000). This mechanism also requires turgor pressure to induce growth,

however, compared to the previous mechanism, it states that cell growth is triggered by the relaxation of the main stress direction by sliding of the fibrils along each other.

Finally, a last mechanism based has been proposed for the local expansion of the cell wall (Haas et al. 2020). In this study, it was observed that homogalacturonan organize as filaments in the cell wall and that these filaments have a different diameter depending on the methylation status of the pectins. The impact on growth was confirmed on plasmolysed cells on which PME were applied exogenously on the cell wall, and triggered growth despite plasmolysis. Other studies reported that pectin polygalacturonases (PG), that cleave homogalacturonan, mutants present decreased cell expansion and PG overexpressors present increased cell expansion (Xiao, Somerville, et al. 2014; Rui, Xiao, et al. 2017). Similarly to in vitro results on pectins, these two result seem counterintuitive and our understanding of pectins still remains elusive. Still, this advocates for the existence of this mechanism of growth in parallel with the previous models, where force generation and deformation of the cell wall would come directly from configurational changes in cell wall components.

It is important to note that all three mechanisms are not exclusive (Figure 2.11). Evidence of consecutive action have been found in the hypocotyl (Peaucelle, Wightman, et al. 2015) and cotyledon (Altartouri et al. 2019). In both cases, the first step is always associated with pectin that breaks an initial symmetry, followed by a reinforcement associated with cellulose strengthening.

Cell wall deformation, and plant morphogenesis in general, is controlled by many factors. Cellulose and pectins are considered as the two elements that influence most growth. The advance in imaging method allowed for a better characterization of the contribution of these two components. However, some of the processes that control their deposition are still poorly understood.

Morphogenesis, millimeters and hours

3

3.1 Organ morphogenesis

Organ morphogenesis is what transforms a group of cells with limited functionality into a structured assembly with a precise shape associated with a specific function. Multicellular organisms present organs of various sizes and shapes. Here we will focus on two organs, one in animals, the drosophila wing or leg disk, and one in plants, the flower, that should describe some of the mechanisms of pluricellular growth in the living world.

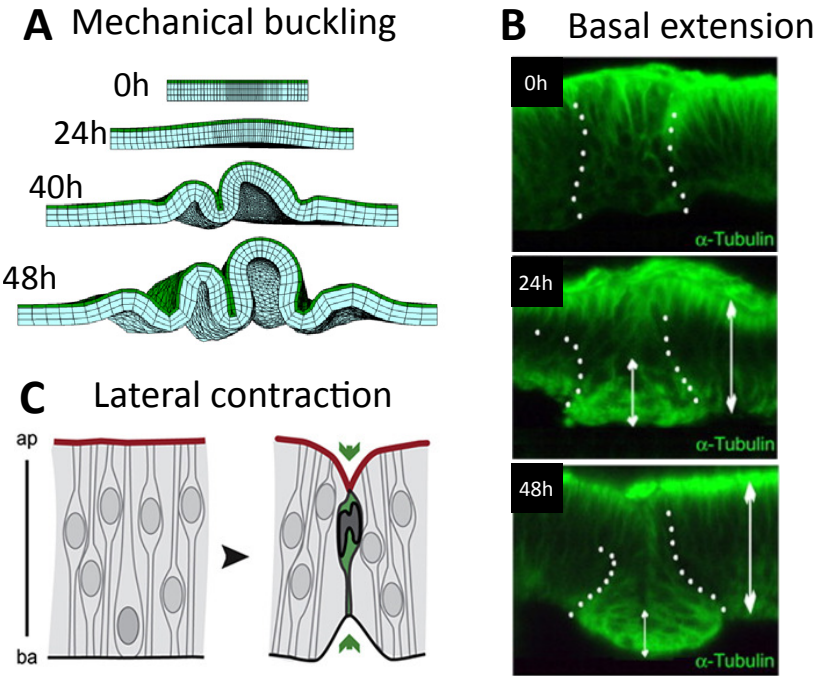

Figure 3.1: Mechanisms of fold formation in drosophila wing disk. A) Heterogeneity in growth rates lead to mechanical buckling. Here, a cross section of a model for the wing disk is represented. Cells grow depending on the size of the element. Boundary extension is limited (extracted from Tozluoğlu et al. 2019) B) Basal cell expansion by microtubule polymerization (extracted from Sui, Pflugfelder, et al. 2012). C) Lateral contraction originating from actin contractility, associated with molecular motors and potentially apoptosis (extracted from Roellig et al. 2022. This drawing initially represents neural tube bending but the same mechanisms are involved in leg and wing fold formation).

Drosophila wing initiates as the wing imaginal disk, a sac-like group of cells forming a monolayered epithelium, that then undergoes a series of steps of morphogenesis before ending up as a proper wing (Figure 3.1 A,Tripathi and Kenneth D Irvine 2022). Drosophila legs present a large number of similarities during the first steps of development with the wing. Here I will discuss mechanisms involved in one and/or the other tissue. The first step of development consists in forming folds that will delimit the boundaries of the organs that the disk will create. Formation of these folds has several origins: 1) Heterogeneity in growth rates in the disk generates mechanical conflict that leads to buckling and fold formation (Figure 3.1A,Tozluoğlu et al. 2019). For instance, if a rapidly growing group of cell in an epidermis is surrounded by slowly growing cells, this generates mechanical stress in the plane, that is released by moving the rapidly growing cells above or below the plane. 2) Asymmetric deformation of

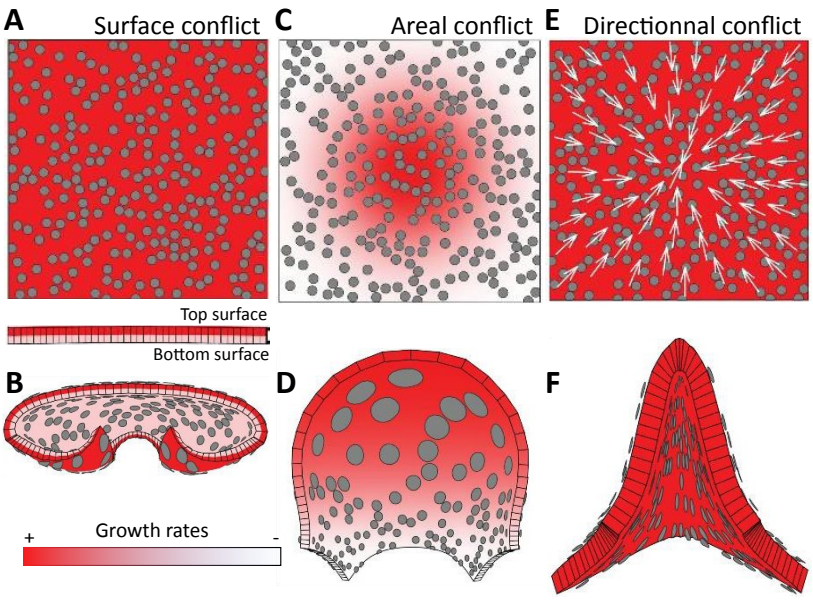

Figure 3.2: Mechanisms of growth conflicts in plants. A) Surface conflicts. Two cell layers are represented here with different growth rates. Grey circle are representative marks used to visualise the deformation of the tissue. B) Resulting shape after growth of the tissue represented in A. C) Areal conflicts. One cell layer with heterogeneities in growth rates. D) Resulting shape after growth of the tissue represented in C. E) Directional conflict. All cells grow homogeneously but with a preferential growth direction represented by the white arrows. F) Resulting shape after growth of the tissue represented in E (extracted from Rebocho et al. 2017).

cells can come from apico-basal contraction. This contraction of the cell apex is linked with microtubule redistribution from an apical position to a basal position in the wing disk (Figure 3.1B,Sui, Pflugfelder, et al. 2012; D. Wang et al. 2016). 3) Lateral contraction of cells leads to the direct apparition of the fold. In the wing disk, actin is recruited laterally by the Rho guanine-nucleotide-exchange factors (RhoGEFs) (Sui and Dahmann 2020) and coupled with molecular motors, this shortens cells (Salbreux et al. 2012). In the leg disk, it was additionally shown that apoptosis contributes to lateral contraction (Figure 3.1C, Monier et al. 2015), where the nucleus acts as a relay for force generation between apical pulling actin and basal adhesions (Ambrosini et al. 2019). 4) Basal extracellular matrix is degraded which may facilitate contraction and cell shape changes (Sui, Pflugfelder, et al. 2012; Bourboulia and Stetler-Stevenson 2010). In the leg disk, the matrix initially is under tension and is degraded at a specific point in time (Proag et al. 2019). Preventing matrix degradation artificially however, did not lead to any defect in leg morphogenesis (Proag et al. 2019).

Wing disk development illustrates four different mechanisms of morphogenesis in animals, with mechanical instability coming from heterogeneity in growth rates, polymerization/depolymerization of cytoskeleton elements that are stiff enough to deform cells, shortening of cell faces by the activity of molecular motors that pull the cytoskeleton, and finally differences in adhesion properties/stiffness of the extracellular matrix.

Plant cells can not exchange place with their neighbor, or modulate their shape without growing. Still plants are able to produce an anthology of shapes. They do so mostly by generating mechanical conflicts of various nature, in terms of growth rate and growth direction (Figure 3.2, Whitewoods and Coen 2017). Similarly to animals, heterogeneity in growth rates induces mechanical instability that triggers displacement orthogonal to the growth direction (Rebocho et al. 2017). Such heterogeneities

can be present at different levels, areal conflicts occur when zones of a same layer of cell grow at different rates. To reduce residual stress, the tissue produces an extrusion at the level of the faster growing zone (Figure 3.2B, Nath et al. 2003; Green 1992). Theoretically there should be no bias about whether the protrusion should be outwards or inwards regarding the surface. Heterogeneities can also be present between two layers of cells, which is then called surface conflict (Figure 3.2A, Rebocho et al. 2017). Here again, this conflict is solved by curving inwards the slower growing zone, which allows the outer zone to grow faster. Lastly, growth conflict could also involve growth direction. As seen above plant cells actively regulate their growth direction by modulating their cell walls. If all cells grow in the same direction, no conflicts are generated, however, if cells grow in different directions, this generates mechanical instability (Figure 3.2C, Rebocho et al. 2017; Kennaway et al. 2011). All these processes potentially are involved in the complex morphogenesis of flower organs such as the snapdragon petal (Rebocho et al. 2017).

Both in plants and animals, numerous mechanisms and physical processes are involved in morphogenesis. The next question is how these mechanisms are patterned. In the next two sections we will describe patterning processes of chemical and mechanical nature.

3.2 Long range chemical patterning: morphogen gradients

Various mechanisms can explain the coordination of cells seen above. The first mechanism that can explain long range coordination relies on morphogen gradients. Morphogens are diffusive molecules of various nature that can influence cell fate or cell growth. Several mechanisms have been proposed for formation of morphogen gradients, including: 1) Unidirectional transport of the morphogen (Figure 3.3A, G. J. Mitchison and Brenner 1980), which has been observed for instance in the shoot apical meristem of Arabidopsis. 2) A so called reflux loop where an upward and a downward flux go through different parts of the tissue (Figure 3.3B, Grieneisen et al. 2007), which has been observed in Arabidopsis root. 3) A synthesis degradation system which is thought to be common in animal tissues. The establishment of a gradient in this latter case requires: a localized production, diffusion, and removal (Figure 3.3C, Crick 1970; Ortrud Wartlick et al. 2009). In the most basic scenario, considering a field of cells, the cell at one end will produce the morphogen. This morphogen diffuses freely in the extracellular space (Yu et al. 2009) or moves via internal transport (Müller et al. 2013). The morphogen is removed homogeneously throughout the tissue via binding followed by degradation, endocytosis, or immobilization (Lander et al. 2009). While there have been debates about whether a dual gradient was required to ensure a robust patterning (Zagorski et al. 2017), single morphogen gradients

Figure 3.3: Mechanisms for the formation of morphogen gradients. A) Unidirectional flux in Arabidopsis shoot apical meristem. Green shades represent auxin concentrations (extracted from Stoma et al. 2008). B) Root reflux-loop of auxin. Colors indicate DII-Venus signal measured in the root tissue. DII-Venus is a negative reporter for auxin signaling. Light colors indicate high DII-Venus response, suggesting a low auxin concentration (extracted from Mellor et al. 2020.). C) Mechanism for synthesis - diffusion - degradation. Conc. = Concentration (redrawn from Inomata 2017).

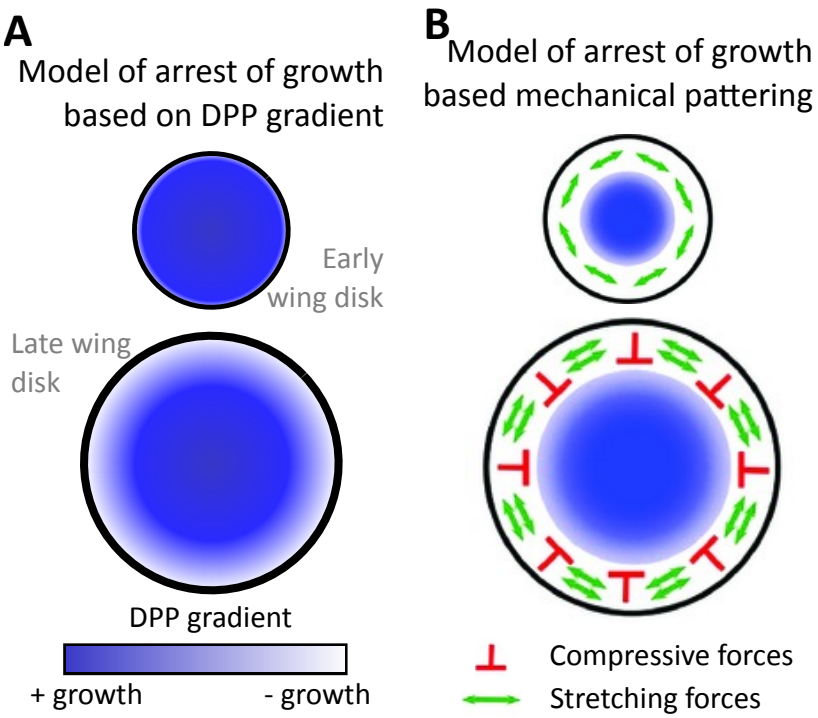

Figure 3.4: Two models for the control of wing disk size. A) Model based on the gradient of a morphogen (DPP), that is produced at the center of the wing disk. When cells grow, they progressively move away from the center of the disk and eventually stop growing. B) Model based on mechanical patterning. Homogeneous growth of the tissue leads to the center expending more rapidly compared to the border of the wing disk. This produces tension at the border, and compression at the center of the disk. When this compression reaches a threshold the wing disk stops growing (adapted from Wada and Kawakami 2015).

have been shown to be sufficient (Vetter and Iber 2022). Gradients are not static and can for instance scale with organ size (O. Wartlick et al. 2011).

In plants, several molecules have been proposed to hold this role of motile growth factor, among which the KLUH/CYP78A5 (KLU) protein (Kazama et al. 2010). *klu* mutants presented decreased growth rates, while KLU overexpressing mutants presented increased growth rates (Anastasiou et al. 2007). Additionally, KLU is expressed only at the base of the leaf and diffuses along the whole organ (Kazama et al. 2010). Similar results were obtained with other factors such as YABBY (Sarojam et al. 2010), LEAFY (van der Graaff et al. 2000) and ANGUSTIFOLIA (Kawade, Horiguchi, et al. 2013; Kawade, Tanimoto, et al. 2017).

Diffusion rate of DPP: 0.1 μm^{-1} (Ibañes and Belmonte 2008)
Diffusion rate of Wingless: 0.5 μm^{-1} (Ibañes and Belmonte 2008)
Size of the wing disk at the establishment of the gradient: 250 µm

Drosophila wing disk development presents a gradient of a morphogen called Decapentaplegic (DPP). DPP is expressed in the medial part of the wing disk, in a stripe aligned with the proximo-distal axis and diffuses freely (Entchev et al. 2000). DPP is required for cell growth in the wing disk (Spencer et al. 1982). Analysis of mutant growth with mosaic expression of DPP revealed that cells next to DPP producing cells had an increased proliferation rate (Rogulja and Kenneth D. Irvine 2005). Surprisingly, overall the wing disk presents no growth gradient (Schwank et al. 2008). Some mechanisms were proposed to explain the discrepancy between DPP gradient and uniform growth (Rogulja and Kenneth D. Irvine 2005; Schwank et al. 2008; Day and P. A. Lawrence 2000). However, DPP gradient was recently shown not to be required for uniform growth; wing disks with uniform low levels of DPP presented growth rates similar to wild-type (Barrio and Milán 2017; Bosch et al. 2017). Similarly to the DPP gradient, the fibroblast growth factor (FGF) morphogen gradient

does not produce a gradient of growth in the vertebrate limb (Boehm et al. 2010).

Morphogen gradient has also been proposed as a mechanism that contributes to the control of organ size. The question being: how does an organ know when to stop growing (Vollmer et al. 2017) ? In the drosophila wing disk, DPP, which presents a gradient in concentration, was proposed as a regulator for organ size (Figure 3.4A, O. Wartlick et al. 2011). In this hypothesis, DPP would be required for cell growth. Because DPP is produced only at the center of the organ, and because the organ is growing, this would lead to cells at the edges of the organ to stop growing once they reach a certain distance from the center of the organ. Together, this produces an organ that scales depending on the diffusibility of the morphogen. Similar patterning of organ size was also suggested in plants with the morphogen mentioned above, and with a proximal production of the morphogen (Kazama et al. 2010).

Recently, it was proposed that these gradients may induce polarization of the cell and influence cell growth direction (Boehm et al. 2010). Such polarization occurs at the cell scale and may be influenced by the morphogen gradients mentioned above.

3.3 Short range chemical patterning: polarization

Cells can be polarized, with elements asymmetrically distributed in the cytoplasm/membrane, and behavior that depends on the direction. One of the polarity networks present in the wing disk is composed of the cadherins Fat and Dachsous. This polarity axis is defined along the proximo distal axis with Fat localized subcellular at the proximal side and Daschous at the distal side (Brittle et al. 2012; Ambegaonkar et al. 2012). Cells then grow, migrate and divide towards this direction (Mangione and Martín-Blanco 2018; Bosveld et al. 2012; Mao, Tournier, Bates, et al. 2011). Such mechanism of coordination of growth direction was also reported in chicken and mouse embryos with the Wnt pathway (B. Gao et al. 2018; Lesnicar-Pucko et al. 2020).

Cell polarity in itself, if it involves adhesion molecules, can also contribute directly to morphogenesis. Nissen et al. 2018 modeled the interaction between polar cells as magnets with two poles. This assumption relies on the asymmetric distribution of surface adhesion proteins that present binding preferences with proteins of the same or different nature (Aigouy and Le Bivic 2016; Beati et al. 2018). Cells in the model thus reorient in a way that align their polarity with that of their neighbors. In a flat surface this does not create conflict, however, if the initial geometry is random or biased, such mechanisms lead to the formation of folds and tubes. Complex morphogenetic events, such as the gastrulation of the sea

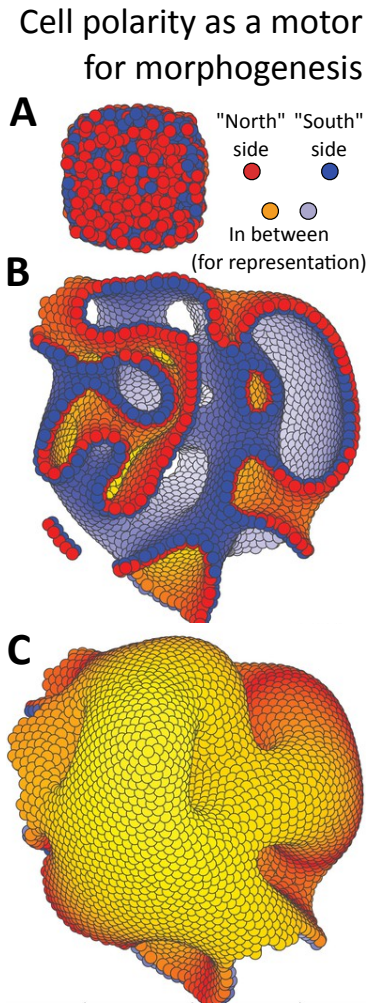

Figure 3.5: Cell polarity and adhesion forces as a motor for morphogenesis. A) Initial group of cells with random orientations. Colors are explained on the right side, the in between colors are used for visual representation of figures B and C. B) Cross section or C) full representation of the same group of cells after free evolution according to magnet-like forces (extracted from Nissen et al. 2018).

urchin, could be explained numerically by simply attributing polarity to cells, and letting them evolve without other instructions (Figure 3.5A-C, Nissen et al. 2018). Plant cell polarity has also been suggested as a potential chemical patterning mechanism for the determination of cell growth direction (Whitewoods and Coen 2017). Different protein have been reported as potential markers for polarity depending on the organ, with ROP proteins in the root (Molendijk et al. 2001), BASL in the leaf (Robinson et al. 2011; Mansfield et al. 2018) and PIN proteins in the embryo (Friml et al. 2003).

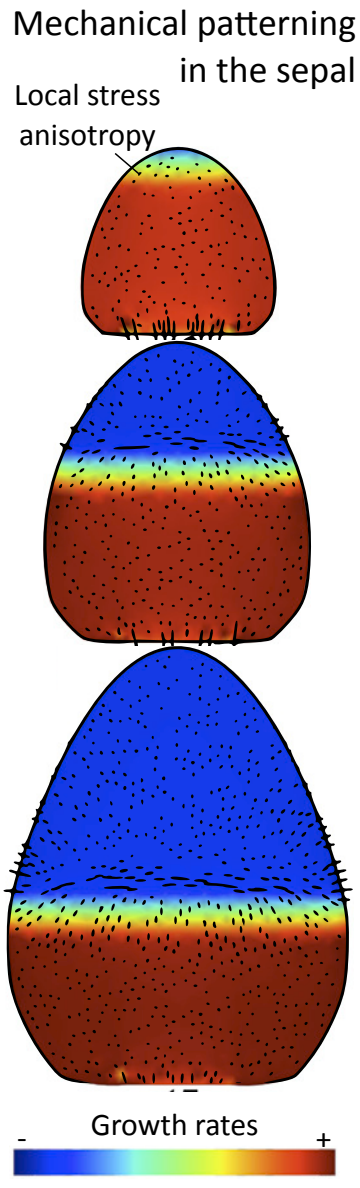

Figure 3.6: Stress patterns in the sepal. Sepals at three stages are represented with growth rates color-coded. The front of arrest of growth moves from the tip to the base of the sepal and generates an anisotropic stress at the boundary (adapted from Hervieux, Dumond, et al. 2016).

3.4 Mechanical patterning of a tissue

Another model has been proposed for the growth arrest of the imaginal wing disc in *Drosophila* using mechanical patterning. The size of this organ was first thought to be regulated mainly by gradients of morphogens such as Decapentaplegic (DPP) (Day and P. A. Lawrence 2000). However, some data were not consistent with this model (Schwank et al. 2008). Other studies proposed that mechanical pressure can be used as an indicator for organ size (Figure 3.4B, Aegerter-Wilmsen et al. 2012; Hufnagel et al. 2007; Shraiman 2005). During the imaginal disk growth, all cells proliferate homogeneously, leading to the expansion of the tissue. Consequently, cells located at the center of the disk are under compression while cells located at the periphery are under tension (Mao, Tournier, Hoppe, et al. 2013). A mechanical gradient is thus generated in the imaginal disk. The model suggests that this organ-scale heterogeneity can be used as an input in the regulatory network to end growth at the appropriate time.

Mechanical forces can also give directional information for growth direction. Sepals, the most external organ of the flower bud, has recently been used as a model for morphogenesis in plants (Roeder 2021). During sepal morphogenesis, a gradient of growth arrest progresses from the tip to the base of the sepal (Figure 3.6, Hervieux, Dumond, et al. 2016). This heterogeneity in growth rates produces a mechanical stress, aligned with the axis of the sepal, to which microtubules respond (Hervieux, Dumond, et al. 2016; Hamant, Heisler, et al. 2008). This alignment of microtubules then leads to cells growing in the direction of the axis of the sepal. Here, it is thought that the sensing of this mechanical pattern generated by the growth gradient acts as a mechanism that enables normal growth of the sepal.

3.5 Case study: Pavement cells

3.5.1 Evolution and function of pavement cells

Pavement cells are jigsaw puzzle shaped cells, with interlocked protrusions, called lobes, and depressions, called necks (Figure 3.7A, B).

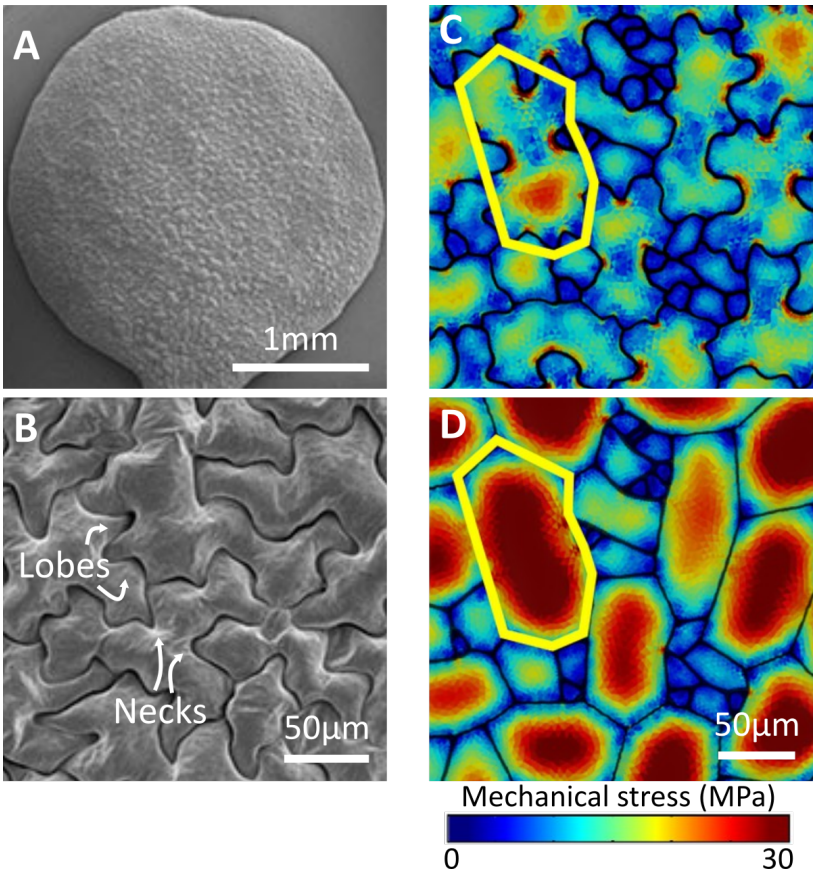

Figure 3.7: Geometry of a pavement cell and stress patterns. A) Scanning electron microscopy image of a cotyledon (the first two leaves) of Arabidopsis, and B) close up (extractedfrom Gunji et al. 2020). C) Real geometry of pavement cells from an Arabidopsis cotyledon. The tissue was modeled and inflated numerically to compute the mechanical stress, color coded here. Necks appear with a higher stress compared to lobes. D) A simplified tissue template using the junctions of the cells in (C). The yellow outline marks a corresponding cell in (C) and (D) (extracted from Sapala, Runions, et al. 2018.)

Pavement cells appear in at least one tissue of all vascular plants that were tested so far (Vőfély et al. 2019). Four main hypotheses explaining their function have been proposed: 1) oscillations in the contact between cells increases the surface of exchange for chemical communication (Galletti and Ingram 2015). 2) Oscillations in the contact between cells increases adhesion between cells (Jacques et al. 2014). The epidermis is indeed likely to break under tension originating from turgor pressure (Verger et al. 2018). However, study of mutants with defects in cell shape did not report defects in cell adhesion, while adhesion defecting mutants presented normal cell shape (Verger et al. 2018). 3) Oscillations also behave has springs which increases the flexibility of the leaf (Sotiriou et al. 2018). 4) At a subcellular level, oscillations in anticlinal walls limits the accumulation of stress in the periclinal cell wall coming from turgor pressure (Sapala, Runions, et al. 2018). This last hypothesis comes from stress computation on realistic cell geometry (Figure 3.7C, D). This study highlighted that the maximum stress in the periclinal cell wall does not necessarily scale with cell size, but rather with the largest open area (LEC), the biggest circle that can fit in the cells. This means that circular cells are exposed to a higher maximal stress compared to pavement cells with similar surface area. As with most evolution related questions it will likely be difficult to pinpoint the phenomena that contributed most to pavement cell shape selection, as all four hypotheses probably influenced it. It is also likely that mechanisms explaining their formation are also conserved.

Arabidopsis cotyledons pavement cells have been extensively studied. Initially, these cells are circular and develop lobes progressively (C. Zhang et al. 2011). A clear developmental timeline, quantified in days after germination with synchronized plants, has been mapped and allows for comparison between studies (C. Zhang et al. 2011). Pavement cell shape acquisition has been separated into two steps, an initiation step followed by a reinforcement.

3.5.2 Lobe mechanical initiation: asymmetry in wall composition or buckling ?

There are currently two hypotheses to explain lobe initiation, one supported by debated experimental data, and one supported by modeling approaches. The study by Majda, Grones, et al. 2017 fixed sections of anticlinal developing walls and used transmission electron microscopy stained with immuno gold, coupled with AFM. This revealed that before wall formation, there is an asymmetry in wall composition with increased de-methylesterification at the lobe site, associated with decreased stiffness (Figure 3.8). Three potential limitations for this study stem from: 1) data comes from measurements on sections, with no possibility of measuring the evolution in time, 2) AFM data on sections does not necessarily reflects the deformability of the wall, 3) this study does not take into account periclinal walls that are thought to greatly contribute to morphogenesis. Acquiring experimental data proved difficult, as visualizing asymmetry in composition at the wall levels requires a high resolution that is not achieved via the simple use of fluorescence compatible with in vivo imaging.

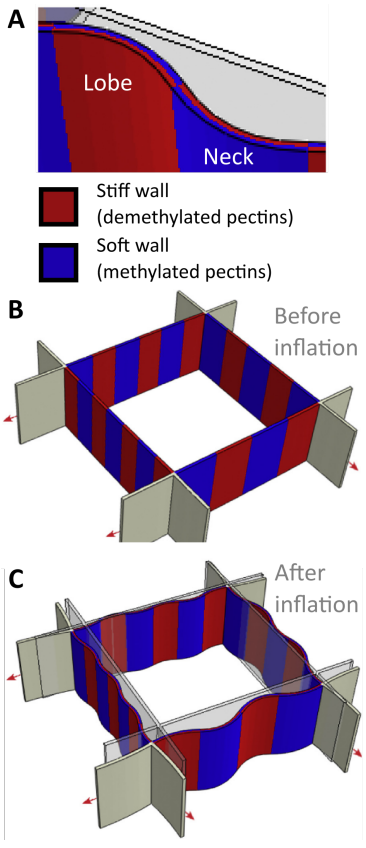

Figure 3.8: Model for lobe initiation by mechanical asymmetry. A) Structure used for the wall asymmetry with alternating stiff walls and thin walls both within a cell and between cells. B) Initial cell shape (before inflation) and C) resulting shape (after inflation). Periclinal walls were not included in the model (extracted from Majda, Grones, et al. 2017.)

Another approach was developed using computational modeling. A. J. Bidhendi, Altartouri, et al. 2019 proposed a mechanism relying on mechanical buckling. Cells are inflated by turgor pressure and, at the cell level, this generates only tension in the cell wall, which in general should not be able to produce buckling in itself. However, in a context where cells are in contact, the swelling of cells aligned with the wall may generate a compressive stress leading to buckling (Figure 3.9). In this study, a modeling approach quantified the stress in the anticlinal cell walls in a group of four jointed cells. When cells were inflated, it was reported that anticlinal cell walls experienced a compressive stress induced by the tension coming from periclinal cell walls, and that this stress was high enough to generate buckling.

Limitations from both studies arised, with most debate occuring on the question of the importance of the periclinal wall (Majda, Krupinski, et al. 2019; A. J. Bidhendi and Geitmann 2019). Future work focusing on the deformability of the 3D wall in a tissue context may answer these questions.

3.5.3 Lobe chemical initiation and maintenance: auxin and brassinosteroids

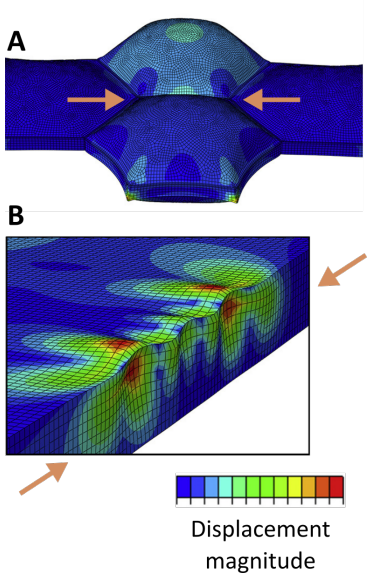

Figure 3.9: Model for lobe initiation by mechanical buckling. A) Structure used for the cells when inflated. Four cells are modeled here. B) Deformations in the cell wall. Arrows indicate the same wall in A and B. Displacement magnitude after inflation is color coded. Note that anticlinal walls form altering necks and lobes rather than a continuous deformation (extracted from A. J. Bidhendi, Altartouri, et al. 2019.)

Auxin is a master phytohormone that regulates cell growth and contributes to pavement cell development. Auxin presents a particular pattern during cotyledon development, with a gradient that forms during early cell shape acquisition (Grones et al. 2020). Plants that were deficient in auxin synthesis, with for instance mutants of YUCCA (Cheng et al. 2006), showed decreased interdigitation that was rescued upon exogenous auxin application (Xu, Wen, et al. 2010). Mutant plants of the auxin efflux carrier *PIN-FORMED 1* (*PIN1*) gene, that presented defects in auxin transport, displayed pavement cells that were long and narrow, with really small lobes (Xu, Wen, et al. 2010). At a subcellular scale, it is thought that auxin is exported via PIN (Gälweiler et al. 1998) from the lobes to the neck of the neighboring cell, and that this particular localisation of PIN is dependent on its phosphorylation status (H. Li et al. 2011). Auxin is then detected apoplastically by the AUXIN BINDING PROTEIN 1 (ABP1) which activates TRANSMEMBRANE KINASE (TMK1) at the neck (Xu, Dai, et al. 2014). Upon activation, TMK1 recruits downstream effector RHO OF PLANTS 6 (ROP6) (Xu, Dai, et al. 2014). ROP6 in turn promotes microtubule ordering which contributes to lobe formation as will be discussed in the following section.

Two studies however present information that question the real role of auxin polar transport in pavement cell shape. Cotyledon of mutants *abp1* (Y. Gao et al. 2015) and *pin1* (Belteton, Sawchuk, et al. 2018) showed no pavement cell shape phenotype, while previous studies suggested an important role for these two proteins. A possible explanation for these contradictory results lies in the organ considered since some of the studies mentioned above were performed on leaves and not in cotyledons. Pan et al. 2020 recently suggested that lobe initiation could be linked with nanoclustering of TMK1 induced by stochastic fluctuations of auxin concentration. This hypothesis relies on the observation of TMK1 clusters that recruits ROP6 (Pan et al. 2020) and initiates microtubule patterning (Xu, Wen, et al. 2010; Pan et al. 2020). This model could explain the lack of phenotype of auxin transport mutants, such as *pin1*, while proposing mechanisms for various mutant phenotypes.

Recently, the plant hormone family brassinosteroids have been proposed as contributing to pavement cell shape complexity (W. Zhang and Staiger 2022). Brassinosteroids have been linked with the patterning of PLECKSTRIN HOMOLOGY GTPase ACTIVATING proteins 1 (PHGAP1) and PHGAP2 (W. Zhang and Staiger 2022), which in turn inhibits ROP2 at the lobe leading to a cascade similar to the one mentioned above (Lauster et al. 2022). Counterintuitively, despite influencing microtubule pattern in the pavement cell, PHGAP1 and PHGAP2 patterning was shown to be dependent on microtubules (Lauster et al. 2022), which suggest that other events initially pattern microtubules.

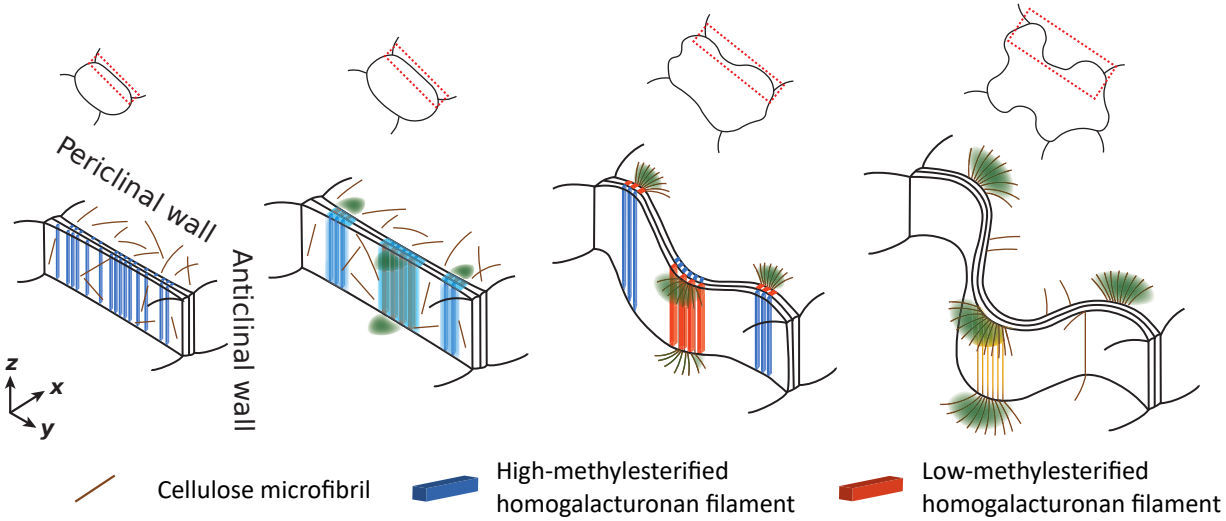

Figure 3.10: Model for pavement cell shape establishement. Evolution of a pavement cell (top) and corresponding wall composition (bottom). Initial patterning of the lobe is triggered either by mechanical buckling or asymetric wall composition. Microtubules then align specifically at the necks. This lead to cellulose being deposited in a fan shaped manner linking periclinal and anticlinal walls, and high-methylesterified pectins being deposited as nanofilaments at the necks. Cellulose then restrains growth direction, while demethylesterification of the pectins induce swelling of the wall (extracted from S. Liu et al. 2021.)

3.5.4 Lobe development: wall reinforcements

Seedlings treated with drugs depolymerizing microtubules presented a drastically altered cell shape, with almost no lobe forming (Panteris et al. 1993; Armour et al. 2015). Cortical microtubules at the surface of the epidermis present a specific pattern going from neck to neck in a fan-like fashion (Sampathkumar et al. 2014; Panteris et al. 1994). Microtubule patterns however do not predict lobe initiation sites (Belteton, Sawchuk, et al. 2018). Two hypotheses are proposed to explain the microtubule pattern: 1) chemical signaling via a relay of auxin patterns as described above, 2) mechanical stress in the pavement cells actually also goes from neck to neck Sampathkumar et al. 2014 in a fan like fashion, and microtubules in plant have been described to align with stress (Hamant, Heisler, et al. 2008). Since microtubules contribute to wall reinforcement, as it will be described below, this creates a feedback loop that reinforces pavement cell shape.

Downstream of microtubules are elements of the cell wall and, again, two non-exclusive hypotheses have been suggested: 1) deposition of cellulose along microtubules leads to a reinforcement of periclinal walls in that direction. Indeed, increased cellulose concentration was observed matching a pattern similar to that of microtubules (Altartouri et al. 2019; A. J. Bidhendi and Geitmann 2019), and that matched also mechanical properties (Sampathkumar et al. 2014; Altartouri et al. 2019). Plants with dysfunctional cellulose synthesis systems, with for instance reduced cellulose content, present reduced lobing (Burn et al. 2002). Genetic perturbation of cellulose crystallinity, without perturbation of total cellulose content, also lead to similar, although less severe, defects (Fujita et al. 2013; Altartouri et al. 2019). Similarly, partial chemical removal of cellulose via

exogenous application of cellulase lead to reduced lobing (Higaki et al. 2017). 2) Deposition of pectin nanofilaments along the anticlinal walls, associated with a de-methyl esterification of these filaments induces swelling. This swelling induces elongation of the anticlinal wall, and because they are bounded by neighboring cells, this increases lobe size. Indeed asymmetry in pectin composition exists from one side of the lobe to the other, with more demethylesterified pectins on the convex side (Majda, Grones, et al. 2017; Haas et al. 2020). Demethylesterification of pectins have been reported to be associated in vitro with swelling (Walkinshaw and Arnott 1981), and with softer cell walls (Peaucelle, Braybrook, et al. 2011; Peaucelle, Wightman, et al. 2015). Exogenous chemical demethylesterification of pectins in plasmolysed conditions lead to growth (Haas et al. 2020). Mutants of PME and PMEI show little to no phenotype (Altartouri et al. 2019), but because of genetic redundancy, it is usually safer to introduce overexpression of the genes Peaucelle, Braybrook, et al. 2011; Peaucelle, Wightman, et al. 2015. Overexpression of PME and PMEI both displayed both reduced lobe frequency and depth (Haas et al. 2020). Both cellulose centered and pectin centered hypotheses present arguments, and it is likely that both mechanisms contribute to pavement cell shape development with potential compensation by the other mechanism in the absence of another.

Pavement cell morphogenesis is a complex process that involves many actors, from microtubules and chemical patterning, to cell wall deposition. Their shape fulfill multiple function and is thought to be important for plant integrity. Despite increasing knowledge on the morphogenetic processes, some elements remain uncertain.

Objectives of the PhD | 4

Truly understanding a biological mechanism (or a real world science mechanism in general) requires being able to explain its behavior at various temporal and spatial scales. For instance, while physicists have theories that work well at describing either really small scales and really large scales, no good theories have been proposed that could unify the two of them. I believe that because biology more easily allows us to propagate theories between scales and test them, we should aim at a comprehension of our system that goes from molecular mechanisms to organism behaviors.

4.1 Cellulose deposition and cell growth coordination

In plant development, one of the popular dogma is that growth is oriented perpendicularly to the direction of cellulose microfibrils (Green 1962). Microfibril deposition is guided by microtubules via CELLULOSE-SYNTHASE INTERACTIVE 1 (CSI1) (S. Li et al. 2012; Gu et al. 2010; Bringmann et al. 2012). In the *csi1* mutant (Xin et al. 2020) or more generally in a context of microtubule depletion (Chan and Coen 2020), cellulose microfibrils were shown to be more aligned compared to wild-type. Surprisingly, such an increase in cellulose microfibril alignment was associated with a decrease of organ elongation (Lei, S. Li, Du, et al. 2013). No satisfying hypothesis has been proposed so far to explain such discrepancy. This suggests that there are still uncertainties about either the dogma of growth aligned with microfibril direction, or the behavior of *csi1* mutant and the function of guidance by microtubules in general. One of the first aspects of my PhD consisted in trying to understand at all scales the consequences of disruption of cellulose deposition in the *csi1* mutant.

This dogma, as popular as it is, only stops at the cellular scale, the size at which it was developed. However, understanding organ and organism development also goes through tissue behavior where properties non trivially linked with cell behavior can emerge. During my PhD, we also decided to scale up this dogma and link cellulose deposition with organ size and shape. To do so, while most results were published in the hypocotyl (Refrégier et al. 2004), we decided to switch to the sepal as model organ for various reasons. 1) Growth of the hypocotyl presents a very stereotyped growth pattern with steps of pure anisotropic growth followed by a complete shift of microfibril deposition orientation (Adamowski et al. 2019). Sepal growth is more continuous in time. 2) All cells of the hypocotyl tend to grow in the same direction. Sepal cell

growth direction is less homogeneous, with potential local reorientation based on local mechanical cues (Hervieux, Tsugawa, et al. 2017). This makes the sepal a more realistic model for the study of tissue growth with respect to cell growth direction. 3) Hypocotyl size depends directly on the environment, with length usually being correlated with the depth of the seed in the soil. There is no clear indication that hypocotyl size and shape is controlled intrinsically. Sepal size and shape, however, is under genetic control, and is important as it covers flowers during development and controls flower opening timing (Hong et al. 2016).

The first chapter of the results will describe both biological questions (discrepancy between scales in *csi1*, and contribution of CSI1 to organ morhogenesis) via the study of *csi1* sepal. Here, we analyzed sepal development at all spatial scales, from cellulose patterns, to cell growth, tissue growth and organ growth.

4.2 Method for quantification of cellulose microfibril angles at various depths

Associated with this project, we tried to develop methods for imaging cellulose in a depth-resolutive manner in a second axis. The initial idea was to analyze the evolution of cellulose after insertion in the wall, which potentially reorients after growth. Another goal was to quantify the contribution of the various cellulose layers to growth, questioning for instance the relative importance of recently deposited microfibrils versus microfibrils far from the membrane.

4.3 Heterogeneity in microtubule dynamics at high temporal resolution in the pavement cell

Upstream of cellulose synthases are microtubules that are very dynamic structures. While a relevant time scale for cellulose deposition is usually in the order of magnitude of the hour (D. Liu et al. 2017), the relevant time scale for microtubules is rather in the order of magnitude of the second (Zwetsloot et al. 2018). In the pavement cell, studies of microtubules usually do not give attention to the temporal resolution and rather give a static view of the microtubule network (Sampathkumar et al. 2014). Similarly, studies claim that factors "influence" microtubule patterning but give no molecular explanation for how this affects microtubule dynamics (W. Lin and Z. Yang 2020). In a third aspect of my PhD, I worked with another PhD student of the lab, Matthieu Cortes, to develop a pipeline of analysis of microtubule dynamics in the pavement cell at short time scales. One of the questions we tried to answer was to link microtubules

dynamics locally, in terms of polymerization, depolymerization, translation, rotation at the second scale, with the emerging apparently stable network at the hour scale.

4.4 Compensatory mechanisms upon cell shape loss in pavement cell

One of the functions of the pavement cell shape has been hypothesized to be resistance to internal pressure (Sapala, Runions, et al. 2018). Surprisingly, pavement cells with defective shape have not been reported to particularly burst (Sapala, Runions, et al. 2018). Here, as a fourth axis of my PhD we decided to investigate potential compensatory mechanisms that could prevent bursting in the absence of pavement cell shape.

Results

"Tout parle à qui sait lire, voir et écouter."

– *Provèrbe marchombre*, Le pacte des marchombres, Pierre Bottero

Spatial consistency of cell growth direction during organ morphogenesis requires CELLULOSE-SYNTHASE INTERACTIVE1

Graphical Abstract

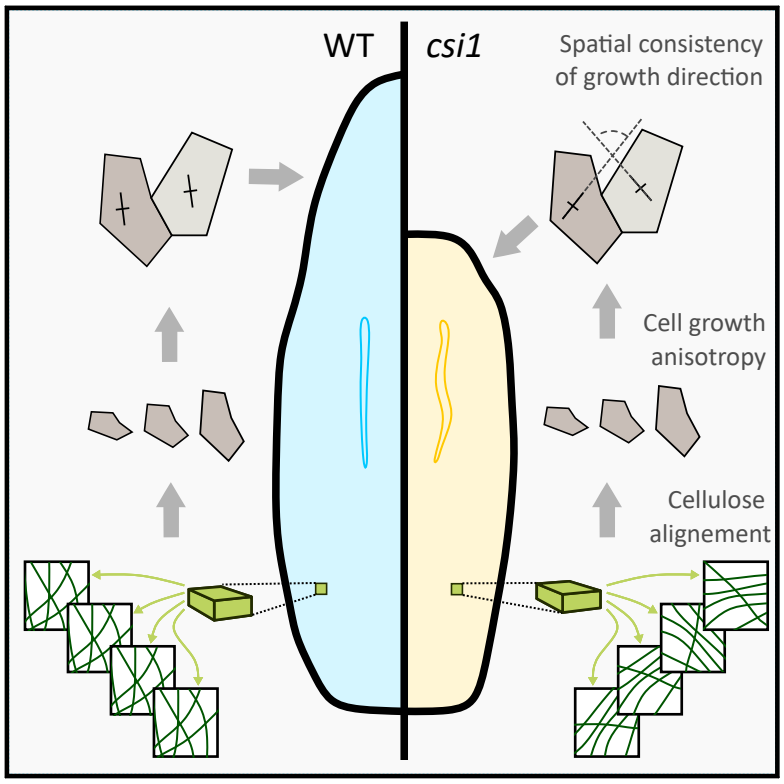

Highlights

- In *csi1*, sepals grow less anisotropically and its cells present a snake-like shape.
- In *csi1*, cellulose is more anisotropic in the most recently deposited plane, but cell walls present similar levels of anisotropy.
- In *csi1*, cells grow with comparable level of anisotropy, but are less consistent spatially in growth direction.

Authors

Corentin Mollier, Joanna Skrzydeł, Dorota Borowska-Wykret, Mateusz Majda, Mateusz Dulski, Antoine Fruleux, Roman Wrzalik, Richard S. Smith, Françoise Monéger, Dorota Kwiatkowska, and Arezki Boudaoud

In Brief

We investigated the contribution of cellulose patterning in organ morphogenesis. We focused on CELLULOSE-SYNTHASE INTERACTIVE 1 (CSI1) that links microtubules and cellulose synthases. We found that in the *csi1* mutant, sepals were less anisotropic. Study of sepal development revealed a decrease in growth anisotropy at organ but not at cell scale. Discrepancies between scales were explained by a lack of spatial consistency of growth direction in the mutant. At a subcellular scale, disruption of guidance led to increased alignment of recently synthesized cellulose microfibrils, but not at the whole wall level.

Contributions

I wrote the article and performed all experiments and analysis except for : AFM, tensile testing, and Raman microspectrometry. For the latter, I contributed to the setup and the first few acquisitions.

Spatial consistency of cell growth direction during organ morphogenesis requires CELLULOSE-SYNTHASE INTERACTIVE1

Corentin Mollier[1], Joanna Skrzydeł[2], Dorota Borowska-Wykret[2], Mateusz Majda[3], Mateusz Dulski[4,5], Antoine Fruleux[1,6], Roman Wrzalik[4,5], Richard S. Smith[3], Françoise Monéger[1], Dorota Kwiatkowska[2,*], and Arezki Boudaoud[1,7,*]

[1]Reproduction et développement des plantes, ENS de Lyon, France; [2]Institute of Biology, Biotechnology and Environmental Protection, University of Silesia in Katowice, Poland; [3]John Innes Centre, Norwich Research Park, Colney Lane, United Kingdom; [4]Silesian Center for Education and Interdisciplinary Research, University of Silesia in Katowice, Poland; [5] August Chełkowski Institute of Physics, University of Silesia in Katowice, Poland; [6]LPTMS, Université Paris-Saclay, France; [7]LadHyX, Ecole polytechnique, CNRS, France ; [*]Corresponding authors: dorota.kwiatkowska@us.edu.pl, arezki.boudaoud@polytechnique.edu

Extracellular matrices generally contain fibril-like polymers that may be organized in parallel arrays. Although their role in morphogenesis has been recognized, it is still unclear how the subcellular control of fibril synthesis translates into well-defined organ shape. Here, we addressed this question using the Arabidopsis sepal as a model organ. In plants, cell growth is driven by turgor pressure and restrained by the extracellular matrix known as the cell wall. Cellulose is the main load-bearing component of the plant cell wall and cellulose microfibrils are thought to channel growth perpendicularly to their main orientation. We investigated the role of the guidance of cellulose synthesis by CELLULOSE SYNTHASE INTERACTIVE 1 (CSI1) in sepal morphogenesis. We observed that sepals are shorter in *csi1* mutants, although the newest cellulose microfibrils are more aligned in *csi1*. Surprisingly, cell growth anisotropy was similar in *csi1* and wild-type plants. We resolved this apparent paradox using polarized Raman microspectroscopy and live imaging of growing sepals. We found that CSI1 is required for spatial consistency of growth direction across the sepal and for the maintenance of overall organ elongation. We confirmed our conclusions at sepal scale, notably using bespoke mechanical assays. Our work illustrates how the subcellular regulation of the extracellular matrix may control morphogenesis at multiple scales.

cellulose | CSI1 | morphogenesis | growth coordination | sepal

Living organisms display an amazing variety of forms. While a given form may be achieved through several morphogenetic trajectories, morphogenesis often involves elongation or anisotropic growth, i.e. more growth along one axis of the organ. Elongated forms may result from coordinated cell rearrangements such as intercalation [1, 2], from patterned heterogeneity in the physical properties of cells [3–6], or from guidance of growth by a matrix surrounding cells or tissues, usually a material reinforced by fibrils [7–9]. Here, we consider the link between fibril arrangement and elongation.

The nature of fibrils and the guidance of fibril synthesis largely vary between kingdoms. In several rod-shaped bacteria, the synthesis of peptidoglycans is guided by MreB, an actin homologue, following membrane curvature [10, 11] and driving bacterial elongation. In Drosophila oocytes, microtubules guide the polar secretion of collagen in the surrounding epithelium [8, 9]. Collagen deposition is associated with a global rotation of the oocyte inside the matrix, which yields a circumferential arrangement of fibrils and a mechanically anisotropic extracellular matrix, which is required for oocyte elongation [7, 11]. Finally in plants, cells are surrounded by a cell wall composed of cellulose microfibrils embedded in a matrix of pectins, hemicelluloses, and structural proteins. Cellulose microfibrils may lead to mechanical anisotropy of the cell wall and channel growth [12]. Despite increasing knowledge about the link between cellulose microfibrils arrangement and cellular growth [12–14], how this yields well-defined organ forms remains poorly understood.

Cellulose chains are polymerized at the plasma membrane by complexes of cellulose synthase (CESA) and bundle into microfibrils in the cell wall. CESA complexes are associated with other proteins such as KORRIGAN that is involved in targeting CESA to the membrane [15, 16], CELLULOSE COMPANION 1 that stabilizes the microtubules guiding the CESA [17], and CELLULOSE SYNTHASE INTERACTIVE PROTEIN 1 (CSI1) that binds microtubules and CESA complexes [18–20]. Two genes closely related to CSI1 have been identified: expression of CSI2 is restricted to pollen, while mutations of CSI3 yield no visible phenotype [21]. *csi1* mutant exhibits hyper aligned cellulose microfibrils in the hypocotyl [22], probably because in the absence of microtubule guidance, CESA are partly guided by previously deposited cellulose microfibrils [23]. Strangely, this hyper alignment of cellulose in *csi1* hypocotyls was not associated with an increased cell/organ growth anisotropy [18, 19] , questioning the link between microfibrils alignment and anisotropic growth. In this work we addressed this link, from cellular to tissue scale.

Growth of etiolated hypocotyls is highly stereotyped [5] and mostly uniaxial, limiting the use of the hypocotyl to explore the relation between cellulose microfibrils deposition and growth direction. We chose to investigate this relation in the Arabidopsis sepal, the green leaf-like organ that protects a flower before its opening. Sepal shape and size are robust [24], despite variability in areal cell growth [25, 26] and putatively in growth direction. We studied the links between cellulose organization, growth anisotropy and main growth direction, from cell to organ scale, using *csi1* mutation to test our conclusions.

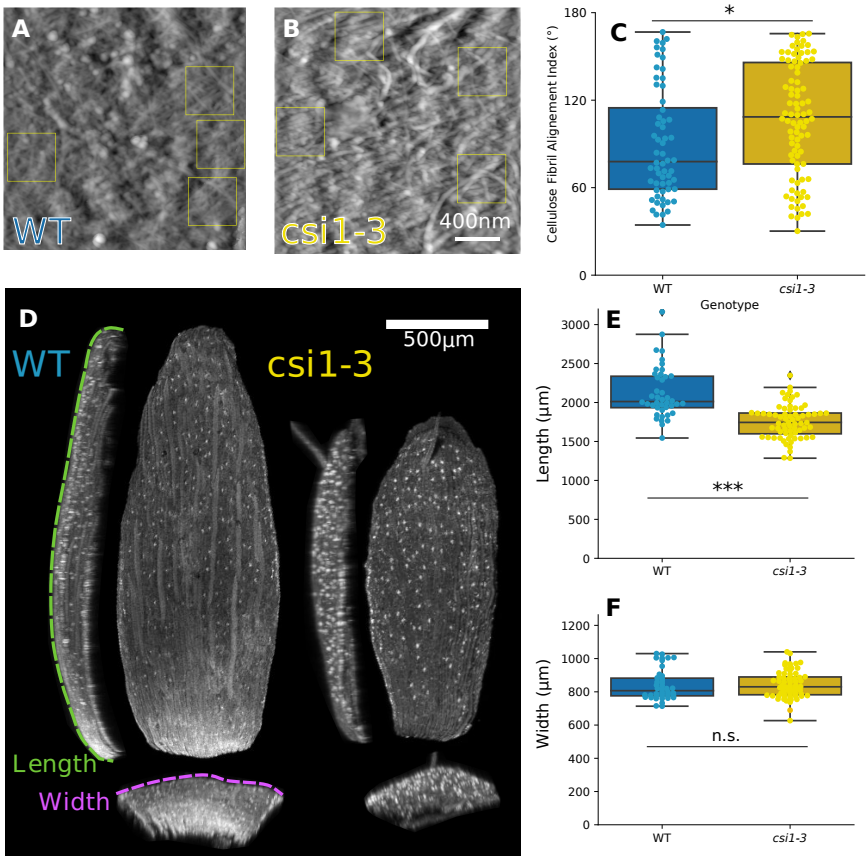

Fig. 1. Recently deposited cellulose microfibrils are more aligned in *csi1* than in wild-type (WT), but *csi1* sepals are shorter
A,B. Representative topography maps, obtained with Atomic Force Microscopy (AFM), of WT and *csi1-3* outer epidermis cell wall imaged from the protoplast side after removing internal tissues and epidermis protoplasts of the sepal (maps corresponding to the median value of the alignment index for each genotype). Yellow squares outline regions used for the index assessment. **C.** Alignment index of cellulose microfibrils, with high values corresponding to more aligned microfibrils. Boxplots for WT and *csi1-3* (N=5 and 6 stage 12 sepals and n=60 and 105 regions of 400nm×400nm from 9 and 14 cells, respectively; p-value of Mann-Whitney test = 0.005). **D.** Representative front, top, and side views of WT and *csi1-3* fully grown sepals (stage 12 of flower development), obtained from projections of confocal images. Cell walls were stained using propidium iodide. The dotted lines show sepal maximal width and length as measured along the outer (abaxial) surface of the sepal. **E,F.** Comparison of length and width of WT and *csi1-3* sepals, measured as in D (n=39 and 67, respectively. t-test p-values = 1×10^{-10}, 0.73, for length and width, respectively.) Here and elsewhere, the boxes extend from the first to the third quartiles of the distributions, the line inside the box indicates the median, the whiskers span the full range of the data (except when outliers are present, corresponding to points further than 1.5 x interquartile range from the corresponding quartile), and the points correspond to individual values. Statistical significance: *= p < 0.05, **=p < 0.005, and ***= p < 0.0005.

Results

Cellulose microfibrils arrangement is more anisotropic in *csi1*.

We first compared cellulose microfibrils patterns between the cell walls of WT and *csi1-3* sepals. To expose the inner surface of the outer epidermal wall before imaging, we gently scratched inner sepal tissues and removed protoplasts using chemical treatment, until we had only one cell-wall remaining. Because this method did not require grinding, this allowed us to keep track of the approximate position of the wall on the sepal, as well as to ensure the observation of the external wall of the epidermis, as confirmed by optical microscopy (Fig. 6B). We then used Atomic Force Microscopy to visualize recently deposited cellulose microfibrils in the outer wall of the abaxial epidermis of sepals [27]: a nanometer-sized probe was used to scan the protoplast-facing surface of the wall sample and measure the height of contact (Fig. 1A,B). Maps presented various orientations of microfibrils (Fig. 1A,B). There was also a proportion of regions with only one apparent orientation (2 out of 62 for WT, 12 out of 100 for *csi1-3*), although the difference between these proportions was not significant (p-value of normal z-test = 0,08). Therefore, we developed an index to quantify to what extent the microfibrils are aligned (Fig. 1 1C). Briefly, microfibrils orientation distribution was decomposed into Gaussians and the alignment index was computed as the maximum angular distance between these Gaussians. We found that cellulose microfibrils were more aligned in *csi1-3* compared to WT (means = 90 and 107 ° for WT and *csi1-3*, respectively; p-value of Mann-Whitney test = 0.005). Next, we examined whether the effect of this mutation on cellulose deposition was associated with affected sepal morphogenesis.

csi1 sepals are shorter owing to reduced elongation rates.

Because Arabidopsis sepals are curved, we used 3D confocal microscopy to quantify their shape parameters (Fig. 1D). We found that *csi1-3* sepals were shorter compared to WT but had a similar width (Fig. 1E,F means = 2140 and 1760µm for length and 840 and 846µm for width, for WT and *csi1-3*, respectively. p-value of t-test = 1×10^{-10}, 0.73, for length and width, respectively). This phenotype was similar for the *csi1-6* allele (Fig. 6A-C), confirming that it is indeed the result of CSI1 loss of function. Sepal contours (as seen from front, Fig. 1D) also differed between genotypes, with for instance a narrower base for *csi1-3*. We quantified curvature and found that *csi1-3* sepals were significantly more curved compared to WT (Fig. 6E,G). Higher anisotropy of microfibrils arrangement is usually associated with a higher cell growth anisotropy [12–14], which would be expected to

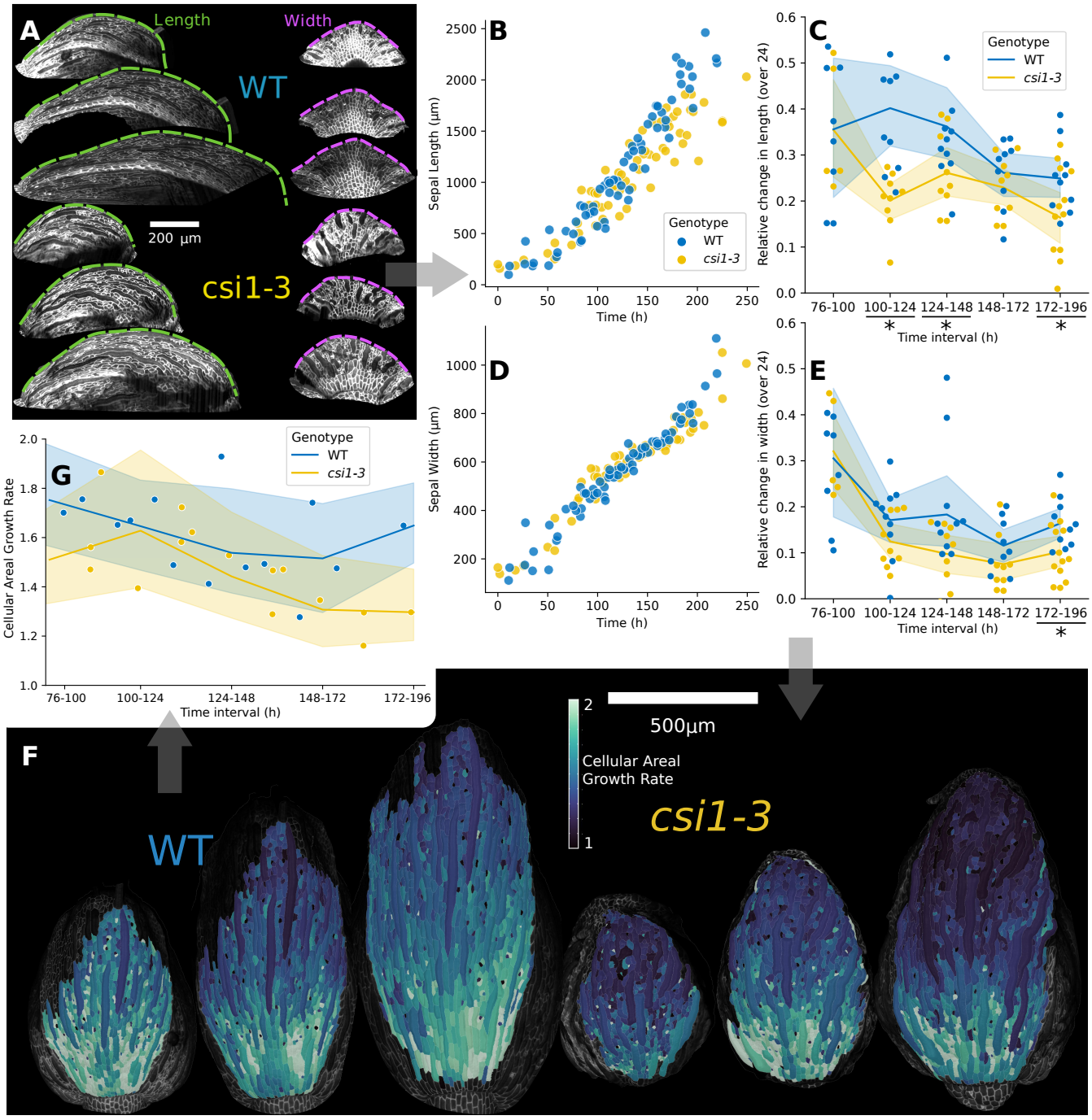

Fig. 2. *csi1* sepals have smaller elongation rates than WT at organ level, but cellular growth rates less different.
A. Representative time series of sepal growth in WT (top) and *csi1-3* (bottom). Cell membranes are labeled using a *pATML1::RCI2A-mCitrine* construct. Colored dashed lines indicate measured sepal length and width. Time between acquisitions = 24h. **B,D.** Sepal length (B) and width (D) as a function of time. Temporal sequences were registered with regard to time to define a common starting time using width, which can be mapped to developmental stages (see Supplementary Figure 2). **C,E.** Relative growth rates in length (C) and width (E) as a function of registered time. Comparisons were made over a sliding 24h window, which corresponds to the imaging interval. Asterisks at the bottom indicate significant differences (p-value of Mann-Whitney test <0.05). WT is in blue and *csi1-3* in yellow. The lines correspond to median, the shading to the interquartile range, and the points to individual sepals. **F.** Top view of representative time series, with cellular growth rate color-coded. Growth was calculated as the ratio of cell surface area between consecutive time points. The first sepals images are associated with the 100-124h interval. Time between acquisitions = 24h. The initial time point of each series was chosen so that sepals have similar width. **G.** Quantification of growth rates as a function of registered time, measured as shown in F. Time registration and symbols are the same as for panels B-E. (p-value of t-test between sepal medians: 0.1, 0.9, 0.5, 0.2 for time intervals 76h-100h, 100h-124h, 124h-148h, 148h-172, respectively. p-value of t-test between all cells of the sepals: 7×10^{-31}, 2×10^{-7}, 2×10^{-14}, 1×10^{-57} for the same time intervals).

yield longer sepals. Surprisingly, higher anisotropy of microfibrils arrangement in *csi1-3* is associated with shorter organs. We therefore analyzed the origin of the differences in elongation of *csi1-3* compared to WT.

To understand the differences in final length between WT and *csi1-3* sepals, we considered sepal morphogenesis and performed live imaging of developing sepals (Fig. 2A). As we used dissected inflorescences grown in vitro, we first checked whether our in vitro growth conditions produced similar organs compared to normally grown plants. We compared sepal length and width between inflorescences growing in the two conditions (Fig. 7A). We found that sepal dimensions are similar throughout development showing that in vitro conditions do not affect sepal morphogenesis. In order to compare developmental trajectories between the two genotypes, WT and *csi1-3*, we developed a common temporal frame for all sepals. Because width is similar between WT and *csi1-3* sepals at a given developmental stage (stage 12 in Fig. 1F; all stages in Fig. 7B), we used width to shift the time of each live imaging sequence and put all sepals into the same time frame, further referred to as registered time (Fig. 7C-F). The outcome is shown in Fig. 2B,D, with a common initial time (0h) that corresponds to stage 5 of flower development. We found that sepal growth can be approximately decomposed in two different phases. In the first, overall sepal growth is isotropic, with length and width increasing similarly, up to a size of about 500µm, corresponding to a time of about 75h in our registered time frame. Differences between WT and *csi1-3* are small in this isotropic growth phase. In the second phase, sepal growth is anisotropic and trajectories of WT and csi1-3 appear to diverge (Fig. 7A). We quantified the rate of increase in dimensions of WT and *csi1-3* sepals during this second phase. We found no differences concerning width except for the last time interval (Fig. 2E). Rate of increase in length is however smaller in *csi1-3* throughout development (Fig. 2C) showing that sepals from *csi1-3* plants are shorter because they elongate less compared to the WT all along the second phase of sepal morphogenesis, and not because of an early arrest of growth.

At cellular scale, neither growth rate nor growth anisotropy can explain differences in sepal elongation.

Next, we sought to understand the cellular basis of the differences in sepal elongation rates. We first focused on the simplest aspect of growth: cell areal growth rate. We imaged sepals in dissected inflorescences with cellular resolution, segmented and tracked over time the surface of outer epidermal cells from the times series of highest quality among those used for Fig. 2F (N=4 for WT and for *csi1-3*). We quantified cell areal growth rate as the ratio of area between two consecutive time points (if a cell has divided, we fuse the daughter cells to compute this ratio). We found cellular growth rates slightly higher in WT compared to *csi1-3* when looking at the whole sepal, which may explain the difference in final sepal area (Fig. 2G). We verified that the possible existence of a base-to-tip growth gradient does not affect this conclusion (Fig. 7G,H). However, these differences in cellular growth rates cannot explain the differences in the ratio of length to width observed for mature sepals. Other cellular parameters that could explain macroscopic differences are the main direction in which cells are growing (i.e. the direction of maximal growth), and how much they grow in this direction compared to the perpendicular direction (i.e. the direction of minimal growth), which is known as cell growth anisotropy.

Using the same live imaging data, we quantified cell growth anisotropy (Fig 3A). We found no differences between WT and *csi1-3* (Fig. 3B). This was unexpected considering that at organ scale sepals grow less anisotropically in *csi1-3* than in WT. In order to find the cause of organ scale differences, we then considered a remaining cellular parameter, the main direction of cell growth.

Spatial consistency of growth direction is lower in *csi1*.

We assessed spatial consistency by measuring the angle between the directions of maximal growth of all pairs of neighboring cells (Fig. 3C,D,E). If the angle is small, it means that the two cells grow in a similar direction. In order to assess the meaning of these values, we computed a theoretical maximum for this angle. When we assigned random orientations to cell growth on a sepal mesh, we found a median of 45° for the angle between growth directions of two cells. In live imaging data, we found that the median angle between the main growth directions of cells in *csi1-3* is higher compared to WT, 30° and 25°, respectively (Fig. 3F). These values are smaller than 45°, which means that there is some level of spatial consistency in the two genotypes, but with higher consistency for WT. Because the definition of cell growth direction is not meaningful in the case of cells with nearly isotropic growth, we also computed the same metrics for cells with a growth anisotropy higher than a threshold of 1.4 and ended up with the same conclusion (Fig. 8A). These results show that CSI1 plays a role in the consistency of growth direction. Cells growing in less consistent directions in *csi1-3*, compared to WT, may explain reduced elongation of *csi1-3* sepals. An outstanding discrepancy is that cellulose appears more aligned in *csi1-3* than in wild-type in AFM maps, whereas anisotropy of cell growth is unaffected. A possible explanation could be that AFM topography only detects the most recently deposited layer of cellulose microfibrils, while all the layers of the cell wall play a role in the control of growth anisotropy. We therefore assessed cellulose alignment over the entire thickness of the cell wall using Raman microspectroscopy.

Cellulose is less aligned at micrometric scale in *csi1* compared to WT.

Polarized Raman microspectroscopy is an imaging mode that provides spatial information on the molecular structure of the cell wall, including crystallinity and,

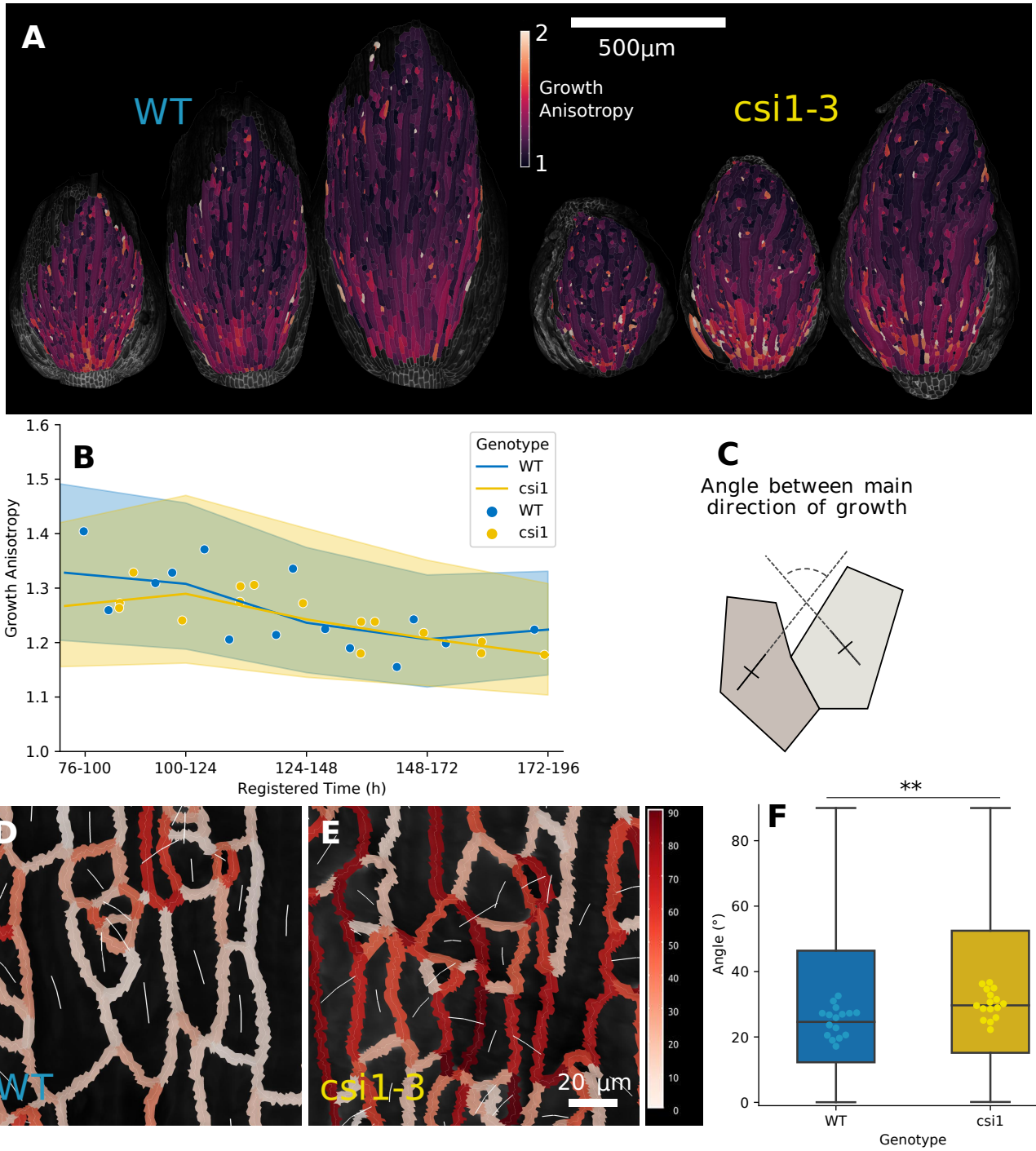

Fig. 3. Growth anisotropy is similar between *csi1* and WT, but spatial consistency of growth direction is affected in *csi1*
A. Representative time series, with cellular growth anisotropy color coded. Growth anisotropy was quantified on the basis of relative displacements of three-way wall junctions — a value of 1 means that growth is isotropic and the highest values of anisotropy are above 2 (the color scale was capped to 2 to avoid saturation). **B.** Quantification of cellular growth anisotropy as a function of registered time, corresponding to all times series as in A. WT is in blue and *csi1-3* in yellow. The lines correspond to median, the shading to the interquartile range, and the points to average values for individual sepals (four series for each genotype). (p-value of t-test between sepal medians: 0.2, 0.7, 0.9, 0.7 for time intervals 76h-100h, 100h-124h, 124h-148h, 148h-172, respectively. p-value of t-test between all cells of the sepals: 8×10^{-4}, 0.23, 0.08, 0.02 for the same time intervals) **C.** Schematic drawing explaining the quantification of spatial consistency of main growth direction shown in panels D and E. The angle is measured between the 3D vectors corresponding to the main growth directions of each pair of neighboring cells. **D,E.** Representative images of main growth direction (white lines, with line length proportional to cell growth anisotropy) and of angle between growth directions of pairs of neighboring cells visualized by the color of their common anticlinal wall (the red colorbar spans angles from 0 to 90°). **F.** Boxplots of the angle between main growth directions in neighboring cells. Box plots were constructed using all pairs of neighboring cells. Points represent the median angles for individual sepals. (Total number of pairs of cells analyzed = 30972, and 27853 for WT, *csi1-3*, respectively. p-value of t-test between every pair of cells = 10^{-88}. p-value of t-test between the median values for individual sepals = 0.002).

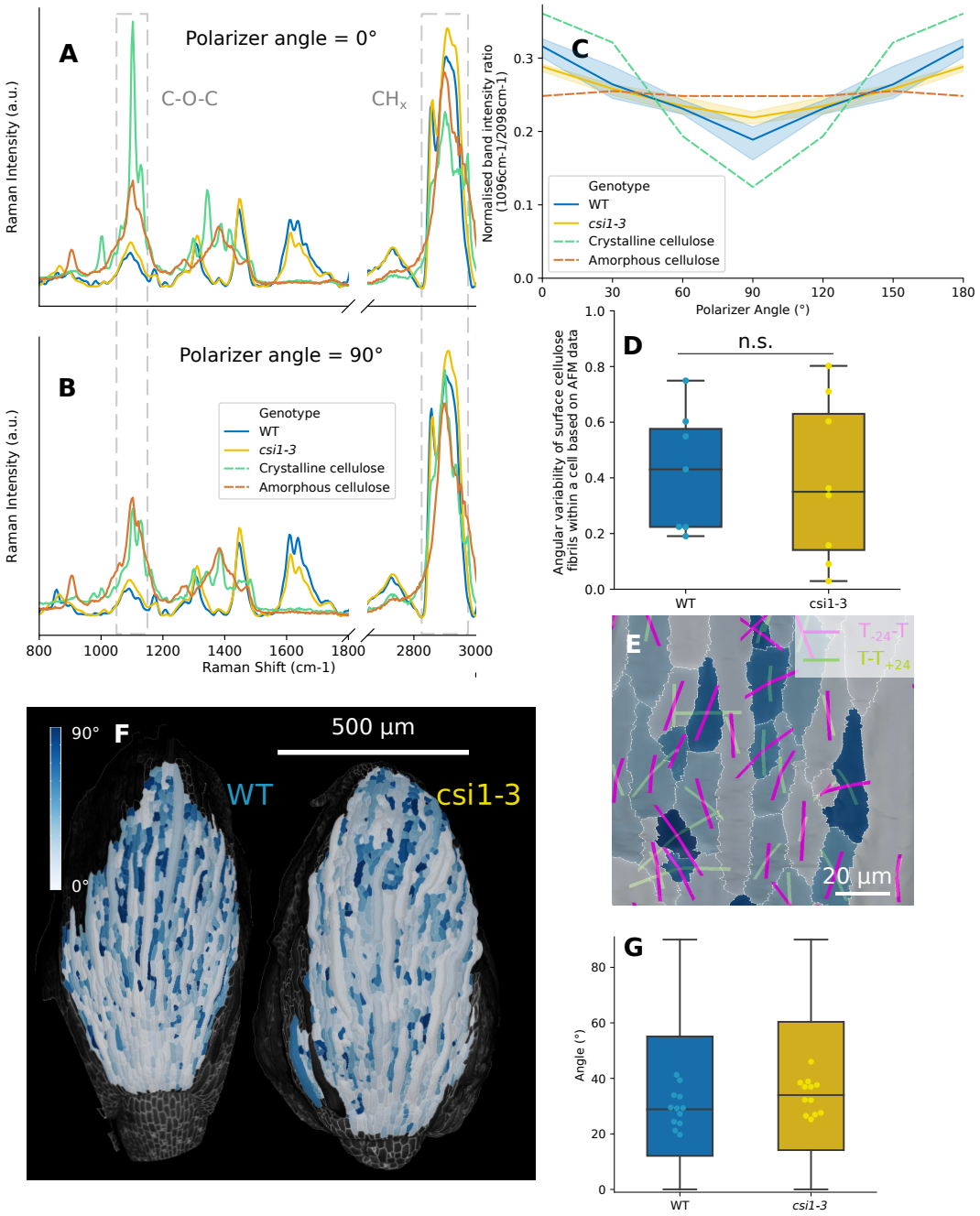

Fig. 4. Cellulose is less aligned at micrometric scale in *csi1* compared to WT, and growth direction is slightly less persistent in *csi1*
A-B. Representative Raman spectra of cell walls from WT and *csi1-3* sepals and purified extract of crystalline and amorphous cellulose collected at different polarization angles (here 0° is shown in panel A and 90° in panel B). Spectrum fragments include two cellulose-specific bands centered at 1096cm^{-1} (related to C-O-C linkage), and at 2898cm^{-1} (CH_x, x=1,2 linkages) **C.** Overall cellulose alignment in the outer epidermal cell walls assessed by ratio of integrated intensity changes from cellulose-specific bands accompanying polarizer angle changes in the 0-180° range. Analysis of WT and csi1 was compared with two reference samples: crystalline and amorphous cellulose. Each ratio value was normalized by the sum of all ratios for the sample to better illustrate the relative changes between samples. The values from 120° to 180° have been duplicated from the 0° to 60° values to show periodicity. The lines correspond to median, the shading to the interquartile range for sepals. (Total number of sepals analyzed = 4 for WT and *csi1-3*. p-values of t-test for each angle between WT and *csi1-3* = 0.02, 0.70, 0.69, 0.09 for angles 0°, 30°, 60° and 90°, respectively). **D.** Angular variability within a cell of the main cellulose microfibrils orientation on the wall surface facing the protoplast, computed on the basis of AFM maps. Angular variability is defined as the circular variance and is therefore bounded between 0 and 1. (Total number of sepals analyzed = 7 and 8, for WT and *csi1-3*, respectively. p-value of t-test between angular variability = 0.78). **E.** Illustration of the quantification shown in F G. Main growth directions of the cells are represented by magenta and green lines, corresponding to growth direction computed with the previous time point, and with the following, respectively. Cells are colored depending on the angle between growth directions at consecutive time intervals. Colorbar is the same as in F. **F.** Representative maps with cell color coded depending on the angle between growth directions at consecutive time intervals. **G.** Angle between growth directions at consecutive time intervals. Points represent the median angle for a given sepal. Box plots were constructed using all cells. (Total number of cells analyzed = 7533, and 7025 for WT, *csi1-3*, respectively. p-value of t-test between every cell = 10^{-14}. p-value of t-test between the median values for sepals = 0.1).

thanks to light polarization, main orientation of the functional groups of cell wall polymers [28, 29]. Cellulose that forms microfibrils is an example of such polarization-sensitive polymer. Thus, to assess the arrangement of cellulose, we compared the Raman spectra of outer cell walls of *csi1-3* and WT sepal epidermis to two reference samples composed of pure crystalline cellulose or pure amorphous cellulose (Fig. 4A,B Fig. 9A,B,C,D). We considered the integrated intensity ratio of two spectral bands: one centered at 1096cm^{-1} that is related to C-O-C linkages, and the other focused at 2898cm^{-1}, related to C-H and H-C-H linkages. If cellulose microfibrils are aligned, the signal intensity of these two bands is anticorrelated (one is maximal while the other is minimal, at the same polarizer angle) [30]. First, we found that for the crystalline cellulose the signal intensity ratio changes dramatically when the polarizer angle changes, as expected for a highly organized material, depicting a strongly anisotropic cellulose arrangement (Fig. 9A). We defined the 0° polarizer angle as that for which the signal of 1096cm^{-1} band attains a maximum value, and 90° as an angle of the minimal signal (Fig. 4A,B, Fig. 9A,B,C,D). Also as expected, amorphous cellulose presented no obvious maximum, but rather a constant signal intensity independent of the polarizer angle, indicating an isotropic material (Fig. 4C, Fig. 9D). In both WT and *csi1-3* changes in the signal ratio lie between the reference samples indicating an intermediate anisotropy of cellulose microfibrils arrangement (Fig. 4C). Furthermore, *csi1-3* cell wall is more similar to amorphous cellulose than WT cell wall (Fig. 4C). This indicates that, at micrometric scale, the arrangement of cellulose is less anisotropic in *csi1-3* sepals. Considering that microfibrils arrangement in recently deposited wall layers in *csi1-3* is more anisotropic than in WT, we interpreted the Raman results as an indication that either microfibrils orientation varies more along the cell wall or across cell wall thickness in the mutant. To test this hypothesis, we looked at variation along the surface of the cell wall in our AFM data. For cells that had several regions that were imaged with high cellulose microfibrils alignment, we measured the main microfibrils orientation on each map and quantified the circular variance associated with each cell (Fig. 4D). We found no significant differences between WT and *csi1-3*, favoring the hypothesis that the differences observed between the AFM and the Raman results come from variability of cellulose microfibrils orientation across the thickness of the wall. If microfibrils orientation across the cell wall layer kept changing in *csi1-3*, we would expect cell growth to be less persistent over time (cells can not maintain growth direction over a long period of time).

Cell capacity to maintain a growth direction over extended periods of time likely depends on how long they are able to keep a consistent reinforcement of their cell walls (dependent on orientation of cellulose microfibrils). To quantify persistence of growth directions, we projected cell growth directions at consecutive time intervals (computed from 3 consecutive segmented images) on the image corresponding to the intermediate image, and quantified the angle between the two vectors corresponding to the main growth direction (Fig. 4E,F,G, Fig. 9F). We found temporal variations of growth direction to be slightly higher in *csi1-3* compared to WT, with medians of 34° and 29°, respectively (see p-values in figure legend). Altogether, we concluded that CSI1 is required for temporal persistence and spatial consistency of growth direction. We further tested this conclusion by examining its potential consequences on cell arrangements and tissue mechanics in fully grown sepals.

Reduced spatial consistency in *csi1* is associated with snakey giant cells and reduced mechanical anisotropy at organ level.

At the scale of a few cells, we expected that mechanical conflicts generated by reduced spatial consistency (differences in growth direction between neighboring cells) in *csi1-3* affects cell shapes, as cells in a tissue are tightly connected through their cell walls. To test this prediction, we used a confocal microscope to image the cells of mature (fully grown) sepals in WT and *csi1-3* (Fig. 5A). The most striking phenotype is observed for giant cells that are approximately straight in WT and snakey in *csi1-3*. To quantify "snakeyness" we computed the ratio between the small side of the rectangle that wraps the cell and the radius of the cell (Fig. 5B). Cells that are straight will present similar values for these two parameters while snakey cells will have the small side of the rectangle bigger than cell radius. We found that giant cells from csi1-3 sepals were indeed more snakey compared to WT (Fig. 5C). Both the absence of spatial consistency and the lack of temporal persistence could explain this phenotype. Because cells are growing in more variable directions with respect to each other in *csi1-3*, cells on one side of a giant cell could grow perpendicularly to the axis of the giant cell while cells on the other side could grow parallel to this axis, leading to the snakey phenotype. At macroscopic scale, we expected that reduced spatial consistency and temporal persistence in *csi1-3* yields less consistent orientation of cellulose microfibrils along mature sepal than in WT and thus decreases the mechanical anisotropy of the whole sepal. To quantify sepal mechanical anisotropy, we assessed shrinkage of the whole sepal upon osmotic treatment [24] and determined sepal shape parameters with our imaging pipeline (Fig. 5D). We measured shrinkage on a length-width axis and shrinkage anisotropy defined as the ratio of shrinkage in length to shrinkage in width (Fig S5A,B,C). We found significant differences in the shrinkage in width (Fig. 10C) but no differences in the shrinkage in length (Fig. 10B). We performed independent measurements of the mechanical properties in length via tensile testing [31], which agreed with the results of osmotic treatments for

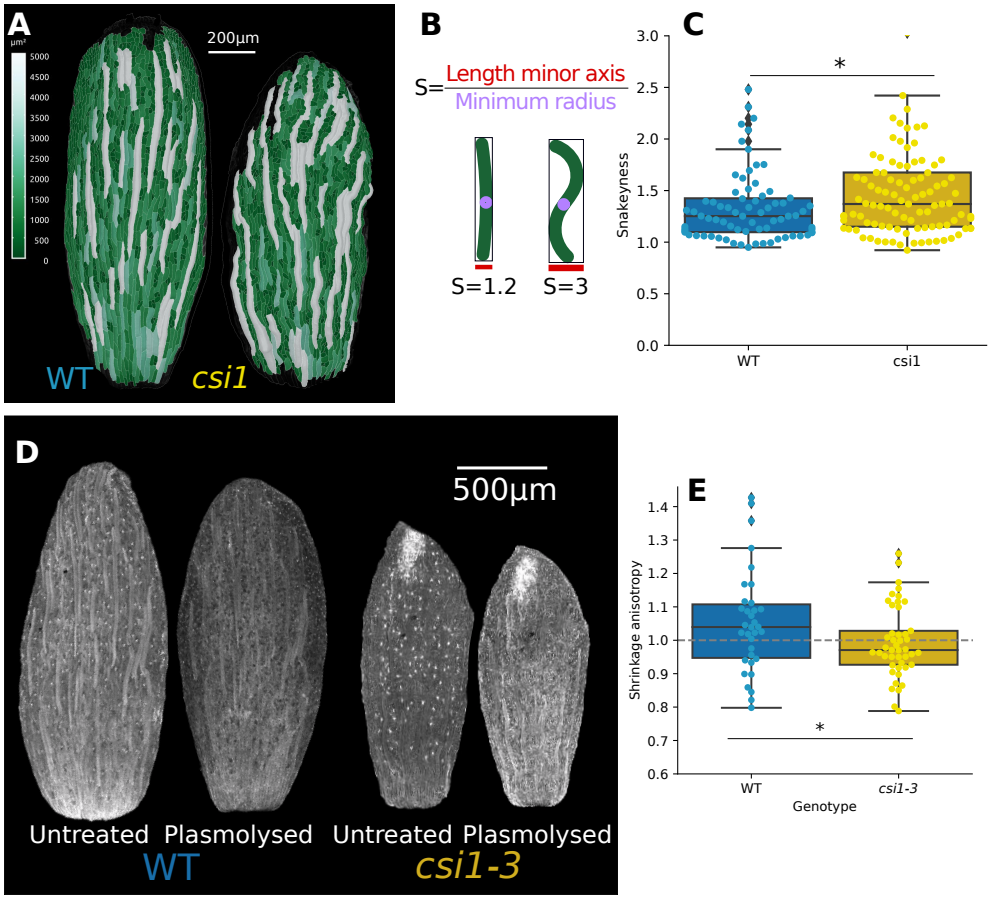

Fig. 5. In *csi1*, giant cells are snakey and sepal mechanical anisotropy is reduced
A. Representative confocal images of cells of WT and *csi1-3* mature sepal. Cell area is color coded. **B.** Illustration of the quantification of snake-yness. C. Box plot of the quantification of cell snakeyness (Total number of cells analyzed = 75 from 4 WT sepals, 101 from 5 *csi1-3* sepals, p-value of t-test = 0.04) **D.** Representative front view of sepals before and after plasmolysis in 0.4M NaCl for 1h. **E.** Box plot of anisotropy of sepal shrinkage upon osmotic treatment. Points represent individual sepals (n = 34 for WT, 45 for *csi1-3*, p value of t-test = 0.04).

the same magnitudes of strain (Fig. 10D). Consequently, csi1-3 shrinks less anisotropically than WT (Fig. 5E), in agreement with expectations.

Discussion

We investigated the link between sepal morphogenesis and the guidance of cellulose synthases by microtubules using the *csi1* mutant. We found that, despite increased anisotropic arrangement of recently deposited cellulose microfibrils, sepals are less elongated in the *csi1* mutant. This could not be ascribed to cell growth anisotropy which is comparable between *csi1* and wild-type (WT). However, we found that growth directions in *csi1* cells are temporally slightly less persistent and spatially less consistent than in WT. This lack of consistency in *csi1* explains shorter sepals and leads to snakey cells and to mechanically less anisotropic organs.

While cellulose microfibrils in *csi1* hypocotyls appear highly aligned [32], we observed that they were not as strongly aligned in *csi1* sepals (Fig. 1). In the absence of guidance by cortical microtubules, cellulose synthases (CESA) were observed to either follow previous microfibrils or to move along a straight line [23, 33]. The relative weight of these modes of CESA motion may depend on the organ, potentially explaining differences in the *csi1* phenotype between hypocotyl and sepal, possibly due to different proteomes between the two types of organs[34]. In addition, other matrix polysaccharides are also likely involved in guidance of CESA[35–37].

Here, we found that guidance of CESA by microtubules does not influence the degree of growth anisotropy but rather growth direction. Disruption of guidance increased spatial and temporal variations of growth direction. As proposed in Chan et al. [23], synthesis along previous fibrils could provide memory of the wall state and help resisting perturbations by forming a template for when cellulose synthesis starts again [38–40], whereas guidance by microtubules provides the control needed for morphogenetic events [41] or to keep track of an organ level direction. Similar ideas might extend to extracellular matrix in animals, with regimes in which direction of matrix synthesis is steady [42], and regimes associated with morphogenetic events [43, 44].

How cells in a tissue all align in the same direction has been partly elucidated in animals. Cell polarity may be oriented by an instructive signal formed by a large-scale gradient or by polarity of neighboring cells via surface proteins [45, 46]. Similar ideas have been proposed for plants [45, 47], in which the coupling between polarities of neighboring cells would involve a large set of actors [48]. Although CSI1 could have other functions than guidance, our work suggests that CSI1 contributes to growth coor-

dination by translating cell polarity into growth direction, through CESA guidance by microtubules. Whereas we did not observe any twisting phenotype in sepal, *csi1* mutation leads to twisting of other organs such as the leaf [49, 50], hypocotyl or shoot [51]. Instead, *csi1* sepal featured snakey cells. Interestingly, Drosophila mutant oocytes with deficient polarity also show snakey cell files [52]. Organ twisting and cell snakyness could be interpreted as impaired orientation by large-scale instructive signals.

Plant hormones are good candidates for such organ-level signals. In particular, auxin presents gradients and its movement is polarly facilitated by PIN proteins [53], notably in lateral organs such as the leaf [54]. PIN1 polarity is coupled with microtubule orientation [55], supporting a potential role for auxin in orienting cell growth direction. Indeed, sepals with affected auxin polarity displayed reduced length [56], although it is unclear whether this involves lack of consistency of growth direction. Mechanical stress is another potential organ-level instructive signal, and studies in animals suggest that it may orient cell polarity [57, 58]. In plants, microtubules align with maximal stress direction [59, 60], which explains the transverse orientations of microtubules seen in sepal [61].

Here, we propose that the main role in organ morphogenesis of guidance of CESA by microtubules is to enable growth direction to follow large scale signals. Interestingly, chemical perturbation of the consistency of cortical microtubules orientation in the root reduces overall organ elongation [62]. We extend these results by describing consistency of cell growth direction and pinpoint the role of CSI1 in consistency. It would be worthwhile to examine whether similar ideas apply to elongation of animal organs. For instance, cell division is oriented during limb bud elongation in the mouse [63], but the spatial consistency of divisions has not been assessed. Altogether, our work illustrates the potential in deciphering the basis of the robustness of morphogenesis by assessing spatial and temporal variability of growth and of its regulators, from subcellular to organ scale.

ACKNOWLEDGMENTS. We acknowledge the contribution of SFR Biosciences (UAR3444/CNRS, US8/Inserm, ENS de Lyon, UCBL) imaging facility, PLATIM / Lymic. We acknowledge A. Lacroix, J. Berger, P. Bolland, H. Leyral and I. Desbouchages for assistance with plant growth and logistics. We thank Mathilde Dumond and Justine Chabredier for the initial exploration of the csi1 phenotype. We thank Olivier Hamant, Adrienne Roeder, and Christophe Tréhin for fruitful discussions and suggestions. We thank Yoshiharu Nishiyama for the generous gift of reference cellulose samples. This work was funded by the French National Research Agency (ANR, grant ANR-17-CAPS-0002-01 V-Morph, to AB) the National Science Centre, Poland (NCN, grant 2017/24/Z/NZ3/00548, to DK), and the German Research Foundation (DFG, grant 355722357, to RS) through a European ERA-NET Coordinating Action in Plant Sciences (ERA-CAPS) grant. This work was also directly funded by the French National Research Agency (ANR, grant ANR-17-CE20-0023-02 WALLMIME, to AB) and by the National Science Centre, Poland (SHENG1 grant 2018/30/Q/00189, to DBW).

Materials and methods

Experimental model and subject details.

Arabidopsis thaliana plant lines used for live imaging and analysis of mature sepal cell shape were pAR169 (ATML1p::mCirtrine-RCI2A,[26]) and *csi1-3* x pAR169. In all other cases the plants used were Col-0, *csi1-3* (SALK_138584,64), *csi1-6* (SALK_115451,[64]). All lines had a Col-0 background. Plants were grown on soil at 22°C in culture rooms with long day conditions (16 h light/8 h darkness). For in vivo imaging, inflorescences were cut off from the plants, dissected up to the desired bud (all buds used in this study were comprised between the 10th and 20th organ initiated along the inflorescence [24]) and grown into apex culture medium plates [65] supplemented by 0.1% V/V plant preservative mixture (PPM; Plant Cell Tech). Plates were then stored in growth cabinets with the same lighting/temperature conditions as in culture rooms.

Method details.

Confocal imaging and analysis. Whole sepal images were collected using a LSM700 confocal microscope (Zeiss, Germany) equipped with a 5x air objective (NA = 0.25). Propidium iodide (PI) was excited using a 555 nm laser and the emitted light filtered through a 560-630 band pass filter.

Live-imaging images were collected using a SP8 confocal microscope (Leica Microsystems, Germany) equipped with a 25× long-distance water objective (NA = 0.95). mCitrine was excited using a 514 nm laser and the emitted light filtered through a 520-550nm band pass filter.

Samples used for whole sepal measurements were stained in PI at 100µM final concentration in water for 15 minutes prior to imaging. Sepals used for osmotic treatments were then plasmolysed for 1h in 0.4M NaCl solution supplemented with PI at 100µM.

Whole sepal measurements were performed following [66]. Quantification of macroscopic growth rates was done by measuring manually sepal curved length and width using oriented images in ImageJ. Live imaging data was analyzed using MorphoGraphX [67], which included segmentation, lineage tracking and computation of the cell areas and principal direction of growth. Principal growth directions of each cell were computed based on the relative displacement of three-way cell junctions between consecutive imaging time points. Growth anisotropy was then calculated as the ratio between magnitudes associated with the maximum and minimum principal directions of growth.

Atomic Force Microscopy (AFM) and quantification of cellulose microfibrils arrangement on protoplast-facing wall surface. Samples of recently formed cell wall surface (i.e. the protoplast-facing surface) were prepared for AFM measurements using a modified protocol of Wuyts et al. [68]. Briefly, the sepals were plasmolysed in 0.4 M NaCl for 10 min and fixed in 70% ethanol (first kept under vacuum for 1 h at

room temperature, next fixed for at least 24 h at 4°C). Afterwards they were treated with absolute chloroform for 10 min (to remove membranes and cuticle), rehydrated in decreasing ethanol series (70%, 50%, 30%) followed by deionized water (5 min in each medium), placed in protoplast lysis buffer of sodium dodecyl sulfate and sodium hydroxide (1% SDS in 0.2M NaOH) for 3 h, treated with 0.01% -amylase (Sigma-Aldrich; from *Bacillus licheniformis*) in PBS (Phosphate Buffered Saline) (pH 7.0) in 37°C overnight (to remove residual starch), moved to over-saturated water solution of chloral hydrate (200 g / 50 ml) for 4 h (to remove protoplast remnants), and rinsed in water (3 x 15 min). Superficial cell walls of the abaxial epidermis were then gently peeled off from the sepal and placed on the glass slide such that the protoplast facing wall surface was exposed. In order to better visualize the cellulose microfibrils in some samples, pectins were removed by treatment with 2% pectinase (Serva, Heidelberg, FRG; from *Aspergillus niger*) in sodium-phosphate buffer (pH 5.7) at room temperature for 30 min, or the buffer alone. The samples were then rinsed in water and dried at room temperature, during which the wall became attached to the glass slide by adhesion. Atomic Force Microscopy (AFM) measurements were performed with a NanoWizard®3 BioScience (JPK Instruments, Berlin, Germany) operating in intermittent contact mode, using HQ:NSC15 rectangular Si cantilevers (MicroMasch, Estonia) with spring constant specified as 40 N/m, cantilever resonant frequency of about 325 kHz, and tip radius 8 nm. All scans were conducted in air in laboratory conditions (22°C, constant humidity of 45%). Images were obtained using the JPK Data Processing software (JPK Instruments). Anisotropy of cellulose microfibrils arrangement was assessed for square regions (400 nm x 400 nm) with distinct microfibrils chosen from measured height images of 2 m x 2 m AFM scans (2-4 regions per scan). Histogram of microfibrils orientation was obtained for each region using Directionality tool (https://imagej.github.io/plugins/directionality) of Fiji (Fourier components method). In the Directionality tool, alignment is assessed for a single curve fitted to the highest peak while in most cell wall regions the distribution of microfibrils orientation was multimodal. Thus, we a developed a bespoke protocol written in Matlab (Mathworks, Nattick, MA, USA) to quantify microfibrils arrangement using the following steps: (i) smooth the histogram by a moving average; (ii) obtain a series of least square approximations of the histogram by a sum of an increasing number of Gaussian models (up to 8); (iii) choose the approximation with the lowest number of Gaussians with adjusted R^2>0.94; (iv) exclude Gaussians with half-width bigger than 180°; (v) concatenate Gaussians with peaks separated by less than 10°; (vi) exclude Gaussians with height smaller than ¼ of the highest peak; (vii) compute the alignment index as the maximal angular distance between the remaining Gaussian peaks. We examined both giant and non-giant epidermal cells of sepals (5 sepals in WT; 6 in *csi1-3*) from stage 12 flowers. In WT we obtained 16 AFM maps from 9 cells, in *csi1-3* - 32 maps from 14 cells. Angular variability was computed on cells on which at least three AFM regions with alignment index greater than 140° were obtained. Angles were periodised and circular variability was measured using the asotropy package [69, 70].

Raman spectroscopy. Sample preparation for Raman microspectroscopy followed the AFM protocol up to the treatment with chloral hydrate and rinsing in water [**?**]. Such prepared sepals were put on glass slides (1 mm thick), immersed in pure deionized water to preserve environmental conditions, and covered by CaF_2 0.15-0.18 mm thick coverslips (CAMS1602, Laser Optex).

Raman data were collected using WITec confocal Raman microscope CRM alpha 300R, equipped with an air-cooled solid-state laser (λ = 532 nm), an thermoelectrically cooled CCD camera, and Zeiss C-Apochromat (100x/1.25 NA) water immersion objective. The excitation laser radiation was coupled to the microscope through a single-mode optical fiber (50 µm diameter). Raman scattered light was focused onto a multi-mode fiber (50 µm diameter) and monochromator with a 600 line mm^{-1} grating. The spectrometer monochromator was calibrated using the emission of a Ne lamp, while the signal of a silicon plate (520.7 cm^{-1}) was used for checking beam alignment.

Surface Raman imaging was applied to differentiate the signal of the cuticular ridges and cell wall. Data were collected in a central fragment of the cell in a 10 m×10 m area using 30 × 30 pixels (=900 spectra) and an integration time of 40 ms per spectrum. The precision of the horizontal movement of the sample during measurements was ± 0.2 m. The lateral resolution (LR) was estimated according to the Rayleigh criterion LR = 0.61λ/NA as LR = 427 nm. All spectra obtained during Raman imaging were collected in the 120 - 4000 cm^{-1} range with a resolution of 3 cm^{-1} and at 30 mW on the sample.

The output data were processed by performing a baseline correction using an autopolynomial function of degree 3, submitted to an automatic cosmic rays removal procedure by comparing each pixel (i.e. each CCD count value at each wavenumber) to its adjacent pixels and finally smoothed by Savitzky–Golay filter. Chemical images were generated using cluster analysis (CA). K-means approach with the Manhattan distance for all Raman imaging maps was carried out to distinguish signal of cuticular ridges and cell wall. Every spectrum obtained from the clustering analysis was normalized by dividing by its total area using WITec Project Five Plus software. The procedure was repeated for ten non-giant pavement cells located in the basal half of different sepals.

Every time data were gathered for 13 consecutive orientations of the polarization plane (the angular range 0-180°), each rotated by 15°. From such obtained set of 13 averaged spectra after the K-means cluster analysis, the spectrum with maximal signal intensity of the C-O-C band (1096 cm^{-1}) was chosen to represent angular position 0°, while the other spectra represent angle-dependent integrated intensity alteration with minimum at 90°. Once positions of the two angular extrema were recognized, the 4 spectra (every 30° from 0° to 90°) were used for further analysis. For each spectrum the spectral parameters like band position, full width at half maximum, intensity and integrated intensity were determined by deconvolution of the spectra through the peak fitting procedure facilitated by GRAMS/AI 9.2 software. For each spectrum, the Voigt function with the minimum number of the components was used to reproduce the experimentally observed band arrangement. The applied procedure allows one to separate cellulose-specific bands, e.g. 1096 cm^{-1} (C-O-C) and 2898 cm^{-1} (CHx, x=1,2) from non-cellulose bands originating from other

polysaccharides present in the cell wall. Finally, the ratio of integrated intensity around the C-O-C and CHx bands was calculated to follow the angle-dependent character of the sample and estimate the extent of cellulose microfibrils ordering. The ratio of integrated intensity values estimated for those two regions was calculated for different polarizer angles (every 30° from 0° to 90°) and normalized by the sum of the four values.

Data from WT and *csi1-3* mutant were compared with purified reference samples of crystalline (*Halocynthia roretzi*) and amorphous (DMAc/LiCl) cellulose[71].

Extensometry. Sepal extensometry and analysis was performed according to Majda et al. [31].

Quantifications and Statistical Analysis.

Analysis and statistical testing were performed with custom made python scripts. Statistical testing was performed using the scipy.stats library[72].

To obtain a default value of spatial consistency, we computed the median angle between neighboring cells in a sepal, ascribing a random orientation to each cell. Indeed, the maximal angle between two cells is 90°, but three neighboring cells cannot all be oriented at 90° to each other. Here, we used one example of segmented sepal mesh and we replaced growth direction with a random vector that is tangential to the surface of the epidermis because we are only considering growth of the sepal outer surface. In practice, the random vector was drawn on the plane best-fitting centroids of neighboring cells. We then applied the same pipeline used for the quantification of spatial consistency of growth direction.

Data and Code Availability.

All data and scripts will be made available with the final version of the article.

References

[1] M. Rauzi, P. Verant, T. Lecuit, and P.-F. Lenne, "Nature and anisotropy of cortical forces orienting Drosophila tissue morphogenesis," *Nature Cell Biology*, vol. 10, pp. 1401–1410, Dec. 2008. Number: 12 Publisher: Nature Publishing Group.

[2] C. Bertet, L. Sulak, and T. Lecuit, "Myosin-dependent junction remodelling controls planar cell intercalation and axis elongation," *Nature*, vol. 429, pp. 667–671, June 2004. Number: 6992 Publisher: Nature Publishing Group.

[3] A. Umeda and K. Amako, "Growth of the Surface of Corynebacterium diphtheriae," *Microbiology and Immunology*, vol. 27, no. 8, pp. 663–671, 1983. _eprint: https://onlinelibrary.wiley.com/doi/pdf/10.1111/j.1348-0421.1983.tb00629.x.

[4] A. Peaucelle, R. Wightman, and H. Höfte, "The Control of Growth Symmetry Breaking in the Arabidopsis Hypocotyl," *Current biology: CB*, vol. 25, pp. 1746–1752, June 2015.

[5] F. Bou Daher, Y. Chen, B. Bozorg, J. Clough, H. Jönsson, and S. A. Braybrook, "Anisotropic growth is achieved through the additive mechanical effect of material anisotropy and elastic asymmetry," *eLife*, vol. 7, p. e38161, Sept. 2018. Publisher: eLife Sciences Publications, Ltd.

[6] A. Singh, T. Saha, I. Begemann, A. Ricker, H. Nüsse, O. Thorn-Seshold, J. Klingauf, M. Galic, and M. Matis, "Polarized microtubule dynamics directs cell mechanics and coordinates forces during epithelial morphogenesis," *Nature Cell Biology*, vol. 20, pp. 1126–1133, Oct. 2018.

[7] S. L. Haigo and D. Bilder, "Global Tissue Revolutions in a Morphogenetic Movement Controlling Elongation," *Science*, vol. 331, pp. 1071–1074, Feb. 2011. Publisher: American Association for the Advancement of Science.

[8] A. J. Isabella and S. Horne-Badovinac, "Rab10-Mediated Secretion Synergizes with Tissue Movement to Build a Polarized Basement Membrane Architecture for Organ Morphogenesis," *Developmental Cell*, vol. 38, pp. 47–60, July 2016.

[9] A. L. Zajac and S. Horne-Badovinac, "Kinesin-directed secretion of basement membrane proteins to a subdomain of the basolateral surface in Drosophila epithelial cells," *Current Biology*, vol. 32, pp. 735–748.e10, Feb. 2022.

[10] C. L. White and J. W. Gober, "MreB: pilot or passenger of cell wall synthesis?," *Trends in Microbiology*, vol. 20, pp. 74–79, Feb. 2012. Publisher: Elsevier.

[11] J. Chlasta, P. Milani, G. Runel, J.-L. Duteyrat, L. Arias, L.-A. Lamiré, A. Boudaoud, and M. Grammont, "Variations in basement membrane mechanics are linked to epithelial morphogenesis," *Development*, vol. 144, pp. 4350–4362, Dec. 2017.

[12] P. B. Green, "Mechanism for Plant Cellular Morphogenesis," *Science*, vol. 138, pp. 1404–1405, Dec. 1962. Publisher: American Association for the Advancement of Science.

[13] D. Suslov and J.-P. Verbelen, "Cellulose orientation determines mechanical anisotropy in onion epidermis cell walls," *Journal of Experimental Botany*, vol. 57, pp. 2183–2192, July 2006. Publisher: Oxford Academic.

[14] T. I. Baskin, "ANISOTROPIC EXPANSION OF THE PLANT CELL WALL," *Annual Review of Cell and Developmental Biology*, vol. 21, pp. 203–222, Nov. 2005.

[15] N. Mansoori, J. Timmers, T. Desprez, C. L. A. Kamei, D. C. T. Dees, J.-P. Vincken, R. G. F. Visser, H. Höfte, S. Vernhettes, and L. M. Trindade, "KORRIGAN1 Interacts Specifically with Integral Components of the Cellulose Synthase Machinery," *PLOS ONE*, vol. 9, p. e112387, Nov. 2014. Publisher: Public Library of Science.

[16] S. Robert, A. Bichet, O. Grandjean, D. Kierzkowski, B. Satiat-Jeunemaître, S. Pelletier, M.-T. Hauser, H. Höfte, and S. Vernhettes, "An Arabidopsis Endo-1,4--d-Glucanase Involved in Cellulose Synthesis Undergoes Regulated Intracellular Cycling[W]," *The Plant Cell*, vol. 17, pp. 3378–3389, Dec. 2005.

[17] A. Endler, C. Kesten, R. Schneider, Y. Zhang, A. Ivakov, A. Froehlich, N. Funke, and S. Persson, "A Mechanism for Sustained Cellulose Synthesis during Salt Stress," *Cell*, vol. 162, pp. 1353–1364, Sept. 2015.

[18] Y. Gu, N. Kaplinsky, M. Bringmann, A. Cobb, A. Carroll, A. Sampathkumar, T. I. Baskin, S. Persson, and C. R. Somerville, "Identification of a cellulose synthase-associated protein required for cellulose biosynthesis," *Proceedings of the National Academy of Sciences of the United States of America*, vol. 107, pp. 12866–12871, July 2010.

[19] M. Bringmann, E. Li, A. Sampathkumar, T. Kocabek, M.-T. Hauser, and S. Persson, "POM-POM2/CELLULOSE SYNTHASE INTERACTING1 Is Essential for the Functional Association of Cellulose Synthase and Microtubules in Arabidopsis," *The Plant Cell*, vol. 24, pp. 163–177, Jan. 2012. Publisher: American Society of Plant Biologists Section: Research Article.

[20] S. Li, L. Lei, C. R. Somerville, and Y. Gu, "Cellulose synthase interactive protein 1 (CSI1) links microtubules and cellulose synthase complexes," *Proceedings of the National Academy of Sciences*, vol. 109, pp. 185–190, Jan. 2012. Publisher: National Academy of Sciences Section: Biological Sciences.

[21] L. Lei, S. Li, J. Du, L. Bashline, and Y. Gu, "CELLULOSE SYNTHASE INTERACTIVE3 Regulates Cellulose Biosynthesis in Both a Microtubule-Dependent and Microtubule-Independent Manner in Arabidopsis[C][W]," *The Plant Cell*, vol. 25, pp. 4912–4923, Dec. 2013. Number: 12.

[22] X. Xin, L. Lei, Y. Zheng, T. Zhang, S. V. Pingali, H. O'Neill, D. Cosgrove, S. Li, and Y. Gu, "CELLULOSE SYNTHASE INTERACTIVE1- and Microtubule-Dependent Cell Wall Architecture Is Required for Acid Growth in Arabidopsis Hypocotyls," preprint, Plant Biology, July 2019.

[23] J. Chan and E. Coen, "Interaction between Autonomous and Microtubule Guidance Systems Controls Cellulose Synthase Trajectories," *Current Biology*, vol. 30, pp. 941–947.e2, Mar. 2020.

[24] L. Hong, M. Dumond, S. Tsugawa, A. Sapala, A.-L. Routier-Kierzkowska, Y. Zhou, C. Chen, A. Kiss, M. Zhu, O. Hamant, R. Smith, T. Komatsuzaki, C.-B. Li, A. Boudaoud, and A. Roeder, "Variable Cell Growth Yields Reproducible Organ Development through Spatiotemporal Averaging," *Developmental Cell*, vol. 38, pp. 15–32, July 2016.

[25] H. M. Meyer, J. Teles, P. Formosa-Jordan, Y. Refahi, R. San-Bento, G. Ingram, H. Jönsson, J. C. W. Locke, and A. H. K. Roeder, "Fluctuations of the transcription factor ATML1 generate the pattern of giant cells in the Arabidopsis sepal," *eLife*, vol. 6, p. e19131, Feb. 2017. Publisher: eLife Sciences Publications, Ltd.

[26] A. H. K. Roeder, V. Chickarmane, A. Cunha, B. Obara, B. S. Manjunath, and E. M. Meyerowitz, "Variability in the Control of Cell Division Underlies Sepal Epidermal Patterning in Arabidopsis thaliana," *PLoS Biology*, vol. 8, p. e1000367, May 2010.

[27] S. J. Hanley, J. Giasson, J.-F. Revol, and D. G. Gray, "Atomic force microscopy of cellulose microfibrils: comparison with transmission electron microscopy," *Polymer*, vol. 33, pp. 4639–4642, Jan. 1992.

[28] N. Gierlinger, S. Luss, C. König, J. Konnerth, M. Eder, and P. Fratzl, "Cellulose microfibril orientation of Picea abies and its variability at the micron-level determined by Raman imaging," *Journal of Experimental Botany*, vol. 61, pp. 587–595, Jan. 2010.

[29] D. Borowska-Wykręt and M. Dulski, "Raman Spectroscopy in Nonwoody Plants," in *Plant Cell Morphogenesis: Methods and Protocols* (F. Cvrčková and V. Žárský, eds.), Methods in Molecular Biology, pp. 83–107, New York, NY: Springer, 2019.

[30] N. Gierlinger, C. Reisecker, S. Hild, and S. Gamsjaeger, "CHAPTER 7:Raman Microscopy: Insights into the Chemistry and Structure of Biological Materials," in *Materials Design Inspired by Nature*, pp. 151–179, May 2013.

[31] M. Majda, N. Trozzi, G. Mosca, and R. S. Smith, "How Cell Geometry and Cellular Patterning Influence Tissue Stiffness," *International Journal of Molecular Sciences*, vol. 23, p. 5651, Jan. 2022. Number: 10 Publisher: Multidisciplinary Digital Publishing Institute.

[32] X. Xin, L. Lei, Y. Zheng, T. Zhang, S. V. Pingali, H. O'Neill, D. J. Cosgrove, S. Li, and Y. Gu, "Cellulose synthase interactive1- and microtubule-dependent cell wall architecture is required for acid growth in Arabidopsis hypocotyls," *Journal of Experimental Botany*, vol. 71, pp. 2982–2994, May 2020.

[33] S. G. Duncombe, S. G. Chethan, and C. T. Anderson, "Super-resolution imaging illuminates new dynamic behaviors of cellulose synthase," *The Plant Cell*, vol. 34, pp. 273–286, Jan. 2022.

[34] J. Mergner, M. Frejno, M. List, M. Papacek, X. Chen, A. Chaudhary, P. Samaras, S. Richter, H. Shikata, M. Messerer, D. Lang, S. Altmann, P. Cyprys, D. P. Zolg, T. Mathieson, M. Bantscheff, R. R. Hazarika, T. Schmidt, C. Dawid, A. Dunkel, T. Hofmann, S. Sprunck, P. Falter-Braun, F. Johannes, K. F. X. Mayer, G. Jürgens, M. Wilhelm, J. Baumbach, E. Grill, K. Schneitz, C. Schwechheimer, and B. Kuster, "Mass-spectrometry-based draft of the Arabidopsis proteome," *Nature*, vol. 579, pp. 409–414, Mar. 2020. Number: 7799 Publisher: Nature Publishing Group.

[35] A. Yoneda, T. Higaki, N. Kutsuna, Y. Kondo, H. Osada, S. Hasezawa, and M. Matsui, "Chemical Genetic Screening Identifies a Novel Inhibitor of Parallel Alignment of Cortical Microtubules and Cellulose Microfibrils," *Plant and Cell Physiology*, vol. 48, pp. 1393–1403, Oct. 2007.

[36] A. Yoneda, T. Ito, T. Higaki, N. Kutsuna, T. Saito, T. Ishimizu, H. Osada, S. Hasezawa, M. Matsui, and

T. Demura, "Cobtorin target analysis reveals that pectin functions in the deposition of cellulose microfibrils in parallel with cortical microtubules," *The Plant Journal*, vol. 64, no. 4, pp. 657–667, 2010. _eprint: https://onlinelibrary.wiley.com/doi/pdf/10.1111/j.1365-313X.2010.04356.x.

[37] C. Xiao, T. Zhang, Y. Zheng, D. J. Cosgrove, and C. T. Anderson, "Xyloglucan Deficiency Disrupts Microtubule Stability and Cellulose Biosynthesis in Arabidopsis, Altering Cell Growth and Morphogenesis1[OPEN]," *Plant Physiology*, vol. 170, pp. 234–249, Jan. 2016.

[38] R. Himmelspach, R. E. Williamson, and G. O. Wasteneys, "Cellulose microfibril alignment recovers from DCB-induced disruption despite microtubule disorganization," *The Plant Journal*, vol. 36, no. 4, pp. 565–575, 2003. _eprint: https://onlinelibrary.wiley.com/doi/pdf/10.1046/j.1365-313X.2003.01906.x.

[39] Z. Liu, R. Schneider, C. Kesten, Y. Zhang, M. Somssich, Y. Zhang, A. R. Fernie, and S. Persson, "Cellulose-Microtubule Uncoupling Proteins Prevent Lateral Displacement of Microtubules during Cellulose Synthesis in Arabidopsis," *Developmental Cell*, vol. 38, pp. 305–315, Aug. 2016.

[40] A. Endler, C. Kesten, R. Schneider, Y. Zhang, A. Ivakov, A. Froehlich, N. Funke, and S. Persson, "A Mechanism for Sustained Cellulose Synthesis during Salt Stress," *Cell*, vol. 162, pp. 1353–1364, Sept. 2015.

[41] M. Sassi, O. Ali, F. Boudon, G. Cloarec, U. Abad, C. Cellier, X. Chen, B. Gilles, P. Milani, J. Friml, T. Vernoux, C. Godin, O. Hamant, and J. Traas, "An Auxin-Mediated Shift toward Growth Isotropy Promotes Organ Formation at the Shoot Meristem in Arabidopsis," *Current Biology*, vol. 24, pp. 2335–2342, Oct. 2014.

[42] Y. Matsubayashi, B. J. Sánchez-Sánchez, S. Marcotti, E. Serna-Morales, A. Dragu, M.-d.-C. Díaz-de-la Loza, G. Vizcay-Barrena, R. A. Fleck, and B. M. Stramer, "Rapid Homeostatic Turnover of Embryonic ECM during Tissue Morphogenesis," *Developmental Cell*, vol. 54, pp. 33–42.e9, July 2020. Publisher: Elsevier.

[43] A. Proag, B. Monier, and M. Suzanne, "Physical and functional cell-matrix uncoupling in a developing tissue under tension," *Development*, vol. 146, p. dev172577, June 2019.

[44] R. Loganathan, B. R. Potetz, B. J. Rongish, and C. D. Little, "Spatial Anisotropies and Temporal Fluctuations in Extracellular Matrix Network Texture during Early Embryogenesis," *PLOS ONE*, vol. 7, p. e38266, May 2012. Publisher: Public Library of Science.

[45] K. Abley, P. B. De Reuille, D. Strutt, A. Bangham, P. Prusinkiewicz, A. F. M. Marée, V. A. Grieneisen, and E. Coen, "An intracellular partitioning-based framework for tissue cell polarity in plants and animals," *Development*, vol. 140, pp. 2061–2074, May 2013.

[46] S. B. Nissen, S. Rønhild, A. Trusina, and K. Sneppen, "Theoretical tool bridging cell polarities with development of robust morphologies," *eLife*, vol. 7, p. e38407, Nov. 2018.

[47] E. E. Kuchen, S. Fox, P. Barbier de Reuille, R. Kennaway, S. Bensmihen, J. Avondo, G. M. Calder, P. Southam, S. Robinson, A. Bangham, and E. Coen, "Generation of Leaf Shape Through Early Patterns of Growth and Tissue Polarity," *Science*, vol. 335, pp. 1092–1096, Mar. 2012. Publisher: American Association for the Advancement of Science.

[48] T. Xu, M. Wen, S. Nagawa, Y. Fu, J.-G. Chen, M.-J. Wu, C. Perrot-Rechenmann, J. Friml, A. M. Jones, and Z. Yang, "Cell Surface- and Rho GTPase-Based Auxin Signaling Controls Cellular Interdigitation in Arabidopsis," *Cell*, vol. 143, pp. 99–110, Oct. 2010. Publisher: Elsevier.

[49] Q. Yang, X. Wan, J. Wang, Y. Zhang, J. Zhang, T. Wang, C. Yang, and Z. Ye, "The loss of function of HEL, which encodes a cellulose synthase interactive protein, causes helical and vine-like growth of tomato," *Horticulture Research*, vol. 7, p. 180, Nov. 2020.

[50] A. Bünder, O. Sundman, A. Mahboubi, S. Persson, S. D. Mansfield, M. Rüggeberg, and T. Niittylä, "CELLULOSE SYNTHASE INTERACTING 1 is required for wood mechanics and leaf morphology in aspen," *The Plant Journal*, vol. 103, no. 5, pp. 1858–1868, 2020. _eprint: https://onlinelibrary.wiley.com/doi/pdf/10.1111/tpj.14873.

[51] B. Landrein, R. Lathe, M. Bringmann, C. Vouillot, A. Ivakov, A. Boudaoud, S. Persson, and O. Hamant, "Impaired Cellulose Synthase Guidance Leads to Stem Torsion and Twists Phyllotactic Patterns in Arabidopsis," *Current Biology*, vol. 23, pp. 895–900, May 2013.

[52] J. M. Carvajal-Gonzalez, S. Balmer, M. Mendoza, A. Dussert, G. Collu, A.-C. Roman, U. Weber, B. Ciruna, and M. Mlodzik, "The clathrin adaptor AP-1 complex and Arf1 regulate planar cell polarity in vivo," *Nature Communications*, vol. 6, p. 6751, Apr. 2015. Number: 1 Publisher: Nature Publishing Group.

[53] J. Nemhauser, L. Feldman, and P. Zambryski, "Auxin and ETTIN in Arabidopsis gynoecium morphogenesis," *Development*, vol. 127, pp. 3877–3888, Sept. 2000.

[54] C. Mansfield, J. L. Newman, T. S. G. Olsson, M. Hartley, J. Chan, and E. Coen, "Ectopic BASL Reveals Tissue Cell Polarity throughout Leaf Development in Arabidopsis thaliana," *Current biology: CB*, vol. 28, pp. 2638–2646.e4, Aug. 2018.

[55] M. G. Heisler, O. Hamant, P. Krupinski, M. Uyttewaal, C. Ohno, H. Jönsson, J. Traas, and E. M. Meyerowitz, "Alignment between PIN1 Polarity and Microtubule Orientation in the Shoot Apical Meristem Reveals a Tight Coupling between Morphogenesis and Auxin Transport," *PLoS Biology*, vol. 8, p. e1000516, Oct. 2010.

[56] N. Yamaguchi, M.-F. Wu, C. M. Winter, and D. Wagner, "LEAFY and Polar Auxin Transport Coordinately Regulate Arabidopsis Flower Development," *Plants*, vol. 3, pp. 251–265, June 2014. Number: 2 Publisher: Multidisciplinary Digital Publishing Institute.

[57] N. A. Dye, M. Popović, K. V. Iyer, J. F. Fuhrmann, R. Piscitello-Gómez, S. Eaton, and F. Jülicher, "Self-organized patterning of cell morphology via mechanosensitive feedback," *eLife*, vol. 10, p. e57964, Mar. 2021. Publisher: eLife Sciences Publications, Ltd.

[58] E. Martin, S. Theis, G. Gay, B. Monier, C. Rouvière, and M. Suzanne, "Arp2/3-dependent mechanical control of morphogenetic robustness in an inherently challenging environment," *Developmental Cell*, vol. 56, pp. 687–701.e7, Mar. 2021.

[59] O. Hamant, M. G. Heisler, H. Jönsson, P. Krupinski, M. Uyttewaal, P. Bokov, F. Corson, P. Sahlin, A. Boudaoud, E. M. Meyerowitz, Y. Couder, and J. Traas, "Developmental Patterning by Mechanical Signals in Arabidopsis," *Science*, vol. 322, pp. 1650–1655, Dec. 2008. Publisher: American Association for the Advancement of Science.

[60] A. Burian, M. Ludynia, M. Uyttewaal, J. Traas, A. Boudaoud, O. Hamant, and D. Kwiatkowska, "A correlative microscopy approach relates microtubule behaviour, local organ geometry, and cell growth at the Arabidopsis shoot apical meristem," *Journal of Experimental Botany*, vol. 64, pp. 5753–5767, Dec. 2013.

[61] N. Hervieux, M. Dumond, A. Sapala, A.-L. Routier-Kierzkowska, D. Kierzkowski, A. K. Roeder, R. Smith, A. Boudaoud, and O. Hamant, "A Mechanical Feedback Restricts Sepal Growth and Shape in Arabidopsis," *Current Biology*, vol. 26, pp. 1019–1028, Apr. 2016.

[62] T. I. Baskin, G. T. Beemster, J. E. Judy-March, and F. Marga, "Disorganization of Cortical Microtubules Stimulates Tangential Expansion and Reduces the Uniformity of Cellulose Microfibril Alignment among Cells in the Root of Arabidopsis," *Plant Physiology*, vol. 135, pp. 2279–2290, Aug. 2004.

[63] B. Boehm, H. Westerberg, G. Lesnicar-Pucko, S. Raja, M. Rautschka, J. Cotterell, J. Swoger, and J. Sharpe, "The Role of Spatially Controlled Cell Proliferation in Limb Bud Morphogenesis," *PLoS Biology*, vol. 8, p. e1000420, July 2010.

[64] J. M. Alonso, A. N. Stepanova, T. J. Leisse, C. J. Kim, H. Chen, P. Shinn, D. K. Stevenson, J. Zimmerman, P. Barajas, R. Cheuk, C. Gadrinab, C. Heller, A. Jeske, E. Koesema, C. C. Meyers, H. Parker, L. Prednis, Y. Ansari, N. Choy, H. Deen, M. Geralt, N. Hazari, E. Hom, M. Karnes, C. Mulholland, R. Ndubaku, I. Schmidt, P. Guzman, L. Aguilar-Henonin, M. Schmid, D. Weigel, D. E. Carter, T. Marchand, E. Risseeuw, D. Brogden, A. Zeko, W. L. Crosby, C. C. Berry, and J. R. Ecker, "Genome-wide insertional mutagenesis of Arabidopsis thaliana," *Science (New York, N.Y.)*, vol. 301, pp. 653–657, Aug. 2003. Number: 5633.

[65] O. Hamant, P. Das, and A. Burian, "Time-Lapse Imaging of Developing Shoot Meristems Using A Confocal Laser Scanning Microscope," in *Plant Cell Morphogenesis: Methods and Protocols* (F. Cvrčková and V. Žárský, eds.), Methods in Molecular Biology, pp. 257–268, New York, NY: Springer, 2019.

[66] D. A. Hartasánchez, A. Kiss, V. Battu, M. Dumond, C. Soraru, A. Delgado-Vaquera, F. Massinon, M. Brasó-Vives, C. Mollier, N. Dubrulle, F. Sénéchal, M.-L. Martin-Magniette, A. Boudaoud, and F. Monéger, "Robustness of organ morphology is associated with modules of co-expressed genes related to plant cell wall," preprint, Plant Biology, Apr. 2022.

[67] P. Barbier de Reuille, A.-L. Routier-Kierzkowska, D. Kierzkowski, G. W. Bassel, T. Schüpbach, G. Tauriello, N. Bajpai, S. Strauss, A. Weber, A. Kiss, A. Burian, H. Hofhuis, A. Sapala, M. Lipowczan, M. B. Heimlicher, S. Robinson, E. M. Bayer, K. Basler, P. Koumoutsakos, A. H. Roeder, T. Aegerter-Wilmsen, N. Nakayama, M. Tsiantis, A. Hay, D. Kwiatkowska, I. Xenarios, C. Kuhlemeier, and R. S. Smith, "MorphoGraphX: A platform for quantifying morphogenesis in 4D," *eLife*, vol. 4, p. e05864, May 2015. Publisher: eLife Sciences Publications, Ltd.

[68] N. Wuyts, J.-C. Palauqui, G. Conejero, J.-L. Verdeil, C. Granier, and C. Massonnet, "High-contrast three-dimensional imaging of the Arabidopsis leaf enables the analysis of cell dimensions in the epidermis and mesophyll," *Plant Methods*, vol. 6, p. 17, July 2010.

[69] T. P. Robitaille, E. J. Tollerud, P. Greenfield, M. Droettboom, E. Bray, T. Aldcroft, M. Davis, A. Ginsburg, A. M. Price-Whelan, W. E. Kerzendorf, A. Conley, N. Crighton, K. Barbary, D. Muna, H. Ferguson, F. Grollier, M. M. Parikh, P. H. Nair, H. M. Günther, C. Deil, J. Woillez, S. Conseil, R. Kramer, J. E. H. Turner, L. Singer, R. Fox, B. A. Weaver, V. Zabalza, Z. I. Edwards, K. A. Bostroem, D. J. Burke, A. R. Casey, S. M. Crawford, N. Dencheva, J. Ely, T. Jenness, K. Labrie, P. L. Lim, F. Pierfederici, A. Pontzen, A. Ptak, B. Refsdal, M. Servillat, and O. Streicher, "Astropy: A community Python package for astronomy," *Astronomy & Astrophysics*, vol. 558, p. A33, Oct. 2013. Publisher: EDP Sciences.

[70] T. A. Collaboration, A. M. Price-Whelan, B. M. Sipőcz, H. M. Günther, P. L. Lim, S. M. Crawford, S. Conseil, D. L. Shupe, M. W. Craig, N. Dencheva, A. Ginsburg, J. T. VanderPlas, L. D. Bradley, D. Pérez-Suárez, M. de Val-Borro, T. L. Aldcroft, K. L. Cruz, T. P. Robitaille, E. J. Tollerud, C. Ardelean, T. Babej, M. Bachetti, A. V. Bakanov, S. P. Bamford, G. Barentsen, P. Barmby, A. Baumbach, K. L. Berry, F. Biscani, M. Boquien, K. A. Bostroem, L. G. Bouma, G. B. Brammer, E. M. Bray, H. Breytenbach, H. Buddelmeijer, D. J. Burke, G. Calderone, J. L. C. Rodríguez, M. Cara, J. V. M. Cardoso, S. Cheedella, Y. Copin, D. Crichton, D. DÁvella, C. Deil, Depagne, J. P. Dietrich, A. Donath, M. Droettboom, N. Earl, T. Erben, S. Fabbro, L. A. Ferreira, T. Finethy, R. T. Fox, L. H. Garrison, S. L. J. Gibbons, D. A. Goldstein, R. Gommers, J. P. Greco, P. Greenfield,

A. M. Groener, F. Grollier, A. Hagen, P. Hirst, D. Homeier, A. J. Horton, G. Hosseinzadeh, L. Hu, J. S. Hunkeler, Ivezić, A. Jain, T. Jenness, G. Kanarek, S. Kendrew, N. S. Kern, W. E. Kerzendorf, A. Khvalko, J. King, D. Kirkby, A. M. Kulkarni, A. Kumar, A. Lee, D. Lenz, S. P. Littlefair, Z. Ma, D. M. Macleod, M. Mastropietro, C. McCully, S. Montagnac, B. M. Morris, M. Mueller, S. J. Mumford, D. Muna, N. A. Murphy, S. Nelson, G. H. Nguyen, J. P. Ninan, M. Nöthe, S. Ogaz, S. Oh, J. K. Parejko, N. Parley, S. Pascual, R. Patil, A. A. Patil, A. L. Plunkett, J. X. Prochaska, T. Rastogi, V. R. Janga, J. Sabater, P. Sakurikar, M. Seifert, L. E. Sherbert, H. Sherwood-Taylor, A. Y. Shih, J. Sick, M. T. Silbiger, S. Singanamalla, L. P. Singer, P. H. Sladen, K. A. Sooley, S. Sornarajah, O. Streicher, P. Teuben, S. W. Thomas, G. R. Tremblay, J. E. H. Turner, V. Terrón, M. H. van Kerkwijk, A. de la Vega, L. L. Watkins, B. A. Weaver, J. B. Whitmore, J. Woillez, and V. Zabalza, "The Astropy Project: Building an inclusive, open-science project and status of the v2.0 core package," *The Astronomical Journal*, vol. 156, p. 123, Aug. 2018. arXiv:1801.02634 [astro-ph].

[71] K. Ruel, Y. Nishiyama, and J.-P. Joseleau, "Crystalline and amorphous cellulose in the secondary walls of Arabidopsis," *Plant Science*, vol. 193-194, pp. 48–61, Sept. 2012.

[72] P. Virtanen, R. Gommers, T. E. Oliphant, M. Haberland, T. Reddy, D. Cournapeau, E. Burovski, P. Peterson, W. Weckesser, J. Bright, S. J. van der Walt, M. Brett, J. Wilson, K. J. Millman, N. Mayorov, A. R. J. Nelson, E. Jones, R. Kern, E. Larson, C. J. Carey, Polat, Y. Feng, E. W. Moore, J. VanderPlas, D. Laxalde, J. Perktold, R. Cimrman, I. Henriksen, E. A. Quintero, C. R. Harris, A. M. Archibald, A. H. Ribeiro, F. Pedregosa, and P. van Mulbregt, "SciPy 1.0: fundamental algorithms for scientific computing in Python," *Nature Methods*, vol. 17, pp. 261–272, Mar. 2020. Number: 3 Publisher: Nature Publishing Group.

[73] D. R. Smyth, J. L. Bowman, and E. M. Meyerowitz, "Early flower development in Arabidopsis," *The Plant Cell*, vol. 2, pp. 755–767, Aug. 1990.

Supplementary Material

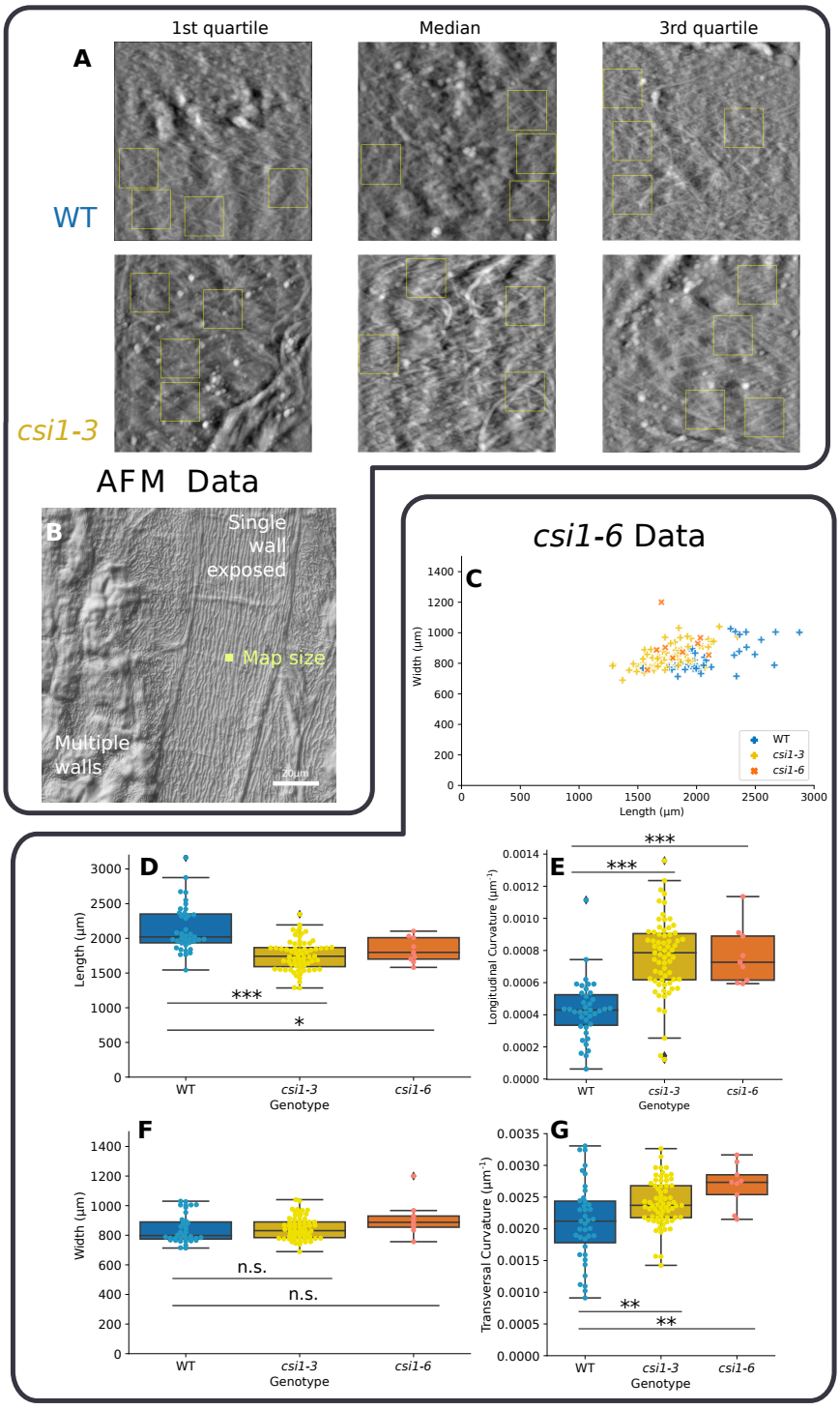

Fig. 6. A. Atomic Force Microscopy (AFM) maps corresponding to first quartile, median, and third quartile for the alignment index (the first quartile corresponds to a low alignment index). Small yellow rectangles show the areas with visible microfibrils used for the analysis. Whole map size = 2µm×2µm, single region analyzed = 400nm×400nm. **B.** Differential interference contrast microscopy image of the samples analyzed in AFM. The yellow square near the image center indicates the size of an AFM map. The protoplast-facing surface of the outer periclinal wall is exposed in the cell slightly to the right, while the cells on the left are covered by walls of inner sepal cells (parenchyma). The lines that are visible in the background correspond to cuticular ridges that are present on the other side of the cell wall. **C.** Length and width of individual WT, *csi1-3* and *csi1-6* sepals. **D,E.** Comparison of length and width of WT, *csi1-3* and *csi1-6* sepals, measured as shown in Figure 1D (n=39, 67 and 9, respectively. t-test p-values between WT and *csi1-6* = 0.01, 0.06 for length and width. See legend of Figure 1 for the comparison with *csi1-3*.) **F,G.** Comparison of curvatures along the main axes of the sepal. Curvature is defined as the inverse of the radius of a circle fitted to the center of the sepal (p-values of t-test for longitudinal curvature = 7×10^{-12} and 8×10^{-6} for comparison between WT and *csi1-3* or *csi1-6*, respectively. p values for transversal curvature = 2×10^{-3} and 9×10^{-3} for comparison between WT and *csi1-3* or *csi1-6*, respectively.)

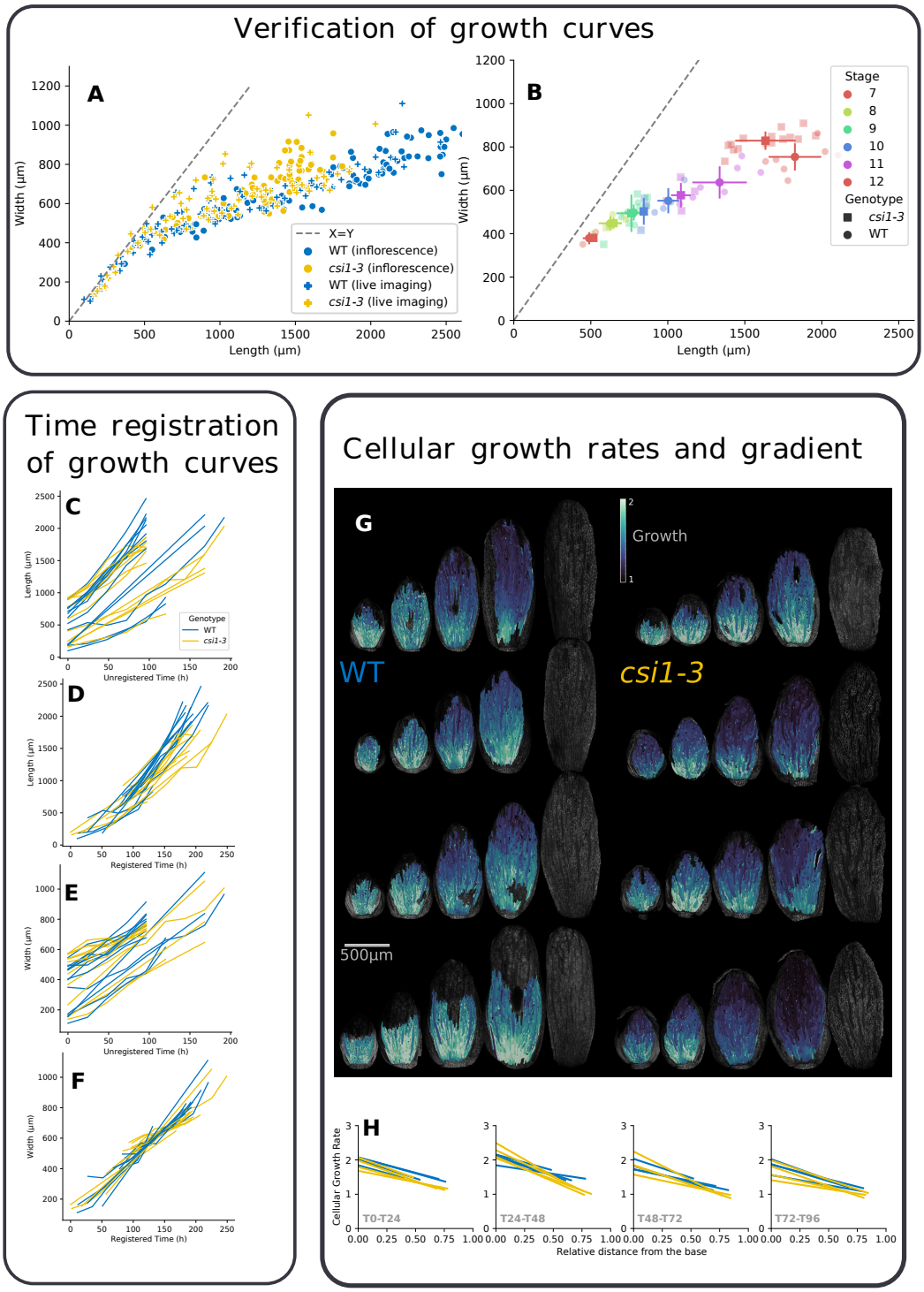

Fig. 7. A. Comparison of growth trajectories between plants used for live imaging (individual flowers imaged live over a few days and grown in vitro following dissection) and culture room grown plants (static images from dissected inflorescences). **B.** Comparison of developmental stage and length-width value between WT and *csi1-3* sepals. Stages used are defined in Smyth et al [73]. Note that width values of WT and *csi1-3* sepals at a given stage overlap more than length values, allowing us to use width to register time (panels C-F). **C-F.** Growth curves from live imaging, before (C,E) and after time registration (D,F) for length (C,D) and width (E,F). **G.** All heatmaps of cellular growth rates in area for all sepals (WT on the left, *csi1-3* on the right); sepals were imaged over 5 days, yielding 4 maps. Regions with a low quality signal were not segmented. **H.** Growth gradients visualized for all the time points. Each line corresponds to a first degree polynomial fit between cellular growth rates and relative distance from cell to the base of the sepal. Sepal total length used here to compute the relative position was measured manually.

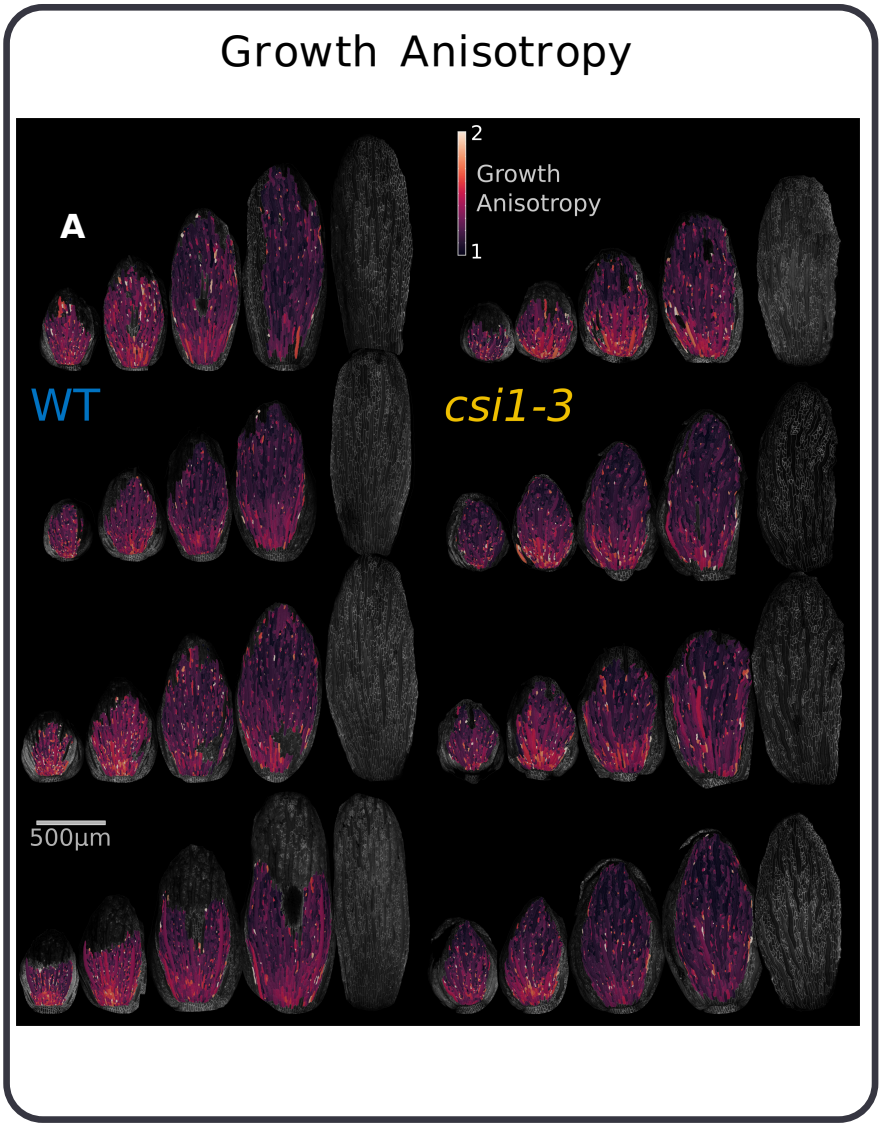

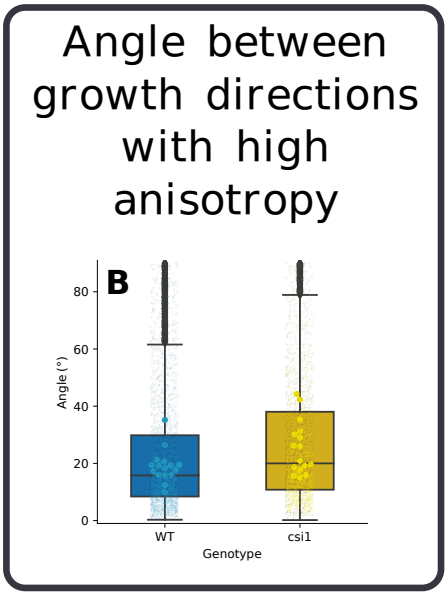

Fig. 8. A. Heatmaps of cellular growth anisotropy for all the examined sepals (WT on the left, *csi1-3* on the right); sepals were imaged over 5 days, yielding 4 maps. Zones with a low quality signal were not segmented. **B.** Angle between main growth directions in neighboring cells with anisotropy of at least 1.4. Large dots represent the median angle for a given sepal. Small points represent individual values between pairs of cells. Box plots were constructed using all the pairs of cells. (Total number of pairs of cells analyzed = 2583, and 2285 for WT, *csi1-3*, respectively. p-value of t-test between the median values for cell pairs = 10^{-11}. p-value of t-test between the median values for sepals = 0.03).

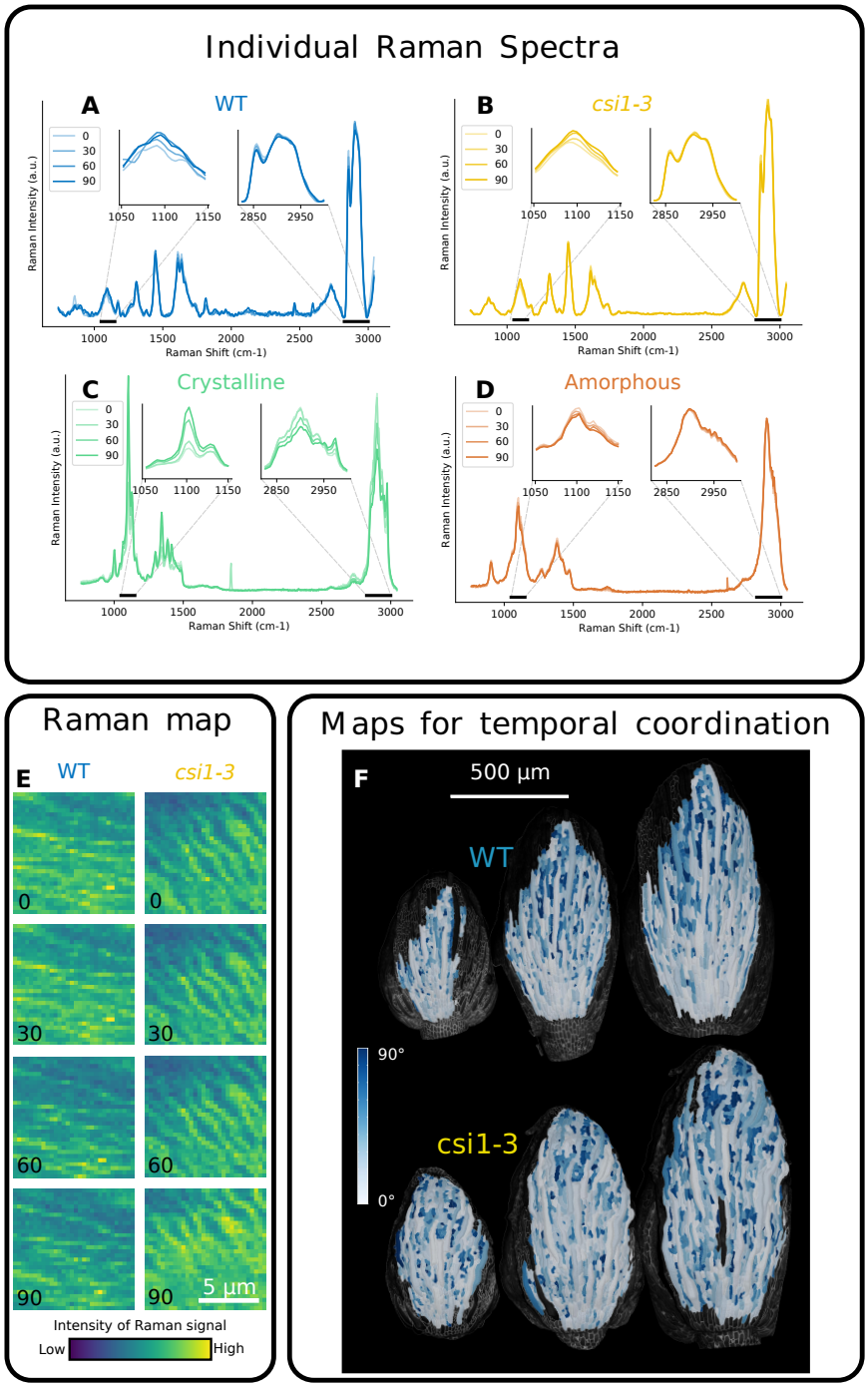

Fig. 9. A-D. Examples of Raman spectra obtained for WT, *csi1-3*, crystalline cellulose and amorphous cellulose at different polarization angles. Insets represent a zoom around the bands centered at 1096cm^{-1} and 2898cm^{-1}, which were considered for the main figure analysis. Differences in color intensity correspond to the different angular positions of the polarizer. **E.** Examples of Raman maps prepared on the basis of the integrated intensity over a C-O-C band at 1096cm^{-1} (10µm×10µm) of WT and *csi1-3* outer wall of epidermis. Numbers at the lower left corner indicate the angle of the polarizer. **F.** Maps of the angle between growth directions at consecutive times.

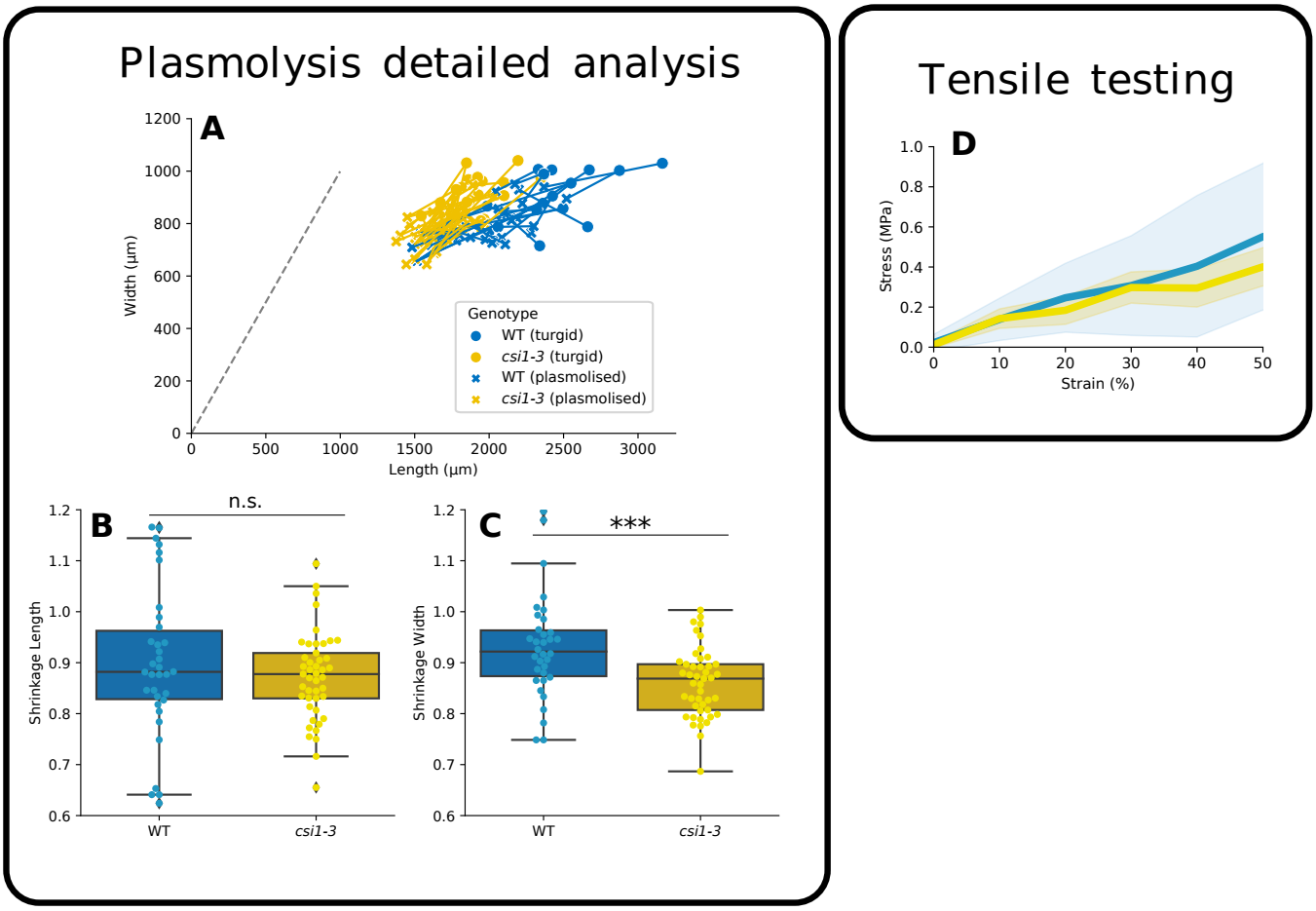

Fig. 10. A. Representation of shrinkage in length/width coordinates. Circles correspond to sepals before osmotic treatment, crosses to after treatment. Points for each sepal are linked by a line. **B,C.** Quantification of sepal shrinkage upon osmotic treatment for length and width, respectively (p values of t-test = 0.3 and 5×10^{-4}); the vertical axis indicates the ratio of dimension (length or width) after treatment to before treatment. **D.** Stress vs. strain for sepals stretched by extensometry. WT is in blue and *csi1-3* in yellow; the lines correspond to median and the shading to the interquartile range (N=8 sepals for WT and *csi1-3*).

Internship report

Cellulose and growth anisotropy in elongated cells

Graphical Abstract

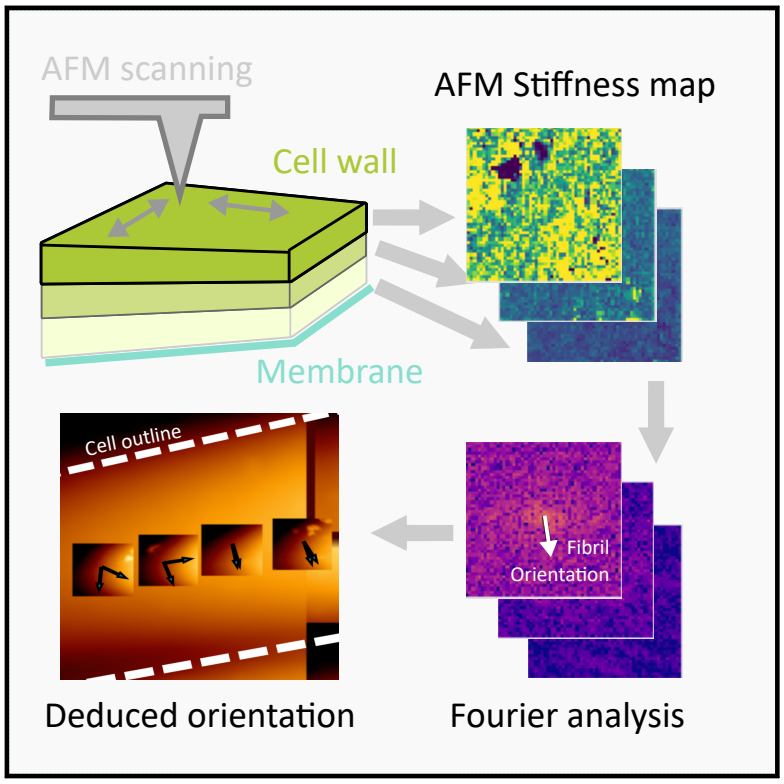

Highlights

- Deduction of fibril orientation from Fourier transform may work well even if the number of fibrils on the map is high.
- Analysis of AFM stiffness maps with Fourier transform did not yield reproducible results.
- A minimal model for the cell wall predicts two regimes for growth anisotropu according to the strength of feedback from mechanical stress on orientation of cellulose fibers

Authors

Emilie Chabert, Corentin Mollier, Antoine Fruleux, and Arezki Boudaoud

In Brief

We performed Atomic Force Microscopy (AFM) stiffness measurement with a resolution of about the size of a cellulose bundle, and analyzed it at various depths. To develop the method we decided to work on the hypocotyl as it should present differences in cellulose orientation in the depth of the cell wall. A small map of 5µm × 5µm was imaged with AFM with a resolution of 50nm, and we extracted stiffness maps at various depths by adjusting the indentation data used to fit the stiffness. These maps were then analyzed with Fourrier transforms, which we first validated using generated data, to recover fibril orientation. Overall, the method did not yield very reproducible results.

Contributions

This part was performed with an intern, Emilie Chabert, which worked on most aspects of the work. I supervised her experimental work throughout her internship, and helped with the measurements and analysis. This is her internship report.

Cellulose and growth anisotropy in elongated cells

Emilie Chabert[1], **Corentin Mollier**[1], **Antoine Fruleux**[1], **and Arezki Boudaoud**[1]

[1]Reproduction et développement des plantes, ENS de Lyon, France

Plant cell walls constitute the extracellular matrix surrounding plant cells and are composed mainly of cellulose microfibrils. The organization of cellulose microfibrils modifies the mechanical properties of the cell wall and partly imposes the growth orientation. Therefore, the visualization of cellulose microfibrils is a crucial tool to understand growth anisotropy. To access cellulose anisotropy across the cell wall depth in living cells, we have developed a method based on the analysis of Young's modulus maps obtained from atomic force microscopy. We used Fast Fourier Transform to analyze the patterns on Young's modulus maps and we have shown that the Fast Fourier Transform can recover fiber orientation and degree of anisotropy from these maps. We found a good match between the cellulose microfibrils orientation recovered with the Fast Fourier Transform applied to Young's modulus maps collected from hypocotyl cells and the microtubules orientation in hypocotyls. We also developed a model to understand how the stress anisotropy modifies growth orientation and cellulose anisotropy. The model demonstrates the existence of different regimes of the orientation of growth relatively to stress, fibers and the intensity of mechanical feedback.

cell wall | cellulose orientation | AFM

Plant cells are surrounded by a cell wall made up of cellulose microfibrils tied together by hemicellulose and embedded in a matrix of pectins and structural proteins. In the cell wall, cellulose microfibrils are organized in layers of parallel fibers [1]. This wall is elastically stretched by turgor pressure, and under particular conditions, it can yield irreversibly leading to cell growth [2].

Plant cell growth is anisotropic which can find different origins: the geometry of plant tissues and the anisotropy of cell walls. Tissues geometry induces anisotropic stress which is the driving force for growth [3]. Additionally, plant cell walls do not have the same mechanical properties in all directions since cellulose fibers often tend to align along a certain direction which lead to different abilities to yield within the cell and so to anisotropic growth [2].

Cellulose microfibrils are deposited along the cortical microtubule network [4] which have been shown to correlate with maximal stress orientation due to a mechanical feedback [5]. Therefore stress, microtubules and cellulose should be aligned together and perpendicularly to growth direction. However, in some cases cortical microtubules are not perpendicular to the axis of growth [6].

Understanding plant growth requires to take into account the stress, the microtubule and cellulose microfibrils orientations and especially to describe precisely their anisotropies. We know how to image growth but so far cellulose imaging methods only give limited information. The first set of methods consists in peeling the cells to detach the cell-wall from the cell and reveal the inner cell-wall for topography analysis by atomic force microscopy (AFM), allowing direct visualisation of cellulose fibers [7]. Because the epidermis is covered by a lipidic cuticle, topography analysis from the outer surface will not show fibers. Cellulose staining combined with confocal analysis may also give information but its results are hard to analyse linked with the number and size of the fibers. Additionally none of these methods allow to have information on the cellulose orientations in the different layers.

Here, we tried to develop a non-destructive method using AFM microscopy to measure wall anisotropy across the cell wall depth. AFM is a method which allows to physically probe samples and provides information about the topography and the mechanical properties such as Young's modulus, a measure of stiffness. Cellulose fibers are thought to be stiffer than the matrix. Therefore, we hoped to be able to recover cellulose microfibrils orientations at different depths from mechanical measurements. Then, we modelled cellulose anisotropy in the dynamic of plant cell walls.

Results

Imaging cellulose with AFM.

To test if we can access the orientation of cellulose microfibrils using AFM microscopy, etiolated hypocotyl cells seemed a good candidate : this tissue is young, thus has a thin cuticle. It also presents aligned microtubules and consequently aligned cellulose fiberss.

AFM can be used to scan the topography of a sample and access to its material mechanical properties. It consists of a tip fixed to a flexible cantilever. When the tip meets the sample, the cantilever bends and the deflection can be measured by a laser. Knowing the sensitivity and spring constant of the tip, the laser deflection and cantilever position can be transformed into tip displacement and force exerted at the tip (Fig1). From then we can fit the obtained curves to extract a mechanical parameter called Young's modulus which describes the elastic behaviour of the material. To access cellulose fibers anisotropy at different depths, we analysed only a portion of the curve - for example on the portion of the curve between the red vertical line and the contact point on the Fig1.

With AFM, we scan regions of area 5 µm x 5 µm with a resolution of 50nm. For each pixel, we used the previous method to extract Young's modulus from the force curve and we constructed Young's modulus maps (Fig3A). As expected, the fibers are not directly visible because of

their number and because they are embedded in a matrix. Thus, we develop a method to analyze these Young's modulus maps and extract information about cellulose fibers anisotropy from them.

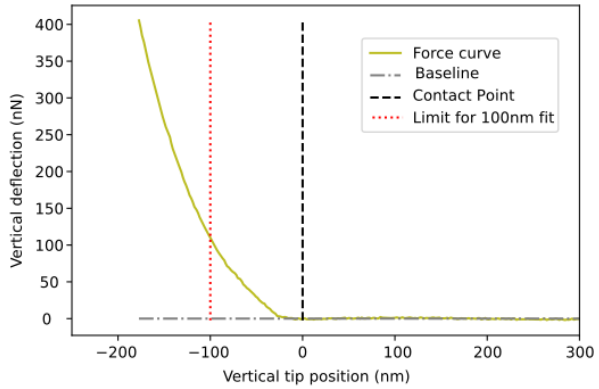

Fig. 1. A force curve obtained from an hypocotyl cell
It represents the force exerted on the tip as a function to its height. For negative values of vertical tip position, a deflection is recorded because the cell wall resists the penetration so the cantilever bends.

Fourier decomposition of fibril maps.

We created a program to analyze the mechanical signature of a fibrillar pattern using Fast Fourier Transform (FFT). 2D FFT decomposes an image in frequencies and gives information about underlying periodic structures like fibers arrangements. From FFT, we aimed at extracting two cell wall properties with an eigen decomposition: the degree of anisotropy and the mean orientation of fibers (see vector on Fig2C).

Before applying the analysis to biological data, we decided to test the FFT on controlled data. To generate these data, we created maps with chosen fiber orientation and degree of anisotropy (Fig2A-2B).The FFT applied to the maps presents an hourglass pattern characteristic of anisotropy (Fig2C).

First, we wanted to make sure that the analysis was insensitive to the orientation of the fibrils. Thus, we calculated the difference between the input main orientation of the generated map and the orientation we deduced from FFT for various input orientations. The FFT can detect all fiber main orientations with good precision(Fig2D).

Then, we tested if it was possible to distinguish anisotropic and isotropic fiber distributions with the FFT by comparing the measured anisotropy with the standard deviation chosen for the angle distribution considered as the theoretical anisotropy (Fig2E). When the fiber distribution tends to isotropy that is the standard deviation increases, the measured anisotropy decreases. Therefore, we can compare the degree of anisotropy between different maps.

We attended to quantify the precision of the measured orientation of anisotropy across a range of degrees of anisotropy (Fig2E). When the fiber distribution of fibers becomes isotropic, logically the measured orientation is less precise. Consequently, to determine if the measured orientation is accurate, the degree of anisotropy needed to be taken into account.

Note that if the fibers are too aligned (low standard deviation), FFT is less precise to determine the degree and orientation of anisotropy.

Finally, we investigated the effect of the numbers of fibers on the map and the noise (Fig2F). The noise is an addition of a random value to each pixel of the map. Without noise, the FFT is quite insensitive to the numbers of fibers. When the noise increases, logically the angle measurement precision decreases. The fact that we can still have quite precise orientation for an intermediate number of fibers even with noise could lead to thinking that we could distinguish the cellulose fibers from the matrix with the FFT.

In conclusion, FFT seemed to be able to analyse potential fibers patterns of Young's modulus maps.

Recovering cellulose microfibrils orientation from Young's modulus map.

Because we want to be able to recover fiber orientation at different depths we generated Young's modulus maps at different depths. Young's modulus maps are more homogeneous at higher depths when a wider portion of the cell wall is analyzed maybe because the indentation area increases with depth (Fig3A).

The orientation of wall anisotropy recovered by FFT changes with depth. This could be due to the modification of the orientation between the stacks (Fig3B). However, the patches with higher values of Young's modulus on the maps could interfere with the analysis.

We then analysed one hypocotyl cell in 5 different positions to determine whether recovered cellulose orientation was compatible with published results on the hypocotyl. If we assume that the pattern of Young's modulus is due to cellulose microfibrils, the wall anisotropy is transverse to the cell axis which is consistent with microtubules orientation in hypocotyls [8] (Fig3C). The difference between orientations found by the FFT taken at the same position can be due to a low degree of anisotropy.

Computational modeling.

We developed a model to understand the interactions between different anisotropies in plant cell walls and especially how the stress anisotropy modifies growth orientation and cellulose anisotropy.

We assumed that tissue geometry imposes wall stress and that wall stress is constant in our model. Furthermore, we considered an elongated organ (hypocotyl, for example) for which the stress is anisotropic, and we chose the x-axis as the main axis of the stress tensor.

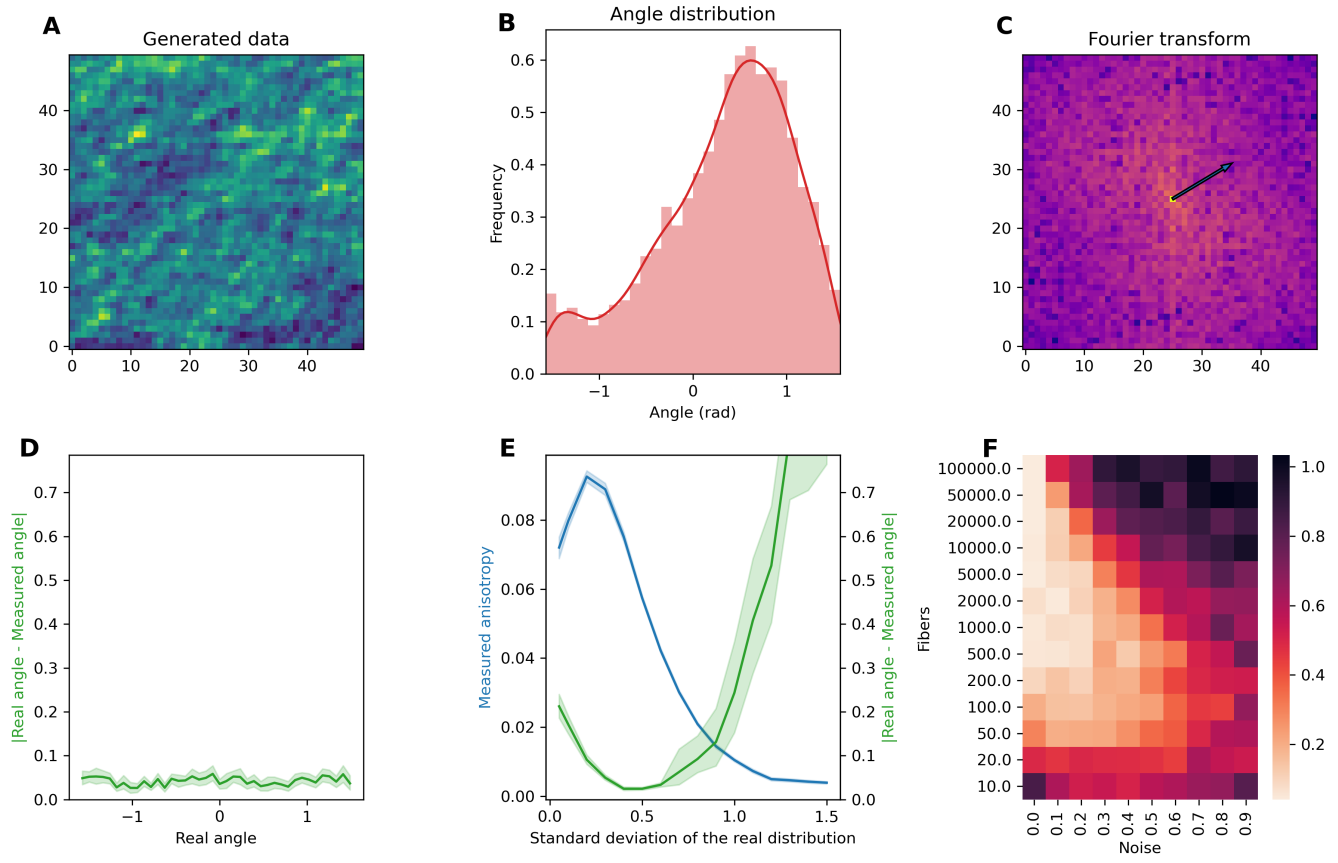

Fig. 2. Fourier decomposition allows recovering fiber orientation
A) A generated map containing 5000 fibers with orientations chosen in a circular normal distribution on the interval $[-\frac{\pi}{2},\frac{\pi}{2}]$ with $\mu = \frac{\pi}{6}, \sigma = 0.7$
B) Distribution of the angles associated to the fibers from A)
C) Result of the FFT applied to A), the vector gives the main fibers orientation found by the FFT
D) Difference between the fiber orientation recovered by the FFT and the orientation chosen for the map with 5000 fibers The bands surrounding the curve represent confidence intervals.
E) Degree of the anisotropy and precision of the angle in function of the standard deviation chosen in the normal distribution
F) Difference between the fiber orientation recovered by the FFT and the orientation chosen for the map in function of numbers of fibers and intensity of noise

In 2D, stress, growth and cellulose fibers can be described by tensors which give the parameters' properties in space. Stress, growth and cellulose microfibrils anisotropy are respectively described by the stress tensor σ, the strain rate γ and the nematic tensor s where s is defined from the cellulose orientation distribution. Using eigendecomposition, it is possible to define a degree of anisotropy and a main orientation for each of these tensors. The degree of anisotropy and the main orientation of s will for example give the degree of alignment of fibers as well as their main orientation.

First, we used the generalized Hooke's law to link the stress σ and the strain rate γ:

$$\begin{pmatrix}\sigma_{11}\\ \sigma_{22}\\ \sigma_{12}\end{pmatrix} = C. \begin{pmatrix}\gamma_{11}\\ \gamma_{22}\\ \gamma_{12}\end{pmatrix}$$

where 1 is the main cellulose microfibrils orientation and 2 the perpendicular direction.

To take into account the influence of cellulose fibers on growth orientation, we defined the matrix C such as the cell wall will be stiffer in the direction 1 (i.e along the main cellulose fibers orientation):

$$C = \begin{pmatrix} A(1+\frac{\alpha_s}{\alpha_0}) & B & 0 \\ B & A(1-\frac{\alpha_s}{\alpha_0}) & 0 \\ 0 & 0 & D \end{pmatrix}$$

where A and D depend on the elastic modulus and the Poisson's ratio, $B = \beta A\sqrt{(1+\frac{\alpha_s}{\alpha_0})(1-\frac{\alpha_s}{\alpha_0})}$ and α_0 quantifies the impact of cellulose anisotropy on the cell wall stiffness. In the following discussion, we took the values for β, A and D found in [9] ($\beta = 0.5$, $A = 1.668$, $D = 2.209$).

To describe the evolution of cellulose anisotropy, we took into account the impact of the deformation and the mechanical feedback.

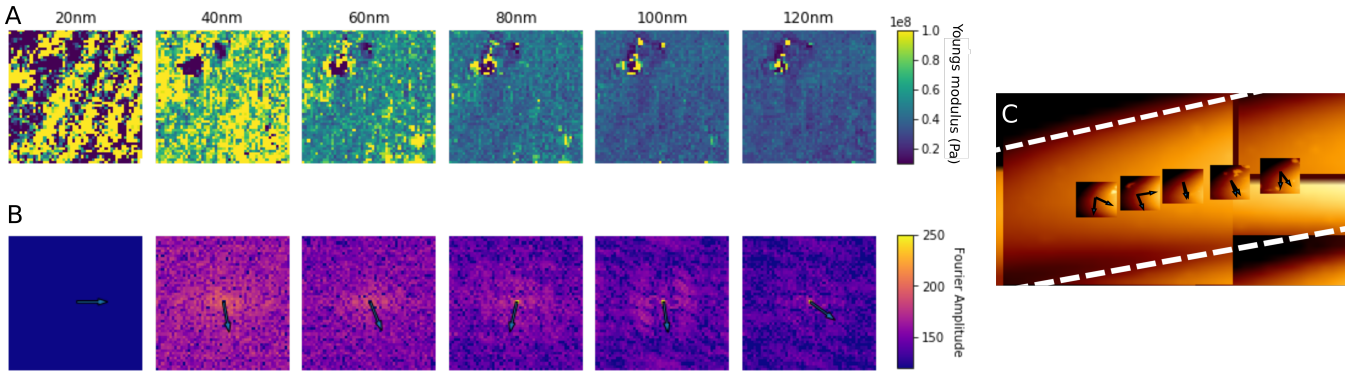

Fig. 3. Analyzing Young's modulus maps with the FFT.
A) Young's modulus maps for different intervals. For example, the first map represents the Young's modulus for the first 20 nm.
B) Result of the FFT applied to A), the vector gives the main fibers orientation found by FFT
C) Combination of topographic maps obtained with AFM on hypocotyl cells. The vectors represent the orientation of anisotropy recovered by FFT. Two measurements were made at the same position. Dashed lines give the cell limits.

$$\frac{ds}{dt} = \alpha_s \gamma - \frac{1}{\alpha_s} s.\gamma.s - \frac{1}{\tau_C}(s - \frac{1}{\sigma_C}(\sigma - \frac{Tr(\sigma)}{2}))$$

The first two terms of the right hand side account for the impact of growth on the cellulose fibers. It assumes that the main fiber orientation follows the deformation while the degree of anisotropy is not impacted. The second last terms of the right hand side corresponds to the mechanical feedback. τ_C is the relaxation time, the time at which the synthesis of fibers responds to changes stresses. $\frac{1}{\sigma_C}$ characterizes the strength of the feedback. $Tr(\sigma)$ is the trace of the matrix sigma.

Exploration of the model.

We investigated the impact of the strength of the mechanical feedback $\frac{1}{\sigma_C}$ and of the relaxation time τ_C on the growth and cell wall anisotropy (Fig4).

The feedback strength has a strong impact on the final alignment of fibers as well as on the final growth, and we could identify two regimes. In all the cases explored, cellulose microfibrils tend to align with the maximal stress direction, on the contrary the resulting maximal direction of strain can be either parallel or perpendicular to the maximal stress direction.

For strong feedback ($\frac{1}{\sigma_C} = 2$ for example), α_s is higher which means cellulose fibers are more aligned in the direction of maximal stress. As a result, the wall is stiffer in the direction of maximal stress therefore the cell grows in the perpendicular direction. For weak feedback (for example $\frac{1}{\sigma_C} = 1$), the stiffness anisotropy is not strong enough to compensate the stress anisotropy.

The relaxation time appears to have a relatively low impact on the final state but is important for the transitory regime and peculiarly in the case where the feedback is strong ($\frac{1}{\sigma_C} = 2$). In this case, if the fibers anisotropy is initially moderate, the main growth orientation initially align along the maximal stress orientation until the fibers anisotropy becomes high enough so that the stiffness anisotropy compensate the stress anisotropy and the growth anisotropy becomes oriented perpendicular to the stress orientation. τ_C characterize the duration of the transition.

Discussion

The analysis of Young's modulus maps turned out to be complex. The first problem is due to technical artifacts. The interference between the laser reflected by the cantilever and the sample distorts the measures and adds a pattern over the one we want to observe. Then, with these preliminary data, we can not be sure that the patterns are actually due to cellulose microfibrils. A cellulase treatment may help us answer this question. However, the method we develop to analyze fiber patterns with FFT can be useful to process other data such as confocal images of cellulose obtained with recent fluorescent dye as current plugins usually work on a small number of fibers [10].

The results of the model are still preliminary but are interesting: it predicts the existence of different regimes of the orientation of growth relatively to stress and fibers. It also predicts the possibility of growth anisotropy to change as the organ grows. This model could help the comprehension of some mutants for which growth does not align on stress anisotropy (as *csi1* mutants may do [11]) as well as to understand the evolution of anisotropies in tissues. The model remains nevertheless simplistic and may require adaptations to fit with the experimental reality. Moreover, the model would need to be explored extensively.

Material and methods

Plant growth condition. We used the p35S::GFP-MBD line. In order to obtain synchronized etiolated hypocotyls,the seeds were placed 4 days in the cold cham-

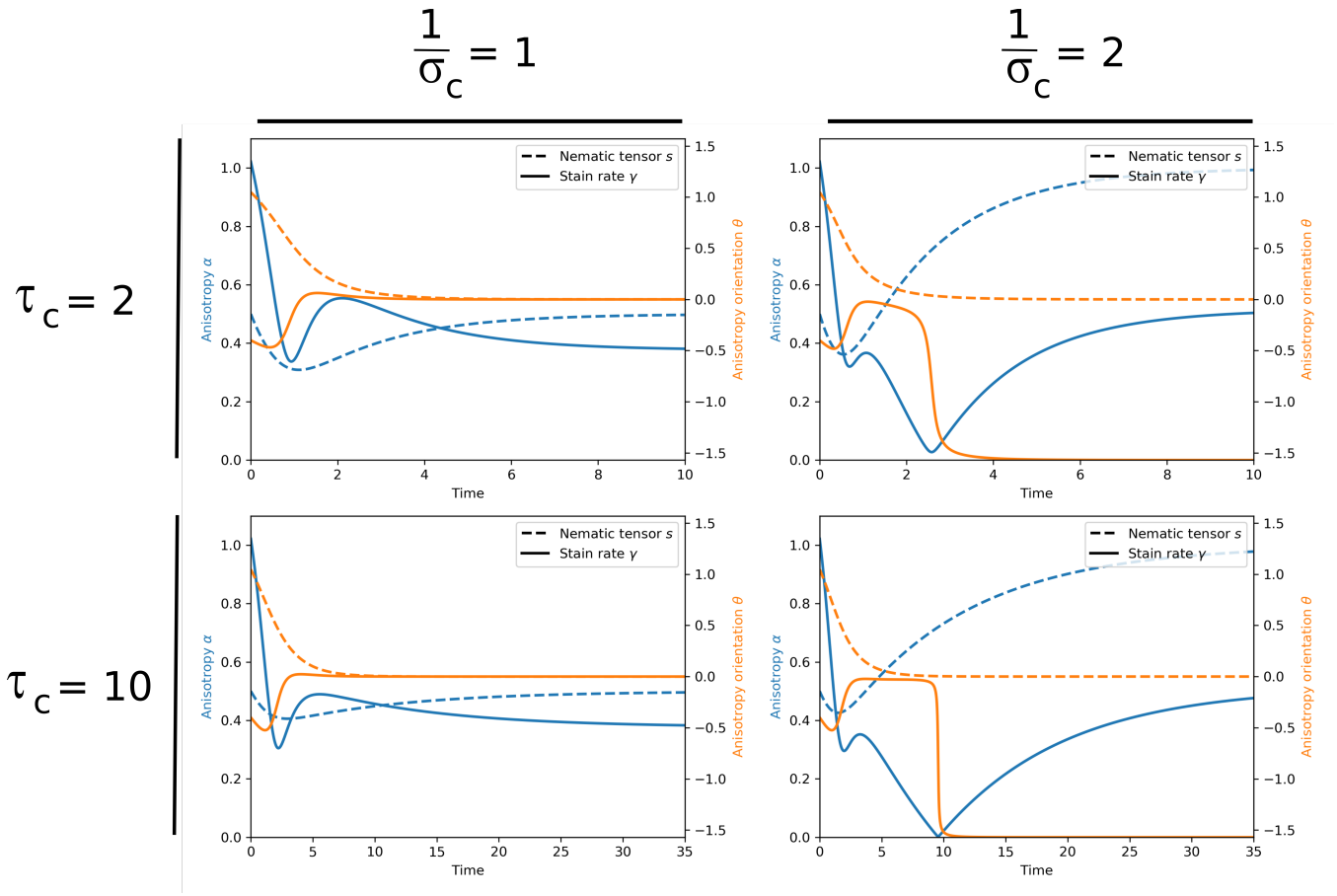

Fig. 4. Simulations of the effect of the mechanical feedback on strain rate and cellulose orientation under constant stress
On each graphic, information about strain rate are represented by dashed lines. The ones about cellulose orientation are in solid lines. θ represents the angle between the maximal stress direction and the maximal strain direction. α represents the degree of anisotropy. The first column presents the result of the simulation when the coupling between the stress and the cellulose orientation is low, the second is for a strong mechanical feedback. The first row shows the result as the relaxation time is low, the second, is for high relaxation time.

ber, then exposed to light during 6 hours and placed in dark for 3 days.

FFT code. The analysis was implemented in Python. Young's modulus maps were first interpolated to fill missing values and then analyzed with numpy.fft.fft2 followed by numpy.fft.fftshift. From the FFT matrix, we defined the order parameter Q classic to describe anisotropic system. $\frac{\lambda_1-\lambda_2}{\lambda_1+\lambda_2}$, where λ_1 and λ_1 are the eigenvalues of Q, quantifies the degree of anisotropy. The eigenvector associated with the higher eigenvalue gives the main direction of anisotropy.

Controls for FFT analysis. We generated a matrix where the fibers were traced by the function skimage.draw.line_aa given an angle chosen in the circular normal distribution on the interval $[-\frac{\pi}{2},\frac{\pi}{2}]$, then displace in the map at a random position.

Atomic force microscopy. The AFM measurements were performed with JPK Nanowizard III using a pyramidal probe (https://www.brukerafmprobes.com/p-3925-rfesp-190.aspx). Samples were glued and immersed in water. We used the tapping mode to produce a 5x5 µm map with a maximal indentation force equals to 400 nN. Young's modulus data were extracted using JPKSPM Data Processing.

Acknowledgments

We thank Simone BOVIO for his help with the AFM acquisition.

References

[1] Alberts, B. et al. *The Plant Cell Wall.* Mol. Biol. Cell 4th Ed. (2002).

[2] Baskin, T. I. & Jensen, O. E. *On the role of stress anisotropy in the growth of stems.* J. Exp. Bot. 64, 4697–4707 (2013).

[3] Sapala, A. et al. *Why plants make puzzle cells, and how their shape emerges.* eLife 7, (2018).

[4] Li, S., Lei, L., Somerville, C. R. & Gu, Y. *Cellulose synthase interactive protein 1 (CSI1) links microtubules and cellulose synthase complexes.* Proc. Natl. Acad. Sci. U. S. A. 109, 185–190 (2012).

[5] Hamant, O., Inoue, D., Bouchez, D., Dumais, J. & Mjolsness, E. *Are microtubules tension sensors?* Nat. Commun. 10, 2360 (2019).

[6] Burian, A. et al. *A correlative microscopy approach relates microtubule behaviour, local organ geometry, and cell growth at the Arabidopsis shoot apical meristem.* J. Exp. Bot. 64, 5753–5767 (2013).

[7] Zhang, T., Mahgsoudy-Louyeh, S., Tittmann, B. & Cosgrove, D. J. *Visualization of the nanoscale pattern of recently-deposited cellulose microfibrils and matrix materials in never-dried primary walls of the onion epidermis.* Cellulose 21, 853–862 (2014).

[8] Crowell, E. F. et al. *Pausing of Golgi Bodies on Microtubules Regulates Secretion of Cellulose Synthase Complexes in Arabidopsis.* Plant Cell 21, 1141–1154 (2009).

[9] Hervieux, N. et al. *Mechanical Feedback Restricts Sepal Growth and Shape in Arabidopsis.* Curr. Biol. 26, 1019–1028 (2016).

[10] Bidhendi, A. J., Chebli, Y. & Geitmann, A. *Fluorescence visualization of cellulose and pectin in the primary plant cell wall.* J. Microsc. 278, 164–181 (2020).

[11] Bringmann, M. et al. *POM-POM2/CELLULOSE SYNTHASE INTERACTING1 Is Essential for the Functional Association of Cellulose Synthase and Microtubules in Arabidopsis[W][OA].* Plant Cell 24, 163–177 (2012).

Subcellular heterogeneity in microtubule dynamics at high temporal resolution in pavement cell

Graphical Abstract

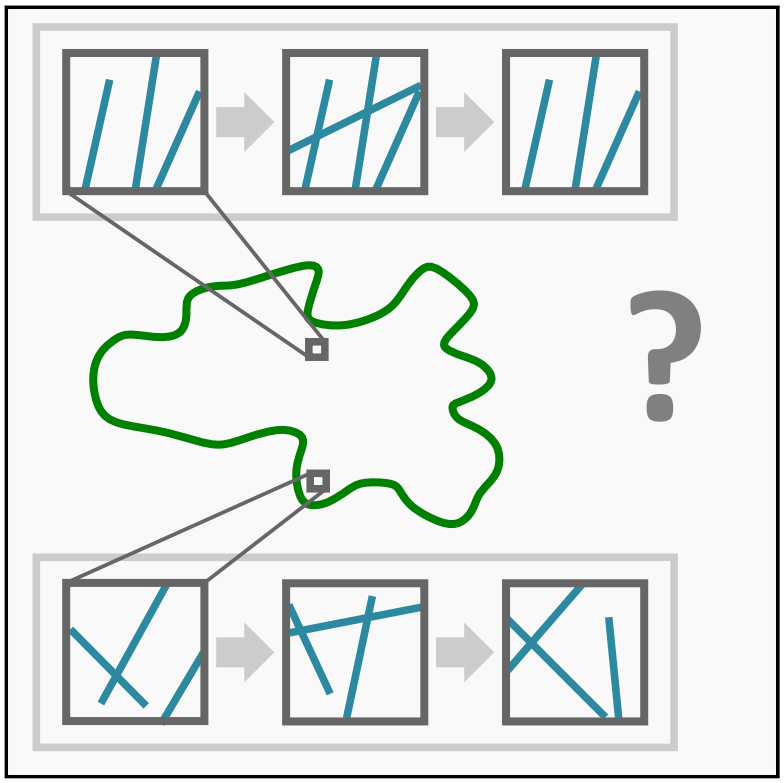

Highlights

- Circular variation of the microtubule orientation does not show differences between lobes, necks and the center of the pavement cells.

Authors

Matthieu Cortes*, Corentin Mollier*, Claire Lionnet, Arezki Boudaoud, Olivier Hamant, and Christophe Tréhin

In Brief

Microtubules are often considered as static structures regarding pavement cell shape development. Their peculiar patterning must however originate from differences in polymerization rates and depolymerization rates (potentially in a spatial and orientation dependant manner). Our goal was to quantify the rapid dynamics of microtubules to highlight the mechanisms that lead to the emergence of the observed patterns.

Contributions

Image acquisition was done exclusively by Matthieu Cortes. Image processing was done by Claire Lionnet and Matthieu Cortes. Matthieu Cortes and I designed the projection method together and I performed all the implementation. I designed and implemented the microtubule dynamics analysis. These preliminary results are, as their name suggest, preliminary.

Subcellular heterogeneity in microtubule dynamics at high temporal resolution in pavement cell

Matthieu Cortes[1,*], **Corentin Mollier**[1,*], **Claire Lionnet**[1], **Arezki Boudaoud**[1,2], **Olivier Hamant**[1], **and Christophe Tréhin**[1]

[1]Reproduction et développement des plantes, ENS de Lyon, France; [2]LadHyX, Ecole polytechnique, CNRS, France; [*]These authors contributed equaly to the work

Microtubules are dynamic structures that alternate between polymerization and depolymerization phases. During polymerization, $\alpha\beta$-tubulin dimers, that compose the microtubule, are added to the tip under a form bound to a GTP nucleotide [1]. This GTP will be hydrolysed over time, which explains why the body of the microtubule is bound to GDP [1, 2]. In vitro dynamics of microtubules has been thoroughly investigated using minimalistic systems of purified tubulin [3]. In vivo dynamics involve many more factors which may influence: polymerization rates, depolymerization rates, and potentially define preferential directions for each of these aspects.

Numerous proteins have been identified as regulators of microtubule dynamics among which: END-BINDING 1 (EB1), CYTOPLASMIC-INKED-ASSOCIATING PROTEINS (CLASPs), and KATANIN. EB1 binds specifically to the GTP cap [4], and globally reduces the catastrophe rates in vivo [5, 6]. CLASP promotes filament assembly and contributes to stabilizing microtubules that have been severed [7]. CLASP may also contribute to the stabilization of microtubules in unstable configurations such as the cell edge of plant cells [8]. KATANIN severs microtubules specifically at the crossovers [9] and at the level of branching [10], which generates new segments. These studies were usually performed with low temporal resolution, and were often not regionalized, which may affect the analysis [11].

Microtubule dynamics is also influenced directly by their environment. Viscosity has been shown to increase polymerization and depolymerization rates [12]. Mechanical stress is one of the only actors shown to pattern directly microtubule orientation [13], via a preferential polymerization orthogonal to the compression direction. In vivo, studies of single cell plant systems demonstrated that microtubules align with stress direction when there is a change in the magnitude of the stress [14]. Despite increasing knowledge in simplified systems, there is currently no overview of the regulation of microtubule dynamics at the subcellular scale in complex and realistic environments.

Pavement cells are epidermal plant cells that present a characteristic shape. This shape is acquired through the patterning of microtubules [15], that control cell wall deposition. Microtubule patterning in pavement cells [16, 17] is thought to be controlled by mainly two factors: 1) Chemical patterning is thought to be directed by interaction between ROP6 and RIC1 [18, 19]. RIC1 has been shown to recruit KATANIN, which then servers branching microtubules to generate two new segments [20]. These new segments would spontaneously align and reinforce the current orientation of microtubules. This hypothesis assumes an already existing patterning of microtubule, and does not explain the recovery of orientation after temporal disruption of microtubule organization [21]. No mechanism has so far been proposed to explain the impact of the ROP6-RIC1 pathway on microtubule dynamics, and how this leads to microtubule patterning.

2) Mechanical patterning relies on the hypothesis that the stress experienced specifically at the neck [22], would stabilize microtubules. Microtubules localized elsewhere, in the lobes for instance, and microtubules present at the neck but not aligned with the stress, would be depolymerized preferentially. Such response to mechanical patterning is thought to be associated with CLASP and KATANIN [23]. Although neither CLASP [24] nor KATANIN [25] have been reported to present a differential pattern between lobes and necks. Spatial heterogeneity in the activity of CLASP and KATANIN may exist, but no experimental evidence has been revealed so far. Again, studies here focused on relatively long time scales and do not propose a model for linking microtubule dynamics with the emerging pattern observed.

Here, we decided to investigate microtubule dynamics at high spatial and temporal scale. We first quantified whole body microtubule dynamics to look at local variations of angle distributions. We then imaged specifically the tip of microtubules to visualize differences in polymerization direction.

Results

Imaging microtubules at high frequency.

To visualize microtubule dynamics at high frequency, we used a light sheet microscope that allowed rapid imaging of a relatively thick section of the cotyledon without inducing photobleaching. With this setup we were able to capture a field of view of at most 200x200 µm with 40 slices spread over 60 µm every 5 second for 10 minutes. Each stack took approximately 2 second for imaging which led to a total exposure time of the sample of 4 minutes.

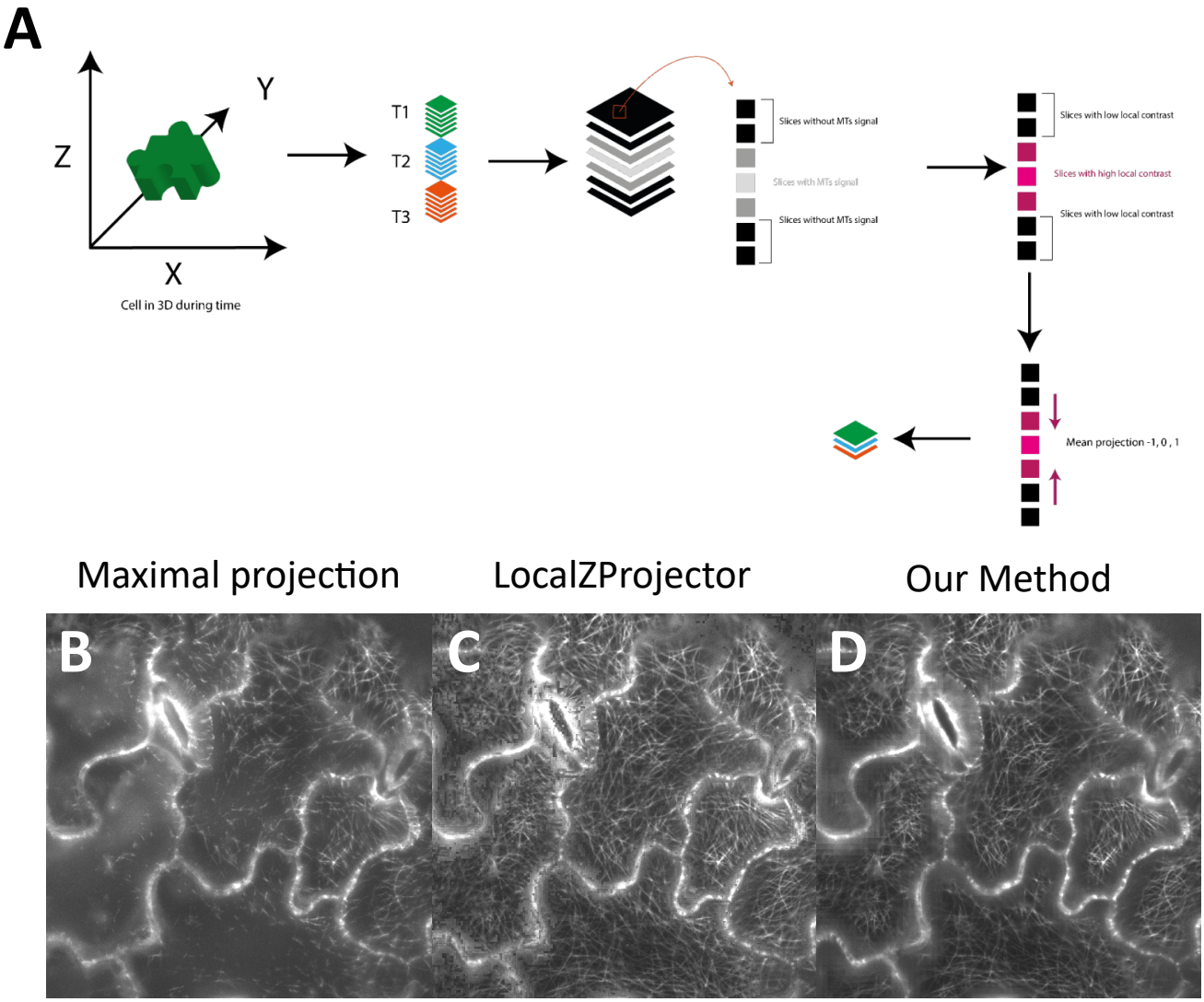

Fig. 1. Method used for the projection of light sheet images
A. Detail of the method used. **B.** Maximum projection of one of the stack obtained. **C.** LocalZProjector projection. **D.** Projection with our method.

Maximum projections of the signal gave relatively poor results (Fig. 1B). This stems from light sheet microscopy generating particular artifacts. The illumination of a thick and opaque sample by a light sheet generates diffraction that diffuses inside the tissue. While the light sheet should only illuminate one plane at a time, the diffraction induces structures above and below the illuminated plane. The deeper in the tissue, the higher the diffraction intensity, and sometimes, this intensity was even higher than the microtubule signal. In order to image cortical microtubules of a whole cell, because pavement cells have a curved surface, we had to image a thick section. We decided to develop a pipeline for the selective projection of the surface signal of light sheet image.

Selective projection of epidermal cortical microtubule signal.

Each stack presented a stereotyped pattern from top to bottom: 1) absence of signal, 2) diffraction at the top of the structures of interest, 3) clear signal from the microtubules, 4) diffraction at the bottom of the structures of interest, 5) absence of signal (Fig. 1A). In order to discriminate between slices of interest and other slices, we took advantage that the slices of interest were the ones with the highest contrast. Slices far from the structures presented a homogeneous low signal. Slices in the diffraction zone presented a homogeneous high signal. Slices in the microtubule zone presented a high microtubule signal and a low intensity background. The use of contrast should then allow us to discriminate between slices.

Pavement cells, however, have an uneven surface and are not positioned orthogonally to the optical axis. Therefore, there is no single plane that contains all the microtubule signal. In order to reliably project the slices containing the microtubule signal, we subdivided the whole

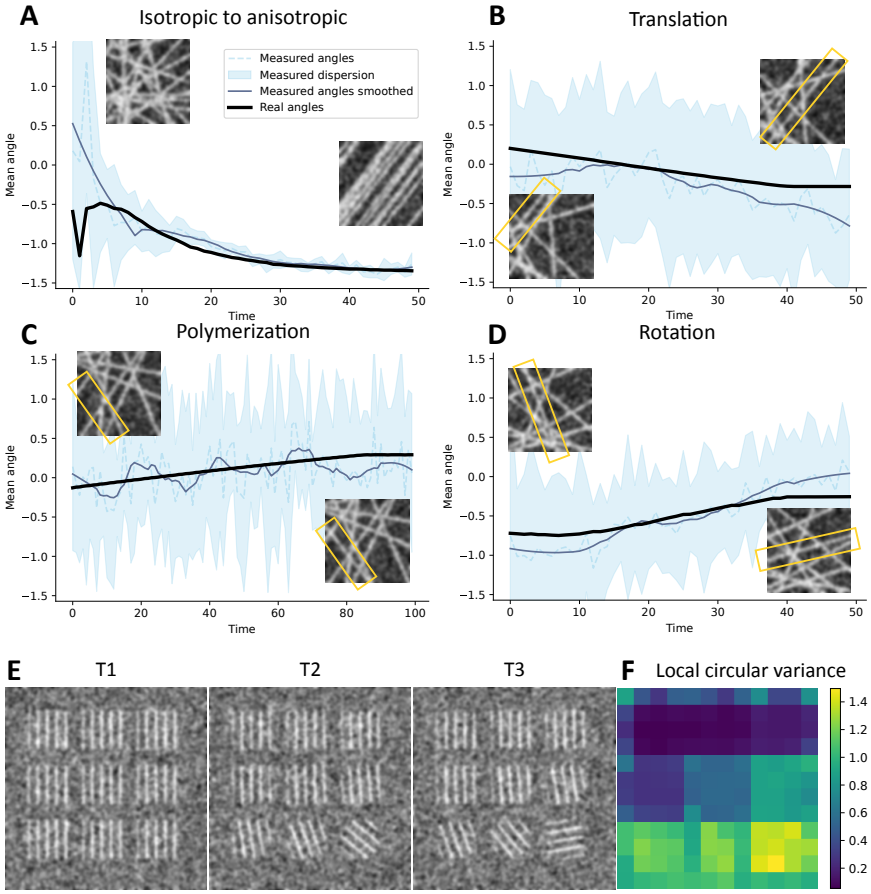

Fig. 2. Verification of the localized variability quantification pipeline on artificial images
A. Comparison of the mean angle generated, and the mean angle obtained with AFT. The inlay images correspond to the first and the last images of the sequence. Here, the exemple of isotropic to anisotropic configuration is represented. **B.** Illustration of microtubule translation. The angle varies despite no change in angle as the weight of the microtubule regarding the mean angle is dependant on the length of the segment. Orange rectangles highlight the microtubule that is dynamic, other microtubules are static. **C.** Illustration of a polymerizing microtubule. Note that depolymerization have the exact reverse dynamic. **D.** Illusrtation of a rotating microtubule. **E.** Three first images of an artificial map generated for the quantification of microtubule local dynamics. Nine groups of microtubules were generated, each group rotates of a fixed angle at each time step. The total sequence is 50 images long. **F.** Associated quantification of the circular variance. The mean angle is calculated for small patches on the map shown on (E). The circular variance is then computed on the list of all the mean angle of the same position over time.

image into overlapping patches of 30 pixels (about 5µm) by 30 pixels in the XY plane every 20 pixels (Fig. 1A). Then, on each of these patches, we computed the local contrast with a radius of 5pixels on every slice and stored the position of its maximum. A map of these positions of maximum contrast of the local maximum was thus created. We noticed local variability in the position of the maximum detected, however, we expect microtubules to run smoothly under the membrane. We thus applied a smoothing step by attributing to each patch the median value of a 3x3 square around the cell. These maps were then used to project the signal of the three slices around the microtubule signal (Fig. 1D). Qualitatively, the selective projection gave improved results compared to a maximum projection, notably with a more homogeneous microtubule signal throughout the cell.

During the development and preparation for publication of this pipeline, a new method for the projection of light sheet images was published: LocalZProjector ([26]). The two methods appeared to be very similar, with the notable exception that our implementation was done with python and their implementation was directly in ImageJ. Additionally, their method proposes two types of selection of the slices that present a signal, one based on the mean intensity, and one based on the standard deviation. Our method based on the local contrast gave slightly better results for the projection of microtubule signal. However, my implementation took a drastically longer time to run compared to their method. For the rest of the analysis, we decided to use their method for the projection of our microtubule signal. Now that we had a satisfying projection of the microtubules, we moved on to the analysis of their dynamics.

Test of the analysis pipeline on artificial images.

To quantify microtubule dynamics, we decided to investigate evolution of the average angle of microtubules at subcellular scale. We divided the cell into patches, and, for each patch, we quantified the average orientation of fibrillar elements using the AFT python package ([27]). AFT performs Fourrier transform analysis and extracts the main orientation of fibrils by using the eigenvalue of the associated covariance matrix. For an image, this gives an orientation and an eccentricity, which evaluates how structured the image is. This method should be less sensitive to noise, but also less sensitive to variations in microtubule orientation.

In order to validate the analysis pipeline we developed, we generated artificial images corresponding to various situations of microtubule dynamics: polymerization, translation, rotation and a switch from isotropic to anisotropic (Fig. 2A-D). In the first three situations we considered an ensemble of static microtubules and one microtubule that

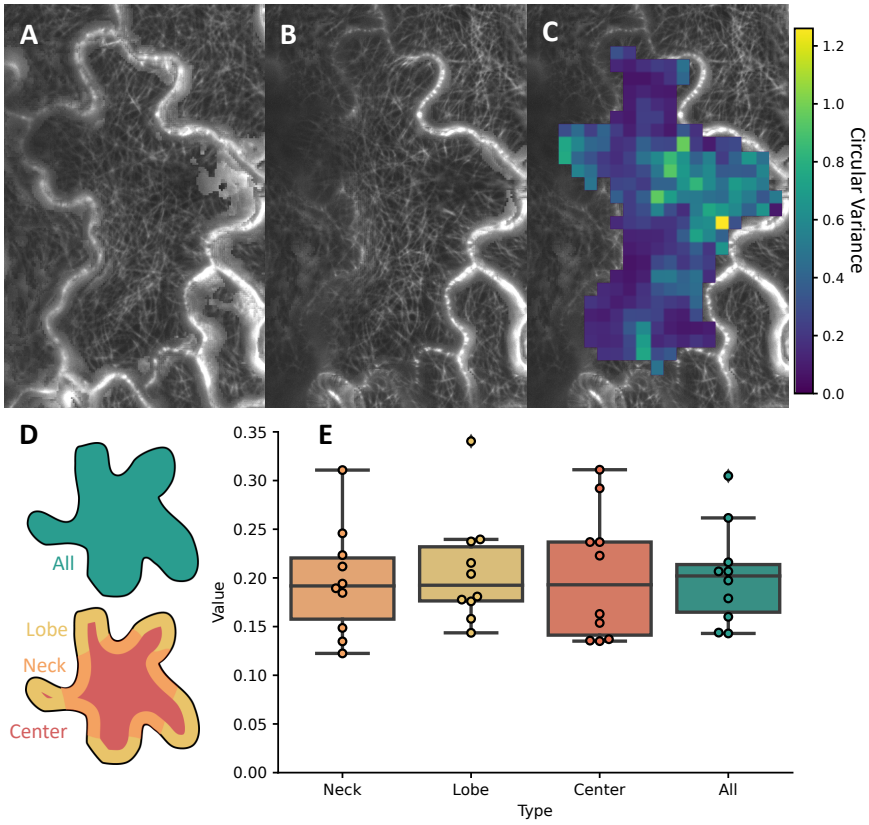

Fig. 3. Dynamics of microtubules at short time scales are similar between regions of the cell
A, B. First (A) and last (B) image of a pavement cell imaged for 10 minutes every 5 seconds. **C.** Panel B with superposed the results for the quantification of circular variance. Each square corresponds to the results of the analysis on a 50 pixel wide area. **D.** Schematic of the different zones considered for the regionnalised analysis. **E.** Quantification of the circular variance in the different regions depicted in (D). Each point represent the median value of cells of one cotyledon. Boxplot depicts median, first and third quartile, and minimum/maximum. Extremum values that are further than three times the interquartile range from the median are considered outsiders.

was dynamic. One situation was represented by a series of 50 images where the dynamic occurred. For instance, for a polymerization sequence, we have 50 images with static microtubules but one that polymerizes over the 50 images. 10 sequences were generated for each category and the orientation of each generated microtubule was recorded. For the last situation, that corresponds to a switch from isotropic to anisotropic, we generated initially isotropic microtubules that converged over 50 images towards the same angle. All sequences yielded satisfying results (Fig. 2A-D).

We then confirmed that our method was able to detect spatial differences in fibril dynamics. We generated a map with nine patches of microtubules that rotate at different speeds (Fig. 2E). We quantified the average orientation of fibrils of small regions using AFT at all time steps. For each region, we then used this sequence of average orientations to compute a circular variance. This produced a map of local circular variance that describes how dynamic the fibrils of an area are (Fig. 2F). Indeed, the map correlated, with regions with fibrils that rotated the fastest presenting the highest values of circular variance. It is important to note that AFT will always detect an orientation even in regions without fibrils (Fig. 2F, top left corner). Regions deprived of fibrils will thus be associated with an orientation computed on noise. Pavement cells present a concentration of microtubules that produces no such zone.

Circular variance of the average microtubule angle does not vary between regions.

We then quantified microtubule dynamics in vivo. We imaged developing pavement cell of cotyledons and computed the circular variance of patches of 50 pixels × 50 pixels (Fig. 3A-C). This produced maps of the circular variance that we could overlay with the original images. By using masks, we then selected the median value of the different regions (Fig. 3D). We found no difference between the circular variance of the different regions (Fig. 3E).

Tracking of microtubule ends.

In order to characterize microtubule polymerization more precisely, we decided to track specifically the growing tips of microtubule. The protein EB1 associates with the GTP cap, and is therefore only present at the growing tip of microtubules. We imaged GFP-EB1 cotyledons with a time interval of 5 to 9 seconds (Fig. 5A,B), which allowed qualitative tracking of particles by eye. Temporal integration also presented linear tracks that suggest that the time interval that we picked is appropriate for the displacement speed of the microtubule tip. We performed tracking of particles using the trackpy python library [28]. The results of the tracking software seemed satisfying by eye when we superposed the signal and the trajectories obtained by tracking (Fig. 4D). We then analyzed particle speed as a function of the tracking time (Fig. 4E). We

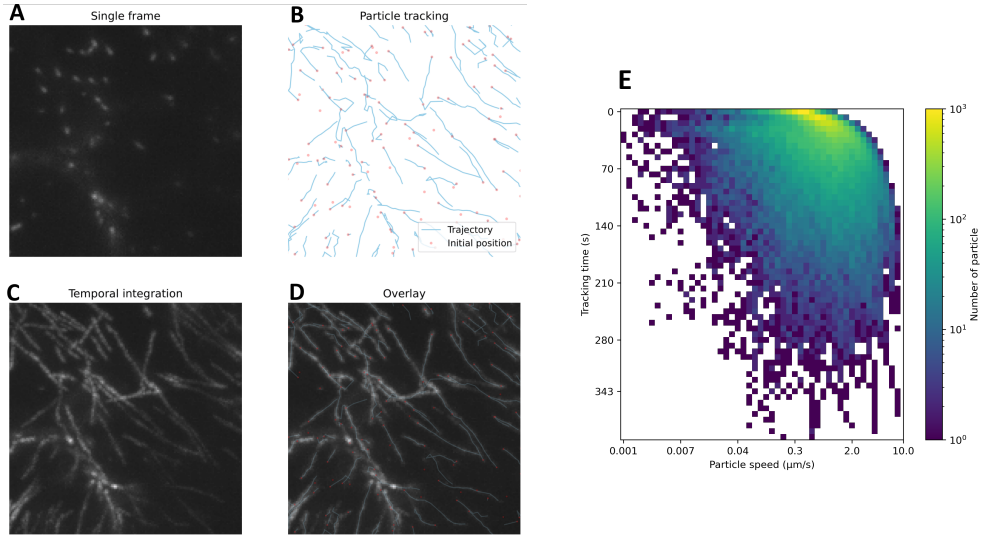

Fig. 4. Tracking of EB1
A. Single time point image of EB1. **B.** Results of particle tracking. Initial position of the particles is indicated by a red circle, trajectory by a blue line. **C.** Temporal integration of EB1 images. **D.** Overlay of B and C.

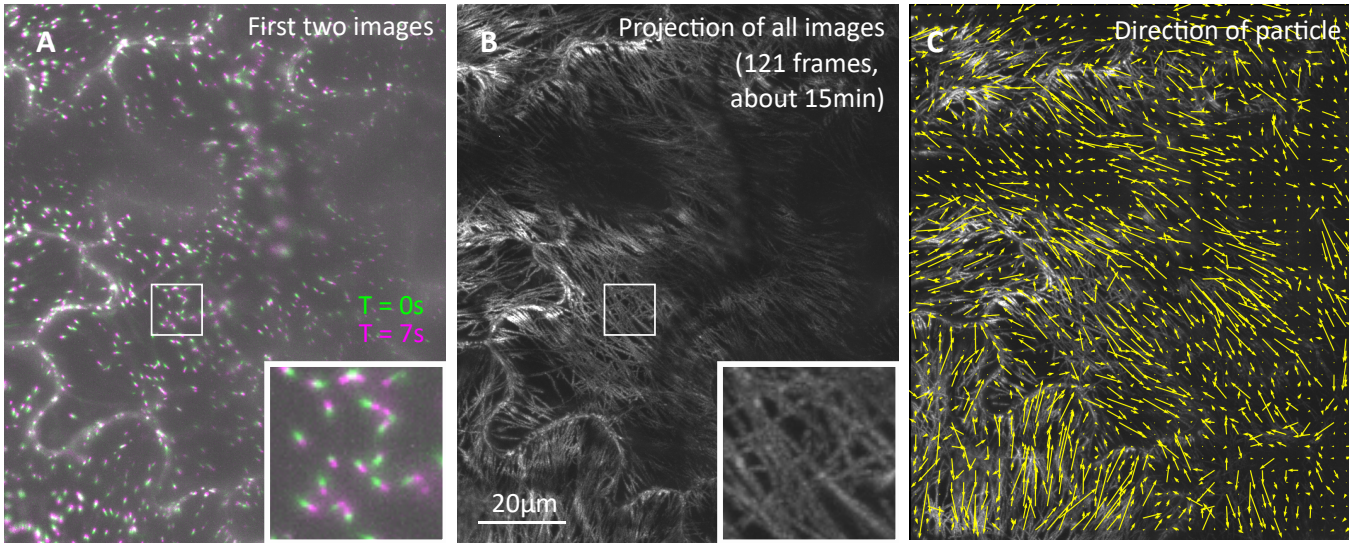

Fig. 5. Tracking of EB1 particles
A. Two consecutive image of EB1 particles colored in green and magenta. White colors indicate a superposition of the two images. **B.** Temporal integration of a complete sequence of EB1 imaging. **C.** Displacement field of particles. We divided the image in small regions of 20 × 20 pixels, and stored the index of particles that were first detected in each region. We then computed the total displacement vector of all the particles that started in a small region.

found an average speed of 500nm/s, which matches the rates observed in animal cells [29, 30], which suggest that we indeed identified growing tip of microtubules.

To qualitatively map differences in polymerization directions, we divided the cell into small regions of 20 × 20 pixels. At each of these positions, we looked at the particles that were first detected in that zone, and computed the mean displacement vector. Regions with particles that move all in the same direction result in vector with a large norm, while region with random growth directions result (Fig. 5C). Qualitatively with our current results, we did not find differences between regions.

Conclusion

Our preliminary results suggest that microtubule dynamics present no differences spatially if we do not account for orientation specific behaviors. Analysis of growing microtubule tips also indicate that there might not be differences in terms of orientation for polymerizing microtubules. Together this may suggest that the regulation that explains microtubule patterning in pavement cells rely on orientation specific depolymerization of microtubules.

Materials & Methods

Lines used and growth conditions. Lines used were 35S::mcitrin-MBD [31] and 35S::AtEB1a-GFP [32]. Seed were sew on on solid custom-made Duchefa 'Arabidopsis'

medium (DU0742.0025, Duchefa Biochemie). The plant growth in "long day" conditions in phytotron, plants were grown under a 16hr (21°C) / 8hr (19°C) light/dark period. Seedling were imaged after 7 days of growth.

Imaging setup. All image were acquired using Alpha 3 Light Sheet with a 40x objective (N = 0.8). Image resolution corresponds to a pixel size of 0,1625 µm and a Z step of 0,5 µm. Seedling were placed on a drop of low melting agar and imaged in water.

Data analysis. All codes used in this study will be made available with the final version of the publication.

References

[1] M. F. Carlier, "Role of Nucleotide Hydrolysis in the Dynamics of Actin Filaments and Microtubules," in *International Review of Cytology* (K. W. Jeon and M. Friedlander, eds.), vol. 115, pp. 139–170, Academic Press, Jan. 1989.

[2] G. J. Brouhard and L. M. Rice, "Microtubule dynamics: an interplay of biochemistry and mechanics," *Nature Reviews Molecular Cell Biology*, vol. 19, pp. 451–463, July 2018. Number: 7.

[3] W. G. Hirst, C. Kiefer, M. K. Abdosamadi, E. Schäffer, and S. Reber, "In Vitro Reconstitution and Imaging of Microtubule Dynamics by Fluorescence and Label-free Microscopy," *STAR Protocols*, vol. 1, p. 100177, Dec. 2020.

[4] J. Roostalu, C. Thomas, N. I. Cade, S. Kunzelmann, I. A. Taylor, and T. Surrey, "The speed of GTP hydrolysis determines GTP cap size and controls microtubule stability," *eLife*, vol. 9, p. e51992, Feb. 2020. Publisher: eLife Sciences Publications, Ltd.

[5] Y. Komarova, C. O. De Groot, I. Grigoriev, S. M. Gouveia, E. L. Munteanu, J. M. Schober, S. Honnappa, R. M. Buey, C. C. Hoogenraad, M. Dogterom, G. G. Borisy, M. O. Steinmetz, and A. Akhmanova, "Mammalian end binding proteins control persistent microtubule growth," *Journal of Cell Biology*, vol. 184, pp. 691–706, Mar. 2009.

[6] A. T. Molines, J. Marion, S. Chabout, L. Besse, J. P. Dompierre, G. Mouille, and F. M. Coquelle, "EB1 contributes to microtubule bundling and organization, along with root growth, in Arabidopsis thaliana," *Biology Open*, vol. 7, p. bio030510, Aug. 2018.

[7] A. Aher, D. Rai, L. Schaedel, J. Gaillard, K. John, Q. Liu, M. Altelaar, L. Blanchoin, M. Thery, and A. Akhmanova, "CLASP Mediates Microtubule Repair by Restricting Lattice Damage and Regulating Tubulin Incorporation," *Current Biology*, vol. 30, pp. 2175–2183.e6, June 2020.

[8] C. Ambrose, J. F. Allard, E. N. Cytrynbaum, and G. O. Wasteneys, "A CLASP-modulated cell edge barrier mechanism drives cell-wide cortical microtubule organization in Arabidopsis," *Nature Communications*, vol. 2, p. 430, Aug. 2011.

[9] M. Uyttewaal, A. Burian, K. Alim, B. Landrein, D. Borowska-Wykręt, A. Dedieu, A. Peaucelle, M. Ludynia, J. Traas, A. Boudaoud, D. Kwiatkowska, and O. Hamant, "Mechanical Stress Acts via Katanin to Amplify Differences in Growth Rate between Adjacent Cells in Arabidopsis," *Cell*, vol. 149, pp. 439–451, Apr. 2012.

[10] M. Nakamura, D. W. Ehrhardt, and T. Hashimoto, "Microtubule and katanin-dependent dynamics of microtubule nucleation complexes in the acentrosomal Arabidopsis cortical array," *Nature Cell Biology*, vol. 12, pp. 1064–1070, Nov. 2010. Number: 11 Publisher: Nature Publishing Group.

[11] M. C. Comes, P. Casti, A. Mencattini, D. Di Giuseppe, F. Mermet-Meillon, A. De Ninno, M. C. Parrini, L. Businaro, C. Di Natale, and E. Martinelli, "The influence of spatial and temporal resolutions on the analysis of cell-cell interaction: a systematic study for time-lapse microscopy applications," *Scientific Reports*, vol. 9, p. 6789, May 2019. Number: 1 Publisher: Nature Publishing Group.

[12] A. T. Molines, J. Lemière, M. Gazzola, I. E. Steinmark, C. H. Edrington, C.-T. Hsu, P. Real-Calderon, K. Suhling, G. Goshima, L. J. Holt, M. Thery, G. J. Brouhard, and F. Chang, "Physical properties of the cytoplasm modulate the rates of microtubule polymerization and depolymerization," *Developmental Cell*, vol. 57, pp. 466–479.e6, Feb. 2022.

[13] O. Hamant, D. Inoue, D. Bouchez, J. Dumais, and E. Mjolsness, "Are microtubules tension sensors?," *Nature Communications*, vol. 10, p. 2360, May 2019.

[14] L. Colin, A. Chevallier, S. Tsugawa, F. Gacon, C. Godin, V. Viasnoff, T. E. Saunders, and O. Hamant, "Cortical tension overrides geometrical cues to orient microtubules in confined protoplasts," *Proceedings of the National Academy of Sciences*, vol. 117, pp. 32731–32738, Dec. 2020.

[15] S. Liu, F. Jobert, Z. Rahneshan, S. M. Doyle, and S. Robert, "Solving the Puzzle of Shape Regulation in Plant Epidermal Pavement Cells," *Annual Review of Plant Biology*, vol. 72, no. 1, pp. 525–550, 2021. _eprint: https://doi.org/10.1146/annurev-arplant-080720-081920.

[16] A. Sapala, A. Runions, A.-L. Routier-Kierzkowska, M. Das Gupta, L. Hong, H. Hofhuis, S. Verger,

G. Mosca, C.-B. Li, A. Hay, O. Hamant, A. H. Roeder, M. Tsiantis, P. Prusinkiewicz, and R. S. Smith, "Why plants make puzzle cells, and how their shape emerges," *eLife*, vol. 7, p. e32794, Feb. 2018.

[17] A. Sapala, A. Runions, and R. S. Smith, "Mechanics, geometry and genetics of epidermal cell shape regulation: different pieces of the same puzzle," *Current Opinion in Plant Biology*, vol. 47, pp. 1–8, Feb. 2019.

[18] Y. Fu, Y. Gu, Z. Zheng, G. Wasteneys, and Z. Yang, "Arabidopsis Interdigitating Cell Growth Requires Two Antagonistic Pathways with Opposing Action on Cell Morphogenesis," *Cell*, vol. 120, pp. 687–700, Mar. 2005.

[19] Y. Fu, T. Xu, L. Zhu, M. Wen, and Z. Yang, "A ROP GTPase Signaling Pathway Controls Cortical Microtubule Ordering and Cell Expansion in Arabidopsis," *Current Biology*, vol. 19, pp. 1827–1832, Nov. 2009. Publisher: Elsevier.

[20] D. Lin, L. Cao, Z. Zhou, L. Zhu, D. Ehrhardt, Z. Yang, and Y. Fu, "Rho GTPase Signaling Activates Microtubule Severing to Promote Microtubule Ordering in Arabidopsis," *Current Biology*, vol. 23, pp. 290–297, Feb. 2013. Publisher: Elsevier.

[21] C. Li, H. Lu, W. Li, M. Yuan, and Y. Fu, "A ROP2-RIC1 pathway fine-tunes microtubule reorganization for salt tolerance in Arabidopsis," *Plant, Cell & Environment*, vol. 40, no. 7, pp. 1127–1142, 2017.

[22] A. Sampathkumar, P. Krupinski, R. Wightman, P. Milani, A. Berquand, A. Boudaoud, O. Hamant, H. Jönsson, and E. M. Meyerowitz, "Subcellular and supracellular mechanical stress prescribes cytoskeleton behavior in Arabidopsis cotyledon pavement cells," *eLife*, vol. 3, p. e01967, Apr. 2014. Publisher: eLife Sciences Publications, Ltd.

[23] R. C. Eng, R. Schneider, T. W. Matz, R. Carter, D. W. Ehrhardt, H. Jönsson, Z. Nikoloski, and A. Sampathkumar, "KATANIN and CLASP function at different spatial scales to mediate microtubule response to mechanical stress in Arabidopsis cotyledons," *Current Biology*, vol. 31, pp. 3262–3274.e6, Aug. 2021.

[24] J. C. Ambrose, T. Shoji, A. M. Kotzer, J. A. Pighin, and G. O. Wasteneys, "The Arabidopsis CLASP Gene Encodes a Microtubule-Associated Protein Involved in Cell Expansion and Division," *The Plant Cell*, vol. 19, pp. 2763–2775, Sept. 2007.

[25] Q. Zhang, E. Fishel, T. Bertroche, and R. Dixit, "Microtubule Severing at Crossover Sites by Katanin Generates Ordered Cortical Microtubule Arrays in Arabidopsis," *Current Biology*, vol. 23, pp. 2191–2195, Nov. 2013.

[26] S. Herbert, L. Valon, L. Mancini, N. Dray, P. Caldarelli, J. Gros, E. Esposito, S. L. Shorte, L. Bally-Cuif, N. Aulner, R. Levayer, and J.-Y. Tinevez, "LocalZProjector and DeProj: a toolbox for local 2D projection and accurate morphometrics of large 3D microscopy images," *BMC Biology*, vol. 19, p. 136, July 2021.

[27] S. Marcotti, D. Belo de Freitas, L. D. Troughton, F. N. Kenny, T. J. Shaw, B. M. Stramer, and P. W. Oakes, "A Workflow for Rapid Unbiased Quantification of Fibrillar Feature Alignment in Biological Images," *Frontiers in Computer Science*, vol. 3, 2021.

[28] D. B. Allan, T. Caswell, N. C. Keim, C. M. van der Wel, and R. W. Verweij, "soft-matter/trackpy: Trackpy v0.5.0," Apr. 2021.

[29] S. Gierke, P. Kumar, and T. Wittmann, "Analysis of microtubule polymerization dynamics in live cells," *Methods in cell biology*, vol. 97, pp. 15–33, 2010.

[30] A. Nakano, H. Kato, T. Watanabe, K.-D. Min, S. Yamazaki, Y. Asano, O. Seguchi, S. Higo, Y. Shintani, H. Asanuma, M. Asakura, T. Minamino, K. Kaibuchi, N. Mochizuki, M. Kitakaze, and S. Takashima, "AMPK controls the speed of microtubule polymerization and directional cell migration through CLIP-170 phosphorylation," *Nature Cell Biology*, vol. 12, pp. 583–590, June 2010.

[31] S. R. Cutler, D. W. Ehrhardt, J. S. Griffitts, and C. R. Somerville, "Random GFP::cDNA fusions enable visualization of subcellular structures in cells of Arabidopsis at a high frequency," *Proceedings of the National Academy of Sciences of the United States of America*, vol. 97, pp. 3718–3723, Mar. 2000.

[32] J. Chan, G. Calder, S. Fox, and C. Lloyd, "Localization of the microtubule end binding protein EB1 reveals alternative pathways of spindle development in Arabidopsis suspension cells," *The Plant Cell*, vol. 17, pp. 1737–1748, June 2005.

Shape, cell wall stiffness and turgor pressure of pavement cells

Graphical Abstract

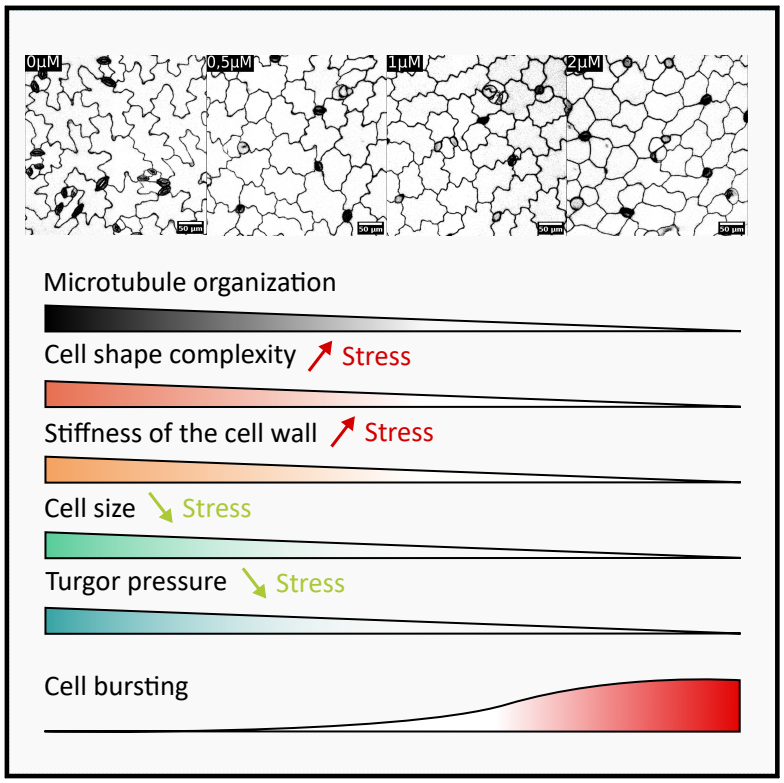

Highlights

- Plants grown on a range of oryzalin concentration produced a range of cell shape defects.
- The largest empty circle (as a proxy for maximum stress) first increases with the defects (as a result of cell shape loss), but then decreases (as a result of cell size reduction).
- Disruption of microtubules seem to lead to a reduction of wall stiffness.
- Defects in cell shape are compensated by a reduction in cell size and a decrease of turgor pressure, but also lead to cell bursting.

Authors

Mylan Ansel, Corentin Mollier, Alice Malivert, and Arezki Boudaoud

In Brief

Plants are complex systems that exhibit various redundant and compensatory mechanisms. Cell shape appears as a critical point for mechanical integrity and associated defects may trigger compensatory pathways. We used a range of oryzalin treatments to depolymerize microtubules, preventing pavement cells from acquiring their particular puzzle shape. This range of treatments generated a range of pavement cells from unaffected to circular. We then evaluated cell wall mechanical properties by measuring cell-wall retractation at the cellular scale under osmotic treatment. Finally, cell shape and wall properties were compared to try and evaluate the existence of compensatory mechanisms.

Contributions

This part was done with an intern, Mylan Ansel. I designed the project, supervised and helped him with the analysis but he performed all the measurements and analysis. This is his internship report.

Shape, cell wall stiffness and turgor pressure of pavement cells

Mylan Ansel[1], **Corentin Mollier**[1], **Alice Malivert**[1], **and Arezki Boudaoud**[1]

[1] Reproduction et développement des plantes, ENS de Lyon, France

Shape and functions of cells are related. In plants, cells display an important diversity of shape. For instance, leaf and cotyledon epidermal cells can have various shapes like trichomes, stomatal or pavement cells. Existing in many eudicot plants, pavement cells present a complex shape composed of necks and lobes making them look like jigsaw-puzzle pieces [1]. Their formation requires a highly regulated cell growth [2–4].

Cell growth depends on two main parameters: turgor pressure and cell wall stiffness [5]. The turgor pressure, caused by the water stored within cells, pushes the membrane against the cell wall, generating a pressure on it. Thus, it causes stress on the cell wall, that elastically or plastically deforms. The primary cell wall, that surrounds plant cells and resists turgor pressure, is notably composed of cellulose. Its disposition, which is guided by microtubules, mainly determines the resistance of the cell wall against the turgor pressure. Because microtubule organization responds to the stress, it creates a stress feedback loop which is essential for puzzle shape formation. In addition, independently of microtubules, other mechanisms control the cell wall stiffness [6].

Functions of puzzle shape are still unclear. It has been suggested that this shape could play a role in chemical signaling or tissue integrity [7–9] and, more recently, that it would allow cell size increase without increasing cell stress [10]. In circular cells, the stress will increase with cell size and become, after reaching a threshold, high enough to break the cell wall. In puzzle shaped cells, the stress will increase more slowly with cell size, turning the threshold for rupture above non physiological stress values.

Nevertheless, some mutant plants display pavement cells without a puzzle shape [4]. While these cells must be exposed to a higher stress, no cell wall rupture has been observed. Two hypotheses are conceivable: either the puzzle shape does not play a role in preventing cell bursting, or compensation mechanisms that prevent cell bursting are triggered in those cells. This compensation could be an increase of cell wall stiffness or a decrease of turgor pressure, both resulting in a stress decrease.

Here we investigated compensation upon loss of puzzle cell shape. For this purpose, we altered pavement cells shape of cotyledons of A*rabidopsis thaliana* by disrupting microtubule organization via oryzalin, and quantified cell wall stiffness as well as turgor pressure.

Results

Puzzle shape is lost when pavement cells grow exposed to oryzalin.

To change pavement cell shape, we made the plants grow in mediums with increasing concentration of oryzalin, a drug which depolymerizes microtubules [11]. We used a fluorescent microtubules reporter (*pPDF1::mCitrine-MBD*) to confirm that they were disturbed (Supp data 1).

Then, to quantify the shape change, we took pavement cells images for each condition with confocal microscopy (Fig 1). We used a propidium iodide (PI) treatment to visualize cell walls. We found that cells became smaller when oryzalin concentration increased (Fig 1A,B). To quantify how lobed cells were, we calculated the solidity [1], defined as the cell area divided by the convex hull area (Fig 1C). The less a cell has lobes, so the further away from a puzzle shape it is, the closer to 1 its solidity is. The solidity increased with oryzalin concentration (from 0.75 without oryzalin to 0.95 from 5µM) meaning that pavement cells progressively lost their puzzle shape (Fig 1D). After 10µM, there were no significant differences of shape between conditions (Fig 1A,D) and some pavement cells started dying, as shown by the PI inside cells. In addition, we found some burst cells (some of them are indicated by red arrows), potential indicators of too high stress (Fig 1A). So, because these pavement cells lost their puzzle shape, were they exposed to a higher stress?

The Largest Empty Circle (LEC) (Fig 2A) is known to be a proxy of the stress [10]. We observed that the LEC increases linearly with cell area (Fig 2B), meaning that the bigger the cell, the larger the LEC, and therefore the higher stress it was exposed to. However, the slope of the ratio LEC/area was steeper the higher the oryzalin concentration. This confirms that puzzle shape is a way to reduce the stress during cell growth. The LEC radius was higher for cells exposed to 0.5, 1 and 2µM of oryzalin than for untreated cells (Fig 2C). This can be explained by the fact that for these conditions, cells were more circular, but their area was still large. Thus, if we make the hypothesis that turgor pressures were similar between these conditions, the stress is predicted to be more important. In contrast, after 5µM of oryzalin, the

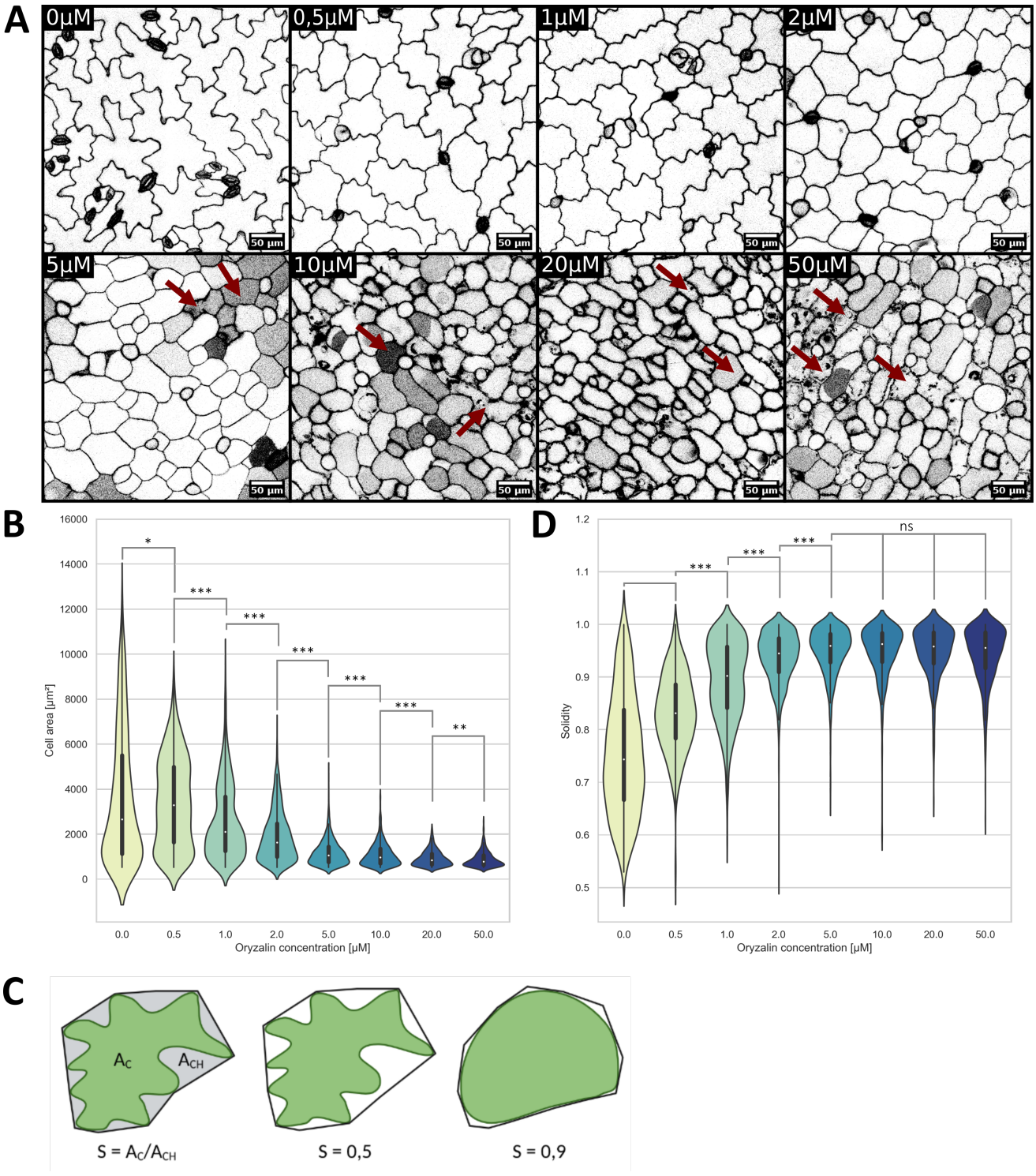

Fig. 1. Pavement cells lose their puzzle shape when plants grow exposed to oryzalin.
Shape analysis of pavement cells of *Col-0* cotyledons. **(A)** Representative confocal images for oryzalin concentrations after a PI treatment (45µM, 30min). Colors are inverted, red arrows indicate some burst cells. **(B)** Cell area for each condition. **(C)** Schematic representation of solidity (cell area divided by convex hull area). **(D)** Solidity for each condition. Statistical analysis on at least 518 cells and 4-6 cotyledons. Mann Whitney test, ns: p-value>0.5, *: p-value<0.05, **: p-value<0.01, ***: p-value<0.001. .

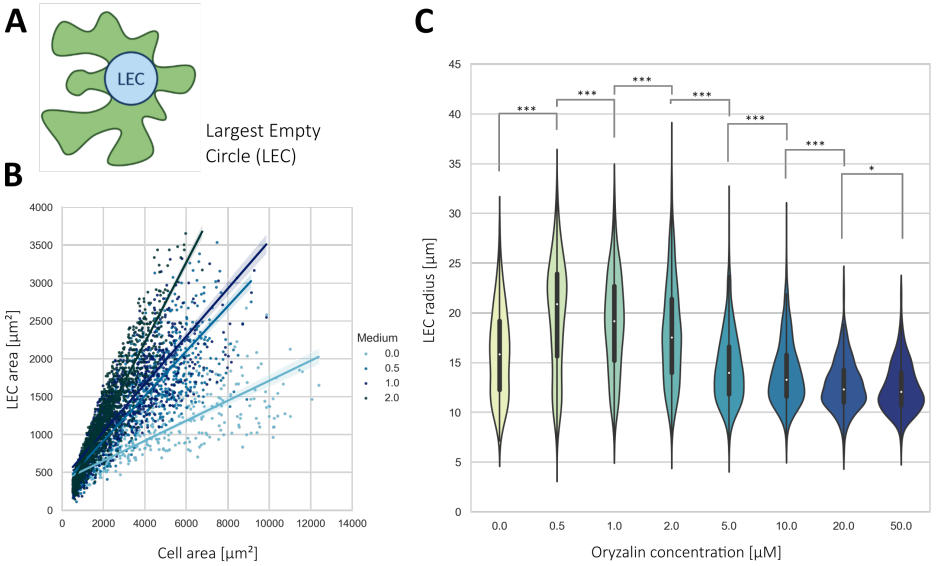

Fig. 2. Pavement cells are not exposed to the same stress in each condition.
Largest Empty Circle (LEC) analysis of pavement cells of *Col-0* cotyledons. **(A)** Schematic representation of the LEC. **(B)** LEC area in function of cell area for 4 oryzalin conditions, R^2 are respectively 0.67, 0.73, 0.74 and 0.87 for 0, 0.5, 1 and 2µM. **(C)** LEC radius for each condition. Statistical analysis at least 518 cells and 4-6 cotyledons. Mann Whitney test, *: p-value<0.05, ***: p-value<0.001.

LEC became smaller than for untreated cells. Surprisingly, while cell area, and therefore LEC were smaller for these concentrations, it was also the only ones in which we observed cells burst.

No detectable compensation for puzzle shape loss by cell wall stiffening.

The stress was predicted to be more important for 0.5, 1 and 2µM of oryzalin. Thus, it is possible that cells compensated for it by stiffening their cell wall. To test it, we determined the relative cell wall stiffness. After a PI treatment, we measured cell area in water and after 50min in a sorbitol solution. This osmotic treatment plasmolyzed cells and thus the plasma membrane no longer pushed on the cell wall (Fig 3A). Therefore, upon relaxation the cell wall shrinks. The more the cell wall shrinks, the less it is stiff [12]. We confirmed that plasmolysis occurred by visualizing the plasma membrane (*pATML1::mCitrine-RCI2A*) for all oryzalin concentrations (Fig 3A for 0µM, data not shown for other concentrations). In addition, we controlled that the cell area did not impact shrinkage measures (Fig 3B), nor the cell shape (Fig 3D). Surprisingly, we noticed a huge variability of measures between cotyledons of the same condition (Fig 3C). The shrinkage increased with oryzalin concentrations, from 10.4% at 0µM to 16.7% at 2µM (Fig 3E). Hence, cell walls became less stiff when cells were grown exposed to oryzalin meaning there is no compensation by cell wall stiffening. However, another possibility is compensation by a decrease of turgor pressure.

Pavement cells might compensate for puzzle shape loss by decreasing their turgor pressure.

To see if turgor pressure changes in response to puzzle shape loss, we measured the global turgor pressure of cotyledons. We successively measured cotyledon area after 15min in solutions with an increasing concentration of NaCl (Fig 4A). We determined the osmotic pressure of each NaCl solution (0, 0.538, 0.841, 0.968, 1.050, 1.139, 1.291, 1.537 and 1.939MPa). Thus, by dividing the cotyledon area in each solution by the one in the solution with no NaCl, we obtained the relative cotyledon area in function of the osmotic pressure of the solution (Fig 4B,C). First, we calculated the shrinkage of cotyledons (Fig 4D). This shrinkage, defined with the relative cotyledon area in the last NaCl solution, increased with increasing oryzalin concentrations (from 17.6% at 0µM to 23% at 2µM). This trend is consistent with our precedent measures (Fig 3E), nevertheless, the values are around 40% higher. Secondly, we obtained relative indications of turgor pressure in cotyledons. Indeed, when the osmotic pressure in the medium increases, the turgor pressure decreases [13]. At the inflexion point (one is indicating by a red arrow in Fig 4B), the turgor pressure is equal to zero. Thus, the lower the osmotic pressure corresponding to this point is, the lower the initial turgor pressure was. It seems that the inflexion point is reached for a lower osmotic pressure when oryzalin concentration increases, 1.49MPa at 0µM and 1.16MPa at 2µM of oryzalin (Fig 4E). This trend might indicate a compensation by a decrease of turgor pressure. However, because of time constraints, only four samples per condition were measured and no statistical conclusions can be drawn.

Discussion

We saw that pavement cells lose their puzzle shape when grown exposed to oryzalin. At higher concentration, they become smaller, and many cells burst and die. At lower concentration they keep practically their standard size.

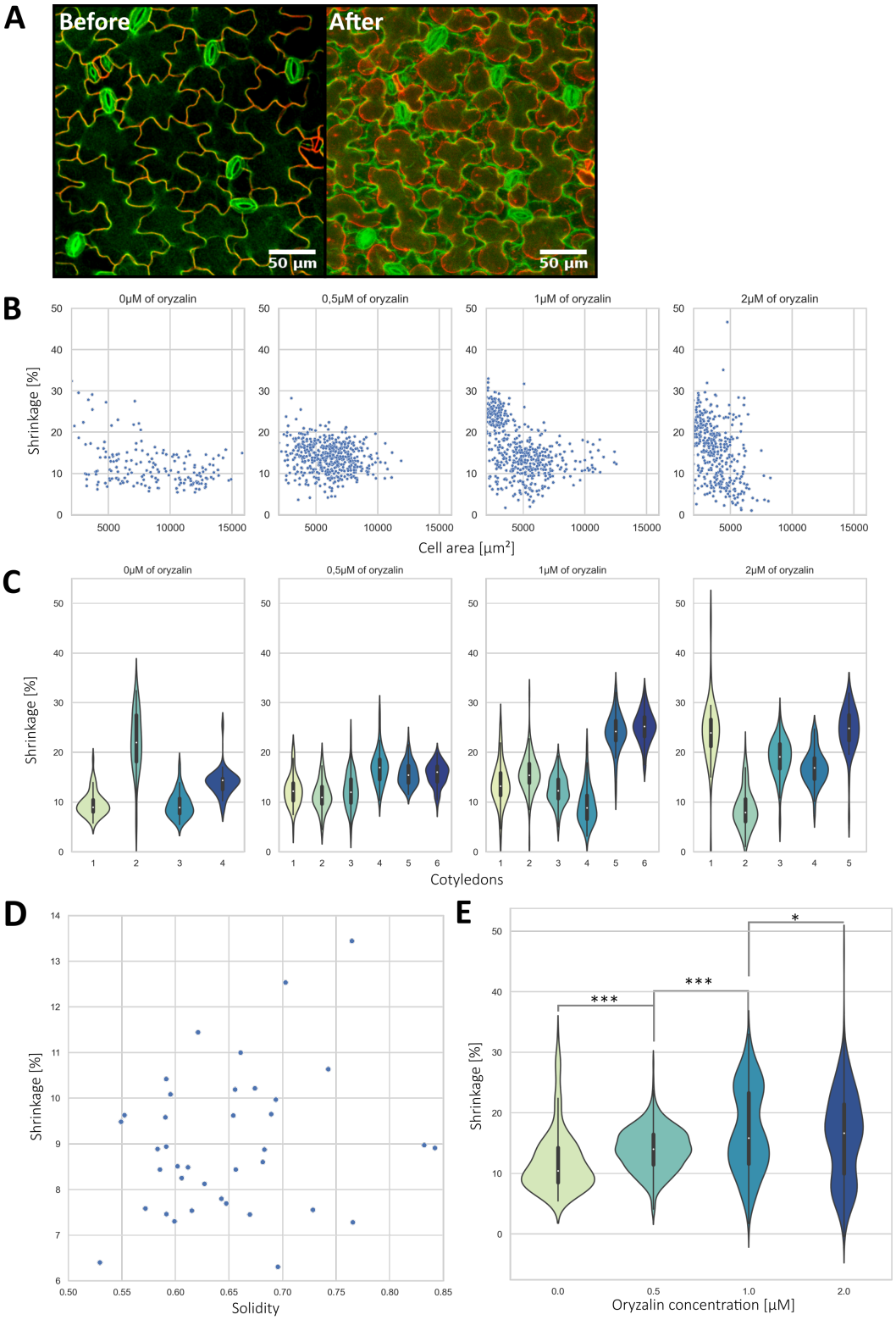

Fig. 3. Pavement cells do not compensate for puzzle shape loss by cell wall stiffening
Shrinkage measures of pavement cells of *Col-0* cotyledons for 4 oryzalin conditions after an osmotic treatment (50min in sorbitol 0.6M). **(A)** Representative image of a cotyledon not exposed to oryzalin, before and after the osmotic treatment. Cell walls are in green (PI) and plasma membrane in red (*pATML1::mCitrine-RCI2A*) **(B)** Shrinkage in function of cell area. **(C)** Shrinkage for each cotyledon. **(D)** Shrinkage in function of solidity for one cotyledon not exposed to oryzalin. **(E)** Shrinkage measures for each condition. Statistical analysis on at least 189 cells and 4-6 cotyledons. Mann Whitney test, *: p-value<0.05, ***: p-value<0.001.

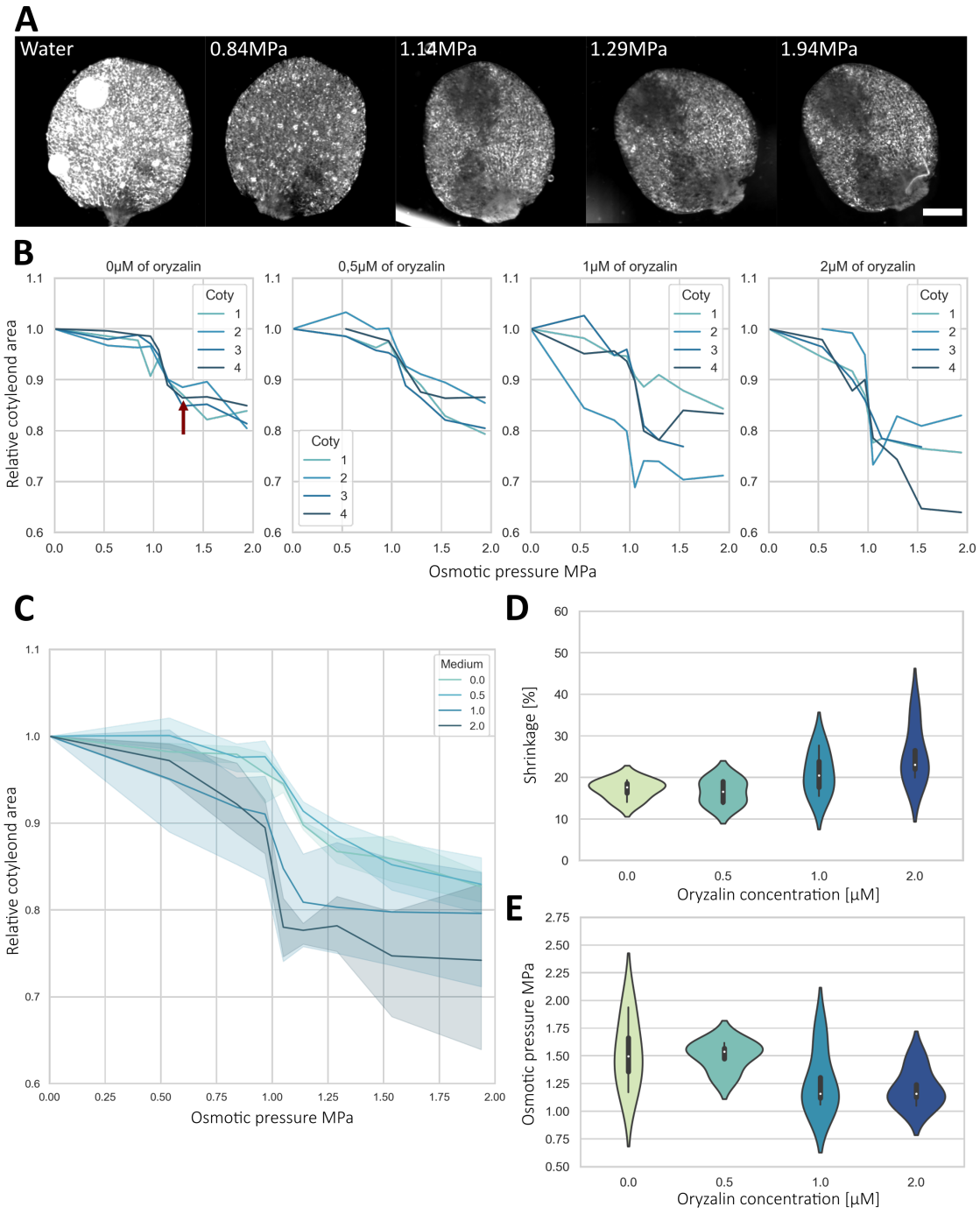

Fig. 4. Pavement cells might compensate for puzzle shape loss by decreasing their turgor pressure
Turgor pressure analysis for 4 oryzalin conditions **(A)** Representative images of a cotyledon not exposed to oryzalin after 15min successively in different NaCl solutions. Scale bar = 100µM **(B)** Relative cotyledon areas in function of the osmotic pressure of the NaCl solutions. The red arrow indicates one inflexion point **(C)** Average relative cotyledon areas for each oryzalin condition (mediums). **(D)** Shrinkage of cotyledons for each condition. **(E)** Osmotic pressure corresponding to the inflexion point of each curve in (B). No statistical analysis because too few repetitions (n=4).

For these conditions, we measured no compensation via cell wall stiffening but our preliminary results seem to indicate a compensation by a decrease of turgor pressure.

We confirmed that oryzalin disturbed pavement cells shape [14], but it could impact more than just the shape. Likely it may affect cell number [15] or cause chemical stresses. To confirm that our results are a direct consequence of shape change, we could use mutants with circular pavement cells like katanin mutants [16]. We could also count the number of pavement cells in each cotyledon to check our results are not due to improper cell numbers, however, it seems that pavement cell divisions are resistant to oryzalin treatments [14].

We saw that cell grown with 5µM of oryzalin have a LEC smaller than untreated cells (Fig 2C) in correlation with a 3 times smaller cell area (Fig 1B). If we expand the cell wall weakening trend we measured, it is also possible that the cell wall becomes so weak that cells cannot even resist the tensile stress applied. In this hypothesis, only small cells (which undergo a lower stress) would resist the tension [10]. Small cell size could then be a direct consequence of cell bursting, even though we cannot rule out a controlled regulation by cells to prevent such bursting or growth limitations due to biotic stress. Quantification of cell bursting (Fig 1A) revealed to be quite difficult with our setup but would likely help answering those questions.

Shrinkage measures are based on two main hypotheses. The first one is that the cell wall must be in the same tensile state for the different conditions before the plasmolysis experiment. The second one is that cell walls must react independently of cell shape to plasmolysis and therefore for the different conditions. We found no correlation between shrinkage and cell area or solidity, suggesting independence of cell shape and plasmolysis (Fig 3B,D). Unfortunately, the first one may not be completely respected because it seems that turgor pressure is not the same in each condition (Fig 4E). However, it would mean that we overvalued the cell wall stiffness for conditions with oryzalin meaning that its reduction would be more important than what we measured. The variability of shrinkage between cotyledons of the same condition (Fig 3C) may indicate imprecisions of quantification or be caused by natural variability between individuals. Increasing the number of repetitions and performing measurements via other methods such as AFM would help answer these questions.

In opposition to our hypothesis, the cell wall stiffness decreases when pavement cells lose their shape (Fig 3E, 4D). It may be because cellulose disposition is less efficient when microtubules are disturbed [17]. Other mechanisms which could reinforce the cell wall would not be sufficient to counterbalance this cellulose loss. A chemical analysis of the cell wall would both reveal how cellulose and other components are affected. The differences between our two measures of cell wall stiffness (Fig 3E, 4D) could be explained because on one side we measured cell contraction and tissue contraction on the other.

Direct measures of turgor pressure are complicated. With our protocol, osmotic pressures at the inflexion point are supposed to be equal to turgor pressures but their values clearly exceed other estimation [13]. It is known that this protocol overestimates real values [13], but we can assume that relative differences are conserved. Thus, our preliminary results seem to indicate a turgor pressure regulation in response to the stress. It could implicate mecanosentive ion transporters, aquaporins and other mechanosensors [13].

In conclusion, we propose here a method which highlights compensation linked with cell wall defects. This method could be used to identify and verify the role of mechanosensors or other actors of this compensation.

Materials & Methods

Plant materials and growth condition.

Three genotypes have been used: *Col-0*, *pAR169* (*pATML1::mCitrine-RCI2A*) to see the plasma membrane, and *mCit-MBD* (*pPDF1::mCit-MBD*) which marks microtubules. We used MS medium (0.7% agar, no sugar and vitamins) with addition of oryzalin at different concentrations (0, 0.5, 1, 2, 5, 10, 20, 50µM) and with compensatory volumes of DMSO. Seed surface sterilized, individually sown and stratified in the cold room for one night. Seedlings were then placed to grow in long-day phytotrons (20°C, 16h light) and observed 6 days after germination.

Image acquisitions.

For shape and cell wall study, cotyledons were dissected and imaged using a Leica SP8 microscope with x25 water immersion objective. *Col-0* and *pAR169* cotyledons were treated with a propidium iodide solution (PI) (45µM, 30min) to visualize cell walls. Using a 514nm laser excitation, the fluorescence signal was collected from 605nm to 642nm for PI and from 521nm to 551nm for *mCit-MBD* and *pAR169*. Each cotyledon was imaged first in water and again after 50min in a sorbitol solution (0.6M).

For turgor pressure study, *Col-0* cotyledons were dissected and imaged using a Nikon SMZ18 stereomicroscope with x6 zoom. They were placed between a curved microscope slide and lamella with water or NaCl solution drops. Pictures were taken after 15min in NaCl solutions of increasing concentrations (0, 0.1, 0.15, 0.175, 0.2, 0.225, 0.25, 0.3, and 0.4M).

Image analysis.

For shape analysis, we projected cell contours of *Col-0* cotyledons with an ImageJ macro, SurfCut [18] and used an ImageJ plugin, PaCeQuant [19], to automatically quantify descriptors of pavement cell shape. For cell wall

study, confocal images of *Col-0* cotyledons were analyzed using MorphoGraphX [20] to extract the shrinkage (Supp data 2). For turgor pressure study, cotyledon areas were determined using a manual segmentation in ImageJ. We determined the osmotic pressure after measuring the average osmotic concentration of each solution via a Gonotec osmomat 030 cryoscopic osmometer.

Bibliography

References

[1] R. V. Vőfély, J. Gallagher, G. D. Pisano, M. Bartlett, and S. A. Braybrook, "Of puzzles and pavements: a quantitative exploration of leaf epidermal cell shape," *The New Phytologist*, vol. 221, pp. 540–552, Jan. 2019.

[2] A. J. Bidhendi and A. Geitmann, "Geometrical Details Matter for Mechanical Modeling of Cell Morphogenesis," *Developmental Cell*, vol. 50, pp. 117–125.e2, July 2019.

[3] M. Majda, P. Grones, I.-M. Sintorn, T. Vain, P. Milani, P. Krupinski, B. Zagórska-Marek, C. Viotti, H. Jönsson, E. J. Mellerowicz, O. Hamant, and S. Robert, "Mechanochemical Polarization of Contiguous Cell Walls Shapes Plant Pavement Cells," *Developmental Cell*, vol. 43, pp. 290–304.e4, Nov. 2017.

[4] D. Lin, L. Cao, Z. Zhou, L. Zhu, D. Ehrhardt, Z. Yang, and Y. Fu, "Rho GTPase Signaling Activates Microtubule Severing to Promote Microtubule Ordering in Arabidopsis," *Current Biology*, vol. 23, pp. 290–297, Feb. 2013.

[5] O. Hamant and J. Traas, "The mechanics behind plant development," *New Phytologist*, vol. 185, pp. 369–385, Jan. 2010.

[6] P. Marowa, A. Ding, and Y. Kong, "Expansins: roles in plant growth and potential applications in crop improvement," *Plant Cell Reports*, vol. 35, pp. 949–965, May 2016.

[7] R. Galletti and G. C. Ingram, "Communication is key: Reducing DEK1 activity reveals a link between cell-cell contacts and epidermal cell differentiation status," *Communicative & Integrative Biology*, vol. 8, p. e1059979, July 2015.

[8] P. Sotiriou, E. Giannoutsou, E. Panteris, B. Galatis, and P. Apostolakos, "Local differentiation of cell wall matrix polysaccharides in sinuous pavement cells: its possible involvement in the flexibility of cell shape," *Plant Biology*, vol. 20, no. 2, pp. 223–237, 2018.

[9] E. Jacques, J.-P. Verbelen, K. Vissenberg, E. Jacques, J.-P. Verbelen, and K. Vissenberg, "Review on shape formation in epidermal pavement cells of the Arabidopsis leaf," *Functional Plant Biology*, vol. 41, pp. 914–921, June 2014. Publisher: CSIRO PUBLISHING.

[10] A. Sapala, A. Runions, A.-L. Routier-Kierzkowska, M. Das Gupta, L. Hong, H. Hofhuis, S. Verger, G. Mosca, C.-B. Li, A. Hay, O. Hamant, A. H. Roeder, M. Tsiantis, P. Prusinkiewicz, and R. S. Smith, "Why plants make puzzle cells, and how their shape emerges," *eLife*, vol. 7, p. e32794, Feb. 2018.

[11] S. D. Strachan and F. D. Hess, "The biochemical mechanism of action of the dinitroaniline herbicide oryzalin," *Pesticide Biochemistry and Physiology*, vol. 20, pp. 141–150, Oct. 1983.

[12] A. Sapala and R. S. Smith, "Osmotic Treatment for Quantifying Cell Wall Elasticity in the Sepal of Arabidopsis thaliana," in *Plant Stem Cells* (M. Naseem and T. Dandekar, eds.), vol. 2094, pp. 101–112, New York, NY: Springer US, 2020. Series Title: Methods in Molecular Biology.

[13] L. Beauzamy, N. Nakayama, and A. Boudaoud, "Flowers under pressure: ins and outs of turgor regulation in development," *Annals of Botany*, vol. 114, pp. 1517–1533, Nov. 2014.

[14] K. Akita, T. Higaki, N. Kutsuna, and S. Hasezawa, "Quantitative analysis of microtubule orientation in interdigitated leaf pavement cells," *Plant Signaling & Behavior*, vol. 10, p. e1024396, May 2015.

[15] F. Corson, O. Hamant, S. Bohn, J. Traas, A. Boudaoud, and Y. Couder, "Turning a plant tissue into a living cell froth through isotropic growth," *Proceedings of the National Academy of Sciences*, vol. 106, pp. 8453–8458, May 2009.

[16] R. C. Eng, R. Schneider, T. W. Matz, R. Carter, D. W. Ehrhardt, H. Jönsson, Z. Nikoloski, and A. Sampathkumar, "KATANIN and CLASP function at different spatial scales to mediate microtubule response to mechanical stress in Arabidopsis cotyledons," *Current Biology*, June 2021.

[17] D. H. Burk, B. Liu, R. Zhong, W. H. Morrison, and Z.-H. Ye, "A Katanin-like Protein Regulates Normal Cell Wall Biosynthesis and Cell Elongation," *The Plant Cell*, vol. 13, pp. 807–828, Apr. 2001.

[18] Erguvan, M. Louveaux, O. Hamant, and S. Verger, "ImageJ SurfCut: a user-friendly pipeline for high-throughput extraction of cell contours from 3D image stacks," *BMC biology*, vol. 17, p. 38, May 2019.

[19] B. Möller, Y. Poeschl, R. Plötner, and K. Bürstenbinder, "PaCeQuant: A Tool for High-Throughput

Quantification of Pavement Cell Shape Characteristics," *Plant Physiology*, vol. 175, pp. 998–1017, Nov. 2017.

[20] P. Barbier de Reuille, A.-L. Routier-Kierzkowska, D. Kierzkowski, G. W. Bassel, T. Schüpbach, G. Tauriello, N. Bajpai, S. Strauss, A. Weber, A. Kiss, A. Burian, H. Hofhuis, A. Sapala, M. Lipowczan, M. B. Heimlicher, S. Robinson, E. M. Bayer, K. Basler, P. Koumoutsakos, A. H. Roeder, T. Aegerter-Wilmsen, N. Nakayama, M. Tsiantis, A. Hay, D. Kwiatkowska, I. Xenarios, C. Kuhlemeier, and R. S. Smith, "MorphoGraphX: A platform for quantifying morphogenesis in 4D," *eLife*, vol. 4, p. e05864, May 2015. Publisher: eLife Sciences Publications, Ltd.

Supplementary data

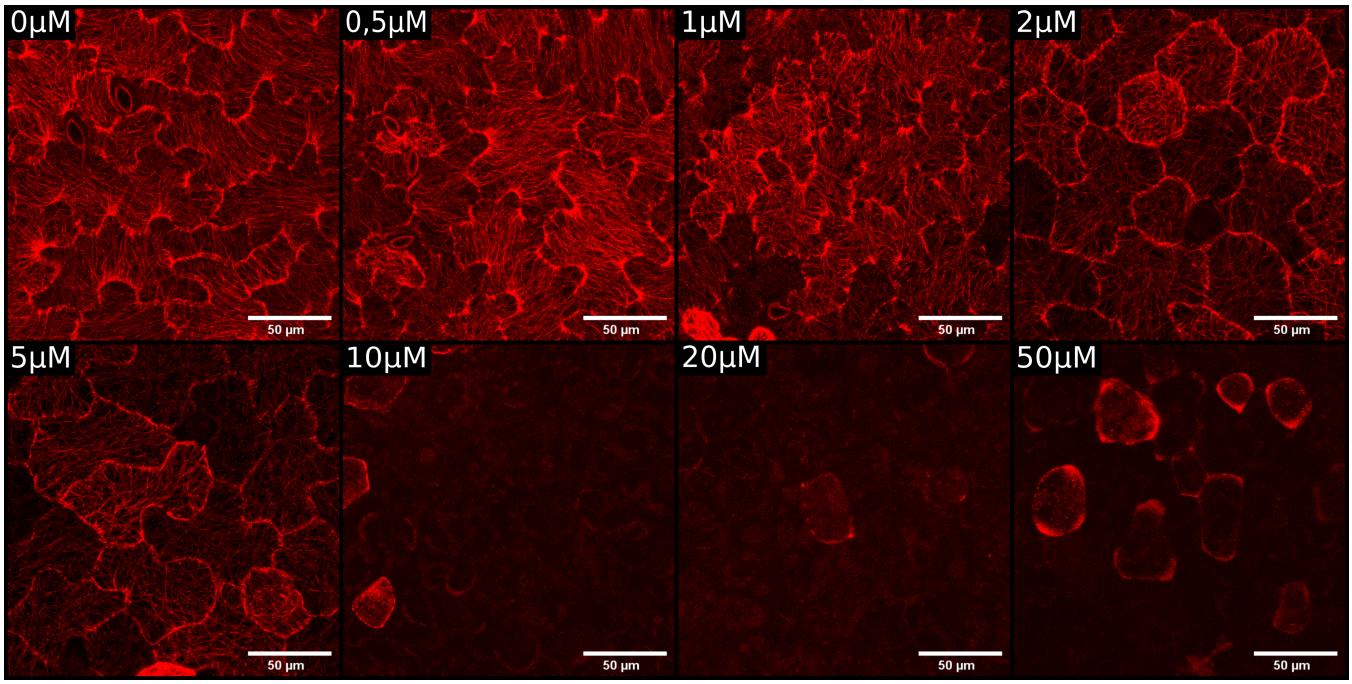

Fig. 5. Microtubules are gradually disturbed when plants grow exposed to oryzalin.
Representative confocal images of microtubules (*pPDF1::mCit-MBD*) of pavement cells for eight oryzalin concentrations. The higher oryzalin concentration is, the less microtubules are visible. Cells seemed to become more circular when oryzalin concentration increases. This confirms that microtubules are gradually disturbed when plants grow exposed to a gradual oryzalin concentration.

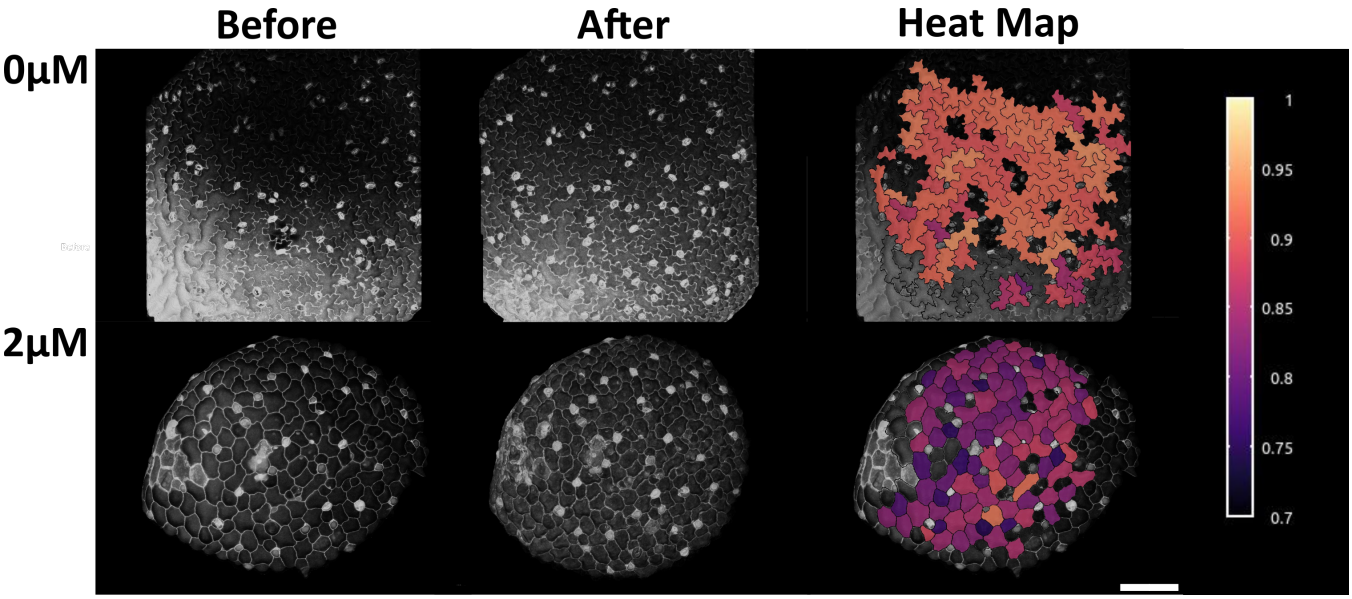

Fig. 6. Segmentation and shrinkage measures on MorphoGraphX.
Visualization of cotyledons from mediums with 0µM and 2µM of oryzalin, before and after the osmotic treatment (sorbitol 0.6M, 50min). Cell walls are visualized by a PI treatment. The comparison of cell area before and after the osmotic treatment defined the shrinkage represented on the Heat Map. The color gradient indicates shrinkage values. Scale bar = 200µm.

Discussion

"Why ask a question whose answer would demand ten more questions ?"

– *Cloud Atlas*, David Mitchell

Well in science that's usually the point.

9 Discussion

Progress in biology is often incremental. We generate small pieces of knowledge that we try to fit in the gigantic puzzle that has been built up over centuries. In this discussion, I will try to give my vision of how the pieces I generated may fit in the current state of the puzzle. Similarly to the introduction, I will go from small to big scales, starting with the results on microtubules, and following with that on cell-wall and finishing with morphogenesis.

9.1 Microtubule discussion

One of the aspects of my PhD was to investigate how patterns of microtubules emerge in the pavement cell (Chapter 7 (Results)). We analyzed the variance of the average angle in small patches and found no differences between regions of the pavement cells. This suggests that the dynamics in terms of polymerization/depolymerization, translation and rotation are similar throughout the cell. In particular, this suggests that there is no factor that induces polymerization/depolymerization at the neck specifically. KATANIN has been proposed as a severing agent specifically at the necks via the ROP6-RIC1 pathway in a way that increases microtubules number (Fu, Gu, et al. 2005; Fu, Xu, et al. 2009; D. Lin et al. 2013). Our results are partly in opposition with this proposal as we detected no differences in average angle variation spatially. However, one possibility is that we only looked at periclinal walls, whereas such recruitment of KATANIN is thought to occur in anticlinal walls. We think that this could potentially lead to differences in periclinal walls as well, as microtubules usually extend from one wall to the other (Belteton, W. Li, et al. 2021), but our method does not enable such quantification.

The second qualitative result that we obtained, regarding increase in polymerization direction as observed by imaging of the microtubule tips, is still preliminary so we will discuss the two possible cases. A) In the case where we would find a preferential orientation for microtubule growth towards the necks, several hypotheses could be formulated : 1) Initiation of microtubules is not random, but is oriented towards the necks. The nucleus has been suggested as an organizing center of cortical microtubules (Ambrose and Wasteneys 2014), however, this does not explain the differences in behavior between lobes and necks in pavement cells as they are both located circumferentially around the nucleus. If this hypothesis is correct, then we expect to find an actor that nucleates microtubules, or induces microtubule branching, in an orientation dependent manner. 2) Reorientation during growth/curving of the microtubule leads to polymerization of microtubules towards necks.

In vitro results suggest that stress may indeed lead to such a reorientation (Kabir et al. 2015). However, in this in vitro study the deformation rate of the substrate supporting the microtubule was far greater (0.42% s^{-1}) than the deformation of the cell wall (a plant cell typically double in size in 24h, so a deformation rate of 0.001% s^{-1}), potentially limiting such an effect. Chemical actors could potentially also lead to a reorientation of individual microtubules, but to our knowledge no evidence of such factors has been found. 3) Depolymerization of microtubules that are not growing towards necks, leading to an apparent increase of microtubules growing towards necks. While the consequence would be the same, the actors involved here would need to be localized outside of the lobe, and would respond to low stress areas.

B) If we find no such preferential orientation for polymerization and if our result regarding overall dynamics holds true, this means that it is the depolymerization that is orientation specific (EB1 only marks synthesizing microtubules). Note that this would be similar to hypothesis A)3) above. For instance, we could hypothesize that KATANIN only depolymerizes microtubules that are not aligned with necks. Molecular mechanisms that could explain such a behavior have not been highlighted yet. Simultaneous imaging of microtubule bodies and tips would help to achieve a clear understanding of the polymerization/depolymerization dynamics locally and to discriminate between the remaining hypotheses.

In plants, microtubules then contribute to the patterning of the cell wall. In the next section I will try to explain the significance of the results I obtained at the cell-wall scale.

9.2 Cell wall scale discussion

9.2.1 On the organization of cellulose in the wall

We found two different wall organizations that lead to similar levels of growth anisotropy (Chapter 5 (Results)). In the csi1 mutant, AFM on the most recently deposited cellulose microfibrils revealed increased alignment compared to WT. However, when looking at the whole thickness of the cell wall via Raman microspectrometry, we found no difference between alignment. We explained this by two different cell wall organization: one with intermediate levels of anisotropy within each plane and likely homogeneous in the depth of the wall (WT), and one with high levels of anisotropy in the plane but decreased layer to layer alignment (csi1). Here, we speculate that, in csi1, the wall is made up of several layers, within which cellulose is highly aligned whereas its orientation varies significantly among layers. This could be explained by a lack of guidance by previously deposited microfibrils in the case of high encountering angle (Chan and Coen 2020). Within a layer in csi1, cellulose microfibrils would guide the deposition of cellulose synthases until a

newly synthesizing fibril initiates with an angle too strong compared to the fibrils present. This new microfibril would then create a new track for cellulose synthases to follow with an orientation that differs from the orientation in the previous layer. Such alternate cellulose organization has actually already been observed in the xylem vessels of trembling aspen (Chafe and Chauret 1974), in the parenchyma of mulberry (Itoh 1975), and in the epidermis of the onion scale (Nicolas et al. 2022).

Surprisingly, our study suggests this organization in a csi1 context, instead of in wild-type plants. This hints that : 1) In Arabidopsis sepal, guidance of cellulose synthase by microtubule prevents the formation of such an organization and leads to more homogeneous walls across thickness. However, the mechanical and physiological properties (resistance to infection, water retention, etc) of the different types of wall organization still remain elusive. In Cardamine pods, cell width has been suggested to be controlled via a wall organization with two main orientations (Gabriella Mosca, unpublished). This double orientation is thought to control the extent of anisotropic growth. This illustrates that the organization of the cell wall contributes to the control of cell shape and growth in general. 2) The establishment of variable orientation in cellulose across the wall does not require guidance of cellulose synthases by microtubules via CSI1. As stated above this could be explained by current models of cellulose guidance (microtubules via CSI1, previously deposited fibrils or no guidance, Chan and Coen 2020), but could also be indicative for other elements contributing to the guidance of cellulose synthases. Indeed, recent advances in microscopy highlighted peculiar motions of cellulose synthases such as U-turns (Duncombe et al. 2022). For instance, membrane composition has been suggested as a potential contributor to the patterning of cellulose synthase motions (Leïa Colin 2021). Cellulose synthases can be affected by multiple post-translational modification (Heidari et al. 2019) and one may wonder about whether these modifications (which could also concern the numerous cellulose synthase partners), trigger switch of the control of the guidance of cellulose deposition.

9.2.2 Compensation and redundancy in plant cells

Biological systems cope with damage to DNA and with environmental variability with two main mechanisms: redundancy and compensation. Redundancy corresponds to the existence of several processes that fulfill the same function. For instance, in the sepal and in the absence of CSI1 or other proteins involved in the complex binding CESA and cortical microtubules, other cell wall elements, such as pectin, may take over the regulation of growth. In the sepal, because microtubules are aligned orthogonally to the growth direction (Hervieux, Dumond, et al. 2016), they make a good candidate for the establishment of growth anisotropy. We found that oryzalin treatments completely abolished cell shape establishment in pavement cells, which also supports microtubule as a

regulator of cell growth. The more microtubules were disrupted, the more cells presented defects in shape. In pavement cells, it was shown that both cellulose and pectin play a role in cell shape acquisition (Altartouri et al. 2019). While it has been known for quite a while that cellulose is deposited along microtubules, a recent study suggests that pectin may actually also be deposited along microtubules (Haas et al. 2020). This also suggests that while there are redundant mechanisms downstream of microtubules, they represent a critical point of plant development. There is still work required to truly define the respective roles of pectins and cellulose.

Compensation corresponds to the mechanisms that are triggered when a process is defective (Sénéchal et al. 2015). In our system, loss of cell shape led to the activation of compensation mechanisms of two natures, both leading to a reduction of stress in the cell wall : reduction of cell size, and reduction of turgor pressure (Chapter 8 (Results)). Such responses are potentially triggered by wall integrity sensing Rui and Dinneny 2020. While reduction of cell size may be a collateral consequence of defects in wall deposition, reduction in turgor pressure has not been documented much as a compensation mechanism and may be actively triggered. Recent studies cue towards FERRONIA as a potential mechanosensor involved in the regulation of water intake (Alice Malivert, unpublished).

I think that single cell experiments, such as protoplast regeneration, with simultaneous imaging of cell shape and cell wall elements may be informative. Associated with genetic perturbation of specific elements, this may clearly draw the line between the contribution of pectin and cellulose. In general, I think that single cells or simplified systems in general are useful because of the smaller number of parameters. When looking at an individual plant cell, cell walls appear as the main regulator of growth. However, when looking at an organ, and morphogenesis in general, several cells are involved. In the following section I will discuss how my results fit with the current understanding of morphogenesis as a multicellular process.

9.3 Morphogenesis discussion

9.3.1 On growth direction spatial consistency

Cells growing in a tissue somehow need to ensure that their collective growth will lead to the morphogenesis of the organ they compose. Such collective behaviors are guided by signals that span the organ. At the sepal level, a large-scale mechanical pattern has been identified. Heterogeneities in growth rates linked with an arrest of growth are thought to induce an orientation of the microtubules coherent throughout the organ (Hervieux, Dumond, et al. 2016). Another global pattern could also exist, this time of chemical nature. Sepals are organs that share a number of similarities

with leaves, for which the implication of an auxin gradient has been reported (Z. Zhang et al. 2020). Such patterns determine the average orientation of growth across a tissue. In our work, we found that average growth direction was not impacted in csi1, but that variability in growth direction was (Chapter 5 (Results)). This could mean either that 1) there is only the large scale signal that determines the average direction of cell growth, and in absence of CSI1, the response to such signal is not strong enough to ensure consistency across the tissue, or 2) there is a large scale that guides global direction, in a CSI1-independent manner, and associated with a local mechanism that controls the polarity of one cell regarding its neighbors, this time dependant of CSI1. Mechanisms ensuring consistency of polarity are relatively well established in animals (Goodrich and Strutt 2011), and while there are some candidates in plants (Q. Yang et al. 2020), their link with local coherence of growth direction has not been highlighted. Interestingly, we think that the sepal makes a good candidate for the screening of such factors, as the peculiar geometry of cells (alternance of small and giant cells) facilitates the quantification of lack of growth consistency.

9.3.2 On organ size and shape variability

Previous work in the team highlighted genetic regulators of organ size and shape variability (Hong et al. 2016). Their work highlighted that spatiotemporal variability in mechanical properties of cells was required to ensure reproducibility of sepals size and shape. Contrarily to animals where the balance of chemical/mechanical patterns has been suggested to determine arrest of growth (Aegerter-Wilmsen et al. 2012; Shraiman 2005), no evidence for such a system has been found in plants. Initially we thought that mechanical patterning could also play a role in shape reproducibility, considering that microtubule response to mechanical stress is active in the sepal (Hervieux, Tsugawa, et al. 2017), but we found no shape variability phenotype in absence of CSI1, which is thought to mediate the microtubule response. What are the other actors that could control growth variability? Considering that organ size scales with temperature (Dambreville et al. 2012), chemical patterning may be a good candidate as temperature determines reaction speed and diffusion. Mechanosensitive channels activity may also depend and scale with temperature (Owada et al. 2019), which may lead to a scaling of organs with temperature. Another possibility is that, again, compensation mechanisms are triggered in csi1 which limit variability of organ shape, leaving open the question: what are the factors that regulate organ shape reproducibility ?

While the faces of the main characters in the puzzle of biology (such as the composition and in vitro dynamics of microtubules, elementary deformation of the cell wall, growth of an organ, etc) start to be assembled, the big empty space between them is blurry (think of the blue sky in the background). Filling this space requires bridging knowledge from various

spatial scales to link characters together. In that sense, developmental biology progressively aims at understanding how a mechanism translates from one scale to another. Hopefully, my work will have helped define the position of a few pieces of the puzzle, as small as they may be.

Bibliography

Abraham, Yael and Rivka Elbaum (2013). 'Quantification of microfibril angle in secondary cell walls at subcellular resolution by means of polarized light microscopy'. en. In: *New Phytologist* 197.3, pp. 1012–1019. DOI: 10.1111/nph.12070 (cited on page 26).

Adamowski, Maciek, Lanxin Li, and Jiří Friml (July 2019). 'Reorientation of Cortical Microtubule Arrays in the Hypocotyl of Arabidopsis thaliana Is Induced by the Cell Growth Process and Independent of Auxin Signaling'. In: *International Journal of Molecular Sciences* 20.13, p. 3337. DOI: 10.3390/ijms20133337 (cited on page 45).

Aegerter-Wilmsen, T. et al. (Sept. 2012). 'Integrating force-sensing and signaling pathways in a model for the regulation of wing imaginal disc size'. en. In: *Development* 139.17, pp. 3221–3231. DOI: 10.1242/dev.082800 (cited on pages 38, 111).

Aher, Amol et al. (June 2020). 'CLASP Mediates Microtubule Repair by Restricting Lattice Damage and Regulating Tubulin Incorporation'. en. In: *Current Biology* 30.11, 2175–2183.e6. DOI: 10.1016/j.cub.2020.03.070 (cited on pages 8, 9).

Ahmad, Fridoon J. et al. (Apr. 1999). 'An Essential Role for Katanin in Severing Microtubules in the Neuron'. In: *The Journal of Cell Biology* 145.2, pp. 305–315 (cited on page 9).

Aigouy, Benoit and André Le Bivic (Sept. 2016). 'The PCP pathway regulates Baz planar distribution in epithelial cells'. en. In: *Scientific Reports* 6.1, p. 33420. DOI: 10.1038/srep33420 (cited on page 37).

Akhmanova, Anna et al. (Mar. 2001). 'CLASPs Are CLIP-115 and -170 Associating Proteins Involved in the Regional Regulation of Microtubule Dynamics in Motile Fibroblasts'. en. In: *Cell* 104.6, pp. 923–935. DOI: 10.1016/S0092-8674(01)00288-4 (cited on page 8).

Altartouri, Bara et al. (Sept. 2019). 'Pectin Chemistry and Cellulose Crystallinity Govern Pavement Cell Morphogenesis in a Multi-Step Mechanism1 [OPEN]'. In: *Plant Physiology* 181.1, pp. 127–141. DOI: 10.1104/pp.19.00303 (cited on pages 31, 43, 110).

Alushin, Gregory M. et al. (May 2014). 'High-Resolution Microtubule Structures Reveal the Structural Transitions in -Tubulin upon GTP Hydrolysis'. en. In: *Cell* 157.5, pp. 1117–1129. DOI: 10.1016/j.cell.2014.03.053 (cited on page 6).

Ambegaonkar, Abhijit A. et al. (July 2012). 'Propagation of Dachsous-Fat Planar Cell Polarity'. English. In: *Current Biology* 22.14, pp. 1302–1308. DOI: 10.1016/j.cub.2012.05.049 (cited on page 37).

Ambrose, Chris, Jun F. Allard, et al. (Aug. 2011). 'A CLASP-modulated cell edge barrier mechanism drives cell-wide cortical microtubule organization in Arabidopsis'. In: *Nature Communications* 2, p. 430. DOI: 10.1038/ncomms1444 (cited on page 9).

Ambrose, Chris and Geoffrey O. Wasteneys (July 2014). 'Microtubule Initiation from the Nuclear Surface Controls Cortical Microtubule Growth Polarity and Orientation in Arabidopsis thaliana'. In: *Plant and Cell Physiology* 55.9, pp. 1636–1645. DOI: 10.1093/pcp/pcu094 (cited on page 107).

Ambrosini, Arnaud et al. (June 2019). 'Mechanical Function of the Nucleus in Force Generation during Epithelial Morphogenesis'. English. In: *Developmental Cell* 0.0. DOI: 10.1016/j.devcel.2019.05.027 (cited on page 34).

Anastasiou, Elena et al. (Dec. 2007). 'Control of Plant Organ Size by KLUH/CYP78A5-Dependent Intercellular Signaling'. English. In: *Developmental Cell* 13.6, pp. 843–856. DOI: 10.1016/j.devcel.2007.10.001 (cited on page 36).

Anderson, Charles T., Ian S. Wallace, and Chris R. Somerville (Jan. 2012). 'Metabolic click-labeling with a fucose analog reveals pectin delivery, architecture, and dynamics in Arabidopsis cell walls'. In: *Proceedings of the National Academy of Sciences* 109.4, pp. 1329–1334. DOI: 10.1073/pnas.1120429109 (cited on pages 20, 26).

Armour, William J. et al. (Sept. 2015). 'Differential Growth in Periclinal and Anticlinal Walls during Lobe Formation in Arabidopsis Cotyledon Pavement Cells'. en. In: *The Plant Cell* 27.9, pp. 2484–2500. DOI: 10.1105/tpc.114.126664 (cited on page 42).

Banks, G et al. (2018). 'A missense mutation in Katnal1 underlies behavioural, neurological and ciliary anomalies'. In: *Molecular Psychiatry* 23.3, pp. 713–722. DOI: 10.1038/mp.2017.54 (cited on page 9).

Barrio, Lara and Marco Milán (July 2017). 'Boundary Dpp promotes growth of medial and lateral regions of the Drosophila wing'. In: *eLife* 6. Ed. by Utpal Banerjee, e22013. DOI: 10.7554/eLife.22013 (cited on page 37).

Bashline, Logan, Shundai Li, Charles T. Anderson, et al. (Sept. 2013). 'The Endocytosis of Cellulose Synthase in Arabidopsis Is Dependent on 2, a Clathrin-Mediated Endocytosis Adaptin1[W][OPEN]'. In: *Plant Physiology* 163.1, pp. 150–160. DOI: 10.1104/pp.113.221234 (cited on page 20).

Bashline, Logan, Shundai Li, Xiaoyu Zhu, et al. (Oct. 2015). 'The TWD40-2 protein and the AP2 complex cooperate in the clathrin-mediated endocytosis of cellulose synthase to regulate cellulose biosynthesis'. In: *Proceedings of the National Academy of Sciences* 112.41, pp. 12870–12875. DOI: 10.1073/pnas.1509292112 (cited on page 20).

Bátori, Veronika et al. (Oct. 2017). 'Production of Pectin-Cellulose Biofilms: A New Approach for Citrus Waste Recycling'. en. In: *International Journal of Polymer Science* 2017, e9732329. DOI: 10.1155/2017/9732329 (cited on page 21).

Baumann, Christoph G. et al. (June 1997). 'Ionic effects on the elasticity of single DNAmolecules'. In: *Proceedings of the National Academy of Sciences* 94.12, pp. 6185–6190. DOI: 10.1073/pnas.94.12.6185 (cited on page 10).

Beati, Hamze et al. (Jan. 2018). 'The adherens junction–associated LIM domain protein Smallish regulates epithelial morphogenesis'. In: *Journal of Cell Biology* 217.3, pp. 1079–1095. DOI: 10.1083/jcb.201610098 (cited on page 37).

Beauzamy, Léna, Julien Derr, and Arezki Boudaoud (May 2015). 'Quantifying Hydrostatic Pressure in Plant Cells by Using Indentation with an Atomic Force Microscope'. en. In: *Biophysical Journal* 108.10, pp. 2448–2456. DOI: 10.1016/j.bpj.2015.03.035 (cited on page 28).

Becker, Robert, Marina Leone, and Felix B. Engel (June 2020). 'Microtubule Organization in Striated Muscle Cells'. en. In: *Cells* 9.6, p. 1395. DOI: 10.3390/cells9061395 (cited on page 14).

Belteton, Samuel A., Wenlong Li, et al. (June 2021). 'Real-time conversion of tissue-scale mechanical forces into an interdigitated growth pattern'. en. In: *Nature Plants* 7.6, pp. 826–841. DOI: 10.1038/s41477-021-00931-z (cited on page 107).

Belteton, Samuel A., Megan G. Sawchuk, et al. (Jan. 2018). 'Reassessing the Roles of PIN Proteins and Anticlinal Microtubules during Pavement Cell Morphogenesis'. In: *Plant Physiology* 176.1, pp. 432–449. DOI: 10.1104/pp.17.01554 (cited on pages 41, 42).

Bidhendi, A.j., Y. Chebli, and A. Geitmann (2020). 'Fluorescence visualization of cellulose and pectin in the primary plant cell wall'. en. In: *Journal of Microscopy* 278.3, pp. 164–181. DOI: 10.1111/jmi.12895 (cited on pages 24, 25).

Bidhendi, Amir J., Bara Altartouri, et al. (July 2019). 'Mechanical Stress Initiates and Sustains the Morphogenesis of Wavy Leaf Epidermal Cells'. en. In: *Cell Reports* 28.5, 1237–1250.e6. DOI: 10.1016/j.celrep.2019.07.006 (cited on pages 40, 41).

Bidhendi, Amir J. and Anja Geitmann (July 2019). 'Geometrical Details Matter for Mechanical Modeling of Cell Morphogenesis'. en. In: *Developmental Cell* 50.1, 117–125.e2. DOI: 10.1016/j.devcel.2019.05.001 (cited on pages 41, 43).

Bisgrove, Sherryl R. et al. (Feb. 2008). 'The microtubule plus-end binding protein EB1 functions in root responses to touch and gravity signals in Arabidopsis'. eng. In: *The Plant Cell* 20.2, pp. 396–410. DOI: 10.1105/tpc.107.056846 (cited on page 8).

Bodrug, Tatyana et al. (Jan. 2020). 'The kinesin-5 tail domain directly modulates the mechanochemical cycle of the motor domain for anti-parallel microtubule sliding'. In: *eLife* 9. Ed. by Andrew P Carter, Suzanne R Pfeffer, and Ryo Nitta, e51131. DOI: 10.7554/eLife.51131 (cited on page 12).

Boehm, Bernd et al. (July 2010). 'The Role of Spatially Controlled Cell Proliferation in Limb Bud Morphogenesis'. en. In: *PLoS Biology* 8.7. Ed. by Alfonso Martinez Arias, e1000420. DOI: 10.1371/journal.pbio.1000420 (cited on page 37).

Boltzmann, Ludwig (Jan. 1995). *Lectures on Gas Theory*. en. Courier Corporation (cited on page 3).

Bosch, Pablo Sanchez et al. (July 2017). 'Dpp controls growth and patterning in Drosophila wing precursors through distinct modes of action'. In: *eLife* 6. Ed. by Utpal Banerjee, e22546. DOI: 10.7554/eLife.22546 (cited on page 37).

Bosveld, Floris et al. (May 2012). 'Mechanical Control of Morphogenesis by Fat/Dachsous/Four-Jointed Planar Cell Polarity Pathway'. In: *Science* 336.6082, pp. 724–727. DOI: 10.1126/science.1221071 (cited on page 37).

Bou Daher, Firas et al. (Sept. 2018). 'Anisotropic growth is achieved through the additive mechanical effect of material anisotropy and elastic asymmetry'. In: *eLife* 7. Ed. by Christian S Hardtke and Dominique C Bergmann, e38161. DOI: 10.7554/eLife.38161 (cited on page 21).

Bourboulia, Dimitra and William G. Stetler-Stevenson (June 2010). 'Matrix metalloproteinases (MMPs) and tissue inhibitors of metalloproteinases (TIMPs): Positive and negative regulators in tumor cell adhesion'. en. In: *Seminars in Cancer Biology*. Adhesive interactions: The multi-task biochemical toolbox of cancer cells 20.3, pp. 161–168. DOI: 10.1016/j.semcancer.2010.05.002 (cited on page 34).

Braybrook, Siobhan A. (Jan. 2015). 'Chapter 13 - Measuring the elasticity of plant cells with atomic force microscopy'. en. In: *Methods in Cell Biology*. Ed. by Ewa K. Paluch. Vol. 125. Biophysical Methods in Cell Biology. Academic Press, pp. 237–254. DOI: 10.1016/bs.mcb.2014.10.006 (cited on page 28).

Bringmann, Martin et al. (Jan. 2012). 'POM-POM2/CELLULOSE SYNTHASE INTERACTING1 Is Essential for the Functional Association of Cellulose Synthase and Microtubules in Arabidopsis'. en. In: *The Plant Cell* 24.1, pp. 163–177. DOI: 10.1105/tpc.111.093575 (cited on pages 23, 45).

Brittle, Amy, Chloe Thomas, and David Strutt (May 2012). 'Planar Polarity Specification through Asymmetric Subcellular Localization of Fat and Dachsous'. English. In: *Current Biology* 22.10, pp. 907–914. DOI: 10.1016/j.cub.2012.03.053 (cited on page 37).

Brouhard, Gary J. and Luke M. Rice (July 2018). 'Microtubule dynamics: an interplay of biochemistry and mechanics'. en. In: *Nature Reviews Molecular Cell Biology* 19.7, pp. 451–463. DOI: 10.1038/s41580-018-0009-y (cited on page 6).

Burian, Agata et al. (Dec. 2013). 'A correlative microscopy approach relates microtubule behaviour, local organ geometry, and cell growth at the Arabidopsis shoot apical meristem'. en. In: *Journal of Experimental Botany* 64.18, pp. 5753–5767. DOI: 10.1093/jxb/ert352 (cited on page 30).

Burn, Joanne E. et al. (June 2002). 'Functional Analysis of the Cellulose Synthase GenesCesA1, CesA2, and CesA3 in Arabidopsis'. In: *Plant Physiology* 129.2, pp. 797–807. DOI: 10.1104/pp.010931 (cited on page 43).

Burns, Roy G. (1991). '-, -, and -tubulins: Sequence comparisons and structural constraints'. en. In: *Cell Motility* 20.3, pp. 181–189. DOI: 10.1002/cm.970200302 (cited on page 5).

Buster, Dan, Karen McNally, and Francis J. McNally (Mar. 2002). 'Katanin inhibition prevents the redistribution of -tubulin at mitosis'. In: *Journal of Cell Science* 115.5, pp. 1083–1092. DOI: 10.1242/jcs.115.5.1083 (cited on page 9).

Cai, Danfeng et al. (Apr. 2016). 'Modeling and analysis of collective cell migration in an in vivo three-dimensional environment'. In: *Proceedings of the National Academy of Sciences* 113.15, E2134–E2141. DOI: 10.1073/pnas.1522656113 (cited on page 3).

Campanacci, Valérie et al. (Mar. 2019). 'Selection and Characterization of Artificial Proteins Targeting the Tubulin Subunit'. en. In: *Structure* 27.3, 497–506.e4. DOI: 10.1016/j.str.2018.12.001 (cited on page 6).

Cao, Lianqi et al. (Aug. 2020). 'Egg-box model-based gelation of alginate and pectin: A review'. en. In: *Carbohydrate Polymers* 242, p. 116389. DOI: 10.1016/j.carbpol.2020.116389 (cited on page 20).

Carazo-Salas, Rafael E. and Paul Nurse (Oct. 2006). 'Self-organization of interphase microtubule arrays in fission yeast'. en. In: *Nature Cell Biology* 8.10, pp. 1102–1107. DOI: 10.1038/ncb1479 (cited on page 14).

Carlier, M. -F. (Jan. 1989). 'Role of Nucleotide Hydrolysis in the Dynamics of Actin Filaments and Microtubules'. en. In: *International Review of Cytology*. Ed. by K. W. Jeon and M. Friedlander. Vol. 115. Academic Press, pp. 139–170. DOI: 10.1016/S0074-7696(08)60629-4 (cited on page 6).

Carminati, Janet and Tim Stearns (Sept. 1997). 'Microtubules Orient the Mitotic Spindle in Yeast through Dynein-dependent Interactions with the Cell Cortex'. In: *The Journal of cell biology* 138, pp. 629–41. DOI: 10.1083/jcb.138.3.629 (cited on page 14).

Cavalier, David M. et al. (June 2008). 'Disrupting two Arabidopsis thaliana xylosyltransferase genes results in plants deficient in xyloglucan, a major primary cell wall component'. eng. In: *The Plant Cell* 20.6, pp. 1519–1537. DOI: 10.1105/tpc.108.059873 (cited on page 22).

Chabin-Brion, Karine et al. (July 2001). 'The Golgi Complex Is a Microtubule-organizing Organelle'. In: *Molecular Biology of the Cell* 12.7, pp. 2047–2060. DOI: 10.1091/mbc.12.7.2047 (cited on page 14).

Chafe, S. C. and G. Chauret (Mar. 1974). 'Cell wall structure in the xylem parenchyma of trembling aspen'. en. In: *Protoplasma* 80.1, pp. 129–147. DOI: 10.1007/BF01666355 (cited on page 109).

Chan, Jordi and Enrico Coen (Mar. 2020). 'Interaction between Autonomous and Microtubule Guidance Systems Controls Cellulose Synthase Trajectories'. en. In: *Current Biology* 30.5, 941–947.e2. DOI: 10.1016/j.cub.2019.12.066 (cited on pages 23, 45, 108, 109).

Chebli, Youssef et al. (Dec. 2012). 'The Cell Wall of the Arabidopsis Pollen Tube—Spatial Distribution, Recycling, and Network Formation of Polysaccharides'. en. In: *Plant Physiology* 160.4, pp. 1940–1955. DOI: 10.1104/pp.112.199729 (cited on page 21).

Cheng, Youfa, Xinhua Dai, and Yunde Zhao (Jan. 2006). 'Auxin biosynthesis by the YUCCA flavin monooxygenases controls the formation of floral organs and vascular tissues in Arabidopsis'. en. In: *Genes & Development* 20.13, pp. 1790–1799. DOI: 10.1101/gad.1415106 (cited on page 41).

Chrétien, D. et al. (June 1992). 'Lattice defects in microtubules: protofilament numbers vary within individual microtubules'. eng. In: *The Journal of Cell Biology* 117.5, pp. 1031–1040. DOI: 10.1083/jcb.117.5.1031 (cited on page 8).

Colin, Leïa (2021). 'How mechanical signals contribute to plant development : the role of the cell cortex in mechano-transduction'. PhD thesis (cited on page 109).

Colin, Leia et al. (Dec. 2020). 'Cortical tension overrides geometrical cues to orient microtubules in confined protoplasts'. en. In: *Proceedings of the National Academy of Sciences* 117.51, pp. 32731–32738. DOI: 10.1073/pnas.2008895117 (cited on pages 12, 13).

Cosgrove, D. J. (Feb. 2000). 'Expansive growth of plant cell walls'. eng. In: *Plant physiology and biochemistry: PPB* 38.1-2, pp. 109–124 (cited on page 31).

Cosgrove, Daniel J. (June 2015). 'Plant expansins: diversity and interactions with plant cell walls'. In: *Current opinion in plant biology* 25, pp. 162–172. DOI: 10.1016/j.pbi.2015.05.014 (cited on page 31).

Coue, M, V A Lombillo, and J R McIntosh (Mar. 1991). 'Microtubule depolymerization promotes particle and chromosome movement in vitro.' en. In: *Journal of Cell Biology* 112.6, pp. 1165–1175. DOI: 10.1083/jcb.112.6.1165 (cited on page 11).

Crick, Francis (Jan. 1970). 'Diffusion in Embryogenesis'. en. In: *Nature* 225.5231, pp. 420–422. DOI: 10.1038/225420a0 (cited on page 35).

Crowell, Elizabeth Faris et al. (Apr. 2009). 'Pausing of Golgi Bodies on Microtubules Regulates Secretion of Cellulose Synthase Complexes in Arabidopsis'. In: *The Plant Cell* 21.4, pp. 1141–1154. DOI: 10.1105/tpc.108.065334 (cited on page 19).

Cuevas-Velazquez, Cesar L. et al. (Sept. 2021). 'Intrinsically disordered protein biosensor tracks the physical-chemical effects of osmotic stress on cells'. en. In: *Nature Communications* 12.1, p. 5438. DOI: 10.1038/s41467-021-25736-8 (cited on page 27).

Daga, Rafael R. et al. (Oct. 2006). 'Self-organization of microtubule bundles in anucleate fission yeast cells'. en. In: *Nature Cell Biology* 8.10, pp. 1108–1113. DOI: 10.1038/ncb1480 (cited on page 14).

Dambreville, Anaëlle et al. (Nov. 2012). 'Plant growth co-ordination in natura: a unique temperature-controlled law among vegetative and reproductive organs in mango'. en. In: *Functional Plant Biology* 40.3, pp. 280–291. DOI: 10.1071/FP12243 (cited on page 111).

David-Pfeuty, T, H P Erickson, and D Pantaloni (Dec. 1977). 'Guanosinetriphosphatase activity of tubulin associated with microtubule assembly.' In: *Proceedings of the National Academy of Sciences* 74.12, pp. 5372–5376. DOI: 10.1073/pnas.74.12.5372 (cited on page 6).

Davies, Lynette M. and Philip J. Harris (2003). 'Atomic force microscopy of microfibrils in primary cell walls'. In: *Planta* 217.2, pp. 283–289 (cited on page 24).

Day, S. J. and P. A. Lawrence (July 2000). 'Measuring dimensions: the regulation of size and shape'. eng. In: *Development (Cambridge, England)* 127.14, pp. 2977–2987 (cited on pages 36, 38).

Derbyshire, Paul et al. (Apr. 2007). 'Cell elongation in Arabidopsis hypocotyls involves dynamic changes in cell wall thickness'. In: *Journal of Experimental Botany* 58.8, pp. 2079–2089. DOI: 10.1093/jxb/erm074 (cited on page 25).

Desai, A. and T. J. Mitchison (1997). 'Microtubule polymerization dynamics'. eng. In: *Annual Review of Cell and Developmental Biology* 13, pp. 83–117. DOI: 10.1146/annurev.cellbio.13.1.83 (cited on page 5).

Desprez, Thierry et al. (Sept. 2007). 'Organization of cellulose synthase complexes involved in primary cell wall synthesis in Arabidopsis thaliana'. In: *Proceedings of the National Academy of Sciences of the United States of America* 104.39, pp. 15572–15577. DOI: 10.1073/pnas.0706569104 (cited on page 17).

Ding, Shi-You, Shuai Zhao, and Yining Zeng (Apr. 2014). 'Size, shape, and arrangement of native cellulose fibrils in maize cell walls'. en. In: *Cellulose* 21.2, pp. 863–871. DOI: 10.1007/s10570-013-0147-5 (cited on page 18).

Diotallevi, Fabiana and Bela Mulder (Apr. 2007). 'The Cellulose Synthase Complex: A Polymerization Driven Supramolecular Motor'. en. In: *Biophysical Journal* 92.8, pp. 2666–2673. DOI: 10.1529/biophysj.106.099473 (cited on page 23).

Dixit, Ram and Richard Cyr (Dec. 2004). 'Encounters between dynamic cortical microtubules promote ordering of the cortical array through angle-dependent modifications of microtubule behavior'. eng. In: *The Plant Cell* 16.12, pp. 3274–3284. DOI: 10.1105/tpc.104.026930 (cited on page 9).

Dmitrieff, Serge et al. (Apr. 2017). 'Balance of microtubule stiffness and cortical tension determines the size of blood cells with marginal band across species'. EN. In: *Proceedings of the National Academy of Sciences* 114.17, pp. 4418–4423. DOI: 10.1073/pnas.1618041114 (cited on page 15).

Doblin, Monika S. et al. (Dec. 2002). 'Cellulose Biosynthesis in Plants: from Genes to Rosettes'. In: *Plant and Cell Physiology* 43.12, pp. 1407–1420. DOI: 10.1093/pcp/pcf164 (cited on page 17).

Dogterom, M. and B. Yurke (Oct. 1997). 'Measurement of the force-velocity relation for growing microtubules'. eng. In: *Science (New York, N.Y.)* 278.5339, pp. 856–860. DOI: 10.1126/science.278.5339.856 (cited on page 11).

Domozych, David S. et al. (Feb. 2014). 'Disruption of the microtubule network alters cellulose deposition and causes major changes in pectin distribution in the cell wall of the green alga, Penium margaritaceum'. In: *Journal of Experimental Botany* 65.2, pp. 465–479. DOI: 10.1093/jxb/ert390 (cited on page 20).

Du, Juan et al. (Nov. 2020). 'Mutations in the Pectin Methyltransferase QUASIMODO2 Influence Cellulose Biosynthesis and Wall Integrity in Arabidopsis'. In: *The Plant Cell* 32.11, pp. 3576–3597. DOI: 10.1105/tpc.20.00252 (cited on page 23).

Duncombe, Sydney G, Samir G Chethan, and Charles T Anderson (Jan. 2022). 'Super-resolution imaging illuminates new dynamic behaviors of cellulose synthase'. In: *The Plant Cell* 34.1, pp. 273–286. DOI: 10.1093/plcell/koab227 (cited on pages 23–25, 109).

Dunleavy, Jessica E. M. et al. (Nov. 2017). 'Katanin-like 2 (KATNAL2) functions in multiple aspects of haploid male germ cell development in the mouse'. In: *PLoS Genetics* 13.11, e1007078. DOI: 10.1371/journal.pgen.1007078 (cited on page 9).

Durand-Smet, Pauline et al. (July 2020). 'Cytoskeletal organization in isolated plant cells under geometry control'. eng. In: *Proceedings of the National Academy of Sciences of the United States of America* 117.29, pp. 17399–17408. DOI: 10.1073/pnas.2003184117 (cited on page 13).

Efimov, Andrey et al. (June 2007). 'Asymmetric CLASP-Dependent Nucleation of Noncentrosomal Microtubules at the trans-Golgi Network'. en. In: *Developmental Cell* 12.6, pp. 917–930. DOI: 10.1016/j.devcel.2007.04.002 (cited on pages 9, 14).

Endler, Anne et al. (Sept. 2015). 'A Mechanism for Sustained Cellulose Synthesis during Salt Stress'. en. In: *Cell* 162.6, pp. 1353–1364. DOI: 10.1016/j.cell.2015.08.028 (cited on page 20).

Eng, Ryan C. et al. (Aug. 2021). 'KATANIN and CLASP function at different spatial scales to mediate microtubule response to mechanical stress in Arabidopsis cotyledons'. en. In: *Current Biology* 31.15, 3262–3274.e6. DOI: 10.1016/j.cub.2021.05.019 (cited on page 10).

Entchev, Eugeni V., Anja Schwabedissen, and Marcos González-Gaitán (Dec. 2000). 'Gradient Formation of the TGF- Homolog Dpp'. English. In: *Cell* 103.6, pp. 981–992. DOI: 10.1016/S0092-8674(00)00200-2 (cited on page 36).

Fedorov, Vladimir A. et al. (Aug. 2019). 'Mechanical properties of tubulin intra- and inter-dimer interfaces and their implications for microtubule dynamic instability'. In: *PLoS Computational Biology* 15.8, e1007327. DOI: 10.1371/journal.pcbi.1007327 (cited on page 5).

Friml, Jiří et al. (Nov. 2003). 'Efflux-dependent auxin gradients establish the apical–basal axis of Arabidopsis'. en. In: *Nature* 426.6963, pp. 147–153. DOI: 10.1038/nature02085 (cited on page 38).

Fu, Ying, Ying Gu, et al. (Mar. 2005). 'Arabidopsis Interdigitating Cell Growth Requires Two Antagonistic Pathways with Opposing Action on Cell Morphogenesis'. en. In: *Cell* 120.5, pp. 687–700. DOI: 10.1016/j.cell.2004.12.026 (cited on page 107).

Fu, Ying, Tongda Xu, et al. (Nov. 2009). 'A ROP GTPase Signaling Pathway Controls Cortical Microtubule Ordering and Cell Expansion in Arabidopsis'. English. In: *Current Biology* 19.21, pp. 1827–1832. DOI: 10.1016/j.cub.2009.08.052 (cited on page 107).

Fujita, Miki et al. (May 2013). 'The anisotropy1 D604N Mutation in the Arabidopsis Cellulose Synthase1 Catalytic Domain Reduces Cell Wall Crystallinity and the Velocity of Cellulose Synthase Complexes1[W][OA]'. In: *Plant Physiology* 162.1, pp. 74–85. DOI: 10.1104/pp.112.211565 (cited on pages 18, 43).

Fygenson, D. Kuchnir, Daniel J. Needleman, and Kim Sneppen (2004). 'Variability-based sequence alignment identifies residues responsible for functional differences in and tubulin'. en. In: *Protein Science* 13.1, pp. 25–31. DOI: 10.1110/ps.03225304 (cited on page 5).

Galletti, Roberta and Gwyneth C Ingram (Sept. 2015). 'Communication is key: Reducing DEK1 activity reveals a link between cell-cell contacts and epidermal cell differentiation status'. In: *Communicative & Integrative Biology* 8.5, e1059979. DOI: 10.1080/19420889.2015.1059979 (cited on page 39).

Gälweiler, L. et al. (Dec. 1998). 'Regulation of polar auxin transport by AtPIN1 in Arabidopsis vascular tissue'. eng. In: *Science (New York, N.Y.)* 282.5397, pp. 2226–2230. DOI: 10.1126/science.282.5397.2226 (cited on page 41).

Gao, Bo et al. (Apr. 2018). 'Coordinated directional outgrowth and pattern formation by integration of Wnt5a and Fgf signaling in planar cell polarity'. In: *Development* 145.8, dev163824. DOI: 10.1242/dev.163824 (cited on page 37).

Gao, Yangbin et al. (Feb. 2015). 'Auxin binding protein 1 (ABP1) is not required for either auxin signaling or Arabidopsis development'. In: *Proceedings of the National Academy of Sciences* 112.7, pp. 2275–2280. DOI: 10.1073/pnas.1500365112 (cited on page 41).

Garner, Rikki M. et al. (May 2022). *Vast heterogeneity in cytoplasmic diffusion rates revealed by nanorheology and Doppelgnger simulations*. en. preprint. Cell Biology. DOI: 10.1101/2022.05.11.491518 (cited on page 12).

Gawkowska, Diana, Justyna Cybulska, and Artur Zdunek (July 2018). 'Structure-Related Gelling of Pectins and Linking with Other Natural Compounds: A Review'. en. In: *Polymers* 10.7, p. 762. DOI: 10.3390/polym10070762 (cited on pages 21, 24).

Geahlen, R L and B E Haley (Oct. 1977). 'Interactions of a photoaffinity analog of GTP with the proteins of microtubules.' In: *Proceedings of the National Academy of Sciences* 74.10, pp. 4375–4377. DOI: 10.1073/pnas.74.10.4375 (cited on page 5).

Gierlinger, Notburga (Aug. 2018). 'New insights into plant cell walls by vibrational microspectroscopy'. In: *Applied Spectroscopy Reviews* 53.7, pp. 517–551. DOI: 10.1080/05704928.2017.1363052 (cited on page 26).

Gittes, F et al. (Feb. 1993). 'Flexural rigidity of microtubules and actin filaments measured from thermal fluctuations in shape.' In: *Journal of Cell Biology* 120.4, pp. 923–934. DOI: 10.1083/jcb.120.4.923 (cited on pages 10, 11).

Goodrich, Lisa V. and David Strutt (May 2011). 'Principles of planar polarity in animal development'. In: *Development (Cambridge, England)* 138.10, pp. 1877–1892. DOI: 10.1242/dev.054080 (cited on page 111).

Graaff, E. van der et al. (Nov. 2000). 'Activation tagging of the LEAFY PETIOLE gene affects leaf petiole development in Arabidopsis thaliana'. In: *Development* 127.22, pp. 4971–4980. DOI: 10.1242/dev.127.22.4971 (cited on page 36).

Green, Paul B. (Dec. 1962). 'Mechanism for Plant Cellular Morphogenesis'. In: *Science* 138.3548, pp. 1404–1405. DOI: 10.1126/science.138.3548.1404 (cited on pages 30, 45).

– (Sept. 1992). 'Pattern Formation in Shoots: A Likely Role for Minimal Energy Configurations of the Tunica'. en. In: *International Journal of Plant Sciences*. DOI: 10.1086/297064 (cited on page 35).

Grieneisen, Verônica A. et al. (Oct. 2007). 'Auxin transport is sufficient to generate a maximum and gradient guiding root growth'. en. In: *Nature* 449.7165, pp. 1008–1013. DOI: 10.1038/nature06215 (cited on page 35).

Grishchuk, E. L. et al. (May 2008). 'Different assemblies of the DAM1 complex follow shortening microtubules by distinct mechanisms'. eng. In: *Proceedings of the National Academy of Sciences of the United States of America* 105.19, pp. 6918–6923. DOI: 10.1073/pnas.0801811105 (cited on page 11).

Grones, Peter et al. (July 2020). 'Fluctuating auxin response gradients determine pavement cell-shape acquisition'. EN. In: *Proceedings of the National Academy of Sciences* 117.27, pp. 16027–16034. DOI: 10.1073/pnas.2007400117 (cited on page 41).

Gu, Ying et al. (July 2010). 'Identification of a cellulose synthase-associated protein required for cellulose biosynthesis'. In: *Proceedings of the National Academy of Sciences of the United States of America* 107.29, pp. 12866–12871. DOI: 10.1073/pnas.1007092107 (cited on pages 23, 45).

Gudimchuk, Nikita B. and J. Richard McIntosh (Dec. 2021). 'Regulation of microtubule dynamics, mechanics and function through the growing tip'. en. In: *Nature Reviews Molecular Cell Biology* 22.12, pp. 777–795. DOI: 10.1038/s41580-021-00399-x (cited on page 6).

Gunji, Shizuka et al. (2020). 'Excess Pyrophosphate Restrains Pavement Cell Morphogenesis and Alters Organ Flatness in Arabidopsis thaliana'. In: *Frontiers in Plant Science* 11 (cited on page 39).

Gutierrez, Ryan et al. (July 2009). 'Arabidopsis cortical microtubules position cellulose synthase delivery to the plasma membrane and interact with cellulose synthase trafficking compartments'. eng. In: *Nature Cell Biology* 11.7, pp. 797–806. DOI: 10.1038/ncb1886 (cited on page 19).

Haas, Kalina T. et al. (Feb. 2020). 'Pectin homogalacturonan nanofilament expansion drives morphogenesis in plant epidermal cells'. en. In: *Science* 367.6481, pp. 1003–1007. DOI: 10.1126/science.aaz5103 (cited on pages 31, 43, 110).

Haigler, C. H. and R. M. Brown (June 1986). 'Transport of rosettes from the golgi apparatus to the plasma membrane in isolated mesophyll cells ofZinnia elegans during differentiation to tracheary elements in suspension culture'. en. In: *Protoplasma* 134.2, pp. 111–120. DOI: 10.1007/BF01275709 (cited on page 19).

Hamant, Olivier, Marcus G. Heisler, et al. (Dec. 2008). 'Developmental Patterning by Mechanical Signals in Arabidopsis'. In: *Science* 322.5908, pp. 1650–1655. DOI: 10.1126/science.1165594 (cited on pages 38, 42).

Hamant, Olivier, Daisuke Inoue, et al. (May 2019). 'Are microtubules tension sensors?' en. In: *Nature Communications* 10.1, p. 2360. DOI: 10.1038/s41467-019-10207-y (cited on page 13).

Harris, Darby M. et al. (Mar. 2012). 'Cellulose microfibril crystallinity is reduced by mutating C-terminal transmembrane region residues CESA1A903V and CESA3T942I of cellulose synthase'. eng. In: *Proceedings of the National Academy of Sciences of the United States of America* 109.11, pp. 4098–4103. DOI: 10.1073/pnas.1200352109 (cited on page 18).

Hartman, J. J. et al. (Apr. 1998). 'Katanin, a microtubule-severing protein, is a novel AAA ATPase that targets to the centrosome using a WD40-containing subunit'. eng. In: *Cell* 93.2, pp. 277–287. DOI: 10.1016/s0092-8674(00)81578-0 (cited on page 9).

He, Xian-Chen et al. (July 2008). 'Molecular cloning, expression profiling, and yeast complementation of 19 -tubulin cDNAs from developing cotton ovules'. In: *Journal of Experimental Botany* 59.10, pp. 2687–2695. DOI: 10.1093/jxb/ern127 (cited on page 5).

Heidari, Parviz et al. (Sept. 2019). 'In silico study of the CESA and CSL gene family in Arabidopsis thaliana and Oryza sativa: Focus on post-translation modifications'. en. In: *Plant Gene* 19, p. 100189. DOI: 10.1016/j.plgene.2019.100189 (cited on page 109).

Herburger, Klaus et al. (July 2020). 'Hetero-trans--Glucanase Produces Cellulose–Xyloglucan Covalent Bonds in the Cell Walls of Structural Plant Tissues and Is Stimulated by Expansin'. en. In: *Molecular Plant* 13.7, pp. 1047–1062. DOI: 10.1016/j.molp.2020.04.011 (cited on page 22).

Hervieux, Nathan, Mathilde Dumond, et al. (Apr. 2016). 'A Mechanical Feedback Restricts Sepal Growth and Shape in Arabidopsis'. In: *Current Biology* 26.8, pp. 1019–1028. DOI: 10.1016/j.cub.2016.03.004 (cited on pages 38, 109, 110).

Hervieux, Nathan, Satoru Tsugawa, et al. (Nov. 2017). 'Mechanical Shielding of Rapidly Growing Cells Buffers Growth Heterogeneity and Contributes to Organ Shape Reproducibility'. eng. In: *Current biology: CB* 27.22, 3468–3479.e4. DOI: 10.1016/j.cub.2017.10.033 (cited on pages 10, 46, 111).

Higaki, Takumi et al. (Jan. 2017). 'Exogenous Cellulase Switches Cell Interdigitation to Cell Elongation in an RIC1-dependent Manner in Arabidopsis thaliana Cotyledon Pavement Cells'. In: *Plant and Cell Physiology* 58.1, pp. 106–119. DOI: 10.1093/pcp/pcw183 (cited on page 43).

Hong, Lilan et al. (July 2016). 'Variable Cell Growth Yields Reproducible Organ Development through Spatiotemporal Averaging'. en. In: *Developmental Cell* 38.1, pp. 15–32. DOI: 10.1016/j.devcel.2016.06.016 (cited on pages 46, 111).

Honnappa, Srinivas et al. (July 2009). 'An EB1-Binding Motif Acts as a Microtubule Tip Localization Signal'. en. In: *Cell* 138.2, pp. 366–376. DOI: 10.1016/j.cell.2009.04.065 (cited on page 8).

Huang, Shixin et al. (Jan. 2020). 'Correlation between crystalline cellulose structure and cellulose synthase complex shape: a spectroscopic study with unicellular freshwater alga Micrasterias'. en. In: *Cellulose* 27.1, pp. 57–69. DOI: 10.1007/s10570-019-02793-3 (cited on page 17).

Hufnagel, Lars et al. (Mar. 2007). 'On the mechanism of wing size determination in fly development'. In: *Proceedings of the National Academy of Sciences* 104.10, pp. 3835–3840. DOI: 10.1073/pnas.0607134104 (cited on page 38).

Huheey, James E, Ellen A Keiter, and Richard L Keiter (1993). *Inorganic chemistry: principles of structure and reactivity*. English. New York, NY: HarperCollins College Publishers (cited on page 18).

Hur, Eun-Mi et al. (Sept. 2011). 'GSK3 controls axon growth via CLASP-mediated regulation of growth cone microtubules'. en. In: *Genes & Development* 25.18, pp. 1968–1981. DOI: 10.1101/gad.17015911 (cited on page 9).

Ibañes, Marta and Juan Carlos Izpisúa Belmonte (2008). 'Theoretical and experimental approaches to understand morphogen gradients'. In: *Molecular Systems Biology* 4.1, p. 176. DOI: https://doi.org/10.1038/msb.2008.14 (cited on page 36).

Igaev, Maxim and Helmut Grubmüller (Sept. 2020). 'Microtubule instability driven by longitudinal and lateral strain propagation'. en. In: *PLOS Computational Biology* 16.9, e1008132. DOI: 10.1371/journal.pcbi.1008132 (cited on pages 5–9).

Ingber, Donald E. (2006). 'Cellular mechanotransduction: putting all the pieces together again'. In: *The FASEB Journal* 20.7, pp. 811–827. DOI: https://doi.org/10.1096/fj.05-5424rev (cited on page 15).

Inomata, Hidehiko (2017). 'Scaling of pattern formations and morphogen gradients'. en. In: *Development, Growth & Differentiation* 59.1, pp. 41–51. DOI: 10.1111/dgd.12337 (cited on page 35).

Inoue, Daisuke et al. (Nov. 2016). 'Sensing surface mechanical deformation using active probes driven by motor proteins'. en. In: *Nature Communications* 7.1, p. 12557. DOI: 10.1038/ncomms12557 (cited on page 13).

Itoh, Takao (June 1975). 'Cell wall organization of cortical parenchyma of angiosperms observed by the freeze etching technique'. en. In: *The botanical magazine = Shokubutsu-gaku-zasshi* 88.2, pp. 145–156. DOI: 10.1007/BF02491249 (cited on page 109).

Jacques, Eveline et al. (June 2014). 'Review on shape formation in epidermal pavement cells of the Arabidopsis leaf'. en. In: *Functional Plant Biology* 41.9, pp. 914–921. DOI: 10.1071/FP13338 (cited on page 39).

Jain, Piyush et al. (June 2021). 'A minimally disruptive method for measuring water potential in planta using hydrogel nanoreporters'. In: *Proceedings of the National Academy of Sciences* 118.23, e2008276118. DOI: 10.1073/pnas.2008276118 (cited on pages 26, 27).

Jakob, Matthias et al. (Apr. 2022). 'The strength and stiffness of oriented wood and cellulose-fibre materials: A review'. en. In: *Progress in Materials Science* 125, p. 100916. DOI: 10.1016/j.pmatsci.2021.100916 (cited on page 18).

Jalili, Nader and Karthik Laxminarayana (Oct. 2004). 'A review of atomic force microscopy imaging systems: application to molecular metrology and biological sciences'. en. In: *Mechatronics* 14.8, pp. 907–945. DOI: 10.1016/j.mechatronics.2004.04.005 (cited on page 28).

Janke, Carsten and Guillaume Montagnac (Dec. 2017). 'Causes and Consequences of Microtubule Acetylation'. eng. In: *Current biology: CB* 27.23, R1287–R1292. DOI: 10.1016/j.cub.2017.10.044 (cited on page 10).

Janková Drdová, Edita et al. (Jan. 2019). 'Developmental plasticity of Arabidopsis hypocotyl is dependent on exocyst complex function'. In: *Journal of Experimental Botany* 70.4, pp. 1255–1265. DOI: 10.1093/jxb/erz005 (cited on page 25).

Kabir, Arif Md Rashedul et al. (Nov. 2015). 'Buckling of Microtubules on a 2D Elastic Medium'. en. In: *Scientific Reports* 5.1, p. 17222. DOI: 10.1038/srep17222 (cited on pages 13, 108).

Kaewthai, Nomchit et al. (Jan. 2013). 'Group III-A XTH Genes of Arabidopsis Encode Predominant Xyloglucan Endohydrolases That Are Dispensable for Normal Growth'. In: *Plant Physiology* 161.1, pp. 440–454. DOI: 10.1104/pp.112.207308 (cited on page 22).

Katrukha, Eugene A et al. (2021). 'Quantitative mapping of dense microtubule arrays in mammalian neurons'. In: *eLife* 10. Ed. by Suzanne R Pfeffer, Kassandra M Ori-McKenney, and Ilaria Testa, e67925. DOI: 10.7554/eLife.67925 (cited on page 14).

Kawade, Kensuke, Gorou Horiguchi, et al. (May 2013). 'ANGUSTIFOLIA3 signaling coordinates proliferation between clonally distinct cells in leaves'. eng. In: *Current biology: CB* 23.9, pp. 788–792. DOI: 10.1016/j.cub.2013.03.044 (cited on page 36).

Kawade, Kensuke, Hirokazu Tanimoto, et al. (Sept. 2017). 'Spatially Different Tissue-Scale Diffusivity Shapes ANGUSTIFOLIA3 Gradient in Growing Leaves'. English. In: *Biophysical Journal* 113.5, pp. 1109–1120. DOI: 10.1016/j.bpj.2017.06.072 (cited on page 36).

Kazama, Toshiya et al. (June 2010). 'The Mechanism of Cell Cycle Arrest Front Progression Explained by a KLUH/CYP78A5-dependent Mobile Growth Factor in Developing Leaves of Arabidopsis thaliana'. In: *Plant and Cell Physiology* 51.6, pp. 1046–1054. DOI: 10.1093/pcp/pcq051 (cited on pages 36, 37).

Kennaway, Richard et al. (June 2011). 'Generation of Diverse Biological Forms through Combinatorial Interactions between Tissue Polarity and Growth'. en. In: *PLOS Computational Biology* 7.6, e1002071. DOI: 10.1371/journal.pcbi.1002071 (cited on page 35).

Kim, Jong Sik and Geoffrey Daniel (Apr. 2018). 'Heterogeneous distribution of pectin and hemicellulose epitopes in the phloem of four hardwood species'. en. In: *Trees* 32.2, pp. 393–414. DOI: 10.1007/s00468-017-1638-z (cited on page 22).

Kim, Sang-Jin and Federica Brandizzi (Apr. 2014). 'The Plant Secretory Pathway: An Essential Factory for Building the Plant Cell Wall'. In: *Plant and Cell Physiology* 55.4, pp. 687–693. DOI: 10.1093/pcp/pct197 (cited on page 20).

Kimura, Satoshi et al. (1999). 'Immunogold Labeling of Rosette Terminal Cellulose-Synthesizing Complexes in the Vascular Plant Vigna angularis'. In: *The Plant Cell* 11.11, pp. 2075–2085. DOI: 10.2307/3871010 (cited on page 17).

Koirala, Rajendra Prasad, Sita Dawanse, and Nurapati Pantha (Jan. 2022). 'Diffusion of glucose in water: A molecular dynamics study'. en. In: *Journal of Molecular Liquids* 345, p. 117826. DOI: 10.1016/j.molliq.2021.117826 (cited on page 3).

Kollman, Justin M. et al. (Oct. 2011). 'Microtubule nucleation by -tubulin complexes'. eng. In: *Nature Reviews. Molecular Cell Biology* 12.11, pp. 709–721. DOI: 10.1038/nrm3209 (cited on pages 5, 6).

Komarova, Yulia et al. (Mar. 2009). 'Mammalian end binding proteins control persistent microtubule growth'. In: *Journal of Cell Biology* 184.5, pp. 691–706. DOI: 10.1083/jcb.200807179 (cited on page 8).

Kononova, Olga et al. (Dec. 2014). 'Tubulin Bond Energies and Microtubule Biomechanics Determined from Nanoindentation in Silico'. In: *Journal of the American Chemical Society* 136.49, pp. 17036–17045. DOI: 10.1021/ja506385p (cited on pages 5, 6).

Kumar, Praveen and Torsten Wittmann (Aug. 2012). '+TIPs: SxIPping along microtubule ends'. en. In: *Trends in Cell Biology* 22.8, pp. 418–428. DOI: 10.1016/j.tcb.2012.05.005 (cited on page 8).

Kurachi, M., M. Hoshi, and H. Tashiro (1995). 'Buckling of a single microtubule by optical trapping forces: direct measurement of microtubule rigidity'. eng. In: *Cell Motility and the Cytoskeleton* 30.3, pp. 221–228. DOI: 10.1002/cm.970300306 (cited on page 11).

Kutschera, U. (1992). 'The Role of the Epidermis in the Control of Elongation Growth in Stems and Coleoptiles'. en. In: *Botanica Acta* 105.4, pp. 246–252. DOI: 10.1111/j.1438-8677.1992.tb00294.x (cited on page 25).

Laan, Liedewij et al. (July 2008). 'Force-generation and dynamic instability of microtubule bundles'. In: *Proceedings of the National Academy of Sciences of the United States of America* 105.26, pp. 8920–8925. DOI: 10.1073/pnas.0710311105 (cited on page 11).

LaCroix, Andrew S et al. (July 2018). 'Tunable molecular tension sensors reveal extension-based control of vinculin loading'. In: *eLife* 7. Ed. by Antoine M van Oijen, e33927. DOI: 10.7554/eLife.33927 (cited on page 27).

LaFrance, Benjamin J. et al. (Jan. 2022). 'Structural transitions in the GTP cap visualized by cryo-electron microscopy of catalytically inactive microtubules'. In: *Proceedings of the National Academy of Sciences* 119.2, e2114994119. DOI: 10.1073/pnas.2114994119 (cited on page 6).

Lagomarsino, Marco Cosentino et al. (Feb. 2007). 'Microtubule Organization in Three-Dimensional Confined Geometries: Evaluating the Role of Elasticity Through a Combined In Vitro and Modeling Approach'. en. In: *Biophysical Journal* 92.3, pp. 1046–1057. DOI: 10.1529/biophysj.105.076893 (cited on page 13).

Lampugnani, Edwin R. et al. (May 2019). 'Cellulose Synthesis – Central Components and Their Evolutionary Relationships'. English. In: *Trends in Plant Science* 24.5, pp. 402–412. DOI: 10.1016/j.tplants.2019.02.011 (cited on page 19).

Lander, Arthur D. et al. (Jan. 2009). 'The Measure of Success: Constraints, Objectives, and Tradeoffs in Morphogen-mediated Patterning'. en. In: *Cold Spring Harbor Perspectives in Biology* 1.1, a002022. DOI: 10.1101/cshperspect.a002022 (cited on page 35).

Lauster, Theresa et al. (Feb. 2022). 'Arabidopsis pavement cell shape formation involves spatially confined ROPGAP regulators'. English. In: *Current Biology* 32.3, 532–544.e7. DOI: 10.1016/j.cub.2021.12.042 (cited on page 42).

Lawrence, Elizabeth J., Marija Zanic, and Luke M. Rice (Apr. 2020). 'CLASPs at a glance'. In: *Journal of Cell Science* 133.8, jcs243097. DOI: 10.1242/jcs.243097 (cited on page 8).

Lei, Lei, Shundai Li, Juan Du, et al. (Dec. 2013). 'CELLULOSE SYNTHASE INTERACTIVE3 Regulates Cellulose Biosynthesis in Both a Microtubule-Dependent and Microtubule-Independent Manner in Arabidopsis[C][W]'. In: *The Plant Cell* 25.12, pp. 4912–4923. DOI: 10.1105/tpc.113.116715 (cited on page 45).

Lei, Lei, Shundai Li, and Ying Gu (July 2012). 'Cellulose synthase interactive protein 1 (CSI1) mediates the intimate relationship between cellulose microfibrils and cortical microtubules'. In: *Plant Signaling & Behavior* 7.7, pp. 714–718. DOI: 10.4161/psb.20338 (cited on page 23).

Lesnicar-Pucko, Gaja et al. (Sept. 2020). *Cellular mechanisms of chick limb bud morphogenesis*. en. DOI: 10.1101/2020.09.10.292359 (cited on page 37).

Li, Hongjiang et al. (June 2011). 'Phosphorylation switch modulates the interdigitated pattern of PIN1 localization and cell expansion in Arabidopsis leaf epidermis'. en. In: *Cell Research* 21.6, pp. 970–978. DOI: 10.1038/cr.2011.49 (cited on page 41).

Li, Shundai et al. (Jan. 2012). 'Cellulose synthase interactive protein 1 (CSI1) links microtubules and cellulose synthase complexes'. en. In: *Proceedings of the National Academy of Sciences* 109.1, pp. 185–190. DOI: 10.1073/pnas.1118560109 (cited on pages 23, 45).

Li, Wenlong et al. (Mar. 2022). 'Protocol for mapping the variability in cell wall mechanical bending behavior in living leaf pavement cells'. In: *Plant Physiology* 188.3, pp. 1435–1449. DOI: 10.1093/plphys/kiab588 (cited on page 28).

Lin, Deshu et al. (Feb. 2013). 'Rho GTPase Signaling Activates Microtubule Severing to Promote Microtubule Ordering in Arabidopsis'. English. In: *Current Biology* 23.4, pp. 290–297. DOI: 10.1016/j.cub.2013.01.022 (cited on page 107).

Lin, Wenwei and Zhenbiao Yang (Oct. 2020). 'Unlocking the mechanisms behind the formation of interlocking pavement cells'. en. In: *Current Opinion in Plant Biology*. Cell signalling and gene regulation 57, pp. 142–154. DOI: 10.1016/j.pbi.2020.09.002 (cited on page 46).

Lindeboom, Jelmer J., Masayoshi Nakamura, Anneke Hibbel, et al. (Dec. 2013). 'A Mechanism for Reorientation of Cortical Microtubule Arrays Driven by Microtubule Severing'. In: *Science* 342.6163, p. 1245533. DOI: 10.1126/science.1245533 (cited on pages 9, 10).

Lindeboom, Jelmer J., Masayoshi Nakamura, Marco Saltini, et al. (Oct. 2018). 'CLASP stabilization of plus ends created by severing promotes microtubule creation and reorientation'. In: *Journal of Cell Biology* 218.1, pp. 190–205. DOI: 10.1083/jcb.201805047 (cited on page 9).

Liu, Derui et al. (Nov. 2017). 'Imaging cellulose synthase motility during primary cell wall synthesis in the grass Brachypodium distachyon'. en. In: *Scientific Reports* 7.1, p. 15111. DOI: 10.1038/s41598-017-14988-4 (cited on page 46).

Liu, Sijia et al. (2021). 'Solving the Puzzle of Shape Regulation in Plant Epidermal Pavement Cells'. In: *Annual Review of Plant Biology* 72.1, pp. 525–550. DOI: 10.1146/annurev-arplant-080720-081920 (cited on page 42).

Liu, Zengyu et al. (Aug. 2016). 'Cellulose-Microtubule Uncoupling Proteins Prevent Lateral Displacement of Microtubules during Cellulose Synthesis in Arabidopsis'. en. In: *Developmental Cell* 38.3, pp. 305–315. DOI: 10.1016/j.devcel.2016.06.032 (cited on page 15).

Lockhart, J. A. (Mar. 1965). 'An analysis of irreversible plant cell elongation'. eng. In: *Journal of Theoretical Biology* 8.2, pp. 264–275. DOI: 10.1016/0022-5193(65)90077-9 (cited on page 28).

Lombino, Franco L. et al. (Nov. 2019). 'The Microtubule Severing Protein Katanin Regulates Proliferation of Neuronal Progenitors in Embryonic and Adult Neurogenesis'. In: *Scientific Reports* 9, p. 15940. DOI: 10.1038/s41598-019-52367-3 (cited on page 9).

Long, Yuchen et al. (Apr. 2020). 'Cellular Heterogeneity in Pressure and Growth Emerges from Tissue Topology and Geometry'. en. In: *Current Biology* 30.8, 1504–1516.e8. DOI: 10.1016/j.cub.2020.02.027 (cited on page 28).

Lynn, Nicole A. et al. (Aug. 2021). 'The Mammalian Family of Katanin Microtubule-Severing Enzymes'. In: *Frontiers in Cell and Developmental Biology* 9, p. 692040. DOI: 10.3389/fcell.2021.692040 (cited on page 9).

Majda, Mateusz, Peter Grones, et al. (Nov. 2017). 'Mechanochemical Polarization of Contiguous Cell Walls Shapes Plant Pavement Cells'. en. In: *Developmental Cell* 43.3, 290–304.e4. DOI: 10.1016/j.devcel.2017.10.017 (cited on pages 28, 40, 43).

Majda, Mateusz, Pawel Krupinski, et al. (July 2019). 'Mechanical Asymmetry of the Cell Wall Predicts Changes in Pavement Cell Geometry'. en. In: *Developmental Cell* 50.1, pp. 9–10. DOI: 10.1016/j.devcel.2019.06.002 (cited on page 41).

Mangione, Federica and Enrique Martín-Blanco (Dec. 2018). 'The Dachsous/Fat/Four-Jointed Pathway Directs the Uniform Axial Orientation of Epithelial Cells in the Drosophila Abdomen'. en. In: *Cell Reports* 25.10, 2836–2850.e4. DOI: 10.1016/j.celrep.2018.11.036 (cited on page 37).

Mansfield, Catherine et al. (Aug. 2018). 'Ectopic BASL Reveals Tissue Cell Polarity throughout Leaf Development in Arabidopsis thaliana'. eng. In: *Current biology: CB* 28.16, 2638–2646.e4. DOI: 10.1016/j.cub.2018.06.019 (cited on page 38).

Mao, Yanlan, Alexander L. Tournier, Paul A. Bates, et al. (Jan. 2011). 'Planar polarization of the atypical myosin Dachs orients cell divisions in Drosophila'. en. In: *Genes & Development* 25.2, pp. 131–136. DOI: 10.1101/gad.610511 (cited on page 37).

Mao, Yanlan, Alexander L. Tournier, Andreas Hoppe, et al. (Oct. 2013). 'Differential proliferation rates generate patterns of mechanical tension that orient tissue growth'. eng. In: *The EMBO journal* 32.21, pp. 2790–2803. DOI: 10.1038/emboj.2013.197 (cited on page 38).

Martin, Douglas S. (2013). 'Measuring Microtubule Persistence Length Using a Microtubule Gliding Assay'. en. In: *Methods in Cell Biology*. Vol. 115. Elsevier, pp. 13–25. DOI: 10.1016/B978-0-12-407757-7.00002-5 (cited on page 11).

Martin, Sophie G. (Sept. 2009). 'Microtubule-dependent cell morphogenesis in the fission yeast'. eng. In: *Trends in Cell Biology* 19.9, pp. 447–454. DOI: 10.1016/j.tcb.2009.06.003 (cited on page 14).

Martínez-Sanz, Marta, Michael J. Gidley, and Elliot P. Gilbert (July 2015). 'Application of X-ray and neutron small angle scattering techniques to study the hierarchical structure of plant cell walls: A review'. en. In: *Carbohydrate Polymers* 125, pp. 120–134. DOI: 10.1016/j.carbpol.2015.02.010 (cited on page 18).

Martinière, Alexandre, Elias Bassil, et al. (Oct. 2013). 'In Vivo Intracellular pH Measurements in Tobacco and Arabidopsis Reveal an Unexpected pH Gradient in the Endomembrane System'. In: *The Plant Cell* 25.10, pp. 4028–4043. DOI: 10.1105/tpc.113.116897 (cited on page 27).

Martinière, Alexandre, Rémy Gibrat, et al. (June 2018). 'Uncovering pH at both sides of the root plasma membrane interface using noninvasive imaging'. In: *Proceedings of the National Academy of Sciences* 115.25, pp. 6488–6493. DOI: 10.1073/pnas.1721769115 (cited on pages 20, 26, 27).

Mathur, Jaideep et al. (Nov. 2003). 'A Novel Localization Pattern for an EB1-like Protein Links Microtubule Dynamics to Endomembrane Organization'. en. In: *Current Biology* 13.22, pp. 1991–1997. DOI: 10.1016/j.cub.2003.10.033 (cited on page 8).

Maurer, Sebastian P. et al. (Feb. 2014). 'EB1 Accelerates Two Conformational Transitions Important for Microtubule Maturation and Dynamics'. In: *Current Biology* 24.4, pp. 372–384. DOI: 10.1016/j.cub.2013.12.042 (cited on page 7).

McKenna, Sylvester T. et al. (Oct. 2009). 'Exocytosis Precedes and Predicts the Increase in Growth in Oscillating Pollen Tubes'. In: *The Plant Cell* 21.10, pp. 3026–3040. DOI: 10.1105/tpc.109.069260 (cited on page 20).

McNally, F. J. and R. D. Vale (Nov. 1993). 'Identification of katanin, an ATPase that severs and disassembles stable microtubules'. eng. In: *Cell* 75.3, pp. 419–429. DOI: 10.1016/0092-8674(93)90377-3 (cited on page 9).

McQueen-Mason, S, D M Durachko, and D J Cosgrove (Nov. 1992). 'Two endogenous proteins that induce cell wall extension in plants.' In: *The Plant Cell* 4.11, pp. 1425–1433. DOI: 10.1105/tpc.4.11.1425 (cited on page 31).

Mellor, Nathan L. et al. (Mar. 2020). 'Auxin fluxes through plasmodesmata modify root-tip auxin distribution'. In: *Development* 147.6, dev181669. DOI: 10.1242/dev.181669 (cited on page 35).

Michaels, Thomas CT et al. (May 2020). 'Mechanics and kinetics of dynamic instability'. In: *eLife* 9. Ed. by Raymond E Goldstein, Detlef Weigel, and Jennifer Ross, e54077. DOI: 10.7554/eLife.54077 (cited on pages 6, 7).

Michels, Lucile et al. (July 2020). 'Complete microviscosity maps of living plant cells and tissues with a toolbox of targeting mechanoprobes'. In: *Proceedings of the National Academy of Sciences* 117.30, pp. 18110–18118. DOI: 10.1073/pnas.1921374117 (cited on pages 26, 27).

Mickolajczyk, Keith J. et al. (Apr. 2019). 'Direct observation of individual tubulin dimers binding to growing microtubules'. In: *Proceedings of the National Academy of Sciences* 116.15, pp. 7314–7322. DOI: 10.1073/pnas.1815823116 (cited on page 6).

Miesenböck, Gero, Dino A. De Angelis, and James E. Rothman (July 1998). 'Visualizing secretion and synaptic transmission with pH-sensitive green fluorescent proteins'. en. In: *Nature* 394.6689, pp. 192–195. DOI: 10.1038/28190 (cited on page 27).

Mirabet, Vincent et al. (Feb. 2018). 'The self-organization of plant microtubules inside the cell volume yields their cortical localization, stable alignment, and sensitivity to external cues'. en. In: *PLOS Computational Biology* 14.2, e1006011. DOI: 10.1371/journal.pcbi.1006011 (cited on page 13).

Mirvis, Mary et al. (July 2019). 'Primary cilium loss in mammalian cells occurs predominantly by whole-cilium shedding'. In: *PLoS Biology* 17.7, e3000381. DOI: 10.1371/journal.pbio.3000381 (cited on page 9).

Mitchison, G. J. and Sydney Brenner (Oct. 1980). 'The dynamics of auxin transport'. In: *Proceedings of the Royal Society of London. Series B. Biological Sciences* 209.1177, pp. 489–511. DOI: 10.1098/rspb.1980.0109 (cited on page 35).

Molendijk, Arthur J et al. (June 2001). 'Arabidopsis thaliana Rop GTPases are localized to tips of root hairs and control polar growth'. In: *The EMBO Journal* 20.11, pp. 2779–2788. DOI: 10.1093/emboj/20.11.2779 (cited on page 38).

Molines, Arthur T., Joël Lemière, et al. (Feb. 2022). 'Physical properties of the cytoplasm modulate the rates of microtubule polymerization and depolymerization'. en. In: *Developmental Cell* 57.4, 466–479.e6. DOI: 10.1016/j.devcel.2022.02.001 (cited on page 12).

Molines, Arthur T., Jessica Marion, et al. (Aug. 2018). 'EB1 contributes to microtubule bundling and organization, along with root growth, in Arabidopsis thaliana'. In: *Biology Open* 7.8, bio030510. DOI: 10.1242/bio.030510 (cited on page 8).

Molines, Arthur T., Virginie Stoppin-Mellet, et al. (June 2020). 'Plant and mouse EB1 proteins have opposite intrinsic properties on the dynamic instability of microtubules'. In: *BMC Research Notes* 13.1, p. 296. DOI: 10.1186/s13104-020-05139-6 (cited on page 8).

Molodtsov, M. I. et al. (2005). 'Force production by depolymerizing microtubules: A theoretical study'. In: *Proceedings of the National Academy of Sciences* 102.12, pp. 4353–4358. DOI: 10.1073/pnas.0501142102 (cited on page 11).

Monier, Bruno et al. (Feb. 2015). 'Apico-basal forces exerted by apoptotic cells drive epithelium folding'. en. In: *Nature* 518.7538, pp. 245–248. DOI: 10.1038/nature14152 (cited on page 34).

Montecinos-Franjola, Felipe, Peter Schuck, and Dan L. Sackett (Apr. 2016). 'Tubulin Dimer Reversible Dissociation'. In: *The Journal of Biological Chemistry* 291.17, pp. 9281–9294. DOI: 10.1074/jbc.M115.699728 (cited on page 5).

Moreau, Hortense, Isabelle Gaillard, and Nadine Paris (May 2022). 'Genetically encoded fluorescent sensors adapted to acidic pH highlight subdomains within the plant cell apoplast'. In: *Journal of Experimental Botany*, erac210. DOI: 10.1093/jxb/erac210 (cited on page 20).

Müller, Patrick et al. (Apr. 2013). 'Morphogen transport'. In: *Development* 140.8, pp. 1621–1638. DOI: 10.1242/dev.083519 (cited on page 35).

Nath, Utpal et al. (Feb. 2003). 'Genetic Control of Surface Curvature'. In: *Science* 299.5611, pp. 1404–1407. DOI: 10.1126/science.1079354 (cited on page 35).

Nawrotek, Agata, Marcel Knossow, and Benoît Gigant (Sept. 2011). 'The Determinants That Govern Microtubule Assembly from the Atomic Structure of GTP-Tubulin'. en. In: *Journal of Molecular Biology* 412.1, pp. 35–42. DOI: 10.1016/j.jmb.2011.07.029 (cited on page 6).

Nicolas, William J. et al. (June 2022). 'Cryo-electron tomography of the onion cell wall shows bimodally oriented cellulose fibers and reticulated homogalacturonan networks'. en. In: *Current Biology* 32.11, 2375–2389.e6. DOI: 10.1016/j.cub.2022.04.024 (cited on pages 24, 25, 109).

Nishita, Michiru et al. (July 2017). 'Regulatory mechanisms and cellular functions of non-centrosomal microtubules'. In: *The Journal of Biochemistry* 162.1, pp. 1–10. DOI: 10.1093/jb/mvx018 (cited on page 14).

Nissen, Silas Boye et al. (Nov. 2018). 'Theoretical tool bridging cell polarities with development of robust morphologies'. In: *eLife* 7. Ed. by Aleksandra M Walczak and Naama Barkai, e38407. DOI: 10.7554/eLife.38407 (cited on pages 37, 38).

O'Neill, Malcolm A. and William S. York (Apr. 2018). 'The Composition and Structure of Plant Primary Cell Walls'. en. In: *Annual Plant Reviews online*. Ed. by Jeremy A Roberts. Chichester, UK: John Wiley & Sons, Ltd, pp. 1–54. DOI: 10.1002/9781119312994.apr0067 (cited on page 17).

Oakley, B. R. (Dec. 2000). 'An abundance of tubulins'. eng. In: *Trends in Cell Biology* 10.12, pp. 537–542. DOI: 10.1016/s0962-8924(00)01857-2 (cited on page 5).

Odermatt, Pascal D et al. (June 2021). 'Variations of intracellular density during the cell cycle arise from tip-growth regulation in fission yeast'. In: *eLife* 10. Ed. by Mohan K Balasubramanian, Naama Barkai, and Matthieu Piel, e64901. DOI: 10.7554/eLife.64901 (cited on page 12).

Okamoto, Hisashi et al. (Jan. 1990). 'Effects of Auxin and Anoxia on the Cell Wall Yield Threshold Determined by Negative Pressure Jumps in Segments of Cowpea Hypocotyl'. In: *Plant and Cell Physiology* 31.6, pp. 783–788. DOI: 10.1093/oxfordjournals.pcp.a077979 (cited on page 29).

Owada, Naoto et al. (May 2019). 'Temperature-sensitive mutants of MscL mechanosensitive channel'. In: *The Journal of Biochemistry* 166.3, pp. 281–288. DOI: 10.1093/jb/mvz035 (cited on page 111).

Paës, Gabriel, Anouck Habrant, and Christine Terryn (Mar. 2018). 'Fluorescent Nano-Probes to Image Plant Cell Walls by Super-Resolution STED Microscopy'. en. In: *Plants* 7.1, p. 11. DOI: 10.3390/plants7010011 (cited on page 25).

Pampaloni, Francesco et al. (July 2006). 'Thermal fluctuations of grafted microtubules provide evidence of a length-dependent persistence length'. eng. In: *Proceedings of the National Academy of Sciences of the United States of America* 103.27, pp. 10248–10253. DOI: 10.1073/pnas.0603931103 (cited on page 11).

Pan, Xue et al. (Aug. 2020). 'Auxin-induced signaling protein nanoclustering contributes to cell polarity formation'. en. In: *Nature Communications* 11.1, p. 3914. DOI: 10.1038/s41467-020-17602-w (cited on page 41).

Panteris, E., P. Apostolakos, and B. Galatis (Nov. 1993). 'Microtubule organization and cell morphogenesis in two semi-lobed cell types of Adiantum capillus-veneris L. leaflets'. eng. In: *The New Phytologist* 125.3, pp. 509–520. DOI: 10.1111/j.1469-8137.1993.tb03899.x (cited on page 42).

– (Aug. 1994). 'Sinuous ordinary epidermal cells: behind several patterns of waviness, a common morphogenetic mechanism'. eng. In: *The New Phytologist* 127.4, pp. 771–780. DOI: 10.1111/j.1469-8137.1994.tb02981.x (cited on page 42).

Paredez, Alexander R., Christopher R. Somerville, and David W. Ehrhardt (June 2006). 'Visualization of Cellulose Synthase Demonstrates Functional Association with Microtubules'. In: *Science* 312.5779, pp. 1491–1495. DOI: 10.1126/science.1126551 (cited on pages 18, 22).

Park, Yong Bum and Daniel J. Cosgrove (Feb. 2015). 'Xyloglucan and its Interactions with Other Components of the Growing Cell Wall'. In: *Plant and Cell Physiology* 56.2, pp. 180–194. DOI: 10.1093/pcp/pcu204 (cited on page 22).

Pauly, Markus and Kenneth Keegstra (Apr. 2016). 'Biosynthesis of the Plant Cell Wall Matrix Polysaccharide Xyloglucan'. en. In: *Annual Review of Plant Biology* 67.1, pp. 235–259. DOI: 10.1146/annurev-arplant-043015-112222 (cited on page 22).

Peaucelle, Alexis, Siobhan A. Braybrook, et al. (Oct. 2011). 'Pectin-Induced Changes in Cell Wall Mechanics Underlie Organ Initiation in Arabidopsis'. en. In: *Current Biology* 21.20, pp. 1720–1726. DOI: 10.1016/j.cub.2011.08.057 (cited on pages 21, 43).

Peaucelle, Alexis, Raymond Wightman, and Herman Höfte (June 2015). 'The Control of Growth Symmetry Breaking in the Arabidopsis Hypocotyl'. eng. In: *Current biology: CB* 25.13, pp. 1746–1752. DOI: 10.1016/j.cub.2015.05.022 (cited on pages 21, 31, 43).

Pedersen, Henriette L. et al. (Nov. 2012). 'Versatile High Resolution Oligosaccharide Microarrays for Plant Glycobiology and Cell Wall Research *'. English. In: *Journal of Biological Chemistry* 287.47, pp. 39429–39438. DOI: 10.1074/jbc.M112.396598 (cited on page 25).

Persson, Staffan et al. (June 2005). 'Identification of genes required for cellulose synthesis by regression analysis of public microarray data sets'. eng. In: *Proceedings of the National Academy of Sciences of the United States of America* 102.24, pp. 8633–8638. DOI: 10.1073/pnas.0503392102 (cited on page 23).

Petry, Sabine et al. (Feb. 2013). 'Branching microtubule nucleation in Xenopus egg extracts mediated by augmin and TPX2'. In: *Cell* 152.4, pp. 768–777. DOI: 10.1016/j.cell.2012.12.044 (cited on page 14).

Picout, David R. et al. (May 2003). 'Pressure Cell Assisted Solubilization of Xyloglucans: Tamarind Seed Polysaccharide and Detarium Gum'. en. In: *Biomacromolecules* 4.3, pp. 799–807. DOI: 10.1021/bm0257659 (cited on page 22).

Pieczywek, Piotr Mariusz et al. (Mar. 2021). 'Aggregation and weak gel formation by pectic polysaccharide homogalacturonan'. eng. In: *Carbohydrate Polymers* 256, p. 117566. DOI: 10.1016/j.carbpol.2020.117566 (cited on page 21).

Pilhofer, Martin et al. (Dec. 2011). 'Microtubules in Bacteria: Ancient Tubulins Build a Five-Protofilament Homolog of the Eukaryotic Cytoskeleton'. en. In: *PLOS Biology* 9.12, e1001213. DOI: 10.1371/journal.pbio.1001213 (cited on page 5).

Pleuger, Christiane et al. (Dec. 2016). 'Expression of katanin p80 in human spermatogenesis'. eng. In: *Fertility and Sterility* 106.7, 1683–1690.e1. DOI: 10.1016/j.fertnstert.2016.08.043 (cited on page 9).

Posé, Sara et al. (Sept. 2015). 'Pectin Nanostructure Visualization by Atomic Force Microscopy'. In: *Bio-protocol* 5.19, e1598–e1598 (cited on page 24).

Proag, Amsha, Bruno Monier, and Magali Suzanne (June 2019). 'Physical and functional cell-matrix uncoupling in a developing tissue under tension'. In: *Development* 146.11, dev172577. DOI: 10.1242/dev.172577 (cited on page 34).

Rai, Ankit et al. (Dec. 2021). 'Lattice defects induced by microtubule-stabilizing agents exert a long-range effect on microtubule growth by promoting catastrophes'. In: *Proceedings of the National Academy of Sciences* 118.51, e2112261118. DOI: 10.1073/pnas.2112261118 (cited on page 8).

Rebocho, Alexandra B et al. (Feb. 2017). 'Generation of shape complexity through tissue conflict resolution'. In: *eLife* 6. Ed. by Naama Barkai, e20156. DOI: 10.7554/eLife.20156 (cited on pages 34, 35).

Refrégier, Guislaine et al. (June 2004). 'Interaction between Wall Deposition and Cell Elongation in Dark-Grown Hypocotyl Cells in Arabidopsis'. en. In: *Plant Physiology* 135.2, pp. 959–968. DOI: 10.1104/pp.104.038711 (cited on page 45).

Riglet, Lucie et al. (Sept. 2020). 'KATANIN-dependent mechanical properties of the stigmatic cell wall mediate the pollen tube path in Arabidopsis'. In: *eLife* 9. Ed. by Sheila McCormick et al., e57282. DOI: 10.7554/eLife.57282 (cited on page 10).

Robinson, Sarah et al. (Sept. 2011). 'Generation of Spatial Patterns Through Cell Polarity Switching'. In: *Science* 333.6048, pp. 1436–1440. DOI: 10.1126/science.1202185 (cited on page 38).

Roeder, Adrienne H. K. (2021). 'Arabidopsis sepals: A model system for the emergent process of morphogenesis'. en. In: *Quantitative Plant Biology* 2, e14. DOI: 10.1017/qpb.2021.12 (cited on page 38).

Roellig, Daniela et al. (Mar. 2022). 'Force-generating apoptotic cells orchestrate avian neural tube bending'. en. In: *Developmental Cell* 57.6, 707–718.e6. DOI: 10.1016/j.devcel.2022.02.020 (cited on page 33).

Rogulja, Dragana and Kenneth D. Irvine (Nov. 2005). 'Regulation of Cell Proliferation by a Morphogen Gradient'. en. In: *Cell* 123.3, pp. 449–461. DOI: 10.1016/j.cell.2005.08.030 (cited on page 36).

Roostalu, Johanna et al. (Feb. 2020). 'The speed of GTP hydrolysis determines GTP cap size and controls microtubule stability'. In: *eLife* 9. Ed. by Anna Akhmanova, e51992. DOI: 10.7554/eLife.51992 (cited on page 7).

Rui, Yue and José R. Dinneny (2020). 'A wall with integrity: surveillance and maintenance of the plant cell wall under stress'. en. In: *New Phytologist* 225.4, pp. 1428–1439. DOI: 10.1111/nph.16166 (cited on pages 21, 110).

Rui, Yue, Chaowen Xiao, et al. (Oct. 2017). 'POLYGALACTURONASE INVOLVED IN EXPANSION3 Functions in Seedling Development, Rosette Growth, and Stomatal Dynamics in Arabidopsis thaliana'. In: *The Plant Cell* 29.10, pp. 2413–2432. DOI: 10.1105/tpc.17.00568 (cited on page 31).

Saladié, Montserrat et al. (July 2006). 'Characterization of a new xyloglucan endotransglucosylase/hydrolase (XTH) from ripening tomato fruit and implications for the diverse modes of enzymic action'. eng. In: *The Plant Journal: For Cell and Molecular Biology* 47.2, pp. 282–295. DOI: 10.1111/j.1365-313X.2006.02784.x (cited on page 22).

Salbreux, Guillaume, Guillaume Charras, and Ewa Paluch (Oct. 2012). 'Actin cortex mechanics and cellular morphogenesis'. en. In: *Trends in Cell Biology* 22.10, pp. 536–545. DOI: 10.1016/j.tcb.2012.07.001 (cited on page 34).

Sampathkumar, Arun et al. (Apr. 2014). 'Subcellular and supracellular mechanical stress prescribes cytoskeleton behavior in Arabidopsis cotyledon pavement cells'. In: *eLife* 3. Ed. by Dominique Bergmann, e01967. DOI: 10.7554/eLife.01967 (cited on pages 14, 28, 42, 43, 46).

Sapala, Aleksandra, Adam Runions, et al. (Feb. 2018). 'Why plants make puzzle cells, and how their shape emerges'. eng. In: *eLife* 7, e32794. DOI: 10.7554/eLife.32794 (cited on pages 39, 47).

Sapala, Aleksandra and Richard S. Smith (2020). 'Osmotic Treatment for Quantifying Cell Wall Elasticity in the Sepal of Arabidopsis thaliana'. en. In: *Plant Stem Cells: Methods and Protocols*. Ed. by Muhammad Naseem and Thomas Dandekar. Methods in Molecular Biology. New York, NY: Springer US, pp. 101–112. DOI: 10.1007/978-1-0716-0183-9_11 (cited on page 28).

Sarojam, Rajani et al. (July 2010). 'Differentiating Arabidopsis Shoots from Leaves by Combined YABBY Activities'. In: *The Plant Cell* 22.7, pp. 2113–2130. DOI: 10.1105/tpc.110.075853 (cited on page 36).

Schneider, René et al. (Aug. 2022). 'Tethering of cellulose synthase to microtubules dampens mechano-induced cytoskeletal organization in Arabidopsis pavement cells'. en. In: *Nature Plants*, pp. 1–10. DOI: 10.1038/s41477-022-01218-7 (cited on page 23).

Schwank, G., S. Restrepo, and K. Basler (Dec. 2008). 'Growth regulation by Dpp: an essential role for Brinker and a non-essential role for graded signaling levels'. en. In: *Development* 135.24, pp. 4003–4013. DOI: 10.1242/dev.025635 (cited on pages 36, 38).

Sénéchal, Fabien et al. (2015). 'Arabidopsis PME17 Activity can be Controlled by Pectin Methylesterase Inhibitor4'. eng. In: *Plant Signaling & Behavior* 10.2, e983351. DOI: 10.4161/15592324.2014.983351 (cited on pages 21, 110).

Sharma, Abhimanyu and Michael Vershinin (Aug. 2020). 'Length dependence of the rigidity of microtubules in small networks'. en. In: *Biochemical and Biophysical Research Communications* 529.2, pp. 303–305. DOI: 10.1016/j.bbrc.2020.06.030 (cited on page 11).

Shraiman, Boris I. (Mar. 2005). 'Mechanical feedback as a possible regulator of tissue growth'. In: *Proceedings of the National Academy of Sciences* 102.9, pp. 3318–3323. DOI: 10.1073/pnas.0404782102 (cited on pages 38, 111).

Sieberer, Björn J. et al. (Sept. 2005). 'Microtubules guide root hair tip growth'. eng. In: *The New Phytologist* 167.3, pp. 711–719. DOI: 10.1111/j.1469-8137.2005.01506.x (cited on page 16).

Silva Braga, Roberta da and Matheus Poletto (Jan. 2020). 'Preparation and Characterization of Hemicellulose Films from Sugarcane Bagasse'. en. In: *Materials* 13.4, p. 941. DOI: 10.3390/ma13040941 (cited on page 22).

Singh, Amrita et al. (Oct. 2018). 'Polarized microtubule dynamics directs cell mechanics and coordinates forces during epithelial morphogenesis'. en. In: *Nature Cell Biology* 20.10, pp. 1126–1133. DOI: 10.1038/s41556-018-0193-1 (cited on page 15).

Song, Bo et al. (2020). 'Direct Measurement of Plant Cellulose Microfibril and Bundles in Native Cell Walls'. In: *Frontiers in Plant Science* 11 (cited on pages 17, 24).

Sotiriou, P. et al. (2018). 'Local differentiation of cell wall matrix polysaccharides in sinuous pavement cells: its possible involvement in the flexibility of cell shape'. en. In: *Plant Biology* 20.2, pp. 223–237. DOI: 10.1111/plb.12681 (cited on page 39).

Spencer, Forrest A., F. Michael Hoffmann, and William M. Gelbart (Mar. 1982). 'Decapentaplegic: A gene complex affecting morphogenesis in Drosophila melanogaster'. en. In: *Cell* 28.3, pp. 451–461. DOI: 10.1016/0092-8674(82)90199-4 (cited on page 36).

Stearns, Tim, Louise Evans, and Marc Kirschner (May 1991). '-Tubulin is a highly conserved component of the centrosome'. en. In: *Cell* 65.5, pp. 825–836. DOI: 10.1016/0092-8674(91)90390-K (cited on page 5).

Stehbens, Samantha and Torsten Wittmann (Aug. 2012). 'Targeting and transport: how microtubules control focal adhesion dynamics'. eng. In: *The Journal of Cell Biology* 198.4, pp. 481–489. DOI: 10.1083/jcb.201206050 (cited on page 16).

Stimpson, Taylor C. et al. (Sept. 2020). 'Xyloglucan Structure Impacts the Mechanical Properties of Xyloglucan–Cellulose Nanocrystal Layered Films—A Buckling-Based Study'. In: *Biomacromolecules* 21.9, pp. 3898–3908. DOI: 10.1021/acs.biomac.0c01031 (cited on page 22).

Stoma, Szymon et al. (Oct. 2008). 'Flux-Based Transport Enhancement as a Plausible Unifying Mechanism for Auxin Transport in Meristem Development'. en. In: *PLOS Computational Biology* 4.10, e1000207. DOI: 10.1371/journal.pcbi.1000207 (cited on page 35).

Stoppin-Mellet, Virginie, Jérémie Gaillard, and Marylin Vantard (July 2002). 'Functional evidence for in vitro microtubule severing by the plant katanin homologue.' In: *Biochemical Journal* 365.Pt 2, pp. 337–342. DOI: 10.1042/BJ20020689 (cited on page 9).

Stratilová, Barbora et al. (Jan. 2020). 'Plant Xyloglucan Xyloglucosyl Transferases and the Cell Wall Structure: Subtle but Significant'. en. In: *Molecules* 25.23, p. 5619. DOI: 10.3390/molecules25235619 (cited on page 22).

Sugimoto, Keiko et al. (June 2003). 'Mutation or Drug-Dependent Microtubule Disruption Causes Radial Swelling without Altering Parallel Cellulose Microfibril Deposition in Arabidopsis Root Cells[W]'. In: *The Plant Cell* 15.6, pp. 1414–1429. DOI: 10.1105/tpc.011593 (cited on page 30).

Sui, Liyuan and Christian Dahmann (Dec. 2020). 'Increased lateral tension is sufficient for epithelial folding in Drosophila'. In: *Development* 147.23, dev194316. DOI: 10.1242/dev.194316 (cited on page 34).

Sui, Liyuan, Gert O. Pflugfelder, and Jie Shen (Aug. 2012). 'The Dorsocross T-box transcription factors promote tissue morphogenesis in the Drosophila wing imaginal disc'. In: *Development* 139.15, pp. 2773–2782. DOI: 10.1242/dev.079384 (cited on pages 33, 34).

Suslov, D. and J.-P. Verbelen (July 2006). 'Cellulose orientation determines mechanical anisotropy in onion epidermis cell walls'. en. In: *Journal of Experimental Botany* 57.10, pp. 2183–2192. DOI: 10.1093/jxb/erj177 (cited on page 30).

Tang, Chao et al. (May 2020). 'Characterization of the pectin methyl-esterase gene family and its function in controlling pollen tube growth in pear (Pyrus bretschneideri)'. en. In: *Genomics* 112.3, pp. 2467–2477. DOI: 10.1016/j.ygeno.2020.01.021 (cited on page 21).

Tas, Roderick P. et al. (Dec. 2017). 'Differentiation between Oppositely Oriented Microtubules Controls Polarized Neuronal Transport'. en. In: *Neuron* 96.6, 1264–1271.e5. DOI: 10.1016/j.neuron.2017.11.018 (cited on page 15).

Taylor, Neil G. et al. (Feb. 2003). 'Interactions among three distinct CesA proteins essential for cellulose synthesis'. In: *Proceedings of the National Academy of Sciences* 100.3, pp. 1450–1455. DOI: 10.1073/pnas.0337628100 (cited on page 17).

Thomas, J., N.a. Idris, and D.a. Collings (2017). 'Pontamine fast scarlet 4B bifluorescence and measurements of cellulose microfibril angles'. fr. In: *Journal of Microscopy* 268.1, pp. 13–27. DOI: 10.1111/jmi.12582 (cited on page 25).

Tillery, Marisa M. L. et al. (Aug. 2018). 'Centrosomal and Non-Centrosomal Microtubule-Organizing Centers (MTOCs) in Drosophila melanogaster'. In: *Cells* 7.9, p. 121. DOI: 10.3390/cells7090121 (cited on page 14).

Toyo-Oka, Kazuhito et al. (Nov. 2005). 'Recruitment of katanin p60 by phosphorylated NDEL1, an LIS1 interacting protein, is essential for mitotic cell division and neuronal migration'. eng. In: *Human Molecular Genetics* 14.21, pp. 3113–3128. DOI: 10.1093/hmg/ddi339 (cited on page 9).

Toyooka, Kiminori et al. (Apr. 2009). 'A Mobile Secretory Vesicle Cluster Involved in Mass Transport from the Golgi to the Plant Cell Exterior'. In: *The Plant Cell* 21.4, pp. 1212–1229. DOI: 10.1105/tpc.108.058933 (cited on page 20).

Tozluoğlu, Melda et al. (Nov. 2019). 'Planar Differential Growth Rates Initiate Precise Fold Positions in Complex Epithelia'. en. In: *Developmental Cell* 51.3, 299–312.e4. DOI: 10.1016/j.devcel.2019.09.009 (cited on page 33).

Tripathi, Bipin Kumar and Kenneth D Irvine (Mar. 2022). 'The wing imaginal disc'. In: *Genetics* 220.4, iyac020. DOI: 10.1093/genetics/iyac020 (cited on page 33).

Uehara, Ryota et al. (Apr. 2009). 'The augmin complex plays a critical role in spindle microtubule generation for mitotic progression and cytokinesis in human cells'. In: *Proceedings of the National Academy of Sciences* 106.17, pp. 6998–7003. DOI: 10.1073/pnas.0901587106 (cited on page 14).

Usov, Ivan et al. (June 2015). 'Understanding nanocellulose chirality and structure-properties relationship at the single fibril level'. eng. In: *Nature Communications* 6, p. 7564. DOI: 10.1038/ncomms8564 (cited on page 18).

Uyttewaal, Magalie et al. (Apr. 2012). 'Mechanical Stress Acts via Katanin to Amplify Differences in Growth Rate between Adjacent Cells in Arabidopsis'. en. In: *Cell* 149.2, pp. 439–451. DOI: 10.1016/j.cell.2012.02.048 (cited on pages 9, 10).

Vain, Thomas et al. (Aug. 2014). 'The Cellulase KORRIGAN Is Part of the Cellulose Synthase Complex'. In: *Plant Physiology* 165.4, pp. 1521–1532. DOI: 10.1104/pp.114.241216 (cited on page 18).

Valentine, Megan T. et al. (May 2006). 'Individual dimers of the mitotic kinesin motor Eg5 step processively and support substantial loads in vitro'. en. In: *Nature Cell Biology* 8.5, pp. 470–476. DOI: 10.1038/ncb1394 (cited on page 12).

Van den Heuvel, M. G. L., M. P. de Graaff, and C. Dekker (June 2008). 'Microtubule curvatures under perpendicular electric forces reveal a low persistence length'. In: *Proceedings of the National Academy of Sciences of the United States of America* 105.23, pp. 7941–7946. DOI: 10.1073/pnas.0704169105 (cited on page 11).

Vandavasi, Venu Gopal et al. (Jan. 2016). 'A Structural Study of CESA1 Catalytic Domain of Arabidopsis Cellulose Synthesis Complex: Evidence for CESA Trimers'. In: *Plant Physiology* 170.1, pp. 123–135. DOI: 10.1104/pp.15.01356 (cited on page 17).

Vemu, Annapurna, Ewa Szczesna, and Antonina Roll-Mecak (2020). 'In vitro reconstitution assays of microtubule amplification and lattice repair by the microtubule severing enzymes katanin and spastin'. In:

Methods in molecular biology (Clifton, N.J.) 2101, pp. 27–38. DOI: 10.1007/978-1-0716-0219-5_3 (cited on page 9).

Verger, Stéphane et al. (Apr. 2018). 'A tension-adhesion feedback loop in plant epidermis'. In: *eLife* 7. Ed. by Christian S Hardtke and Dominique C Bergmann, e34460. DOI: 10.7554/eLife.34460 (cited on page 39).

Verhertbruggen, Yves et al. (Sept. 2009). 'An extended set of monoclonal antibodies to pectic homogalacturonan'. en. In: *Carbohydrate Research*. Pectin: Structure and Function 344.14, pp. 1858–1862. DOI: 10.1016/j.carres.2008.11.010 (cited on page 25).

Vetter, Roman and Dagmar Iber (Mar. 2022). 'Precision of morphogen gradients in neural tube development'. en. In: *Nature Communications* 13.1, p. 1145. DOI: 10.1038/s41467-022-28834-3 (cited on page 36).

Villares, Ana et al. (Aug. 2015). 'Kinetic aspects of the adsorption of xyloglucan onto cellulose nanocrystals'. en. In: *Soft Matter* 11.32, pp. 6472–6481. DOI: 10.1039/C5SM01413A (cited on page 22).

Vitre, Benjamin et al. (Apr. 2008). 'EB1 regulates microtubule dynamics and tubulin sheet closure in vitro'. en. In: *Nature Cell Biology* 10.4, pp. 415–421. DOI: 10.1038/ncb1703 (cited on pages 7, 8).

Vőfély, Róza V. et al. (2019). 'Of puzzles and pavements: a quantitative exploration of leaf epidermal cell shape'. en. In: *New Phytologist* 221.1, pp. 540–552. DOI: 10.1111/nph.15461 (cited on page 39).

Volkov, Vladimir A. et al. (May 2013). 'Long tethers provide high-force coupling of the Dam1 ring to shortening microtubules'. eng. In: *Proceedings of the National Academy of Sciences of the United States of America* 110.19, pp. 7708–7713. DOI: 10.1073/pnas.1305821110 (cited on page 11).

Vollmer, Jannik, Fernando Casares, and Dagmar Iber (Nov. 2017). 'Growth and size control during development'. eng. In: *Open Biology* 7.11, p. 170190. DOI: 10.1098/rsob.170190 (cited on page 37).

Wada, Hironori and Koichi Kawakami (2015). 'Size control during organogenesis: Development of the lateral line organs in zebrafish'. en. In: *Development, Growth & Differentiation* 57.2, pp. 169–178. DOI: 10.1111/dgd.12196 (cited on page 36).

Walker, R. A. et al. (Oct. 1988). 'Dynamic instability of individual microtubules analyzed by video light microscopy: rate constants and transition frequencies'. eng. In: *The Journal of Cell Biology* 107.4, pp. 1437–1448. DOI: 10.1083/jcb.107.4.1437 (cited on page 6).

Walkinshaw, M. D. and Struther Arnott (Dec. 1981). 'Conformations and interactions of pectins: II. Models for junction zones in pectinic acid and calcium pectate gels'. en. In: *Journal of Molecular Biology* 153.4, pp. 1075–1085. DOI: 10.1016/0022-2836(81)90468-X (cited on page 43).

Wang, Chaofeng et al. (Dec. 2017). 'KTN80 confers precision to microtubule severing by specific targeting of katanin complexes in plant cells'. In: *The EMBO Journal* 36.23, pp. 3435–3447. DOI: 10.15252/embj.201796823 (cited on page 9).

Wang, Dan et al. (Aug. 2016). 'Complementary expression of optomotor-blind and the Iroquois complex promotes fold formation to separate wing notum and hinge territories'. en. In: *Developmental Biology* 416.1, pp. 225–234. DOI: 10.1016/j.ydbio.2016.05.020 (cited on page 34).

Wang, Maojun et al. (Aug. 2013). 'A Comparative Genome Analysis of PME and PMEI Families Reveals the Evolution of Pectin Metabolism in Plant Cell Walls'. In: *PLoS ONE* 8.8, e72082. DOI: 10.1371/journal.pone.0072082 (cited on page 20).

Wang, Ning, James P. Butler, and Donald E. Ingber (1993). 'Mechanotransduction Across the Cell Surface and Through the Cytoskeleton'. In: *Science* 260.5111, pp. 1124–1127. DOI: 10.1126/science.7684161 (cited on page 15).

Wang, Xuan, Liza Wilson, and Daniel J Cosgrove (May 2020). 'Pectin methylesterase selectively softens the onion epidermal wall yet reduces acid-induced creep'. In: *Journal of Experimental Botany* 71.9, pp. 2629–2640. DOI: 10.1093/jxb/eraa059 (cited on pages 20, 21).

Wartlick, O. et al. (Mar. 2011). 'Dynamics of Dpp Signaling and Proliferation Control'. In: *Science* 331.6021, pp. 1154–1159. DOI: 10.1126/science.1200037 (cited on pages 36, 37).

Wartlick, Ortrud, Anna Kicheva, and Marcos González-Gaitán (Sept. 2009). 'Morphogen gradient formation'. eng. In: *Cold Spring Harbor Perspectives in Biology* 1.3, a001255. DOI: 10.1101/cshperspect.a001255 (cited on page 35).

Waters, Aoife M. and Philip L. Beales (July 2011). 'Ciliopathies: an expanding disease spectrum'. In: *Pediatric Nephrology (Berlin, Germany)* 26.7, pp. 1039–1056. DOI: 10.1007/s00467-010-1731-7 (cited on page 9).

Whitewoods, Christopher D. and Enrico Coen (Sept. 2017). 'Growth and Development of Three-Dimensional Plant Form'. English. In: *Current Biology* 27.17, R910–R918. DOI: 10.1016/j.cub.2017.05.079 (cited on pages 34, 38).

Wiedemeier, Allison M. D. et al. (Oct. 2002). 'Mutant alleles of Arabidopsis RADIALLY SWOLLEN 4 and 7 reduce growth anisotropy without altering the transverse orientation of cortical microtubules or cellulose microfibrils'. eng. In: *Development (Cambridge, England)* 129.20, pp. 4821–4830. DOI: 10.1242/dev.129.20.4821 (cited on page 30).

Wittmann, Torsten and Clare M. Waterman-Storer (June 2005). 'Spatial regulation of CLASP affinity for microtubules by Rac1 and GSK3beta in migrating epithelial cells'. eng. In: *The Journal of Cell Biology* 169.6, pp. 929–939. DOI: 10.1083/jcb.200412114 (cited on page 8).

Wohlert, Malin et al. (Jan. 2022). 'Cellulose and the role of hydrogen bonds: not in charge of everything'. en. In: *Cellulose* 29.1, pp. 1–23. DOI: 10.1007/s10570-021-04325-4 (cited on pages 17, 18).

Wolf, Sebastian et al. (Sept. 2012). 'Plant Cell Wall Homeostasis Is Mediated by Brassinosteroid Feedback Signaling'. en. In: *Current Biology* 22.18, pp. 1732–1737. DOI: 10.1016/j.cub.2012.07.036 (cited on page 21).

Wormit, Alexandra and Björn Usadel (Sept. 2018). 'The Multifaceted Role of Pectin Methylesterase Inhibitors (PMEIs)'. eng. In: *International Journal of Molecular Sciences* 19.10, E2878. DOI: 10.3390/ijms19102878 (cited on page 21).

Xiao, Chaowen, Chris Somerville, and Charles T. Anderson (Mar. 2014). 'POLYGALACTURONASE INVOLVED IN EXPANSION1 Functions in Cell Elongation and Flower Development in Arabidopsis[C][W]'. In: *The Plant Cell* 26.3, pp. 1018–1035. DOI: 10.1105/tpc.114.123968 (cited on page 31).

Xiao, Chaowen, Tian Zhang, et al. (Jan. 2016). 'Xyloglucan Deficiency Disrupts Microtubule Stability and Cellulose Biosynthesis in Arabidopsis, Altering Cell Growth and Morphogenesis1[OPEN]'. In: *Plant Physiology* 170.1, pp. 234–249. DOI: 10.1104/pp.15.01395 (cited on pages 22, 23, 25).

Xin, Xiaoran et al. (May 2020). 'Cellulose synthase interactive1- and microtubule-dependent cell wall architecture is required for acid growth in Arabidopsis hypocotyls'. In: *Journal of Experimental Botany* 71.10, pp. 2982–2994. DOI: 10.1093/jxb/eraa063 (cited on pages 25, 45).

Xiong, Xue et al. (2013). 'A Single Amino-Acid Substitution at Lysine 40 of an Arabidopsis thaliana-tubulin Causes Extensive Cell Proliferation and Expansion Defects'. en. In: *Journal of Integrative Plant Biology* 55.3, pp. 209–220. DOI: 10.1111/jipb.12003 (cited on page 10).

Xu, Tongda, Ning Dai, et al. (Feb. 2014). 'Cell Surface ABP1-TMK Auxin-Sensing Complex Activates ROP GTPase Signaling'. In: *Science* 343.6174, pp. 1025–1028. DOI: 10.1126/science.1245125 (cited on page 41).

Xu, Tongda, Mingzhang Wen, et al. (Oct. 2010). 'Cell Surface- and Rho GTPase-Based Auxin Signaling Controls Cellular Interdigitation in Arabidopsis'. English. In: *Cell* 143.1, pp. 99–110. DOI: 10.1016/j.cell.2010.09.003 (cited on page 41).

Xue, Jie, Maurice Bosch, and J. Paul Knox (Nov. 2013). 'Heterogeneity and Glycan Masking of Cell Wall Microstructures in the Stems of Miscanthus x giganteus, and Its Parents M. sinensis and M. sacchariflorus'. en. In: *PLOS ONE* 8.11, e82114. DOI: 10.1371/journal.pone.0082114 (cited on page 22).

Yagi, Noriyoshi et al. (June 2021). 'An anchoring complex recruits katanin for microtubule severing at the plant cortical nucleation sites'. en. In: *Nature Communications* 12.1, p. 3687. DOI: 10.1038/s41467-021-24067-y (cited on page 10).

Yang, Qihong et al. (Nov. 2020). 'The loss of function of HEL, which encodes a cellulose synthase interactive protein, causes helical and vine-like growth of tomato'. eng. In: *Horticulture Research* 7.1, p. 180. DOI: 10.1038/s41438-020-00402-0 (cited on page 111).

Yokoyama, Ryusuke et al. (2010). 'Biological implications of the occurrence of 32 members of the XTH (xyloglucan endotransglucosylase/hydrolase) family of proteins in the bryophyte Physcomitrella patens'. en. In: *The Plant Journal* 64.4, pp. 645–656. DOI: 10.1111/j.1365-313X.2010.04351.x (cited on page 22).

Yoneda, Arata, Takumi Higaki, et al. (Oct. 2007). 'Chemical Genetic Screening Identifies a Novel Inhibitor of Parallel Alignment of Cortical Microtubules and Cellulose Microfibrils'. In: *Plant and Cell Physiology* 48.10, pp. 1393–1403. DOI: 10.1093/pcp/pcm120 (cited on page 23).

Yoneda, Arata, Takuya Ito, et al. (2010). 'Cobtorin target analysis reveals that pectin functions in the deposition of cellulose microfibrils in parallel with cortical microtubules'. en. In: *The Plant Journal* 64.4, pp. 657–667. DOI: 10.1111/j.1365-313X.2010.04356.x (cited on page 23).

Yu, Shuizi Rachel et al. (Sept. 2009). 'Fgf8 morphogen gradient forms by a source-sink mechanism with freely diffusing molecules'. en. In: *Nature* 461.7263, pp. 533–536. DOI: 10.1038/nature08391 (cited on page 35).

Zagorski, Marcin et al. (June 2017). 'Decoding of position in the developing neural tube from antiparallel morphogen gradients'. In: *Science* 356.6345, pp. 1379–1383. DOI: 10.1126/science.aam5887 (cited on page 36).

Zanic, Marija et al. (June 2013). 'Synergy between XMAP215 and EB1 increases microtubule growth rates to physiological levels'. eng. In: *Nature Cell Biology* 15.6, pp. 688–693. DOI: 10.1038/ncb2744 (cited on page 7).

Zdunek, Artur, Piotr M. Pieczywek, and Justyna Cybulska (2021). 'The primary, secondary, and structures of higher levels of pectin polysaccharides'. en. In: *Comprehensive Reviews in Food Science and Food Safety* 20.1, pp. 1101–1117. DOI: 10.1111/1541-4337.12689 (cited on page 21).

Zhang, Chunhua, Leah E. Halsey, and Daniel B. Szymanski (Feb. 2011). 'The development and geometry of shape change in Arabidopsis thalianacotyledon pavement cells'. In: *BMC Plant Biology* 11.1, p. 27. DOI: 10.1186/1471-2229-11-27 (cited on page 40).

Zhang, Rui et al. (Aug. 2015). 'Mechanistic Origin of Microtubule Dynamic Instability and Its Modulation by EB Proteins'. In: *Cell* 162.4, pp. 849–859. DOI: 10.1016/j.cell.2015.07.012 (cited on page 7).

Zhang, Tian, Dimitrios Vavylonis, et al. (May 2017). 'Nanoscale movements of cellulose microfibrils in primary cell walls'. en. In: *Nature Plants* 3.5, p. 17056. DOI: 10.1038/nplants.2017.56 (cited on page 24).

Zhang, Tian, Yunzhen Zheng, and Daniel J. Cosgrove (Jan. 2016). 'Spatial organization of cellulose microfibrils and matrix polysaccharides in primary plant cell walls as imaged by multichannel atomic force microscopy'. eng. In: *The Plant Journal: For Cell and Molecular Biology* 85.2, pp. 179–192. DOI: 10.1111/tpj.13102 (cited on pages 17, 24).

Zhang, Weiwei and Christopher J. Staiger (Jan. 2022). 'Revising the Role of Cortical Cytoskeleton during Secretion: Actin and Myosin XI Function in Vesicle Tethering'. en. In: *International Journal of Molecular Sciences* 23.1, p. 317. DOI: 10.3390/ijms23010317 (cited on pages 19, 41, 42).

Zhang, Yao et al. (May 2021). 'Molecular insights into the complex mechanics of plant epidermal cell walls'. eng. In: *Science (New York, N.Y.)* 372.6543, pp. 706–711. DOI: 10.1126/science.abf2824 (cited on page 29).

Zhang, Zhongjuan et al. (Dec. 2020). 'A WOX/Auxin Biosynthesis Module Controls Growth to Shape Leaf Form'. en. In: *Current Biology* 30.24, 4857–4868.e6. DOI: 10.1016/j.cub.2020.09.037 (cited on page 111).

Zheng, Yunzhen et al. (2018). 'Xyloglucan in the primary cell wall: assessment by FESEM, selective enzyme digestions and nanogold affinity tags'. en. In: *The Plant Journal* 93.2, pp. 211–226. DOI: 10.1111/tpj.13778 (cited on page 22).

Zhu, Chuanmei et al. (Mar. 2015). 'The Fragile Fiber1 Kinesin Contributes to Cortical Microtubule-Mediated Trafficking of Cell Wall Components1[OPEN]'. In: *Plant Physiology* 167.3, pp. 780–792. DOI: 10.1104/pp.114.251462 (cited on page 20).

Zhu, Xiaoyu et al. (Apr. 2018). 'CSI1, PATROL1, and exocyst complex cooperate in delivery of cellulose synthase complexes to the plasma membrane'. In: *Proceedings of the National Academy of Sciences of the United States of America* 115.15, E3578–E3587. DOI: 10.1073/pnas.1800182115 (cited on pages 19, 21).

Zwetsloot, Alexander James, Gokhan Tut, and Anne Straube (Oct. 2018). 'Measuring microtubule dynamics'. In: *Essays in Biochemistry* 62.6, pp. 725–735. DOI: 10.1042/EBC20180035 (cited on pages 7, 46).